AFIT/GAE/ENY/93D-27

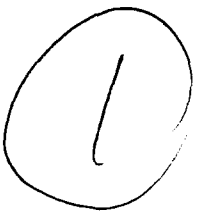

OPTIMAL CONTROL DESIGN ADVANTAGES UTILIZING TWO-DEGREE-OF-FREEDOM CONTROLLERS

THESIS

Michael J. Stephens, Captain, USAF

AFIT/GAE/ENY/93D-27

Approved for public release; distribution unlimited

AFIT/GAE/ENY/93D-27

OPTIMAL CONTROL DESIGN ADVANTAGES UTILIZING TWO-DEGREE-OF-FREEDOM CONTROLLERS

THESIS

Presented to the Faculty of the Graduate School of Engineering

of the Air Force Institute of Technology

Air University

In Partial Fulfillment of the

Requirements for the Degree of

Master of Science in Aeronautical Engineering

Michael J. Stephens, B.S., M.B.A.

Captain, USAF

December 1993

Acknowledgements

This thesis is the culmination of many hours and long days and nights of hard work. First of all, I would like to thank my advisor, Dr. Ridgely, not only for providing me with an interesting topic, but for being there to explain difficult concepts in ways that I could understand and giving me the confidence that I could complete this momentus project successfully. There are also many friends I have made at AFIT who have helped me to see the lighter side of things when times were tough -- I salute you all.

Furthermore, I cannot forget the unwavering support of my family -- Mom and Steph -- in whatever I do. Nor can I forget the one individual who has basically had to put her life on hold while I stumbled through school -- my wife, Carolyn. Words cannot properly express the gratitude I feel toward her.

I would like to dedicate this thesis to the person whose example and approach to life helped mold me into the person I am today -- my father, the late Dr. James L. Stephens, Jr.

-- Michael J. Stephens

Table of Contents

Page

List of Figures

Figure | Page

Notation

1-DOF	One-Degree-of-Freedom
2-DOF	Two-Degree-of-Freedom
SISO	Single-Input-Single-Output
MIMO	Multiple-Input-Multiple-Output
IGM	Independent Gain Margin
IPM	Independent Phase Margin
ARE	Algebraic Riccati Equation
LFT	Linear Fractional Transformation
$G(s)$	Plant transfer function
$K(s)$	Compensator transfer function
L	Loop Transfer Function
S	Sensitivity Function $\equiv \left(\frac{1}{1+L}\right)$ or $[I+L]^{-1}$
T	Complimentary Sensitivity Function $\equiv \left(\frac{L}{1+L}\right)$ or $[I+L]^{-1}L$
$\lvert A \rvert$	magnitude of A
$\sigma_i(A)$	singular values of A
$\bar{\sigma}(A)$	maximum singular value of A
$\underline{\sigma}(A)$	minimum singular value of A
$\mathrm{tr}(A)$	trace of $A \equiv \sum_{i=1}^{n} a_{ii}$

$\lambda_i(A)$	eigenvalues of A
A^*	complex conjugate transpose of A
$\|\cdot\|_2$	2-norm
inf	infimum
α_0	$\inf_{K\ adm} \|T_{zw}\|_2$
K_{2opt}	unique $K(s)$ that yields $\|T_{zw}\|_2 = \alpha_0$
RH_2	space of all stable, strictly proper transfer functions with real, rational coefficients
$\left[\begin{array}{c\|c} A & B \\ \hline C & D \end{array}\right]$	transfer function notation $\equiv C(sI - A)^{-1}B + D$
ω	frequency variable
ω_0	bandwidth frequency
s	Laplace variable ($s = j\omega$)
z	controlled outputs
y	measured outputs
u	control inputs
r_c	reference command inputs
w_d	plant disturbance noise
w_n	sensor or measurement noise
$\in$	element of

Abstract

The purpose of this study was to investigate and describe the differences between a one-degree-of-freedom (1-DOF) controller, in which a controller is placed in a single location in the control loop, and a two-degree-of-freedom (2-DOF) controller, in which two separate controllers are designed -- one in the feedback loop and the other as a prefilter in the forward loop. The approach involved summarizing the major rules governing loop shaping for performance and robustness in the 1-DOF case and then extending the concepts to the 2-DOF case. H_2 optimization was utilized to perform several types of SISO examples and one MIMO example to verify the concepts. In all cases, the 2-DOF controller exhibited superior tracking performance over a wide range of plant disturbances and measurement noises compared to the 1-DOF model.

OPTIMAL CONTROL DESIGN ADVANTAGES UTILIZING TWO-DEGREE-OF-FREEDOM CONTROLLERS

I. Introduction

1.1 Background

Current linear control system design depends primarily upon the principles of either cascade or feedback compensation. Employing these methods allows the use of such design techniques as root locus and other classical design techniques. In any case, the basic block diagram used in the mathematical model requires that the compensator be placed in a single location in the control loop, as shown in Figure 1-1(a). Hence, systems that are modeled by such a block diagram are referred to as one-degree-of-freedom (1-DOF) systems. The basic control design objective examined in this thesis is achieving favorable command following performance in the face of plant disturbances and sensor or measurement noise. In 1-DOF systems, the single compensator is designed to accomplish all of the tasks required for this objective. The problem typically encountered with this type of system is that there is an inherent tradeoff between tracking low frequency commands and rejecting high frequency measurement noise.

A more successful way to deal with this problem is to use a two-degree-of-

freedom (2-DOF) system, which is shown in Figure 1-1(b). Using this type of setup, there are now two separate compensators available to accomplish the design objectives. The idea behind this type of system is that the compensator in the feedback loop, K_1, takes care of the disturbance and measurement noise rejection objectives, while the prefilter, K_2, takes care of command following properties. From the outset, it is expected that 2-DOF controllers will provide better overall tracking performance than 1-DOF controllers; two of the questions that this thesis proposes to answer are how much better and under what conditions they are better.

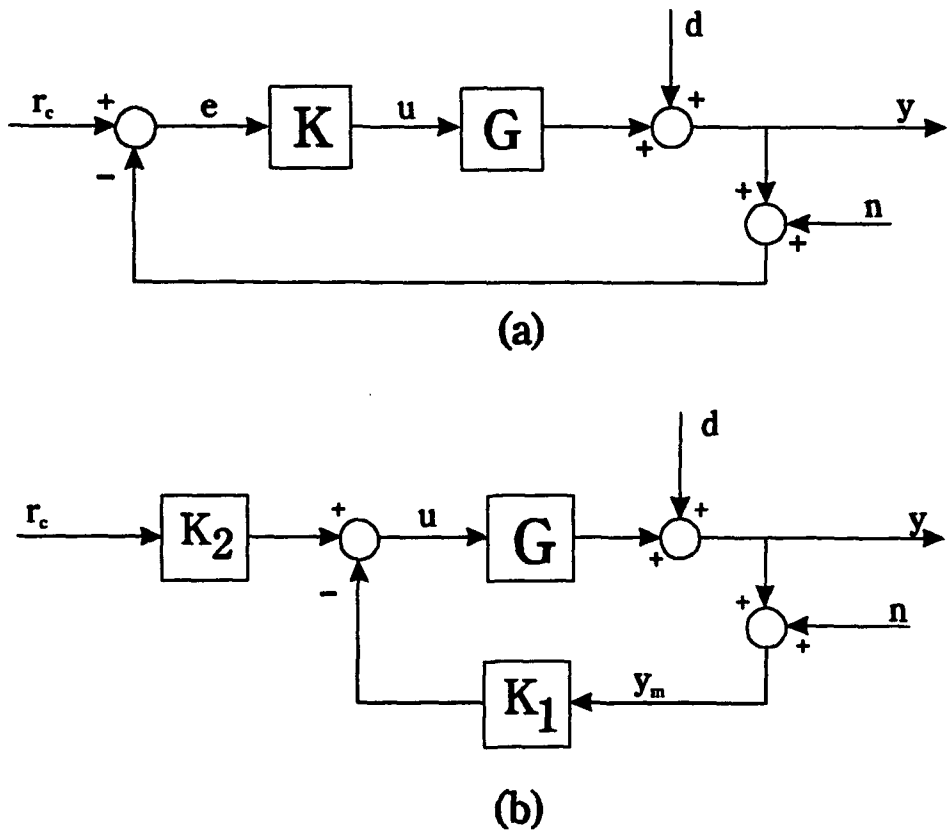

Figure 1-1. **(a)** 1-DOF Control System Block Diagram
(b) 2-DOF Control System Block Diagram

1.2 Objectives

The primary objective of this thesis is to investigate and quantify the differences between the 1-DOF and 2-DOF design methodologies. This objective is accomplished by observing the trends in the closed loop frequency and time responses of both systems as plant disturbances and measurement noises are varied.

1.3 Scope

The approach followed is to first summarize the major rules governing loop shaping for performance and robustness in the 1-DOF case and then extend these concepts to the 2-DOF case. Then, several types of examples are examined in order to illustrate the differences between the two systems. The first set of examples are single-input-single-output (SISO): a stable, minimum phase system; an unstable, minimum phase system; a stable, nonminimum phase system; and an unstable, nonminimum phase system. This first set of SISO examples is explored in detail to show the basic trends that can be expected from each type of system. The next set of SISO examples involves designing each system to be a particular system type and observing its time responses to higher order inputs. The last SISO example examines the effect of low frequency measurement noise on the tracking performance of both 1-DOF and 2-DOF systems. Finally, a multiple-input-multiple-output (MIMO) point design for a missile autopilot system is analyzed to verify the concepts for the MIMO case.

There are several limitations regarding this thesis that are worth noting here. It is not the purpose of this thesis to actually perform designs, in either the SISO or

MIMO case. Representative disturbance and measurement noise sizes are repeated in all of the examples to show the trends in the frequency response plots and time responses -- not to provide design data. Also, all of the controllers used in the examples in this thesis were designed using H_2 optimization, which has certain limitations, such as the two compensators in the 2-DOF system being constrained to share the same poles. In keeping with thrust of the thesis objectives, however, H_2 optimization represents a consistent design method with which the design characteristics of 1-DOF and 2-DOF systems can be compared.

1.4 Related Work

In section 1.1 of this thesis, it was stated that 2-DOF controllers are expected to perform better than 1-DOF controllers. This general conclusion has come about due to the previous published work of others in this field. While the 2-DOF controllers in this work are designed simultaneously using H_2 optimization, most of the work in this field has made use of other methods, such as H_∞ optimization, or describes methods of designing the two compensators separately and parameterizing the class of all compensators that satisfy some criteria. For references utilizing these techniques, the reader is referred to [4, 5, 8, 9, 10]. Since the intent of thesis is not to perform actual designs, but to provide insight into the fundamental differences between 1-DOF and 2-DOF systems, other optimization techniques were not investigated.

1.5 Thesis Outline

This thesis consists of eight chapters. Chapter I provides general background information on the potential benefits of the 2-DOF design method and outlines the

scope of this work.

Chapter II covers fundamental design concepts for the 1-DOF case, for both SISO and MIMO cases. Specifically, the attributes which comprise a "good" loop shape with regard to tracking, disturbance rejection, and measurement noise rejection are described. System type concepts are also reviewed..

Chapter III mirrors the previous chapter by extending the ideas of loop shaping for performance and robustness to the 2-DOF case, emphasizing key differences.

Chapter IV provides an overview of the benefits and limitations of the H_2 optimization design method, which is used for all of the examples in this thesis.

The general H_2 control problem, as it is applied to the examples in this thesis, is described in Chapter V. In addition to showing the appropriate transfer function matrices and state spaces for the 1-DOF and 2-DOF cases, the rationale behind all of the weight selections used in the examples is provided.

Chapter VI features SISO examples to illustrate the concepts of Chapters II and III. First, an exhaustive frequency and time response plot analysis is performed for 1) a stable, minimum phase system; 2) an unstable, minimum phase system; 3) a stable, nonminimum phase system; and 4) an unstable, nonminimum phase system. Secondly, the unstable, nonminimum phase example is used in conjunction with altered H_2 tracking weights to compare the effects of higher order inputs on different system types. Finally, the same unstable, nonminimum phase plant is used to illustrate the effects of low frequency measurement noise on 1-DOF and 2-DOF systems. This last example represents a prime case where the advantages of utilizing a 2-DOF controller should be apparent.

Chapter VII presents a MIMO missile autopilot example and explores the trends in loop shape and tracking performance as the plant disturbance and measurement noise are varied.

Chapter VIII provides the overall conclusions for this work, as well as recommendations for further study.

II. Fundamental Concepts for 1-DOF Controllers

The purpose of this chapter is to review the basic concepts of feedback control of linear systems in the 1-DOF case (both SISO and MIMO) in order to provide a basis for comparison to the 2-DOF case. Chapter III extends these basic concepts to the 2-DOF case and highlights the key differences. Since the overall objectives in control system design include command following, disturbance rejection, and measurement noise rejection, each of these concepts will be examined in detail -- specifically, how the shape of the closed loop system should look in order to achieve these objectives. In addition, the idea of system type and different types of inputs will be compared between the two cases. Although the differences between 1-DOF and 2-DOF systems are best illustrated through the use of examples, this background chapter lays the groundwork for what should be expected in the examples in the latter chapters.

2.1 Loop Shaping

One of the most important aspects of control system design is the concept of "good" loop shaping. In most cases, a control system designer has at least one objective in mind: to build a set or multiple point tracker, to reject plant disturbances or measurement noises, or to achieve performance in the face of plant uncertainty. Often, all of these objectives are important. The shape of a favorable loop for a closed loop system depends upon what performance criteria are desired. This chapter is devoted to detailing what characteristics a 1-DOF control system must exhibit to

satisfy each design objective. A more complete treatment of loop shaping is contained in [7:Ch. 4].

2.1.1 SISO Case. Figure 2-1 shows the standard 1-DOF, SISO, unity feedback, cascade compensation block diagram which is taught in most basic control system fundamentals courses.

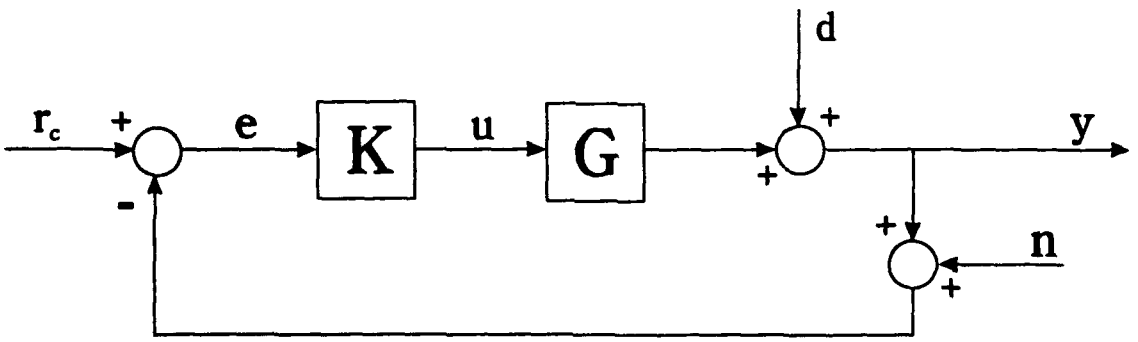

Figure 2-1. *1-DOF SISO Control System Block Diagram*

where

r_c = reference command input signal

e = error signal

u = control input signal

d = output disturbance signal

n = sensor noise signal

y = output signal

Relating the outputs to the inputs in closed loop form yields

$$y = \left(\frac{GK}{1 + GK}\right) r_c + \left(\frac{1}{1 + GK}\right) d - \left(\frac{GK}{1 + GK}\right) n \qquad (2.1)$$

It is appropriate here to define two quantities which will prove important in the design process. First, the quantity $\left(\frac{1}{1 + GK}\right)$ (or $[I + GK]^{-1}$ in the MIMO case) is known as the system's *sensitivity*. Second, the quantity $\left(\frac{GK}{1 + GK}\right)$ (or $[I + GK]^{-1}GK$ in the MIMO case) is known as the system's *complimentary sensitivity*. Denoting the sensitivity as S and the complimentary sensitivity as T, equation (2.1) can be rewritten as

$$y = Tr_c + Sd - Tn \qquad (2.2)$$

From this equation, the appropriate size of the magnitude of GK (denoted $|GK|$) can be determined depending on the particular objective desired.

2.1.1.1 Command Following. For good tracking, consider first only the input r_c and the output y. The transfer function from r_c to y is simply the complimentary sensitivity. It is apparent that if $|1 + GK|$ (and hence $|GK|$) is made "large" over the frequency range where commands are expected, usually low frequencies, then the transfer function will be close to unity over those frequencies, and the system will exhibit good tracking characteristics.

2.1.1.2 Disturbance Rejection. Good disturbance rejection is attained by examining the transfer function from d to y, which is equal to the sensitivity. Given this, it is clear that when $|GK|$ is large over the frequency where disturbances

are expected (usually low frequencies), the transfer function becomes very small, and the disturbance is effectively rejected. Of note is the fact that the requirement that $|GK|$ be large applies to both the command following and disturbance rejection performance objectives.

2.1.1.3 Sensor or Measurement Noise Rejection. Finally, the transfer function from n to y can be examined in order to achieve sensor noise rejection. From equation (2.1), this transfer function is equal to the negate of the complimentary sensitivity. In order to reject measurement noises, this quantity must be made "small" at frequencies where noises are expected. It is important to note that the output y is related to the command input r_c and the sensor noise input signal n by the same transfer function, the complimentary sensitivity. In the command following case, $|GK|$ needs to be made large, and in the sensor noise rejection case, $|GK|$ needs to be made small, presenting what could be a serious conflict in design objectives. If the measurement noise has any low frequency content, it will be passed through to the output since $|GK|$ is large at low frequencies. Measurement noise, however, is typically a high frequency phenomenon, so as long as there is adequate separation between the frequency range where most command inputs fall and the range where measurement noises fall, there is no problem in meeting both design objectives.

2.1.1.4 Bode Magnitude Plot Analysis. The aforementioned requirements can be combined together and represented on a Bode magnitude plot that incorporates all of the objectives by presenting "barriers" that $|GK|$ must avoid. Figure 2-2 represents such a Bode plot. The control system designer then tries to find a compensator that produces a stable closed loop system whose loop transfer function

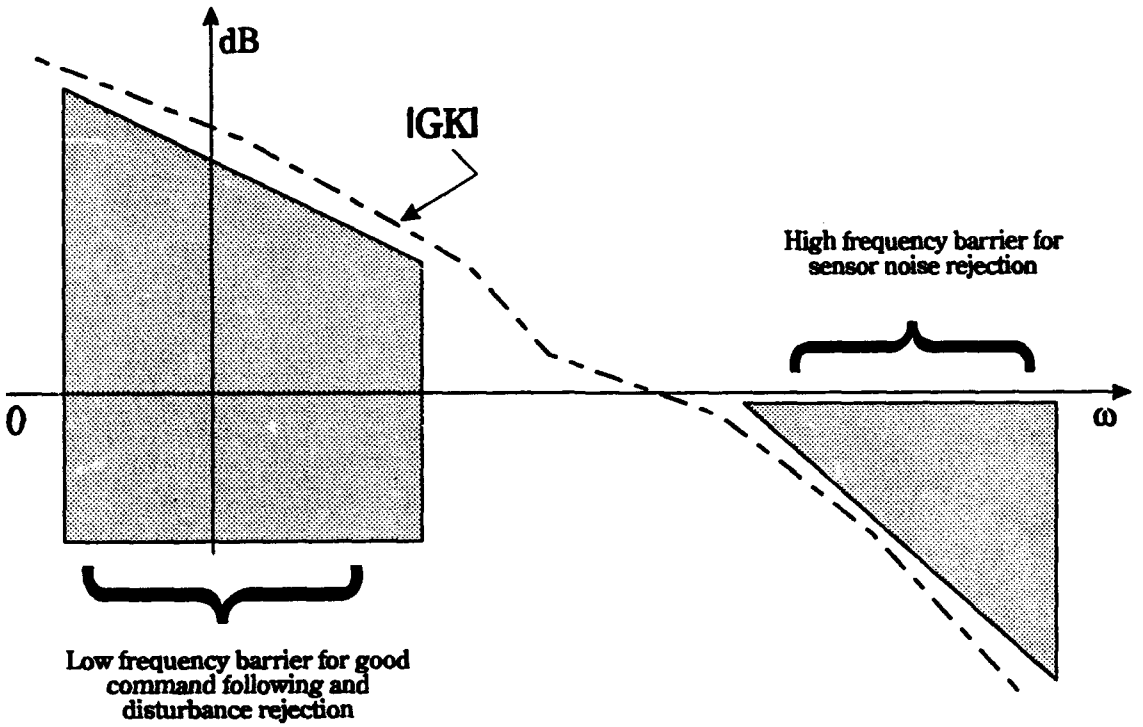

Figure 2-2. Bode Magnitude Plot of a "Good" Loop Transfer Function for a 1-DOF, SISO System

$|GK|$ satisfies the properties shown in Figure 2-2. In addition to a Bode magnitude plot of the loop transfer function $|GK|$, it is also beneficial to examine magnitude plots of the sensitivity function $|S|$ and the complimentary sensitivity function $|T|$. These Bode plots can be judged "good" or "bad" according to the same requirements that produce good command following, disturbance rejection, and measurement noise rejection.

In the case of the sensitivity function, there are two barriers that $|S|$ must avoid in order to meet all of the objectives. First, since $|GK|$ has high gain at low frequency, $|S|$ must be sufficiently small at low frequency in order to achieve a small steady state

error in the step response (other types of inputs will be discussed later in the chapter). The sensitivity function must also cross the 0 dB line at a high enough frequency that the system will have a sufficiently fast transient response (the speed of the system's transient response is proportional to how high the crossover frequency of $|GK|$ is). Secondly, $|S|$ must not exhibit too much overshoot above the 0 dB line because then the stability margins begin to deteriorate (stability margins will be discussed more fully later in this chapter). Combining these ideas yields a Bode magnitude plot like the one shown in Figure 2-3.

A Bode plot of the complimentary sensitivity function exhibits the same information contained in the sensitivity plot, but the information is not quite as explicit. Once again, if $|GK|$ is large at low frequency and small at high frequency, then the system exhibits good tracking characteristics, disturbance rejection, and noise

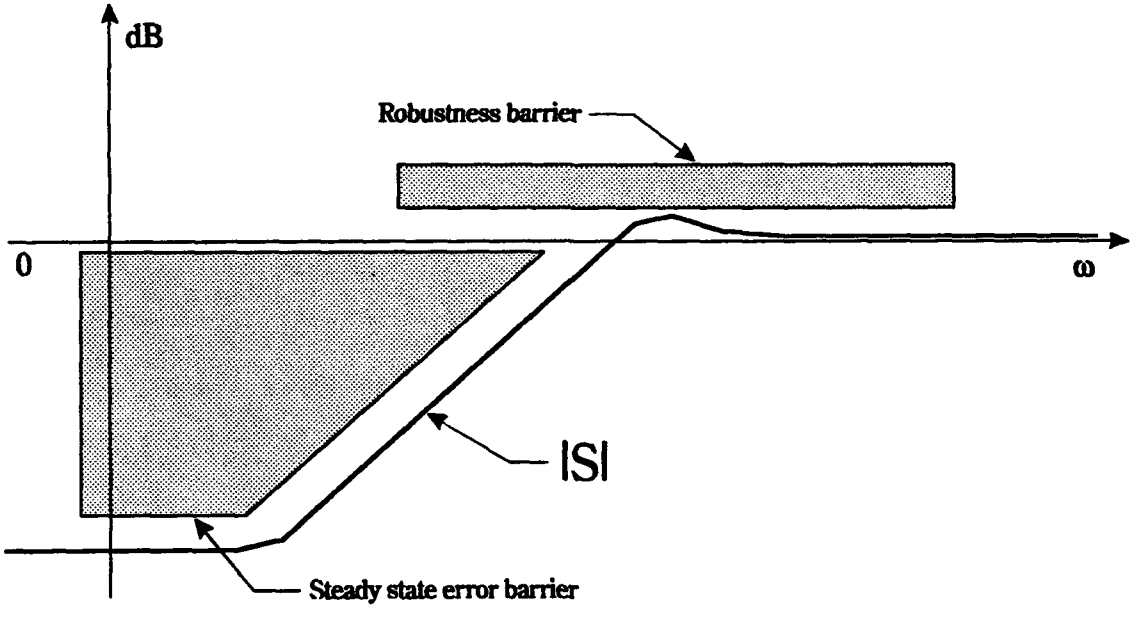

Figure 2-3. Bode Magnitude Plot of a "Good" Sensitivity Function for a 1-DOF, SISO Transfer Function

rejection. On a magnitude plot of $|T|$, the function is unity (0 dB) at low frequency and "rolls off" at high frequency in order to achieve these characteristics. The real utility of this plot is in noting the point at which the frequency passes the -3 dB point, which is known as the system's *bandwidth*, which will be denoted ω_0. The bandwidth is a measure of the frequency range over which the system will track command inputs. Incidentally, if any measurement noises fall below the system bandwidth, then they will be passed through to the output y. Additionally, like the sensitivity function, the complimentary sensitivity function must not exhibit too much oversh or the stability margins begin to deteriorate. Thus, there is a robustness, as well as a bandwidth, barrier on a Bode plot of $|T|$. Figure 2-4 shows a Bode plot of a "good" system complimentary sensitivity function.

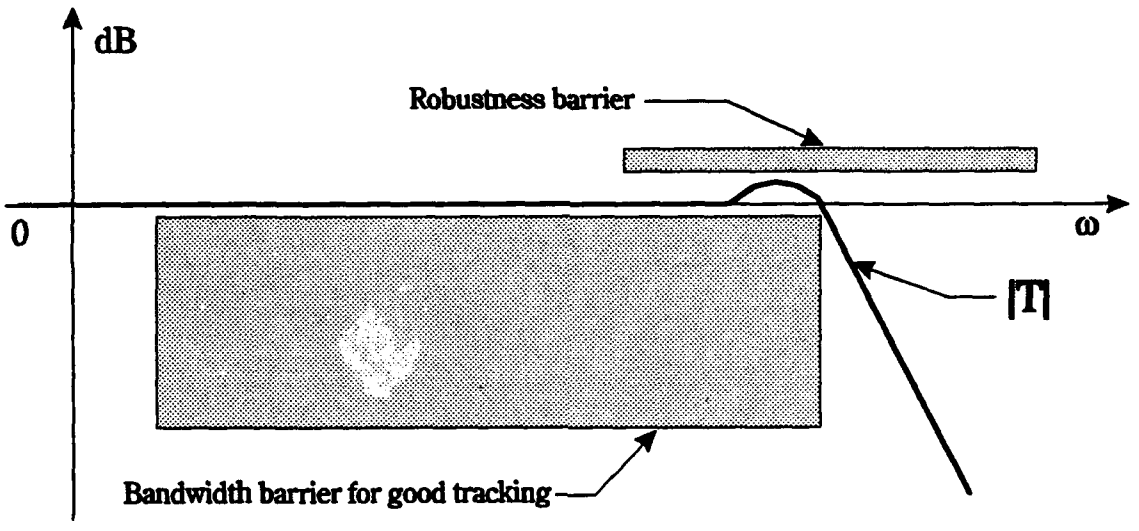

Figure 2-4. Bode Magnitude Plot of a "Good" Complimentary Sensitivity Function for a 1-DOF, SISO System

2.1.2 MIMO Case. Any discussion of system loop shaping would be incomplete without considering the multivariable case. Problems of this type employ the same basic principles as in the SISO case, but require some minor modifications. Figure 2-1 is still applicable to this discussion, with the primary difference being that all signals are now vector signals, and the plant is a transfer function matrix relating several inputs to several outputs.

2.1.2.1 Singular Values. The first principle that applies to multivariable loop shaping is the concept of singular values. In the SISO case, the "size" of a transfer function is simply its magnitude at the particular frequency of interest. When the magnitudes are plotted over a range of frequencies, a Bode plot results. In the MIMO case, however, the plant is described by a transfer function matrix, whose size cannot be described by so simple a notion. Instead, it is described in terms of its singular values. The singular values of a given matrix, A, are given by

$$\sigma_i(A) = [\lambda_i(A^*A)]^{\frac{1}{2}} \tag{2.3}$$

where

$\sigma_i(A)$ = singular values of A

A^* = complex conjugate transpose of A

$\lambda_i(A^*A)$ = eigenvalues of A^*A

The minimum singular value of A, denoted $\underline{\sigma}(A)$, is a measure of the maximum attenuation of a signal by the transfer function matrix. The maximum singular value, $\bar{\sigma}(A)$, is a measure of the maximum amplification of the signal. Hence, if $\underline{\sigma}(A)$ is

large, then the matrix A is said to be large; if $\bar{\sigma}(A)$ is small, then A is said to be small. As frequency changes, each individual transfer function in the transfer matrix also changes, just as in the SISO case. Therefore, the minimum and maximum singular values of the transfer function matrix are also functions of frequency and can be plotted. The resulting plot is called a singular value plot and is the MIMO equivalent of a Bode plot.

2.1.2.2 MIMO Performance Measures. The concept of singular values can be used to extend the SISO ideas of command following, disturbance rejection, and measurement noise rejection to the MIMO case. First of all, the MIMO equation relating the outputs to the inputs is

$$y = [I + GK]^{-1}GK\,r_c + [I + GK]^{-1}\,d - [I + GK]^{-1}GK\,n \qquad (2.4)$$

Beginning with an analysis of command following performance, the transfer function from r_c to y needs to approach unity over the low frequency range where commands are expected. This means that for all frequencies below the bandwidth frequency,

$$[I + GK]^{-1}GK \approx I \qquad \forall\ \omega < \omega_0 \qquad (2.5)$$

For disturbance rejection, the sensitivity function must be minimized at low frequency, just as in the SISO case, except now the condition becomes

$$[I + GK]^{-1} \approx 0 \qquad \forall\ \omega < \omega_0 \qquad (2.6)$$

Saying that the sensitivity function should be "small" at low frequency, is equivalent to saying

$$\bar{\sigma}[\{I + GK\}^{-1}] \quad \text{"small"} \qquad \forall \ \omega < \omega_0 \tag{2.7}$$

Using the singular value identity

$$\bar{\sigma}(A) = \frac{1}{\underline{\sigma}(A^{-1})} \tag{2.8}$$

condition (2.7) becomes

$$\underline{\sigma}[I + GK] \quad \text{"large"} \qquad \forall \ \omega < \omega_0 \tag{2.9}$$

which, in turn, may be simplified to read

$$\underline{\sigma}[GK] \quad \text{"large"} \qquad \forall \ \omega < \omega_0 \tag{2.10}$$

Once again, the measurement noise-to-output transfer function, *n* to *y*, is the negate of the complimentary sensitivity, so for all frequencies above the bandwidth frequency (where hopefully all of the measurement noises are),

$$[I + GK]^{-1}GK << 1 \qquad \forall \ \omega > \omega_0 \tag{2.11}$$

It can be shown that at high frequency, equation (2.11) holds if

$$\bar{\sigma}[GK] \quad \text{"small"} \qquad \forall \ \omega > \omega_0 \tag{2.12}$$

Putting all of this information together, it follows that a singular value plot of a "good" MIMO loop shape ($\sigma[GK]$) can be constructed by satisfying equation (2.10) at low frequency and equation (2.12) at high frequency, as in Figure 2-5.

2.1.2.3 Stability Margins. Thus far, little mention has been made regarding a system's *robustness*, or ability to maintain closed loop stability in the face of plant uncertainty, gain changes, phase changes, or simultaneous gain and phase

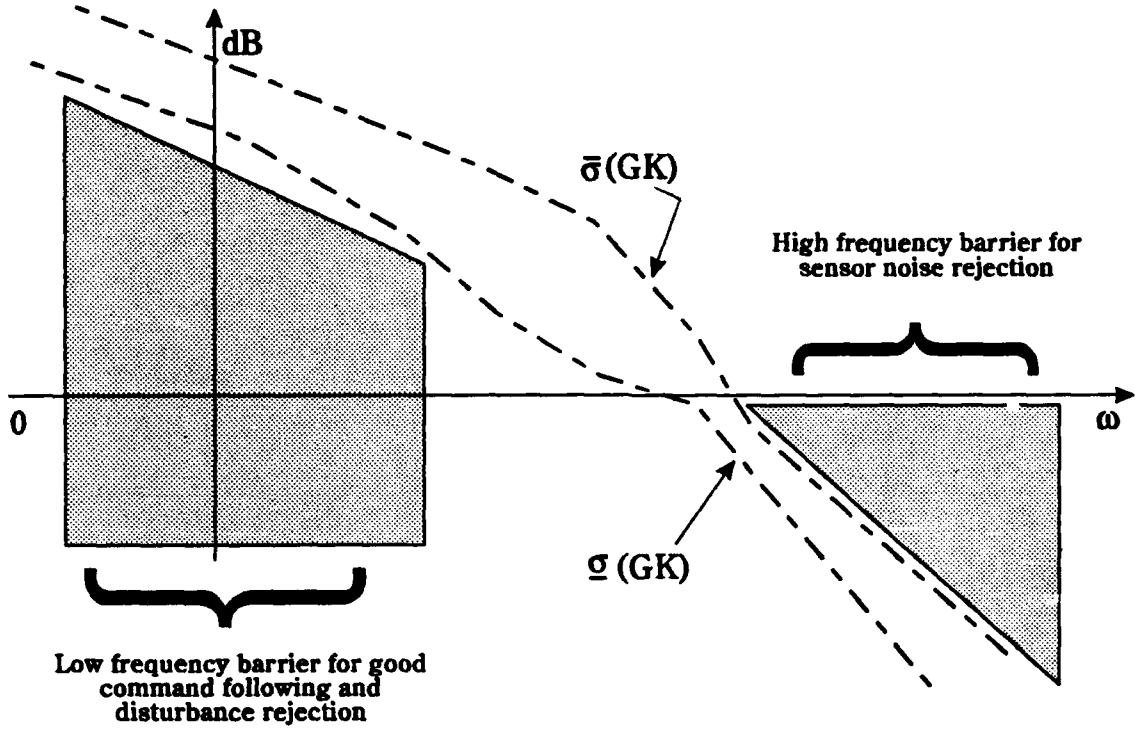

Figure 2-5. Singular Value Plot of a "Good" Loop Transfer Function for a 1-DOF, MIMO System

changes. To maintain consistency, this thesis will only be concerned with simultaneous gain and phase changes, which are measured by *independent gain* and *phase margins*. This approach could be considered somewhat conservative, in that the margins will almost always come out to be less than margins obtained classically or one-loop-at-a-time. However, in cases where the plant has unstable poles or nonminimum phase zeros, simultaneous gain and phase changes can sometimes easily destabilize the system, while gain or phase changes alone could not. The independent gain margin (IGM) and independent phase margin (IPM) of a system are given by

$$IGM = \left[\frac{1}{1+\alpha_0}, \frac{1}{1-\alpha_0}\right] \cup [1-a_0, 1+a_0]$$

$$IPM = \left[\pm 2\sin^{-1}\left(\frac{\alpha_0}{2}\right)\right] \cup \left[\pm 2\sin^{-1}\left(\frac{a_0}{2}\right)\right] \tag{2.13}$$

where

$$\alpha_0 = \min_{\omega} \underline{\sigma}[I+L] = \max_{\omega} \overline{\sigma}\{[I+L]^{-1}\} = \max_{\omega} \overline{\sigma}[S]$$

$$a_0 = \min_{\omega} \underline{\sigma}[I+L^{-1}] = \max_{\omega} \overline{\sigma}\{[I+L]^{-1}L\} = \max_{\omega} \overline{\sigma}[T] \tag{2.14}$$

Note that the variable L represents the loop transfer function (GK in the 1-DOF case). From these definitions it is apparent that the shape of the sensitivity and complimentary sensitivity functions plays a direct role in the determination of stability margins, in both the SISO and MIMO cases. From Figures 2-3 and 2-4, the extent to which $|S|$ and $|T|$ "bubble up" above the 0 dB line indicates the amount that the margins deteriorate. Thus, the robustness barriers in these two figures ensure that the closed loop system has reasonable stability margins. Although no singular value plot is shown for the MIMO sensitivity or complimentary sensitivity functions, the line representing the maximum singular values will usually exhibit the same sort of "hump" above the 0 dB line, and equation (2.13) can be used to calculate the independent margins.

2.2 *System Type*

In addition to defining characteristics of a linear system's loop shape, one may also be interested in quantifying its tracking performance to a variety of inputs. One approach is to approximate the inputs as linear polynomial functions of time. The steady state error resulting when each type of input is applied to the system reveals important information about the system. Specifically, for a stable system, the degree of the polynomial input for which the steady state error is constant is referred to as the *system type*. The following discussion is excerpted from [3:125-132].

For the unity feedback, 1-DOF setup in Figure 2-1, consider the transfer function from r_c to e, which is equal to the sensitivity function, or, in terms of Laplace variables

$$e(s) = \frac{1}{1 + L(s)} r_c(s) \tag{2.15}$$

where $L(s)$ is equal to the loop transfer function $G(s)K(s)$. If the reference input is assumed to be a polynomial of degree k and is represented in the time domain as

$$r_c(t) = \left(\frac{t^k}{k!}\right) u_{-1}(t) \tag{2.16}$$

where $u_{-1}(t)$ represents the unit step function, then the Laplace transform of the input is written

$$r_c(s) = \frac{1}{s^{k+1}} \tag{2.17}$$

Therefore, if $k = 0$, then the input is a step of unit amplitude; if $k = 1$, the input is a

ramp with unit slope; if $k = 2$, the input is a parabola with unit second derivative; and so on.

From the final value theorem, the system steady state error is then defined as

$$e_{ss} = \lim_{s \to 0} s \frac{1}{[1 + L(s)]\, s^{k+1}} = \lim_{s \to 0} \frac{1}{[1 + L(s)]\, s^{k}} \tag{2.18}$$

If the system is type 0, then L has no poles at the origin and setting k equal to zero (step input) produces the following error:

$$e_{ss} = \frac{1}{1 + L(0)} = \frac{1}{1 + K_p} \tag{2.19}$$

where K_p is the position error constant, which is equal to the DC gain of $L(s)$ (for unity feedback). In other words, if the loop transfer function L has no poles at the origin, then this error cannot be zero. Likewise, if the system is type I, then L has one pole at the origin, and if the input is a ramp ($k = 1$), then the steady state error is

$$e_{ss} = \lim_{s \to 0} \frac{1}{[1 + L(s)]\, s} = \lim_{s \to 0} \frac{1}{s\, L(s)} = \frac{1}{K_v} \tag{2.20}$$

where K_v is the velocity constant. If the system is type II, L has two poles at the origin, and if the input is a parabola ($k = 2$), then the steady state error is

$$e_{ss} = \lim_{s \to 0} \frac{1}{[1 + L(s)]\, s^2} = \lim_{s \to 0} \frac{1}{s^2 L(s)} = \frac{1}{K_a} \tag{2.21}$$

where K_a is the acceleration constant.

It is important to note that although a system of type k produces a constant

error for inputs whose Laplace transform have a degree of $(k + 1)$, it perfectly tracks inputs which have a degree of k or lower. If the degree of the input is $(k + 2)$ or higher, however, the system will produce an infinite steady state error. It is also important to note that the above results are only valid for the unity feedback case. For the non-unity feedback case, the error constants must be derived by solving for the reference command-to-error transfer function from the particular block diagram and applying the final value theorem as appropriate.

III. Fundamental Concepts for 2-DOF Controllers

At first it may not seem necessary to provide a separate chapter on the basic linear system theory behind 2-DOF controllers, since the principles from which it is derived were just described in Chapter II. However, in keeping with the main thrust of this thesis, the linear system fundamentals as they apply to 2-DOF systems must be described in detail so that the expected performance advantages have a sound basis in theory as well as in practice. This chapter mirrors all of the concepts covered in Chapter II, except the ideas are extended to the 2-DOF case for comparison and contrast.

3.1 Loop Shaping

In the 2-DOF case, many of the same principles of loop shaping from the 1-DOF case still apply, but the added flexibility of having two different compensators manifests itself in several ways.

3.1.1 SISO Case. The basic block diagram for the 2-DOF system is shown in Figure 3-1. All of the variables are the same as those defined in the 1-DOF setup in Figure 2-1 except in this figure, the measured output, y_m, is shown. Of special note is the fact that the 2-DOF block diagram is derived from a block diagram manipulation of the 1-DOF diagram, and the two are equivalent if K_1 and K_2 are equal. If they are not equal, however, then the equations describing the system become quite different because K_1 is in the feedback loop, while K_2 is a completely separate compensator, acting as a prefilter.

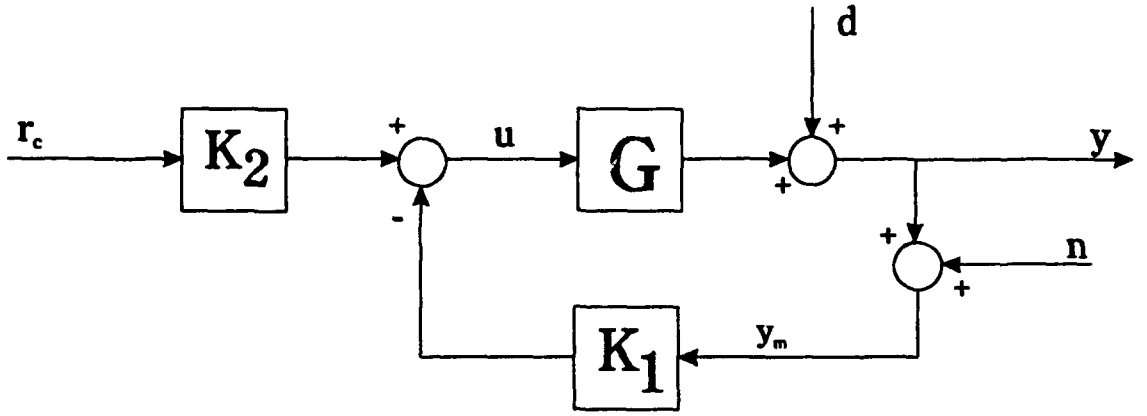

Figure 3-1. 2-DOF SISO Control System Block Diagram

Relating the output to the inputs in equation form yields

$$y = \left(\frac{GK_2}{1 + GK_1}\right) r_c + \left(\frac{1}{1 + GK_1}\right) d - \left(\frac{GK_1}{1 + GK_1}\right) n \tag{3.1}$$

or, more compactly,

$$y = SGK_2 r_c + Sd - Tn \tag{3.2}$$

It is immediately apparent that the transfer function from r_c to y, which will be referred to as $\tilde{T}$, is not equal to the complimentary sensitivity, which is still the transfer function from n to y. Also, the sensitivity and complimentary sensitivity functions depend only upon K_1, not K_2. The implications of these observations will become clear as each of the design objectives is explored in detail.

3.1.1.1 Disturbance Rejection. To simplify the analysis, the objectives dealing with the K_1 compensator will be discussed first. As in the 1-DOF case, good disturbance rejection is attained by examining the d to y transfer function, which is the sensitivity function. In order to reject a disturbance, the magnitude of GK_1, denoted $|GK_1|$, must be sufficiently large at low frequency, where disturbances are expected.

3.1.1.2 Sensor or Measurement Noise Rejection. Measurement noise rejection is dependent upon the n to y transfer function, which is equal to the negate of the complimentary sensitivity function, as in the SISO case. In order to reject measurement noises, $|GK_1|$ must be sufficiently small at high frequency, where noises are expected.

3.1.1.3 Command Following. Thus far, it has been shown that in order to attain good disturbance rejection and measurement noise rejection, restrictions are placed on the size of $|GK_1|$ which are essentially the same as those for the 1-DOF case. However, favorable tracking of commands is attained through a combination of requirements on both $|GK_1|$ and $|GK_2|$, as evidenced by the $\tilde{T}$ transfer function, which is the product of the sensitivity function, S, and GK_2. This transfer function must approach unity over the frequency range where commands are expected (low frequencies). It is this characteristic of the 2-DOF model that sets it apart from the 1-DOF model.

When both $|GK_1|$ and $|GK_2|$ are very large and nearly equal to each other, the system will track commands that are in the frequency range of interest. However, it is not necessary for $|GK_1|$ to be large at low frequency in order to achieve good tracking

-- it only needs to be large enough to reject the specific disturbance expected. $|GK_2|$ can be adjusted to have its magnitude be whatever it needs to be to make $\tilde{T}$ equal to unity.

3.1.1.4 Bode Magnitude Plot Analysis. The requirements just mentioned present some interesting possibilities in the way of Bode plots. Although there are countless combinations of different command, disturbance, and measurement noise sizes, the two cases presented here are low frequency commands with: 1) moderate-sized high frequency noise with a *large* low frequency disturbance; and 2) moderate-sized high frequency noise with a *small* low frequency disturbance. The plant in all cases is assumed to be stable and minimum phase.

In the first case, the large disturbance is the driving factor in determining the shape of the loop transfer functions. At low frequency, $|GK_1|$ must be large in order to reject the disturbance, while at high frequency, the measurement noise is large enough to drive down the size of $|GK_1|$. Meanwhile, $|GK_2|$ matches $|GK_1|$ almost identically at low frequency, but when $|GK_1|$ starts to roll off after it passes the bandwidth frequency, $|GK_2|$ is able to level out at the 0 dB line in order to maintain near-perfect tracking out to a much higher frequency. The trends just described for this first case are shown in Figure 3-2.

In the second case, the disturbance is not so large anymore, but the size of the measurement noise is still moderately large, so the measurement noise exerts the most influence on the shape of the loop transfer functions. The overall effect of a dominant measurement noise is to hold down $|GK_1|$ as much as possible over all frequencies,

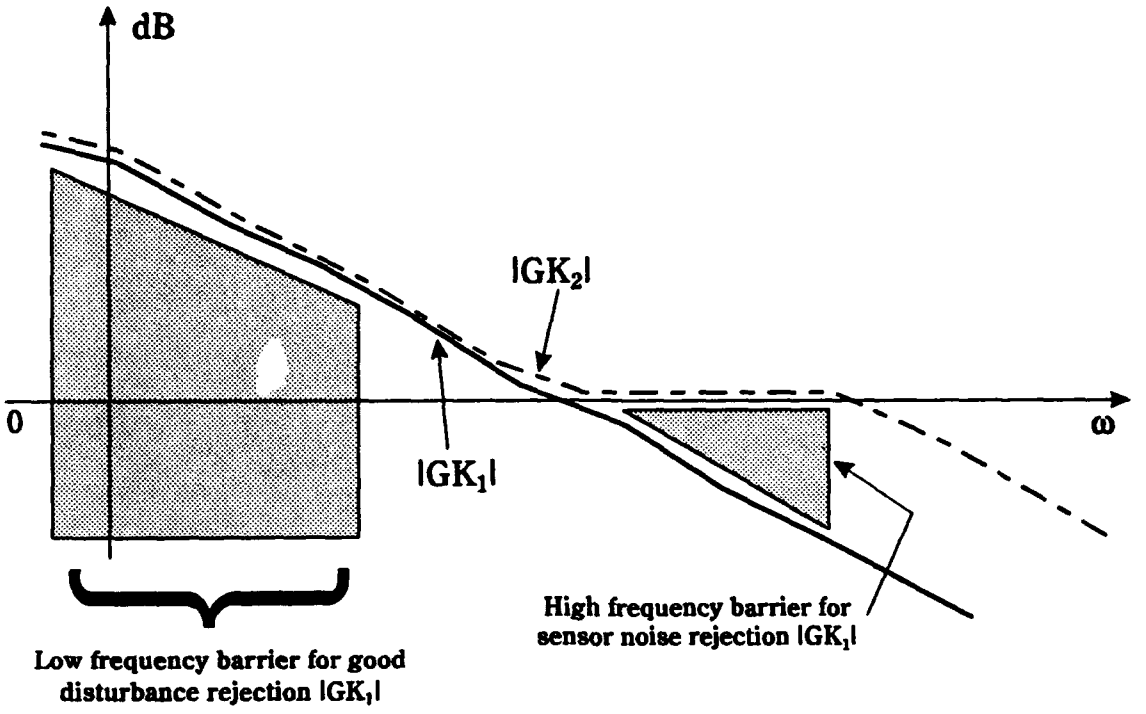

Figure 3-2. Bode Magnitude Plot of "Good" Loop Transfer Functions for a 2-DOF, SISO System (Large Disturbance Case)

especially high frequencies. $|GK_1|$ will still be sufficiently large at low frequency to reject the disturbance, however. $|GK_2|$ accommodates this situation by remaining at or around 0 dB over as wide a frequency range as possible, thereby keeping $\tilde{T}$ equal to unity and achieving good tracking. Figure 3-3 shows the trends just described for the second case.

Another interesting point regarding the 2-DOF setup is the shape of the sensitivity function. Recall from Figure 2-3 that in the 1-DOF case there were two separate barriers on the sensitivity function Bode plot which corresponded to a steady state error and speed of response boundary and a robustness boundary. As previously

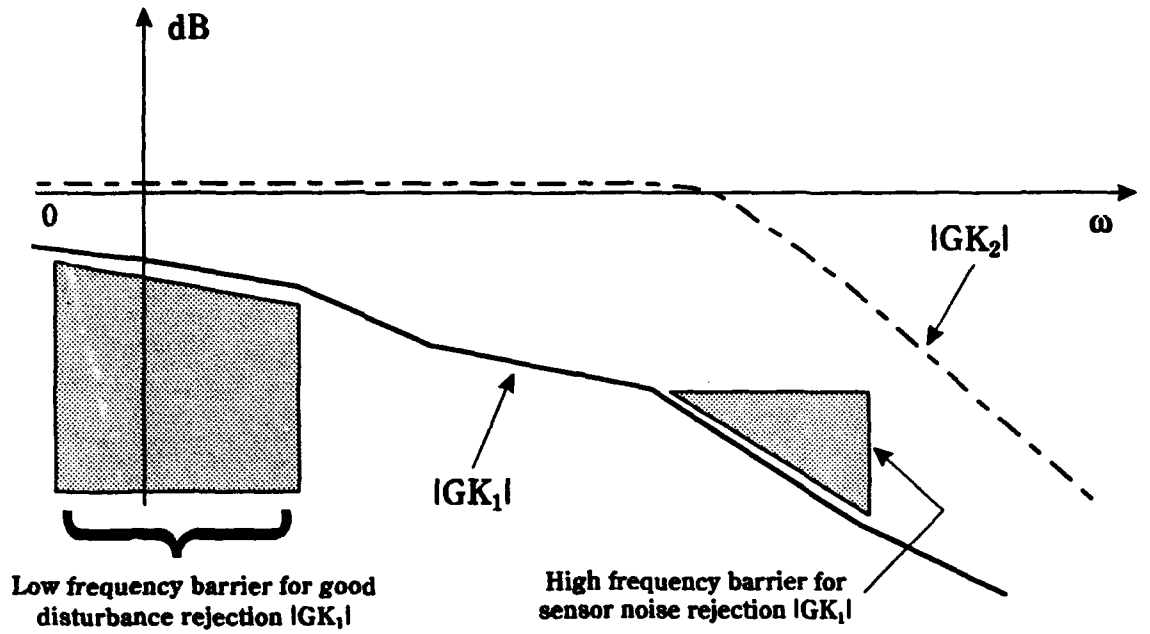

Figure 3-3. Bode Magnitude Plot of "Good" Loop Transfer Functions for a 2-DOF, SISO System (Small Disturbance Case)

mentioned, there is no low frequency barrier which corresponds to good command following in a 2-DOF system. Instead, $|GK_1|$ must only be large enough to reject the appropriate size disturbance encountered. In fact, a closer examination of the 2-DOF sensitivity term, $\left(\frac{1}{1 + GK_1}\right)$, reveals that if the quantity GK_1 takes on a very small (or negative) value, then $|S|$ could take on values ranging between 0 and ∞ (or $-\infty$ to ∞ dB). Most practical or realizable plants and control systems would never utilize many of these $|S|$ values due to poor stability margins, but if this were not a consideration, then those values would theoretically be possible. Therefore, the only consideration remaining for the 2-DOF sensitivity function Bode plot is the robustness barrier on the

maximum magnitude of $|S|$. The 2-DOF $|S|$ plot resembles the 1-DOF $|S|$ plot in that the curve eventually steadies out at the 0 dB line, but it does not necessarily approach the 0 dB line from low frequency. Figure 3-4 shows the results of the foregoing analysis of the 2-DOF sensitivity function.

In a similar fashion, an examination of the 2-DOF complimentary sensitivity function, $\left(\frac{GK_1}{1 + GK_1}\right)$, reveals that if the quantity GK_1 takes on very small (or negative) values, then $|T|$ could also take on values ranging between 0 and ∞ (or $-\infty$ and ∞ dB). Once again, deteriorating stability margins are the main consideration in the shape of the 2-DOF complimentary sensitivity function Bode magnitude plot. It should be noted that even in the 2-DOF setup, disturbance rejection and measurement

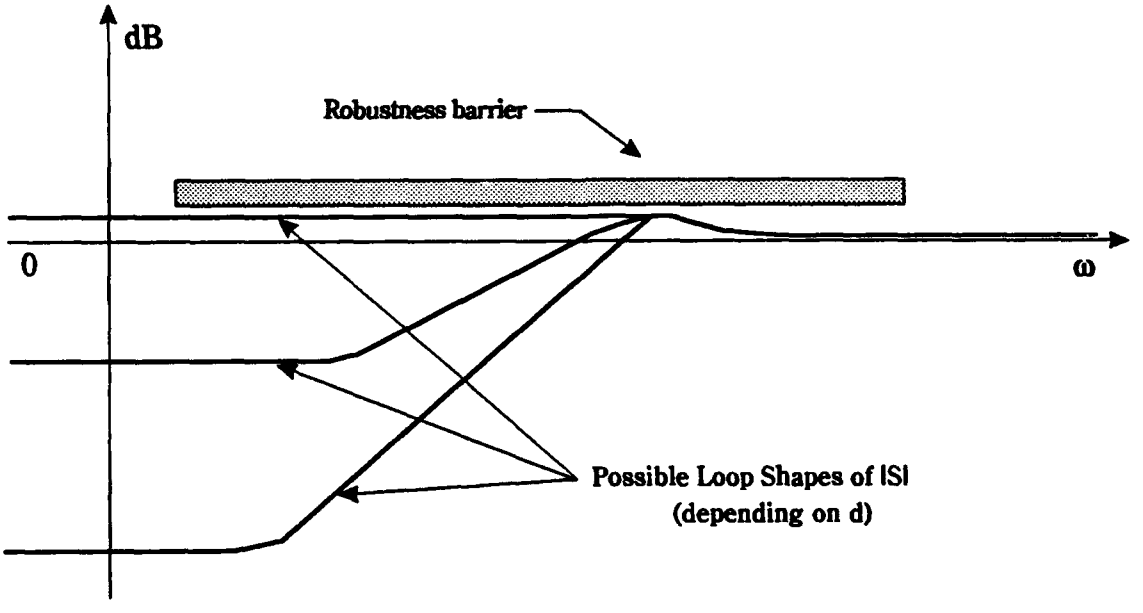

Figure 3-4. Bode Magnitude Plot of Possible "Good" Sensitivity Functions for a 2-DOF, SISO System

noise rejection are competing objectives. The plot will still maintain the general shape of the 1-DOF complimentary sensitivity plot and roll off at some bandwidth cutoff frequency, but the overall magnitude at low frequency is quite variable in the 2-DOF case. The resulting 2-DOF complimentary sensitivity function from this analysis is shown in Figure 3-5.

Another idea to reiterate here is the fact that the complimentary sensitivity function does not provide information about the frequency range over which a 2-DOF system will track commands. The 2-DOF equivalent to the 1-DOF input-to-output transfer function is SGK_2. This transfer function needs to be equal to unity over as wide a frequency range as possible to provide favorable tracking. Since GK_1 and GK_2

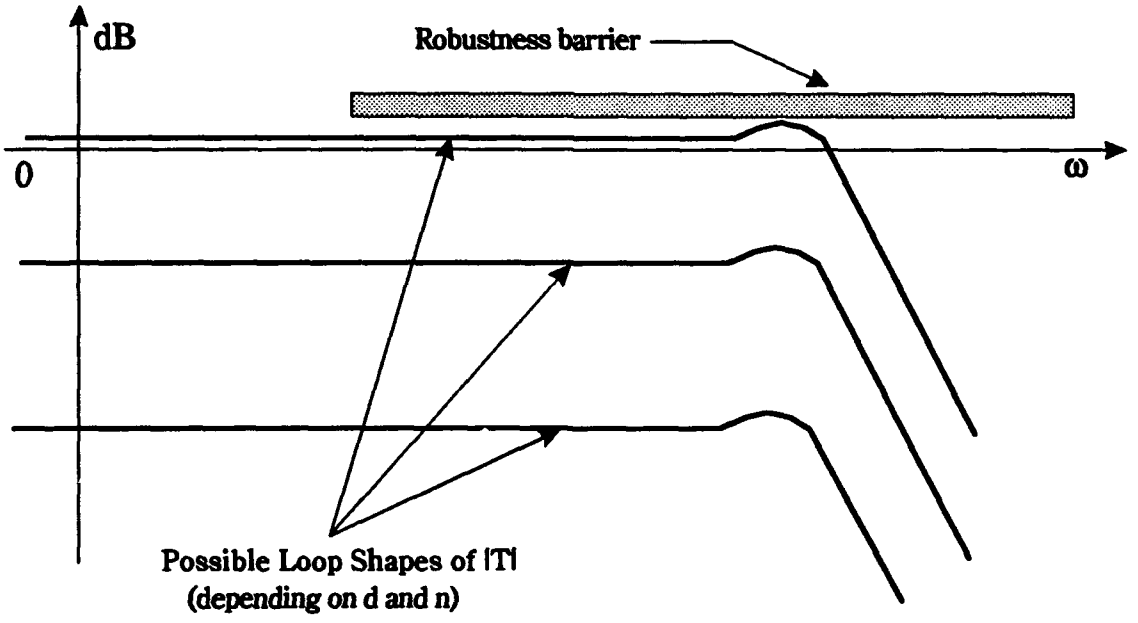

Figure 3-5. Bode Magnitude Plot of Possible "Good" Complimentary Sensitivity Functions for a 2-DOF, SISO System

are independent, a decrease in the size of one can be offset by an increase in the size of the other in order to maintain tracking performance. This is the essence of having *two* degrees of freedom. Therefore, a "good" Bode magnitude plot of $|SGK_2|$ is identical to the one shown for the 1-DOF case in Figure 2-4.

3.1.2 MIMO Case. The extension of the 2-DOF SISO loop shaping ideas to the MIMO case is relatively straightforward, making use of singular values to define the sizes of transfer function matrices. Starting with the overall r_c to y transfer function, equation (3.1) becomes

$$y = [I + GK_1]^{-1} GK_2 r_c + [I + GK_1]^{-1} d - [I + GK_1]^{-1} GK_1 n \qquad (3.3)$$

Equation (3.3) can also be written in terms of S, T, and $\tilde{T}$, as in equation (3.2). Good disturbance rejection requires that the sensitivity function be sufficiently small at low frequency to accommodate any disturbances expected, which can be expressed as

$$\underline{\sigma}[GK_1] \quad \textit{"sufficiently large"} \qquad \forall \ \omega < \omega_0 \qquad (3.4)$$

Conversely, good measurement noise rejection requires that $|T|$ be small at high frequency, which can be written as

$$\overline{\sigma}[GK_1] \quad \textit{"sufficiently small"} \qquad \forall \ \omega > \omega_0 \qquad (3.5)$$

As far as MIMO command following performance goes, once again the output is dependent upon the behavior of both K_1 and K_2. In the case where the disturbance

is relatively large, then $\underline{\sigma}[GK_1]$ will be large at low frequency in order to reject the disturbance, and $\underline{\sigma}[GK_2]$ will also be large at low frequency to match $\underline{\sigma}[GK_1]$. At high frequency, however, $\overline{\sigma}[GK_1]$ must roll off in order to reject the appropriate measurement noise. Tracking is maintained by $\underline{\sigma}[GK_2]$ staying at 0 dB out to a higher frequency. In the case where the disturbance is relatively small and the measurement noise is relatively large, then $\overline{\sigma}[GK_1]$ may well be below 0 dB over all frequencies. In that case, $\underline{\sigma}[GK_2]$ must remain at 0 dB from low frequency out to as high a frequency as possible to provide satisfactory tracking requirements.

The MIMO sensitivity and complimentary sensitivity functions essentially follow the same rules as they do in the SISO case. Both singular value plots have only robustness barriers, with no barriers regarding speed of response, steady state error, or bandwidth. The maximum singular values of both $|S|$ and $|T|$ must stay below the robustness barrier in order for the system to maintain adequate stability margins. There are no figures shown for the 2-DOF MIMO loop shapes, but it is hoped that the foregoing discussion provides adequate insight.

Overall, there are several marked differences between the loop shaping characteristics of a 1-DOF and a 2-DOF system, the key one being in the tracking requirements. In the 1-DOF system, the tracking and disturbance rejection requirements dictate that $|GK|$ be large at low frequency, while it must be small at high frequency in order to reject any measurement noise. These two competing requirements limit how well a 1-DOF system can track because $|GK|$ can only have a

large magnitude out to a certain frequency before it must start to roll off. In the 2-DOF case, there still exists the same conflict between disturbance and measurement noise rejection requirements (this time with $|GK_1|$) but the system's tracking ability is not exclusively tied to $|GK_1|$. $|GK_2|$ provides the needed flexibility in the system by being free to be whatever magnitude it needs to be in order to follow commands out to a much higher frequency. In fact, the example presented in Chapter VI of this thesis puts that added flexibility to the test by introducing measurement noise falling in the same low frequency range that commands and plant disturbances do. The 2-DOF system, therefore, can be considered to have two main parts: an "inner loop", which takes care of noise and robustness requirements, and an "outer loop" (even though it is not really a loop at all), which takes care of tracking requirements. These conclusions apply to both the SISO and MIMO cases, as appropriate.

3.2 System Type

For a 2-DOF system, or any non-unity feedback system for that matter, the simple rules governing system type and the computation of the error constants in the 1-DOF unity feedback case do not apply. The basic principle is the same, however. Once again, from the basic 2-DOF block diagram from Figure 3-1, the analysis begins with the error signal $r_c(s) - y(s)$. In the 1-DOF case, the transfer function between this signal and the reference command was equal to the sensitivity function, which made the subsequent calculations more straightforward. In the 2-DOF case, however, there is no signal directly on the block diagram which represents the quantity $r_c(s) - y(s)$, so one must be created. Figure 3-6 is a modified version of Figure 3-1 that shows the

error signal explicitly.

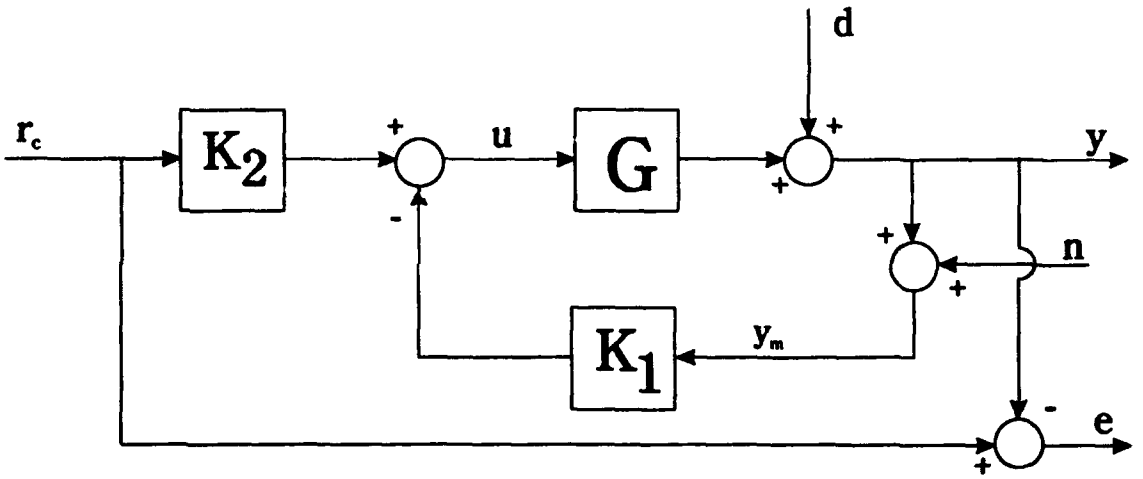

Figure 3-6. 2-DOF Block Diagram Showing Error Signal

From this modified block diagram, the error signal e can be shown to be

$$e(s) = r_c(s) - y(s) = r_c(s) - \left(\frac{GK_2}{1 + GK_1}\right) r_c(s) \tag{3.6}$$

or

$$e(s) = [1 - F(s)]\, r_c(s) \tag{3.7}$$

where $F(s)$ is defined as

$$F(s) = \frac{GK_2}{1 + GK_1} \tag{3.8}$$

Since $F(s)$ contains both K_1 and K_2, it is clear that the error-to-reference command transfer function will not have a clean, clear-cut solution like the 1-DOF case.

Instead, the expression for the steady state error becomes

$$e_{ss} = \lim_{s \to 0} \; s \; \frac{[1 - F(s)]}{s^{k+1}} = \lim_{s \to 0} \; \frac{[1 - F(s)]}{s^{k}} \qquad (3.9)$$

Once again, the system type is the smallest value of k at which the steady state error is a nonzero constant (not infinity). The input tracking characteristics for the 2-DOF system are also the same as the 1-DOF case. If a system is type 0 and the input is a step, then a constant steady state error will result. If the system is type I, then it will track a step perfectly and produce a constant steady state to a ramp input. If the system is type II, then it will track a step and a ramp perfectly and produce a constant steady state error to a parabolic input. The same logic applies to systems of greater type and inputs modeled by higher order polynomials. The primary difference between 1-DOF and 2-DOF systems with regard to system type is that in the 2-DOF case, one cannot necessarily attribute the number of poles or zeros at the origin in either GK_1 or GK_2 to the determination of the system type, as in the 1-DOF case.

IV. H_2 Optimization

In comparing and contrasting the single- and two-degree-of-freedom design methodologies, it is appropriate to use one design technique that is consistent between the two. H_2 optimization represents a relatively straightforward design technique which, because it is an optimization procedure, produces the "best" compensator for the particular model specified. It is particularly appropriate here, as the system is modeled with noises acting on it. It also allows for direct comparison between the two methodologies under varying input parameters. The following summary of H_2 optimization was largely taken from [6] and [2], which should be consulted for a more detailed description of this method.

The objective of H_2 optimization is to produce a compensator which minimizes the 2-norm of a transfer function or transfer function matrix from exogenous inputs (commands, disturbances, or measurement noises) to controlled outputs. The standard H_2 design setup is shown in the diagram in Figure 4-1, with w representing the exogenous inputs (assumed to be zero mean, unit intensity white Gaussian noises) and z representing the controlled outputs. P is the plant, which includes all system dynamics and weights on the exogenous inputs and controlled outputs. K is the compensator, u is the controlled input to the plant, and y is the measured plant outputs. P can be partitioned in such a way that

$$\begin{bmatrix} z \\ y \end{bmatrix} = \begin{bmatrix} P_{zw} & P_{zu} \\ P_{yw} & P_{yu} \end{bmatrix} \begin{bmatrix} w \\ u \end{bmatrix} \tag{4.1}$$

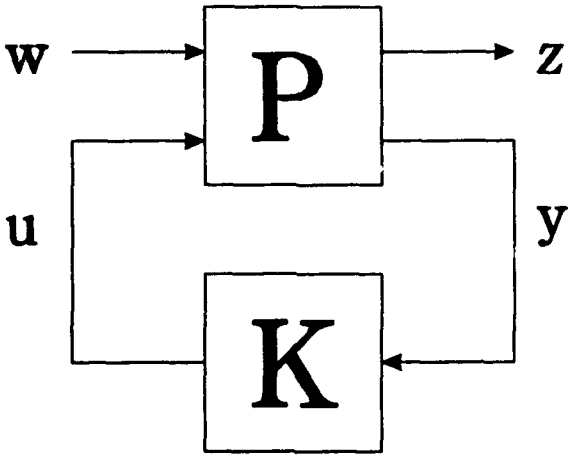

Figure 4-1. H_2 Design Diagram

The closed-loop transfer function T_{zw} is the transfer function from w to z and can be written as a linear fractional transformation (LFT) of P and K from Figure 4-1 as

$$T_{zw} = P_{zw} + P_{zu}K(I - P_{yu}K)^{-1}P_{yw} \tag{4.2}$$

The H_2 design procedure involves designing a stabilizing compensator K that minimizes the 2-norm of z, which is equivalent to minimizing the 2-norm of T_{zw}, given by

$$\inf_{K\ adm} \|z\|_2 = \inf_{K\ adm} \|T_{zw}\|_2 \equiv \alpha_0 \tag{4.3}$$

where

$$\|T_{zw}\|_2 = \left(\frac{1}{2\pi} \int_{-\infty}^{\infty} tr\left[T_{zw}^{*}(j\omega)\ T_{zw}(j\omega)\right] d\omega \right)^{\frac{1}{2}} \tag{4.4}$$

Since the H_2 algorithms utilized in this thesis employ state space methods, it is first necessary to represent the plant differential equations in state space form. The state space representation of the nine matrices that comprise the P matrix are

$$\dot{x} = Ax + B_w w + B_u u \tag{4.5a}$$

$$z = C_z x + D_{zw} w + D_{zu} u \tag{4.5b}$$

$$y = C_y x + D_{yw} w + D_{yu} u \tag{4.5c}$$

which can be written in transfer matrix form as

$$P = \left[\begin{array}{c|cc} A & B_w & B_u \\ \hline C_z & D_{zw} & D_{zu} \\ C_y & D_{yw} & D_{yu} \end{array}\right] \tag{4.6}$$

There are several assumptions regarding these nine matrices which are inherent to the well-posedness and solvability of the H_2 control problem:

(i) $D_{zw} = 0$

(ii) $D_{yu} = 0$

(iii) (A, B_u) stabilizable and (C_y, A) detectable

(iv) $D_{zu}^T D_{zu}$ and $D_{yw} D_{yw}^T$ full rank

(v) $\begin{bmatrix} A - j\omega I & B_u \\ C_z & D_{zu} \end{bmatrix}$ has full column rank for all ω

(vi) $\begin{bmatrix} A - j\omega I & B_w \\ C_y & D_{yw} \end{bmatrix}$ has full row rank for all ω

Condition (i) arises due to the fact that the transfer function 2-norm is also proportional to the area under the singular value plot of T_{zw}, which must be finite. If D_{zw} is nonzero, then the closed loop transfer function will be infinite. Condition (ii), on D_{yu}, is not necessary but facilitates an easier development of a solution. Condition (iii) is necessary for stabilizing compensators to exist. Condition (iv) is required so that there is a penalty on control usage and so that there are no perfect measurements; otherwise, a singular control problem results. Conditions (v) and (vi) ensure the existence of stabilizing solutions to the algebraic Riccati equations that appear in the problem solution. Condition (iv) can be strengthened to $D_{zu}^T D_{zu} = I$ and $D_{yu} D_{yu}^T = I$ in order to simplify the final form of the equations by scaling u and y. A detailed explanation of this scaling process is contained in [7:70-71]. The H_2 solution that follows assumes that u and y have been properly scaled; scaled quantities will be shown with a tilde (~).

If suboptimal compensators are considered, the family of all compensators that satisfy $\|T_{zw}\|_2 \leq \alpha$, with $\alpha \geq \alpha_0$, is given by the LFT of $J(s)$ and the constrained freedom parameter $Q(s)$, shown in Figure 4-2. In the suboptimal case, the constraints on $Q(s)$ are $Q \in RH_2$ and $\|Q\|_2^2 \leq \alpha^2 - \alpha_0^2$. RH_2 is the space of all stable, strictly proper transfer functions with real, rational coefficients. For the case where $Q(s)$ is equal to zero, the transfer function $J_{uy}(s)$ is equal to the optimal H_2 compensator K_{2opt}; a nonzero $Q(s)$ parameter produces suboptimal compensators. The transfer function $J(s)$ is given by

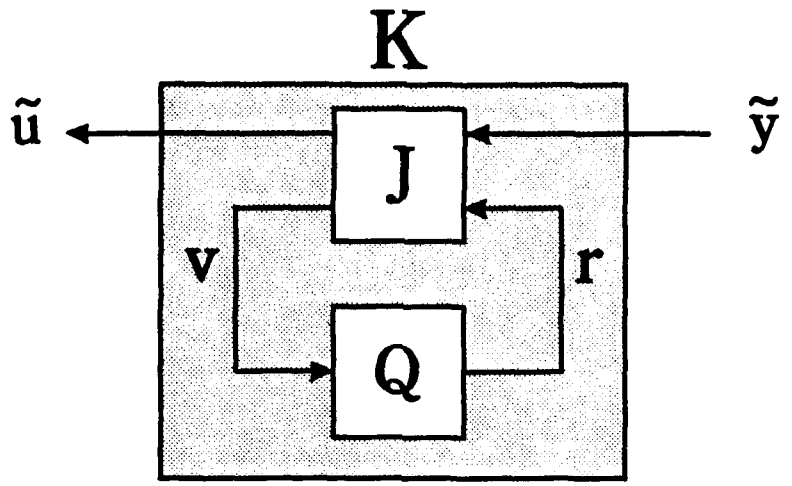

Figure 4-2. (J, Q) Parameterization Diagram for H_2 Suboptimal Compensator

$$J(s) = \begin{bmatrix} J_{uy} & J_{ur} \\ J_{vy} & J_{vr} \end{bmatrix} = \left[\begin{array}{c|cc} A_J & K_f & K_{fl} \\ \hline -K_c & 0 & I \\ K_{cl} & I & 0 \end{array}\right] \tag{4.7}$$

where

$$\begin{aligned} A_J &= A - K_f\tilde{C}_y - \tilde{B}_u K_c \\ K_c &= \tilde{B}_u^T X_2 + \tilde{D}_{zu}^T C_z \qquad & K_{cl} &= -\tilde{C}_y \\ K_f &= Y_2 \tilde{C}_y^T + B_w \tilde{D}_{yw}^T \qquad & K_{fl} &= \tilde{B}_u \end{aligned} \tag{4.8}$$

with the scaled matrices given by

$$\begin{aligned} \tilde{B}_u &= B_u S_u^{-1} \qquad & \tilde{C}_y &= S_y C_y \\ \tilde{D}_{zu} &= D_{zu} S_u^{-1} \qquad & \tilde{D}_{yw} &= S_y D_{yw} \end{aligned} \tag{4.9}$$

S_u and S_y are internal scalings such that

$$S_u^T S_u = D_{zu}^T D_{zu} \qquad S_y^{-1}(S_y^{-1})^T = D_{yw} D_{yw}^T \tag{4.10}$$

The X_2 and Y_2 matrices are the real, unique, symmetric positive semidefinite solutions to the algebraic Riccati equations

$$(A - \tilde{B}_u\tilde{D}_{zu}^T C_z)^T X_2 + X_2(A - \tilde{B}_u\tilde{D}_{zu}^T C_z) - X_2\tilde{B}_u\tilde{B}_u^T X_2 + \hat{C}_z^T\hat{C}_z = 0 \quad (4.11)$$

and

$$(A - B_w\tilde{D}_{yw}^T\tilde{C}_y)Y_2 + Y_2(A - B_w\tilde{D}_{yw}^T\tilde{C}_y)^T - Y_2\tilde{C}_y^T\tilde{C}_y Y_2 + \hat{B}_w\hat{B}_w^T = 0 \quad (4.12)$$

where

$$\hat{C}_z = (I - \tilde{D}_{zu}\tilde{D}_{zu}^T)C_z \quad (4.13)$$

and

$$\hat{B}_w = B_w(I - \tilde{D}_{yw}^T\tilde{D}_{yw}) \quad (4.14)$$

The resulting reverse scaled optimal compensator state space is given by

$$K_{2opt}(s) = \left[\begin{array}{c|c} A_J & \tilde{K}_f \\ \hline -\tilde{K}_c & 0 \end{array}\right] \quad (4.15)$$

where

$$\tilde{K}_f = K_f S_y \quad (4.16a)$$

$$\tilde{K}_c = S_u^{-1} K_c \quad (4.16b)$$

The final item of interest regarding H_2 optimization centers around the order of the compensators produced by the algorithms. In general, the H_2 algorithm produces a compensator that has the same order as the plant, plus the number of states contained in the dynamic weights used to shape the closed loop system (weight shapes will be discussed in Chapter V). It should be noted that in the 2-DOF case, the H_2 algorithm

produces two compensators that share the same A matrix and thus, the same poles (the zeros of each may be different, however). The fact that K_1 and K_2 must share the same poles could be considered a limitation to utilizing the method of designing both compensators simultaneously. However, all of the examples in this thesis make use of the H_2 method of designing both compensators simultaneously because this method still illustrates the advantages of using 2-DOF controllers when tracking is one of the primary control objectives. Furthermore, under the assumption that the exogenous inputs are white Gaussian noise and the output energy is to be minimized, this controller order is optimal.

V. General Problem Formulation

The purpose of this chapter is to present the setup of the general H_2 problem for the 1-DOF and 2-DOF cases, along with all of the assumptions inherent to the problem and the rationale for selecting the dynamic weight shapes for the H_2 optimization algorithm. The analysis begins with a state space description of each system, which provides all of the variables necessary for the P matrix. Since H_2 optimization minimizes the 2-norm of T_{zw}, or the energy of selected outputs to white noise inputs, the outputs chosen for the z vector are not arbitrary. These outputs must be representative of the "errors" to be minimized. In general, dynamic weights reflect the desired frequency range of an input that gets fed through to the corresponding output. All of these factors will be discussed in this chapter, and the dynamic weights chosen to illustrate design trends in the latter examples will be shown.

5.1 1-DOF Case

The 1-DOF block diagram used for the H_2 formulation is shown in Figure 5-1. For this figure, w_d is the disturbance signal and w_n is the measurement noise signal. The governing control law for H_2 optimization is $u = Ky$, with all of the transfer functions relating the outputs to the inputs being derived from this law. The most noticeable difference between Figure 5-1 and Figure 2-1 is the presence of weighting blocks in the block diagram of Figure 5-1. As mentioned in the introduction to this chapter, the weights help in the design of a compensator which produces a system with a closed loop shape that suits the desires of the control system designer. It is

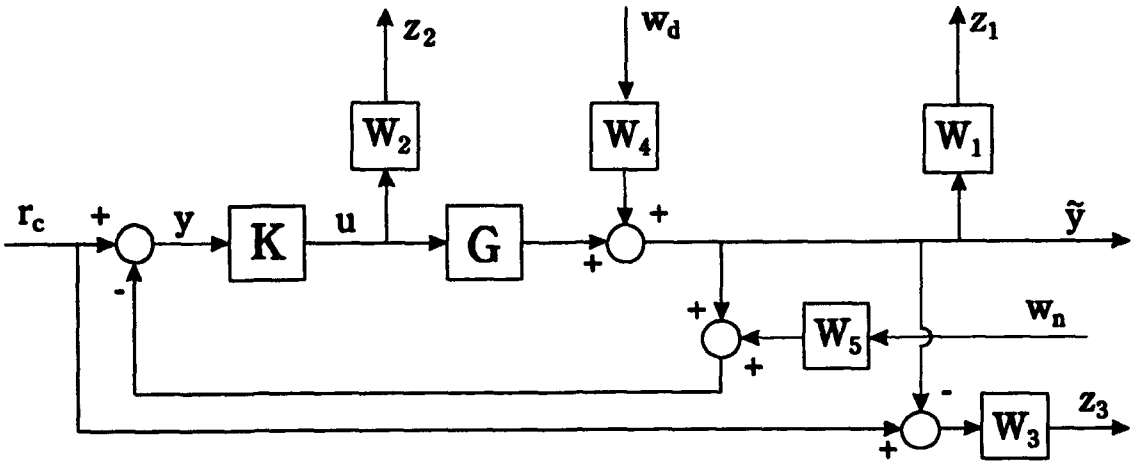

Figure 5-1. 1-DOF H_2 Optimization Block Diagram

easy to see how the different weights affect different aspects of the system by examining the transfer function matrix between the outputs (ideal output (z_1), control usage (z_2), and tracking error (z_3)) and the exogenous inputs (commands (r_c), disturbances (w_d), and measurement noises (w_n)). It is given by

$$\begin{bmatrix} z_1 \\ z_2 \\ z_3 \end{bmatrix} = \begin{bmatrix} W_1T & W_1SW_4 & -W_1TW_5 \\ W_2KS & -W_2KSW_4 & -W_2KSW_5 \\ W_3S & -W_3SW_4 & W_3TW_5 \end{bmatrix} \begin{bmatrix} r_c \\ w_d \\ w_n \end{bmatrix} \tag{5.1}$$

Incidentally, minimizing the transfer function between r_c and z_1 is not a control objective, since it is desired for it to be unity for favorable tracking. However, z_1 is included in the H_2 setup so that the w_d to z_1 and w_n to z_1 transfer functions can be minimized.

The parameters of interest in most control system designs are the sensitivity, S,

and the complimentary sensitivity, T. From the given transfer function matrix, S is affected by W_1, W_3, and W_4, while T is affected by W_1, W_3, and W_5. At first glance, it may seem as if these weights would conflict with each other if they were set to different values, and as it turns out, this is true. However, there is a logical method for choosing the weights such that their values make intuitive sense and the resulting compensator produces a good closed loop shape.

The state space representation of Figure 5-1 provides some insight into the weight selection rationale. The nine matrices comprising the P matrix are given by

$$A = \begin{bmatrix} A_g & 0 & 0 & 0 & 0 & 0 \\ B_1C_g & A_1 & 0 & 0 & B_1C_4 & 0 \\ 0 & 0 & A_2 & 0 & 0 & 0 \\ -B_3C_g & 0 & 0 & A_3 & -B_3C_4 & 0 \\ 0 & 0 & 0 & 0 & A_4 & 0 \\ 0 & 0 & 0 & 0 & 0 & A_5 \end{bmatrix} \tag{5.2a}$$

$$B_w = \begin{bmatrix} 0 & 0 & 0 \\ 0 & B_1D_4 & 0 \\ 0 & 0 & 0 \\ B_3 & -B_3D_4 & 0 \\ 0 & B_4 & 0 \\ 0 & 0 & B_5 \end{bmatrix} \quad B_u = \begin{bmatrix} B_g \\ B_1D_g \\ B_2 \\ -B_3D_g \\ 0 \\ 0 \end{bmatrix} \tag{5.2b}$$

$$C_z = \begin{bmatrix} D_1C_g & C_1 & 0 & 0 & D_1C_4 & 0 \\ 0 & 0 & C_2 & 0 & 0 & \\ -D_3C_g & 0 & 0 & C_3 & -D_3C_4 & 0 \end{bmatrix}$$

$$C_y = \begin{bmatrix} -C_g & 0 & 0 & 0 & -C_4 & -C_5 \end{bmatrix} \tag{5.2c}$$

$$D_{zw} = \begin{bmatrix} 0 & D_1 D_4 & 0 \\ 0 & 0 & 0 \\ D_3 & -D_3 D_4 & 0 \end{bmatrix} \quad D_{zu} = \begin{bmatrix} D_1 D_g \\ D_2 \\ -D_3 D_g \end{bmatrix}$$

$$D_{yw} = \begin{bmatrix} I & -D_4 & -D_5 \end{bmatrix} \quad D_{yu} = \begin{bmatrix} -D_g \end{bmatrix} \tag{5.2d}$$

The state vector is given by

$$\bar{x} = \begin{bmatrix} x_g \\ x_1 \\ x_2 \\ x_3 \\ x_4 \\ x_5 \end{bmatrix} = \begin{bmatrix} \textit{plant states} \\ \textit{controlled output weight states} \\ \textit{control usage weight states} \\ \textit{tracking weight states} \\ \textit{disturbance weight states} \\ \textit{measurement noise weight states} \end{bmatrix}$$

If the assumptions discussed in Chapter IV regarding H_2 optimization are applied to the above state space, then certain characteristics of some of the weights can be determined, such as whether they are strictly proper or just proper. To begin with, D_{zw} must equal zero, so all of the terms in that matrix must be set to zero, including D_3 and D_1 and/or D_4. Since D_{yu} is equal to zero, then $D_g = 0$, which means that the plant must be strictly proper. Since $D_{zu}{}^T D_{zu}$ must have full rank, then D_2 must be nonzero (actually $D_2{}^T D_2$ must be full rank). The fact that $D_{yw} D_{yw}{}^T$ must have full rank indicates that D_4 and D_5 may or may not be equal to zero. For all of the examples illustrated in this thesis, the following assumptions will be made regarding the dynamic weights:

(i) W_1 is a constant (D_1 nonzero, with no x_1 states and thus no A_1, B_1, or C_1)

(ii) W_2 is a constant (D_2 nonzero, with no x_2 states and thus no A_2, B_2, or C_2)

(iii) W_3 is represented by a strictly proper transfer function ($D_3 = 0$)

(iv) W_4 is represented by a strictly proper transfer function ($D_4 = 0$)

(v) W_5 is represented by a (nonstrictly) proper transfer function (D_5 nonzero)

If these assumptions are applied to the state space given in the equations of (5.2), the new state space becomes

$$A = \begin{bmatrix} A_g & 0 & 0 & 0 \\ -B_3C_g & A_3 & -B_3C_4 & 0 \\ 0 & 0 & A_4 & 0 \\ 0 & 0 & 0 & A_5 \end{bmatrix} \quad B_w = \begin{bmatrix} 0 & 0 & 0 \\ B_3 & 0 & 0 \\ 0 & B_4 & 0 \\ 0 & 0 & B_5 \end{bmatrix} \quad B_u = \begin{bmatrix} B_g \\ 0 \\ 0 \\ 0 \end{bmatrix}$$

$$C_z = \begin{bmatrix} D_1C_g & 0 & D_1C_4 & 0 \\ 0 & 0 & 0 & 0 \\ 0 & C_3 & 0 & 0 \end{bmatrix} \quad D_{zw} = \begin{bmatrix} 0 & 0 & 0 \\ 0 & 0 & 0 \\ 0 & 0 & 0 \end{bmatrix} \quad D_{zu} = \begin{bmatrix} 0 \\ \rho \\ 0 \end{bmatrix} \qquad (5.3)$$

$$C_y = \begin{bmatrix} -C_g & 0 & -C_4 & -C_5 \end{bmatrix} \quad D_{yw} = \begin{bmatrix} I & 0 & -D_5 \end{bmatrix} \quad D_{yu} = [0]$$

Whenever a weight is assigned to be a constant, as in the case of W_1 and W_2, only the D term remains, and that state can be removed from the original state space. Also, W_2 is a measure of the amount of control power used in the system, and it is given the symbol ρ (a diagonal matrix) to show that it can be "tuned" to speed up or slow down the system.

5.2 2-DOF Case

The 2-DOF block diagram used in the H_2 optimization algorithm is shown in

Figure 5-2. All of the weights are located in the same places as the 1-DOF system, although block diagram interpretation yields a slightly different transfer function matrix relating the z outputs to the exogenous inputs. It is given by

$$\begin{bmatrix} z_1 \\ z_2 \\ z_3 \end{bmatrix} = \begin{bmatrix} W_1SGK_2 & W_1SW_4 & -W_1TW_5 \\ W_2[I - K_1SG]K_2 & -W_2K_1SW_4 & -W_2K_1SW_5 \\ W_3[I - SGK_2] & -W_3SW_4 & W_3TW_5 \end{bmatrix} \begin{bmatrix} r_c \\ w_d \\ w_n \end{bmatrix} \tag{5.4}$$

Once again the sensitivity and complimentary sensitivity functions are affected by the same weights as in the 1-DOF case. Thus, the same approach to weight selection will be used in this case. The primary difference between the 1-DOF and 2-DOF cases is the implementation of the control law $u = Ky$. In the 1-DOF case, there was a single compensator, K, and only one control input, y. For the 2-DOF system, the control law must be modified to read

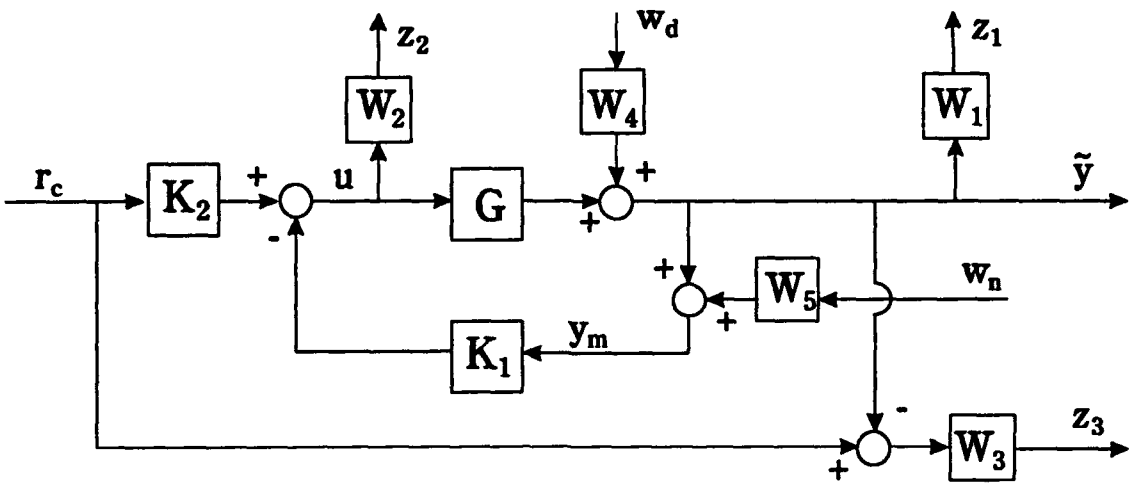

Figure 5-2. 2-DOF H_2 Optimization Block Diagram

$$u = Ky = \begin{bmatrix} -K_1 & K_2 \end{bmatrix} \begin{bmatrix} y_m \\ r_c \end{bmatrix} \tag{5.5}$$

As discussed in Chapter III, the addition of the second compensator changes the input-output relationships and accounts for the differences between the 1-DOF and 2-DOF transfer function matrices in (5.1) and (5.4).

The 2-DOF state space representation of Figure 5-2 is actually quite similar to the 1-DOF state space, the only differences being in the matrices relating to the control input, y (C_y, D_{yw}, and D_{yu}). With all of the assumptions regarding H_2 optimization taken into account, the final 2-DOF state space is given by

$$A = \begin{bmatrix} A_g & 0 & 0 & 0 \\ -B_3C_g & A_3 & -B_3C_4 & 0 \\ 0 & 0 & A_4 & 0 \\ 0 & 0 & 0 & A_5 \end{bmatrix} \quad B_w = \begin{bmatrix} 0 & 0 & 0 \\ B_3 & 0 & 0 \\ 0 & B_4 & 0 \\ 0 & 0 & B_5 \end{bmatrix} \quad B_u = \begin{bmatrix} B_g \\ 0 \\ 0 \\ 0 \end{bmatrix}$$

$$C_z = \begin{bmatrix} D_1C_g & 0 & D_1C_4 & 0 \\ 0 & 0 & 0 & 0 \\ 0 & C_3 & 0 & 0 \end{bmatrix} \quad D_{zw} = \begin{bmatrix} 0 & 0 & 0 \\ 0 & 0 & 0 \\ 0 & 0 & 0 \end{bmatrix} \quad D_{zu} = \begin{bmatrix} 0 \\ \rho \\ 0 \end{bmatrix} \tag{5.6}$$

$$C_y = \begin{bmatrix} -C_g & 0 & -C_4 & -C_5 \\ 0 & 0 & 0 & 0 \end{bmatrix} \quad D_{yw} = \begin{bmatrix} 0 & 0 & -D_5 \\ I & 0 & 0 \end{bmatrix} \quad D_{yu} = \begin{bmatrix} 0 \\ 0 \end{bmatrix}$$

Since there is no substantial change in the 2-DOF state space regarding the D terms of the dynamic weights, all of the assumptions regarding whether a weight is strictly proper, proper, or equal to a constant (assumptions (i) through (v) in Section 5.1) are still applicable from the 1-DOF case.

5.3 Weight Selection

As far as choosing actual values for the weights, there are basically two schools of thought. First, a weight can be viewed as a filter through which only the frequencies of interest are allowed to pass. This logic is particularly applicable to noise weights. Since all of the disturbances and measurement noises in H_2 optimization are assumed to be white Gaussian noises, it makes sense to only pass through certain frequency ranges of interest to the system. Second, a weight can be viewed as a penalty on a signal over a particular frequency range. In other words, the weight is chosen in such a way that its magnitude plot looks like the inverse of what the designer wants the signal of interest to look like. It is possible for these two weight selection approaches to conflict with each other, but in general, they are not mutually exclusive. The weights chosen in this section are typical of many aircraft control problems and will be used in all of the examples in this thesis.

Beginning with the weight selections for the disturbance, it is logical to utilize the first method described above. If the system is assumed to be that of a typical aircraft, a disturbance would be a low frequency event with varying magnitude. With the noise signal itself assumed to be white noise, the disturbance weight will be approximated by a low pass filter with a pole at s = -2. For comparison purposes, the magnitudes of this weight were chosen somewhat arbitrarily, corresponding to a small, medium, and large disturbance. The disturbance weights are given by

$$W_4 = \frac{0.0002}{s+2}, \quad \frac{20}{s+2}, \quad \frac{200}{s+2} \tag{5.7}$$

and their Bode magnitude plots are shown in Figure 5-3. For clarity, however, the

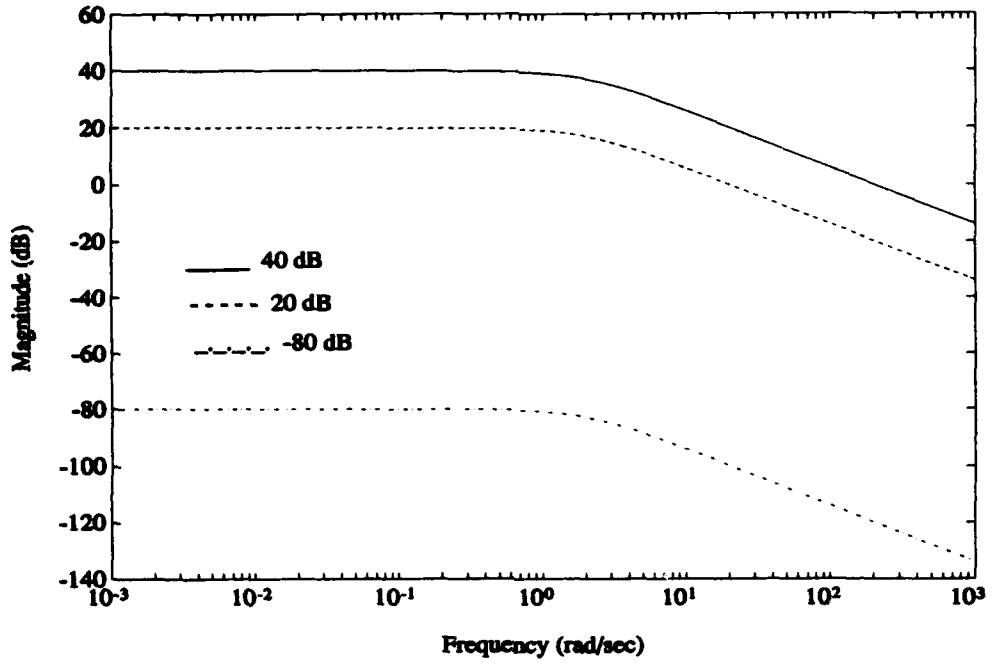

Figure 5-3. Bode Magnitude Plot of Disturbance Weights

weights will be described on example plots by their DC gain, which are -80 dB, 20 dB, and 40 dB, respectively.

The measurement noise weights utilize the same logic described for the disturbance weights, only in this case, measurement noise is a high frequency phenomenon with varying magnitude. The measurement noise weights will be approximated by a high pass filter with a zero at -0.01 and a pole at -10. The magnitudes of this weight were chosen to reflect what would be considered a "small" measurement noise level versus a "large" noise level. The measurement noise weights are plotted in Figure 5-4 and are given by

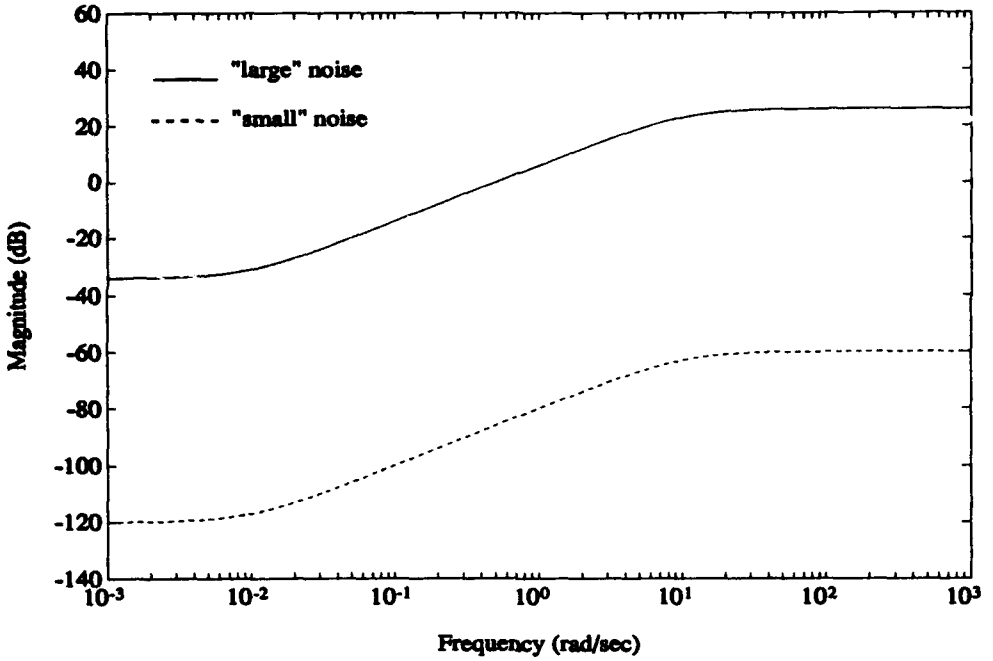

Figure 5-4. Bode Magnitude Plot of Measurement Noise Weights

$$W_5 = \frac{0.001\,(s + 0.01)}{s + 10}, \quad \frac{20\,(s + 0.01)}{s + 10} \tag{5.8}$$

On example plots, these two noise weights will be referred to as either a "small" noise or "large" noise to reflect the magnitude of the noise weight.

The only remaining dynamic weight for this system is W_3, the tracking weight. This weight is of the type that should be chosen as a penalty on the signal over the frequency range of interest. As the name implies, the tracking weight penalizes deviations of the output signal, y, from the reference command, r_c. Therefore, in order to apply this penalty over the relevant frequency range, the weight should be shaped like a low pass filter with a low frequency pole. There is another factor to consider,

however. If the tracking weight is set to be a low pass filter (a constant gain divided by a single pole near the origin), then the weight actually resembles an integrator over the frequency range where commands come in. If the tracking weight resembles an integrator, then the actual error signal will reflect the inverse of the integrator and the system will exhibit type I behavior. Likewise, if the tracking weight is set to be a low pass filter with two poles near the origin, then the system will exhibit type II behavior; and so on. This system type behavior will be examined more closely in an example in a later chapter. Since most of the illustrative examples in the coming chapters concern themselves only with step responses, the tracking weight used in those examples is

$$W_3 = \frac{10}{s + 0.01} \tag{5.9}$$

Its Bode plot is shown in Figure 5-5.

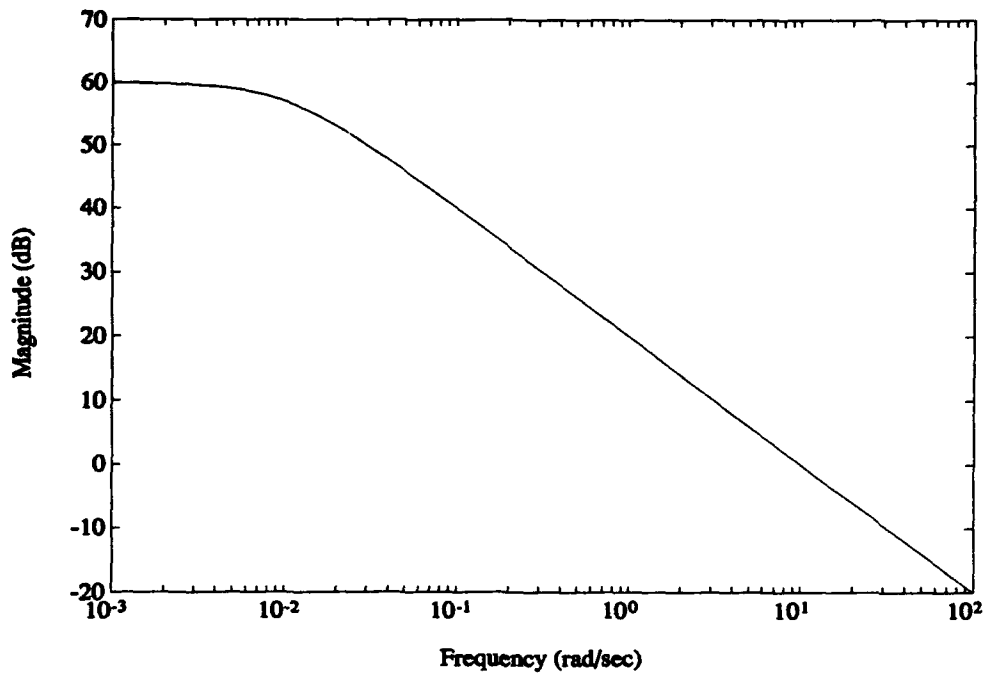

Figure 5-5. Bode Magnitude Plot of Tracking Weight

As mentioned previously, it is not a control objective to minimize the 2-norm of the r_c to y transfer function. Thus, it would not make sense to place a weight on W_1. For simplicity, W_1 was chosen to be 1.0. Control usage is often a limiting factor in aircraft control problems, since actuators and control surfaces have limited range and speed. Since the primary purpose of this thesis is to show trends in the speed and robustness of 1-DOF and 2-DOF systems as disturbances and measurement noises are varied, the control usage weight was set to a value which allows these parameter variations to be seen easily -- $W_2 = 0.001$.

It also bears mentioning here that the weight choices described previously in this section are applicable to the multivariable case. The primary difference, of course, is that in the MIMO case, the weights represent transfer function matrices instead of individual transfer functions. While it is true that it is often desirable to tailor the weights to each individual element in a vector signal, it is not necessary for observing trends. For the purposes of this thesis, the SISO weights will be multiplied by an appropriate sized identity matrix in order to come up with a MIMO weight.

5.4 Evaluation Model

Once all of the weights have been selected, an H_2 algorithm is utilized to calculate the optimal compensator K_{2opt}, as described in Chapter 4. Since the controller is designed while taking all of the weights into consideration, it would follow that if a simulation were set up that incorporated disturbances and measurement noises of intensity and frequency similar to the weights used in the design of the compensator, then the system with the newly designed controller would perform quite

well. For the purposes of this thesis, however, it is of greater interest to observe the effects of weight changes on both 1-DOF and 2-DOF systems using a model that purely tests the performance of the controller.

The evaluation model used throughout this thesis is simply an unweighted version of the basic feedback setup with no noises or "errors" included. The block diagrams of the evaluation models for the 1-DOF and 2-DOF cases are shown in Figures 5-6 and 5-7, respectively. These may not be "real world" simulation models with accurate noises, but they do provide a consistent basis for comparison of different controllers. The purpose of these evaluation models is not to evaluate the "goodness" of an H_2 design; rather, it is to examine the basic differences between 1-DOF and 2-DOF controllers.

The next two chapters of this thesis illustrate the concepts described thus far through examples that highlight the differences between the 1-DOF and 2-DOF design methodologies. All of the weights given in this chapter will be used in each problem to maintain consistency for comparison purposes.

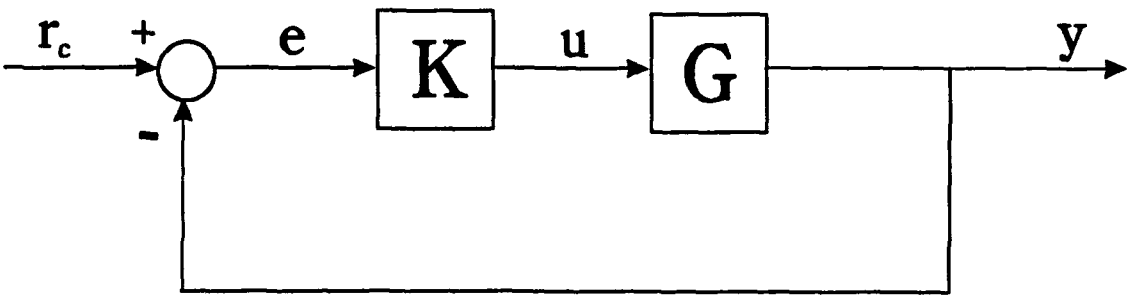

Figure 5-6. 1-DOF Evaluation Model Block Diagram

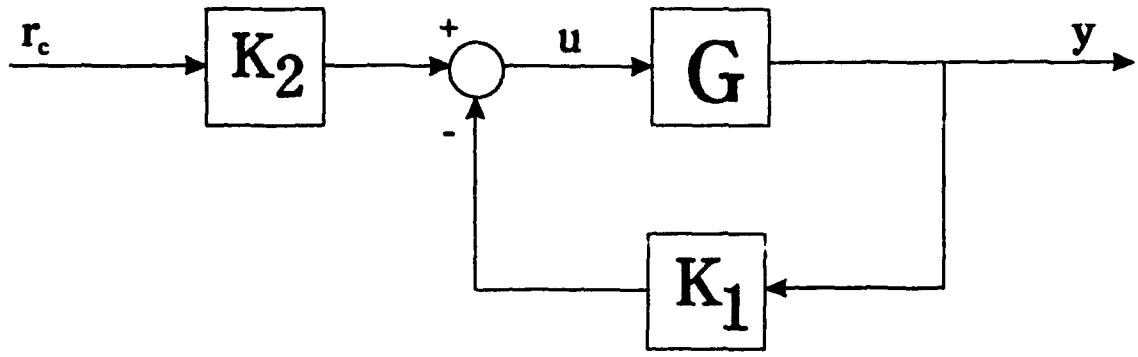

Figure 5-7. 2-DOF Evaluation Model Block Diagram

VI. SISO Examples

To best illustrate the differences between 1-DOF and 2-DOF control systems, it is perhaps best to explore a simple example that is representative of the types of problems encountered in control system design. In this chapter, the plant consists of a *transfer function* with one zero and two poles. This example can be manipulated to produce a stable, minimum phase system, an unstable, minimum phase system, a stable, nonminimum phase system, and an unstable, nonminimum phase system. The transfer functions used in the examples are as follows:

$$G(s) = \frac{s + 2}{(s + 1)(s + 5)} \qquad \textit{stable, minimum phase} \qquad (6.1)$$

$$G(s) = \frac{s + 2}{(s - 1)(s + 5)} \qquad \textit{unstable, minimum phase} \qquad (6.2)$$

$$G(s) = \frac{s - 2}{(s + 1)(s + 5)} \qquad \textit{stable, nonminimum phase} \qquad (6.3)$$

$$G(s) = \frac{s - 2}{(s - 1)(s + 5)} \qquad \textit{unstable, nonminimum phase} \qquad (6.4)$$

Although these transfer functions initially appear to be quite simple, it turns out that as far as general trends are concerned (regarding the effects of stable vs. unstable poles and minimum phase vs. nonminimum phase zeros), they are representative of the behavior of each class of transfer function.

For each example type, there are many graphs of loop shapes and time responses to observe in order to make comparisons between the 1-DOF and 2-DOF model, so it would be prudent here to explain the order in which the graphs will be

presented. In each class of problem, the 1-DOF plots will be presented first, with plots of sensitivity, complimentary sensitivity, loop transfer function, and step responses, followed by the same plots for the 2-DOF case. Since the objectives of this thesis include observing similarities and differences between the two design methodologies as plant disturbances and measurement noises are varied, each individual plot will contain three curves, corresponding to the small, medium, and large disturbances defined in equation (5.7). As mentioned in Chapter V, each curve will be identified by the appropriate DC gain of the disturbance (-80, 20, and 40 dB, respectively). Also, the graphs will appear in pairs, with "small" measurement noise plots (as defined in equation (5.8)) being on the top of the page and "large" measurement noise plots on the bottom.

The first four sections of this chapter will concern themselves with examining the frequency response plots and step responses of each of the four classes of example, making relevant comparisons and contrasts where appropriate. The fifth section of the chapter will explore the effects of different types of inputs on the time responses of one of the examples. Specifically, the chosen plant will be given step, ramp, and parabolic inputs, and the 1-DOF and 2-DOF time responses will be compared. The final section of the chapter will examine the possible tracking advantages of using a 2-DOF compensator when the system is subjected to measurement noise which contains low frequency content.

6.1 Stable, Minimum Phase System

The stable, minimum phase example serves as a baseline for comparison to all

of the other types of examples, but it is still instructive to analyze all of the plots in order to reiterate the concepts from Chapters II and III.

6.1.1 1-DOF Case. For the basic 1-DOF case, all of the loop shape plots should closely resemble the plots of "good" loop shapes in Chapter II. Beginning with the sensitivity function, Figure 6-1 shows that $|S|$ is small at low frequency and levels out at 0 dB at higher frequencies. As the disturbance becomes larger, $|GK|$ also becomes larger at low frequency. In the large measurement noise case in Figure 6-2, the shape of $|S|$ is exactly the same, but it does not have as small a magnitude at low frequency. This is expected due to the fact that with a large measurement noise, $|GK|$ must be smaller at high frequency to reject it, and the overall magnitude of GK is lower over all frequencies.

The complimentary sensitivity plots reflect that when $|GK|$ is large at low frequency, $|T|$ approaches unity, or 0 dB, and rolls off at high frequency. As the disturbance becomes larger, $|GK|$ becomes larger at low frequency, and the bandwidth of the system increases. A comparison of Figures 6-3 and 6-4 verifies the effect of a large measurement noise on the system -- $|T|$ rolls off sooner when the noise is large because $|GK|$ is smaller at high frequency.

Figures 6-5 and 6-6 illustrate the shape of a "good" loop transfer function, with high gain at low frequency and low gain at high frequency. Once again, $|GK|$ increases as the disturbance gets larger. The effect of the large measurement noise is to shift the magnitude of $|GK|$ downward for each disturbance.

Figures 6-7 and 6-8 feature the step responses of the 1-DOF system, utilizing the evaluation model from Chapter V, with no plant disturbances or measurement

noises acting on the system. As the magnitude of the assumed disturbance increases, so does the magnitude of GK in the resulting controller at low frequency, which makes the steady state error smaller. Differences in steady state error are not visible in the figures because they are so small, however. The bandwidth frequency also increases as $|GK|$ gets larger, which has a much more noticeable effect on the response by making the rise times much faster. In the large measurement noise case, the same trends are present, but since $|GK|$ is not as large at low frequency, and the bandwidth frequency is lower for each disturbance, the settling times are much longer. When the disturbance is large enough, the system steadies out in less than a second, but the large noise manifests itself by making the initial overshoot larger than that of the corresponding small noise case.

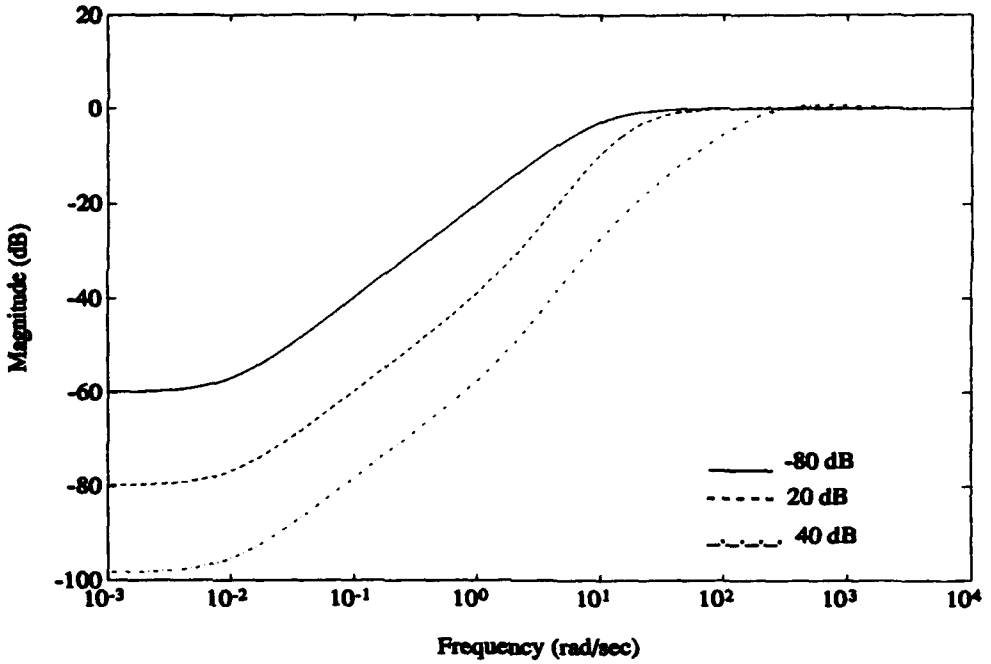

Figure 6-1. 1-DOF Bode Magnitude Plot of |S| for Stable, Minimum Phase System Example (Small Noise Case)

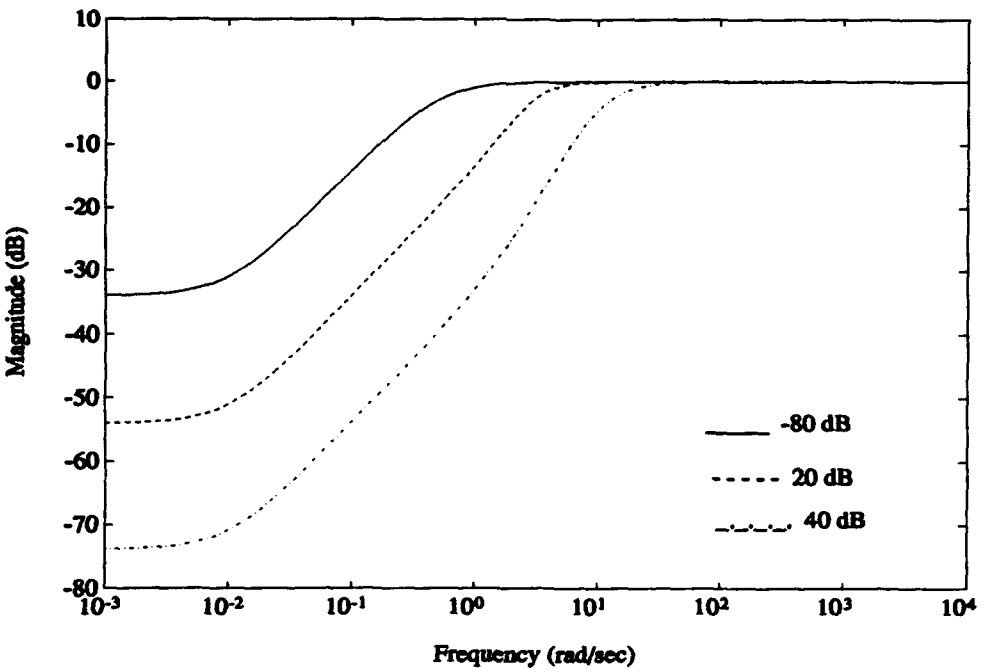

Figure 6-2. 1-DOF Bode Magnitude Plot of |S| for Stable, Minimum Phase System Example (Large Noise Case)

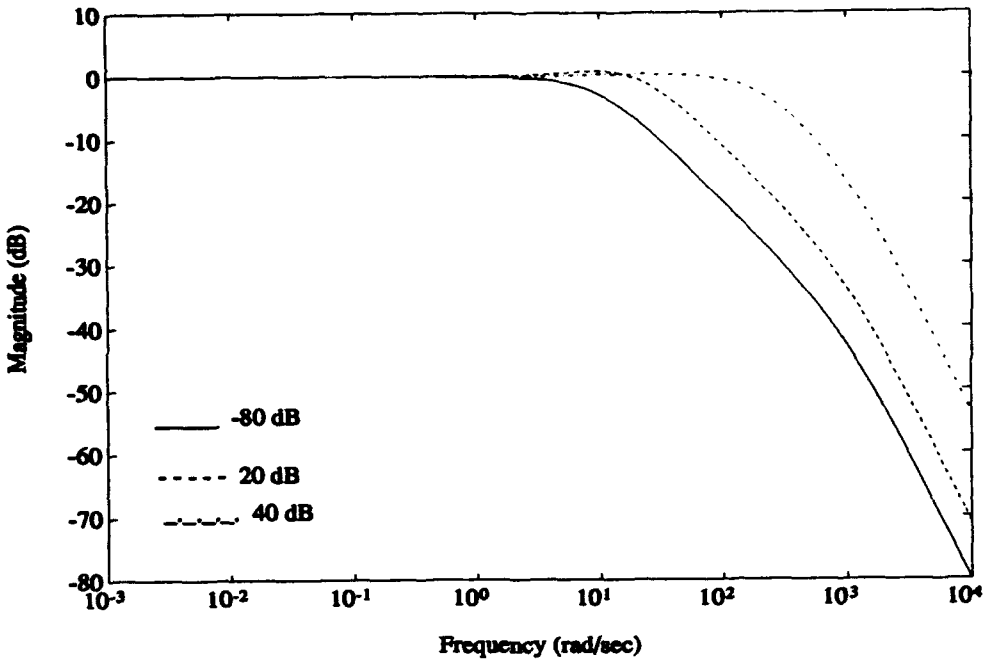

Figure 6-3. 1-DOF Bode Magnitude Plot of |T| for Stable, Minimum Phase System Example (Small Noise Case)

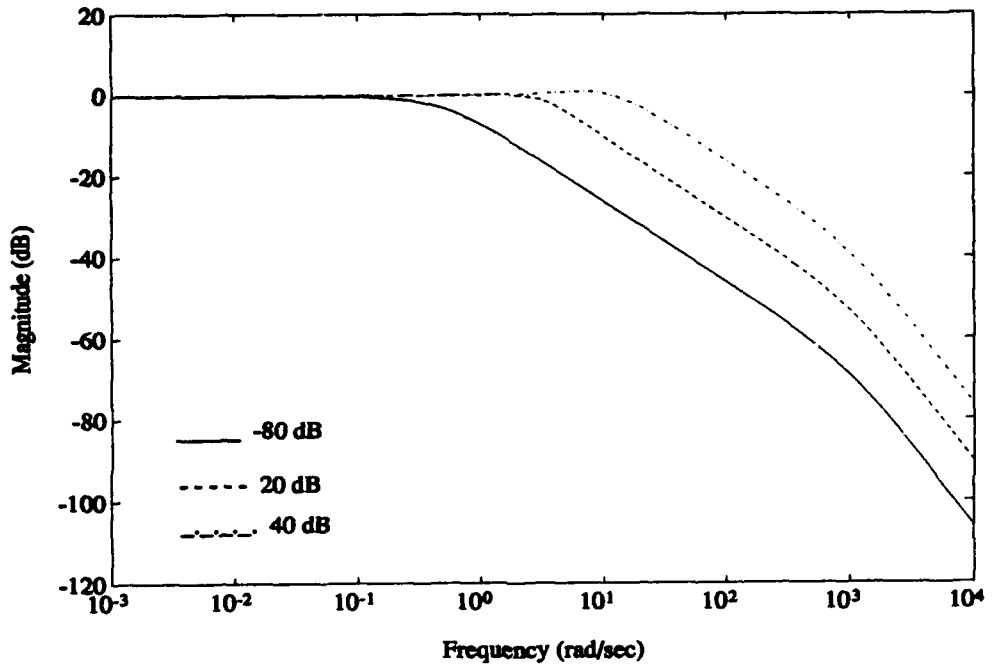

Figure 6-4. 1-DOF Bode Magnitude Plot of |T| for Stable, Minimum Phase System Example (Large Noise Case)

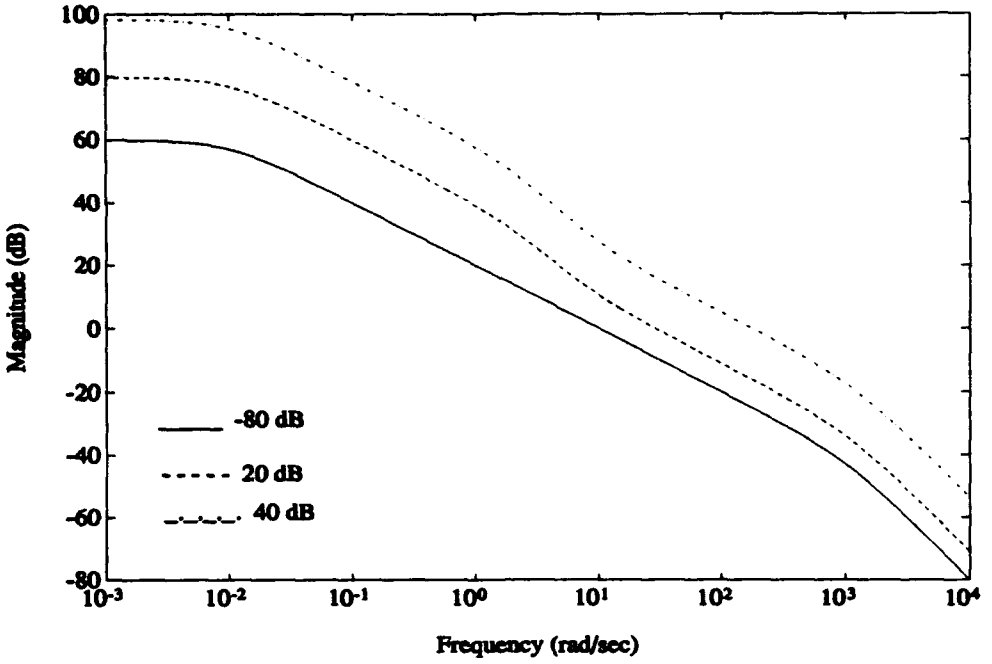

Figure 6-5. 1-DOF Bode Magnitude Plot of $|GK|$ for Stable, Minimum Phase System Example (Small Noise Case)

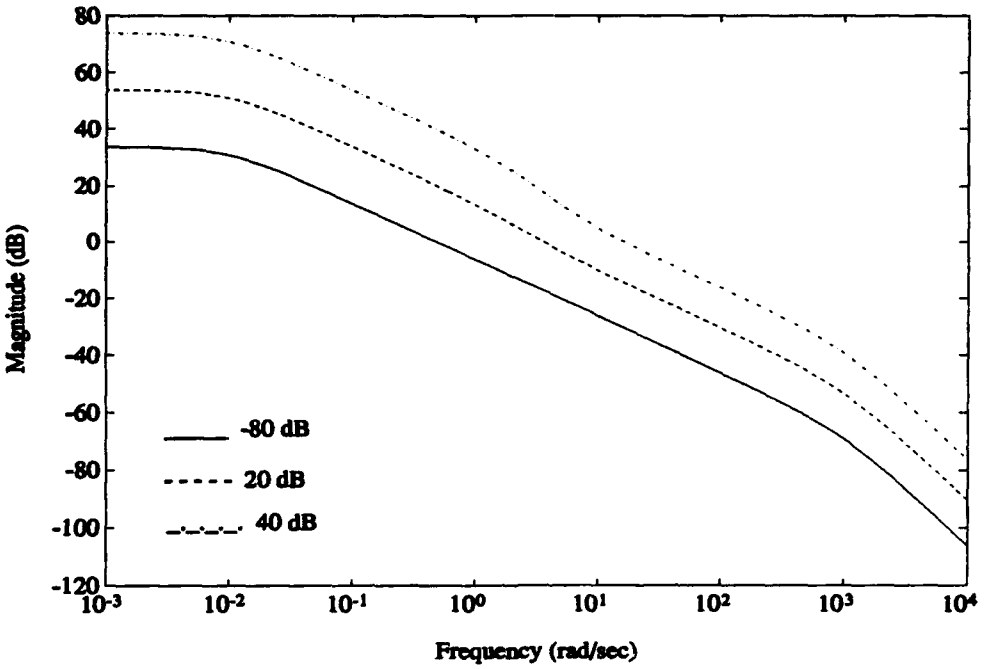

Figure 6-6. 1-DOF Bode Magnitude Plot of $|GK|$ for Stable, Minimum Phase System Example (Large Noise Case)

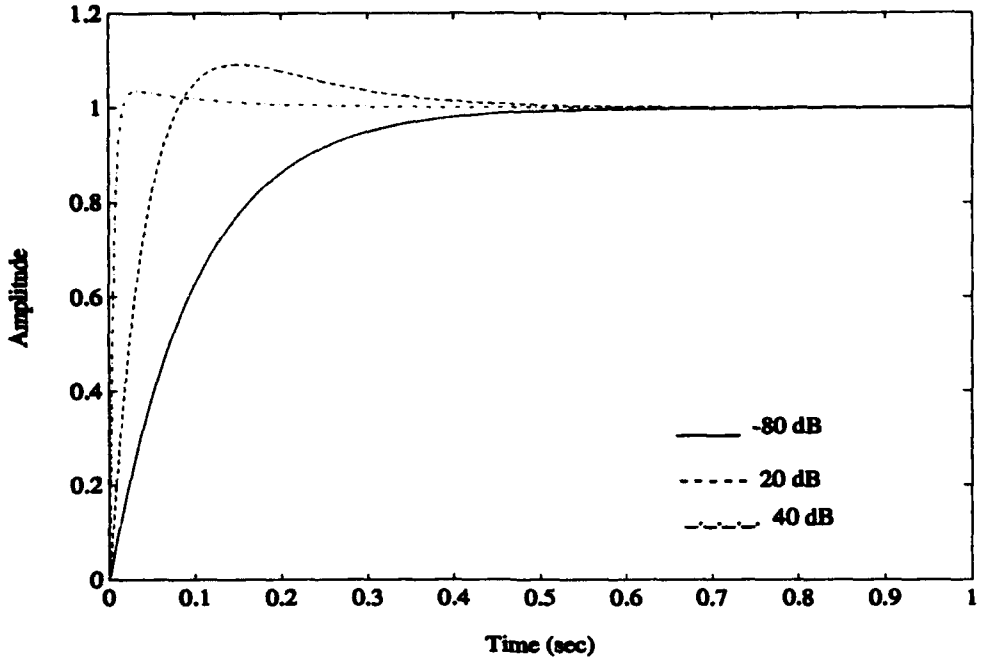

Figure 6-7. 1-DOF Step Responses for Stable, Minimum Phase System Example (Small Noise Case)

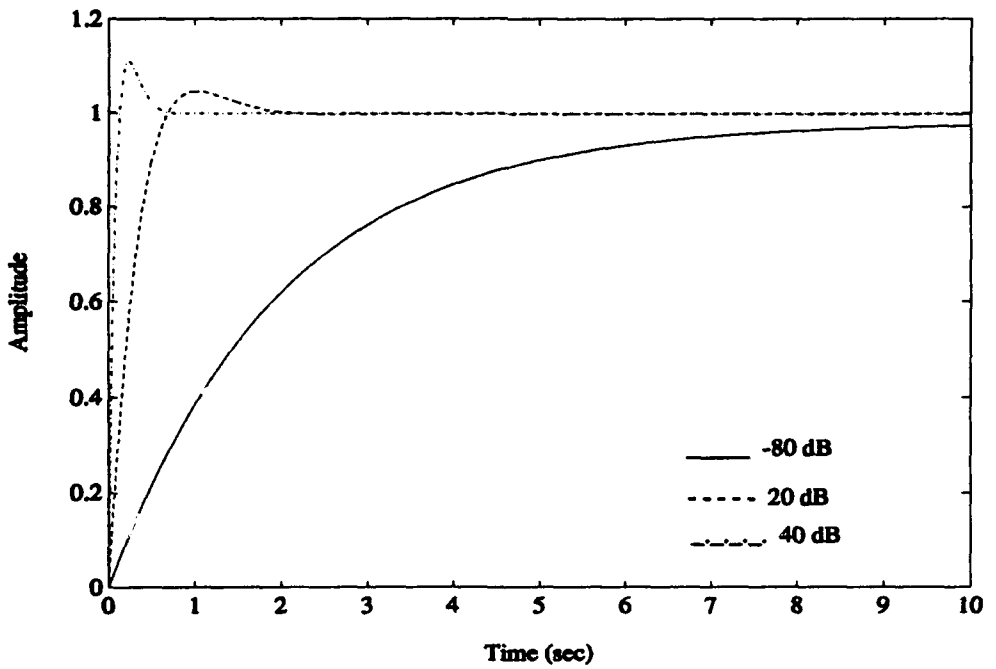

Figure 6-8. 1-DOF Step Responses for Stable, Minimum Phase System Example (Large Noise Case)

6.1.2 2-DOF Case. The 2-DOF case also serves as a baseline for the other types of 2-DOF examples in that the loop shape plots resemble those of "good" loop shapes as described in Chapter III. Figures 6-9 and 6-10 show magnitude plots of the sensitivity function. In both the small and large noise cases, $|S|$ exhibits the characteristic "good" shape of being small at low frequency and leveling out at 0 dB at high frequency. As the assumed plant disturbance level is increased, the magnitude of GK is increased at low frequency; thus, the magnitude of $|S|$ decreases at low frequency. In the large noise-small disturbance case, $|S|$ is at 0 dB at virtually all frequencies because the large noise forces down the size of $|GK_1|$ over all frequencies, and the disturbance is not large enough to offset this.

Figures 6-11 and 6-12 show plots of the 2-DOF complimentary sensitivity function. These plots also exhibit the characteristics of a good loop shape, in that most of the plots are at 0 dB at low frequency and roll off at some bandwidth frequency. In the small noise case, the disturbance is always large enough for $|T|$ to be 0 dB at low frequency. As the disturbance gets larger, the bandwidth frequency increases. In the large noise case, however, the size of the noise holds down $|GK_1|$ since the disturbance is small, and $|T|$ is not even guaranteed to be at 0 dB at low frequency. In fact, when the disturbance is at its smallest, the DC gain of $|T|$ is nearly -100 dB. The roll-off frequencies for all of the disturbances are significantly lower for the large noise case than those for the small noise case.

Figures 6-13 and 6-14 show plots of $|GK_1|$ and $|GK_2|$ for the small noise case. The plots of $|GK_1|$ reflect the trends observed in the plots of $|S|$ and $|T|$, with high gain at low frequency and low gain at high frequency. As the size of the disturbance

increases, the overall size of $|GK_1|$ also increases. For the two larger disturbances, $|GK_2|$ virtually matches $|GK_1|$, but in the small disturbance case, $|GK_2|$ must compensate for the effects of the measurement noise by flattening out at 0 dB until around 10 rad/sec before rolling off. In the large noise case (Figures 6-15 and 6-16), the overall magnitudes of $|GK_1|$ decrease much more rapidly with decreasing disturbances than in the 1-DOF case, especially in the smallest disturbance case, where $|GK_1|$ has a DC gain of -100 dB. Since the overall system bandwidth of the 2-DOF system is about 10 rad/sec, $|GK_2|$ shapes itself to roll off at this frequency, even if $|GK_1|$ falls below 0 dB before this frequency. If the disturbance is large enough (relative to the noise), it means that $|GK_2|$ will probably match the shape of $|GK_1|$; if the disturbance is small enough, then $|GK_2|$ will probably have to stay 0 dB until it reaches 10 rad/sec. This trend is repeated here because it will recur in all of the remaining examples in this thesis.

Figure 6-17 shows a plot of the system transfer function from r_c to y, given by $|SGK_2|$, which (from Chapter III) is the 2-DOF equivalent of $|T|$ for the 1-DOF case insofar as evaluating the frequency range over which the system will track commands. It shows that the 2-DOF system bandwidth for command following is indeed about 10 rad/sec.

The final graph for the stable, minimum phase case, Figure 6-18, is the step response for the 2-DOF system. It is immediately apparent that there is only one line on the graph, as there always is for H_2 2-DOF controllers. With the flexibility of two compensators, the 2-DOF system is able to produce the optimal time response, regardless of the size of the disturbance or measurement noise. In this case, the

response exhibits the shape of a critically damped system, with the settling time being as fast as possible without any overshoot .

6.1.3 Comparison Between 1-DOF and 2-DOF Cases. The differences between the 1-DOF and 2-DOF cases for this first basic example are centered around the different requirements for good loop shapes, as described in Chapters II and III. The 2-DOF sensitivity function shows the same trends as in the 1-DOF example in the small noise case, except that for the smallest disturbance, it is not as small at low frequency as it is in the 1-DOF case. The reason for $|S|$ not being as small at low frequency in the 2-DOF case stems from the idea that $|GK_1|$ is only as large as it needs to be to reject the appropriate sized disturbance at low frequency. In both the small and large noise cases, $|S|$ is at least as small at low frequency as the corresponding 1-DOF case when the disturbance is at its largest, reflecting the fact that $|GK_1|$ must be sufficiently large at low frequency to reject a large disturbance. The 2-DOF Bode magnitude plot of $|T|$ differs from that of the 1-DOF case in that it is not even guaranteed to be at 0 dB at low frequency when the measurement noise level is large, due to the fact that $|GK_1|$ is held down over all frequencies. Since the 2-DOF loop transfer function, GK_1, does not have the same restrictions on command following that the 1-DOF loop transfer function does, the plots of $|GK_1|$ show the variability in the magnitudes, depending on the size of the assumed disturbance.

The rise time and settling time of the 2-DOF step response are not as fast as some of the 1-DOF responses in the small noise case, but they are faster than those of the large noise case (note the time scale differences in the figures). The advantage of the 2-DOF controller is that although the response is not as fast as some 1-DOF

special cases, it always produces the same response (for a given tracking weight), no matter what the size of the disturbance or measurement noise is. On the other hand, a large measurement noise has a detrimental effect on the 1-DOF responses. It should be noted that the shape of the 2-DOF step response can be altered by changing the tracking weight. For instance, if the gain of the tracking weight is increased so that its magnitude plot crosses the 0 dB line at a higher frequency, the resulting step response will have a faster rise time, but more overshoot. Most of the examples in this thesis, however, have been completed using the tracking weight mentioned in Chapter V, since this weight produces step responses in which the differences between the 1-DOF and 2-DOF case can readily be seen.

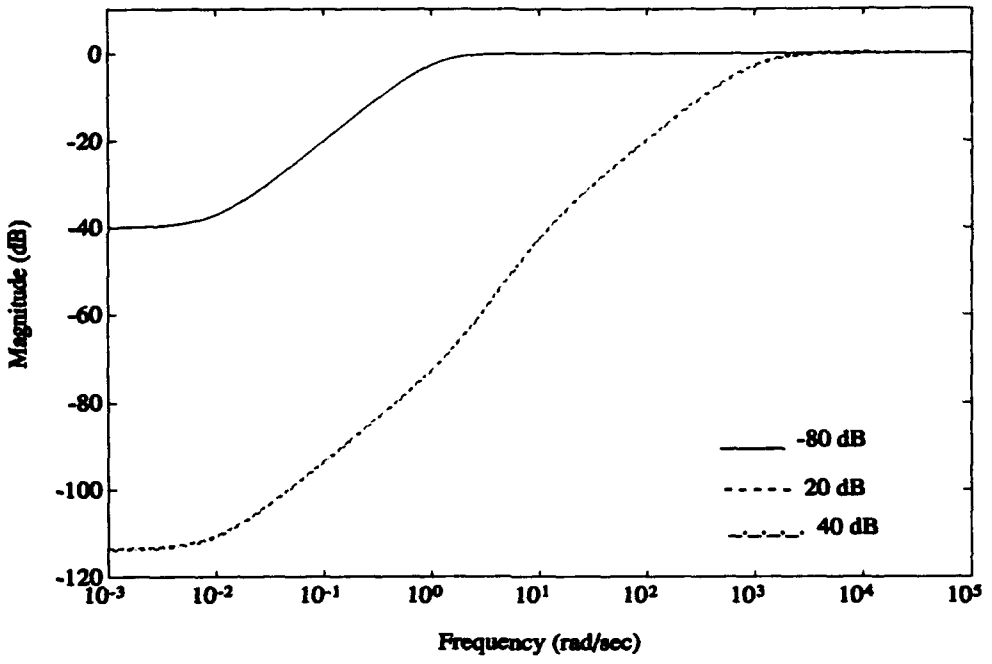

Figure 6-9. 2-DOF Bode Magnitude Plot of |S| for Stable, Minimum Phase System Example (Small Noise Case)

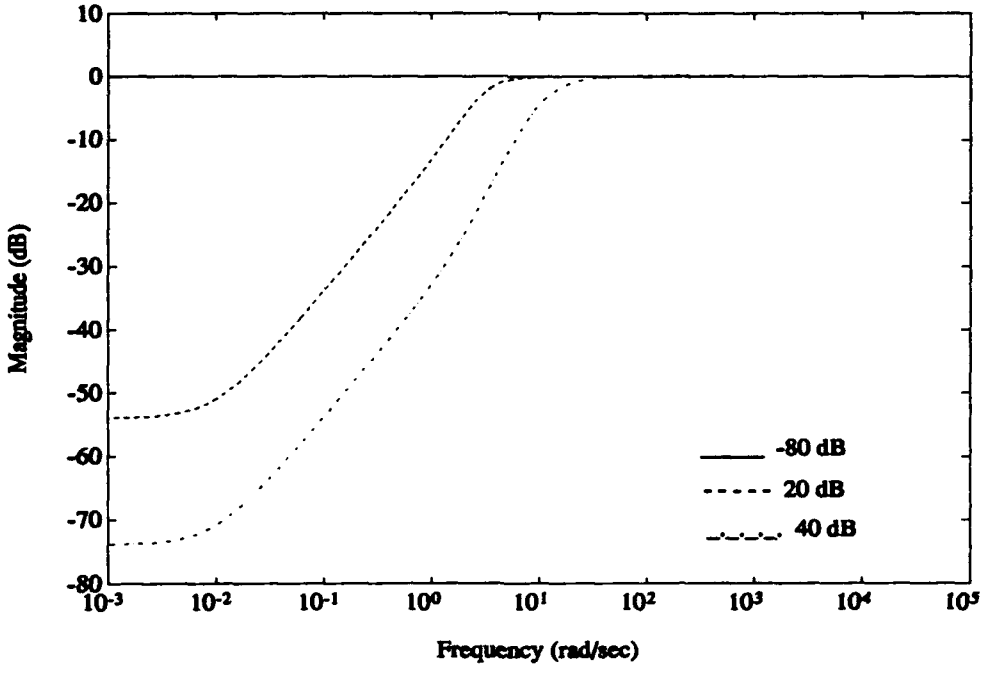

Figure 6-10. 2-DOF Bode Magnitude Plot of |S| for Stable, Minimum Phase System Example (Large Noise Case)

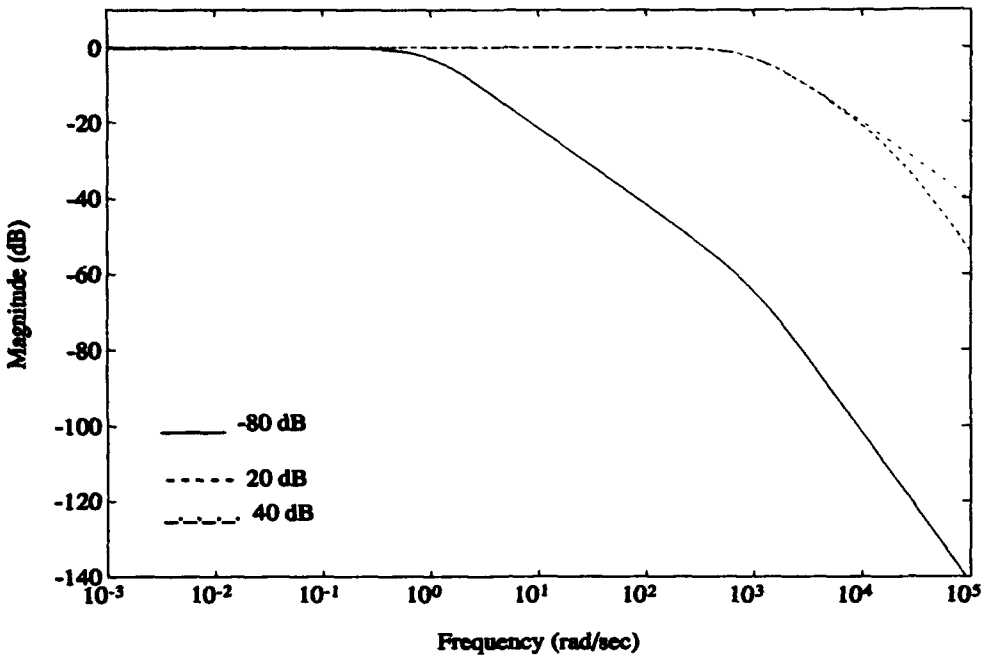

Figure 6-11. 2-DOF Bode Magnitude Plot of $|T|$ for Stable, Minimum Phase System Example (Small Noise Case)

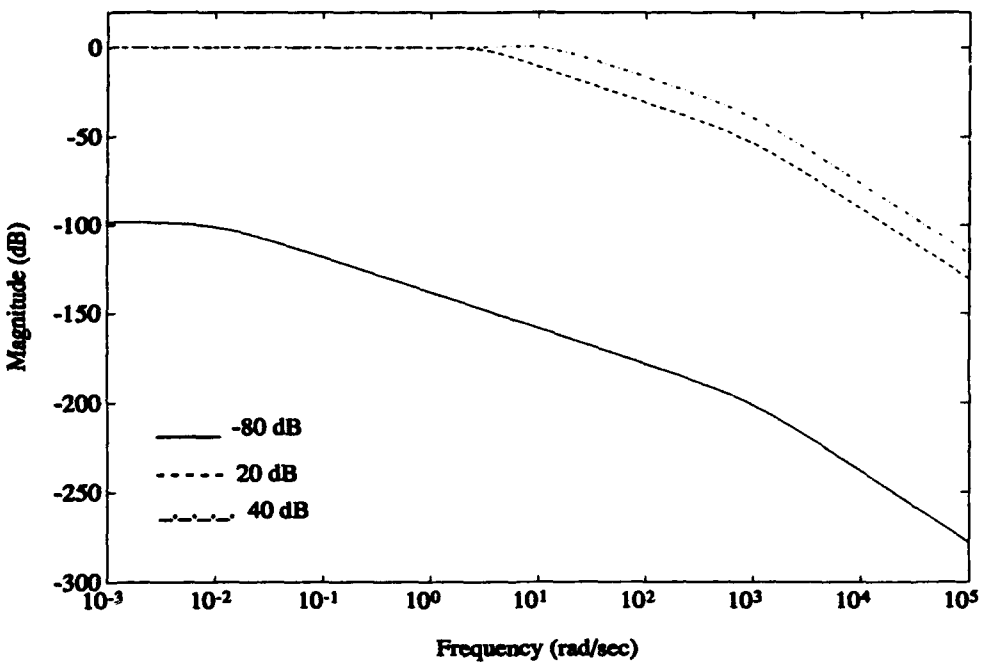

Figure 6-12. 2-DOF Bode Magnitude Plot of $|T|$ for Stable, Minimum Phase System Example (Large Noise Case)

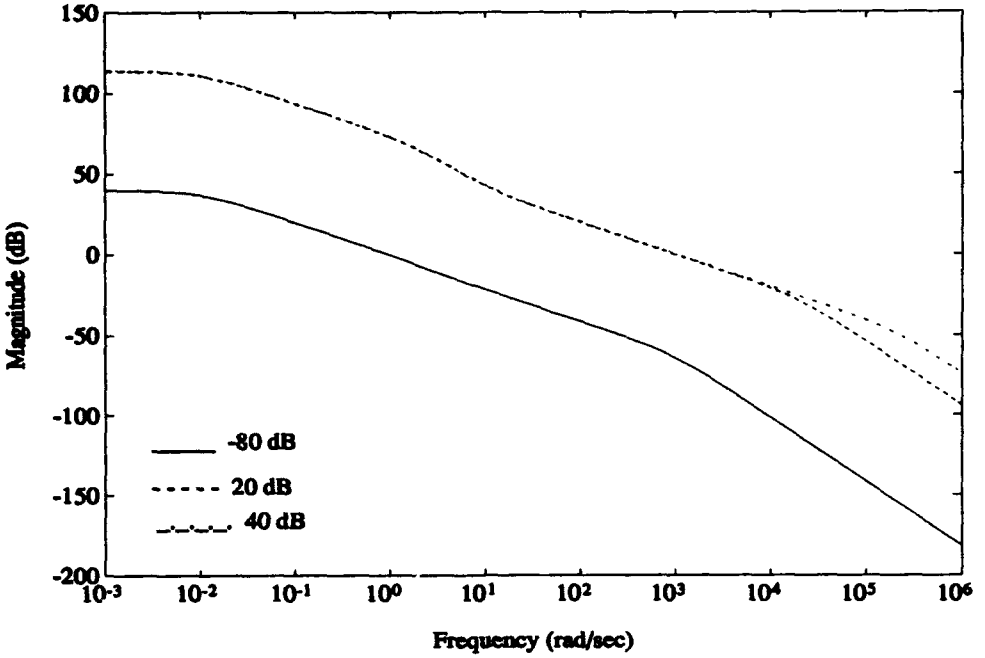

Figure 6-13. 2-DOF Bode Magnitude Plot of $|GK_1|$ for Stable, Minimum Phase System Example (Small Noise Case)

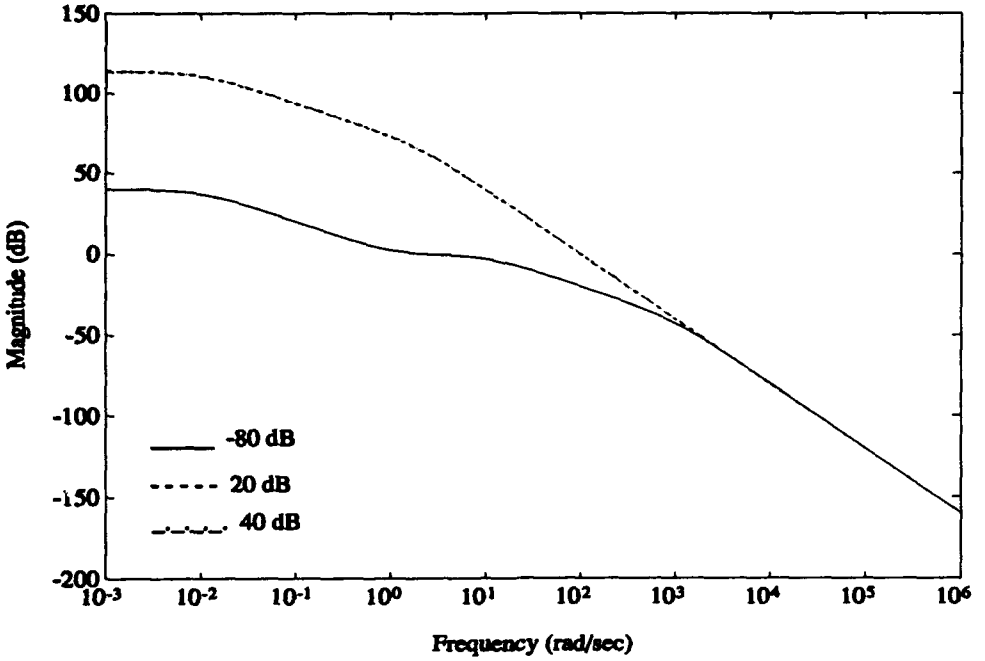

Figure 6-14. 2-DOF Bode Magnitude Plot of $|GK_2|$ for Stable, Minimum Phase System Example (Small Noise Case)

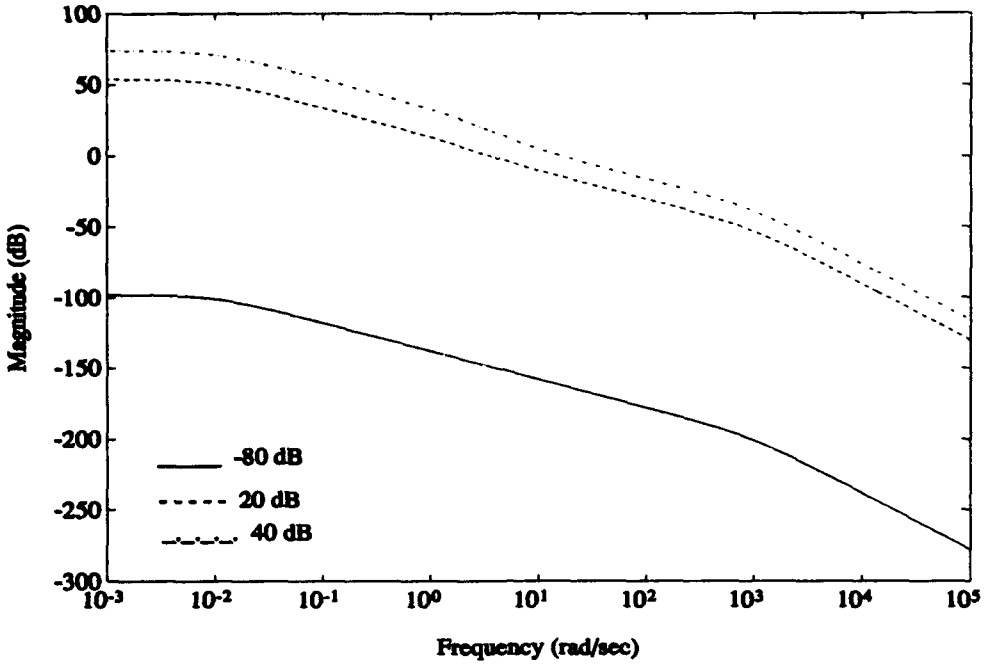

Figure 6-15. 2-DOF Bode Magnitude Plot of $|GK_1|$ for Stable, Minimum Phase System Example (Large Noise Case)

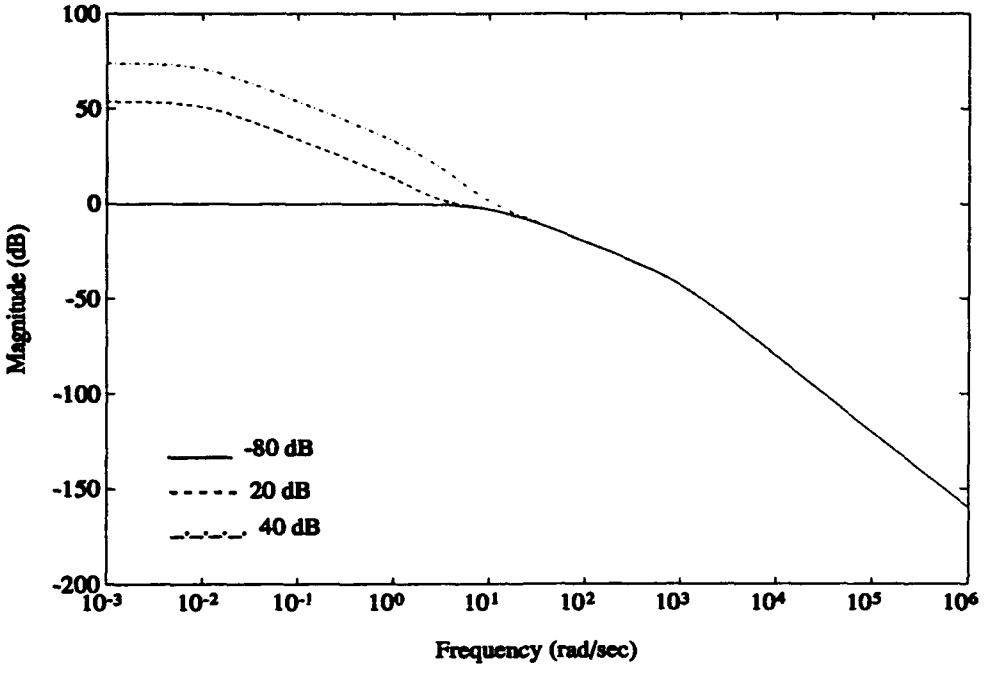

Figure 6-16. 2-DOF Bode Magnitude Plot of $|GK_2|$ for Stable, Minimum Phase System Example (Large Noise Case)

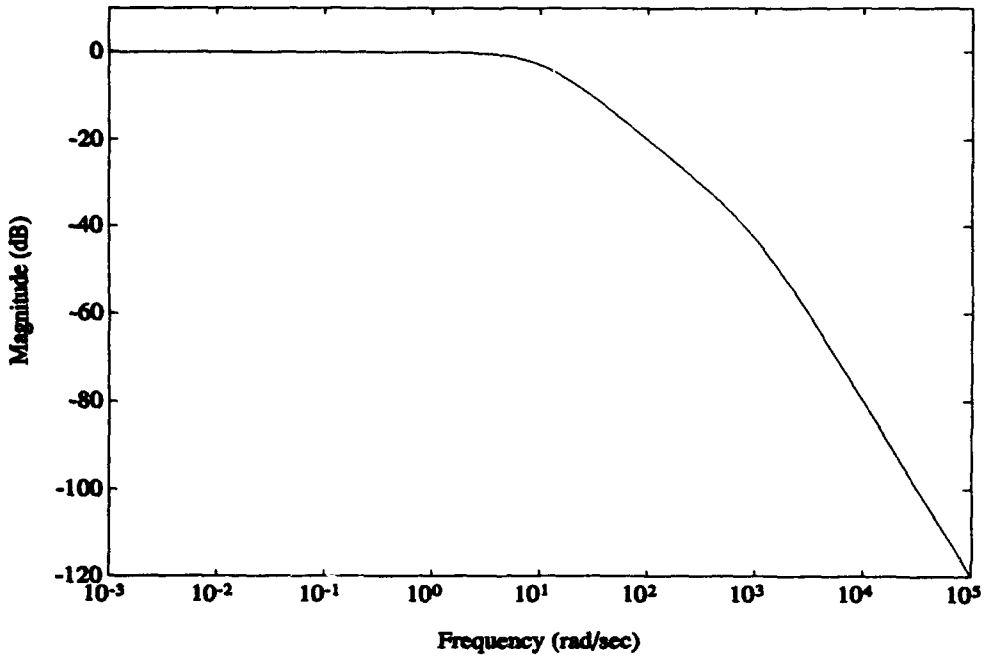

Figure 6-17. 2-DOF Bode Magnitude Plot of $|SGK_2|$ for Stable, Minimum Phase System Example (any size noise)

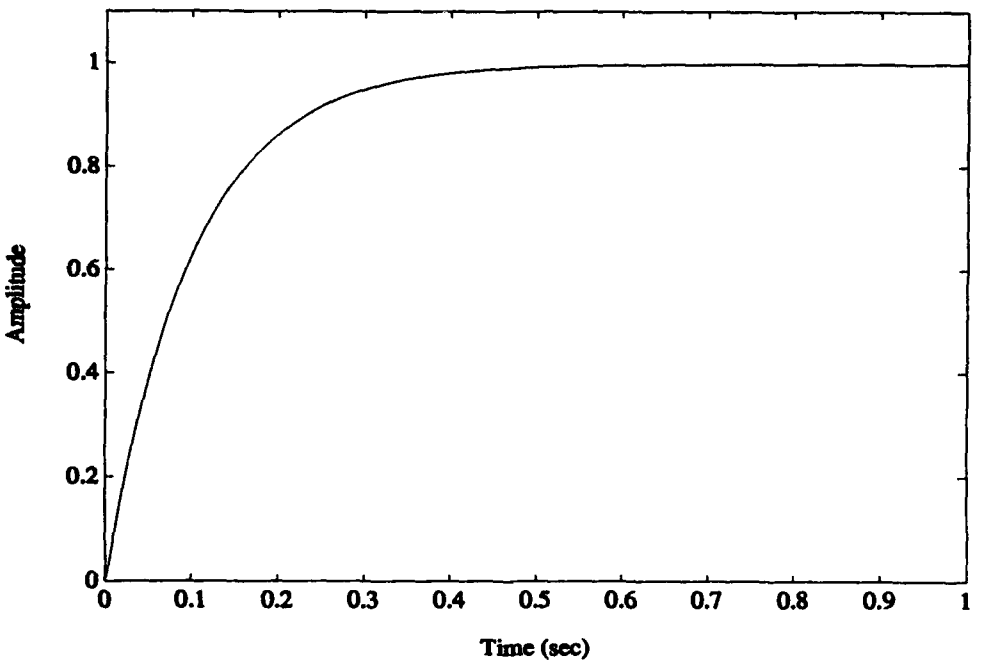

Figure 6-18. 2-DOF Step Response for Stable, Minimum Phase System Example (any size noise)

6.2 *Unstable, Minimum Phase System*

6.2.1 1-DOF Case. In this case, the only difference in the plant transfer function is that now there is an unstable pole at s = +1. Figures 6-19 and 6-20 show plots of the 1-DOF sensitivity function, $|S|$. In both the small and large noise cases, there is no significant change from the stable, minimum phase example in trends or in the actual magnitudes of the function. Figures 6-21 and 6-22 show plots of the complimentary sensitivity function, $|T|$. Again, the same trends are present as in the stable, minimum phase example, except that the function exhibits a small increase in magnitude before rolling off, especially in the large noise case. This "bubble" indicates deteriorating stability margins, which should be expected since the plant is unstable to begin with, and the stability margins will not be as good as they would be with a stable plant. The plots of $|GK|$ are shown in Figures 6-23 and 6-24. They are virtually identical to the plots of $|GK|$ in the stable, minimum phase case.

The real differences between the stable, minimum phase and the unstable, minimum phase systems are evident in the step responses, shown in Figures 6-25 and 6-26. In the small noise-large disturbance case, the responses are nearly identical, but when the disturbance gets smaller, the responses begin to settle out in the neighborhood of two seconds in the unstable system instead of one second in the stable system. In the large noise case, the settling times are generally much slower, ranging from just under a second for the large disturbance case to over 10 seconds for the small disturbance case. As the assumed plant disturbance gets smaller, the settling time produced by the resulting compensator gets longer, and the peak overshoot gets larger.

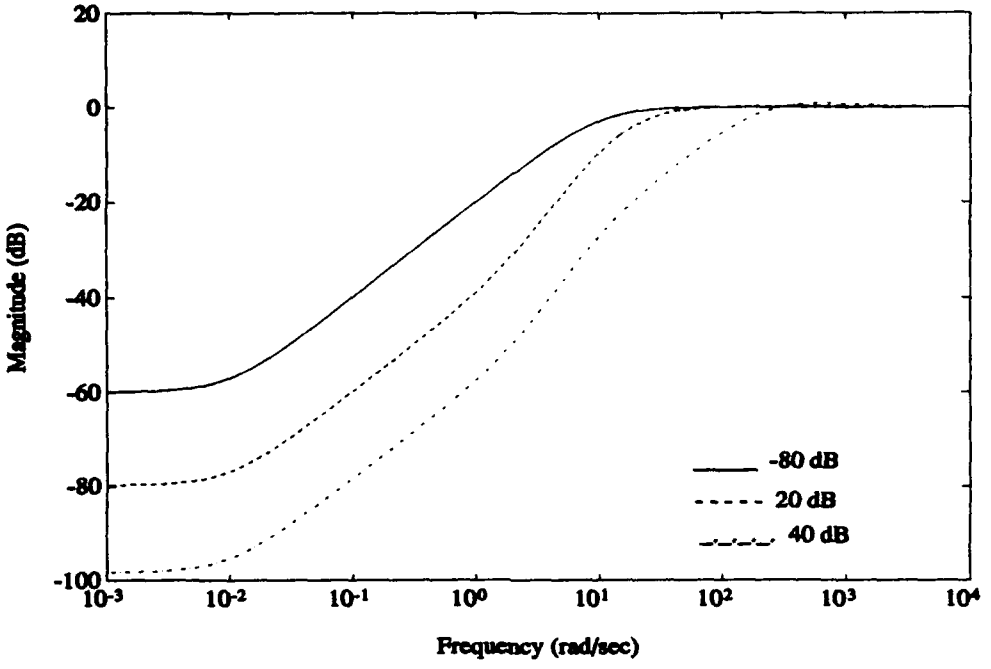

Figure 6-19. 1-DOF Bode Magnitude Plot of |S| for Unstable, Minimum Phase System Example (Small Noise Case)

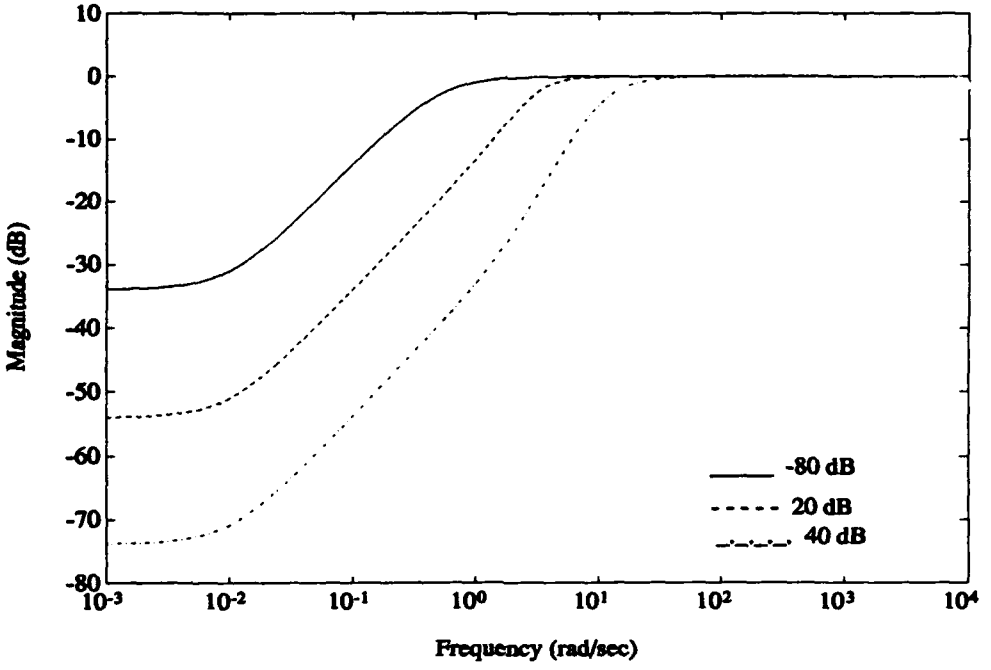

Figure 6-20. 1-DOF Bode Magnitude Plot of |S| for Unstable, Minimum Phase System Example (Large Noise Case)

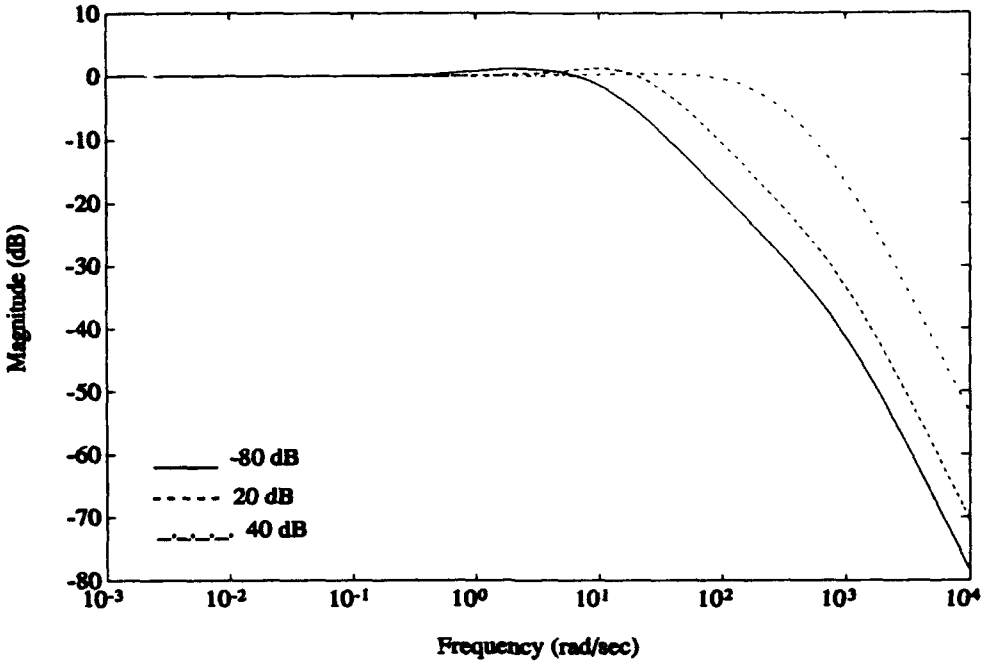

Figure 6-21. 1-DOF Bode Magnitude Plot of $|T|$ for Unstable, Minimum Phase System Example (Small Noise Case)

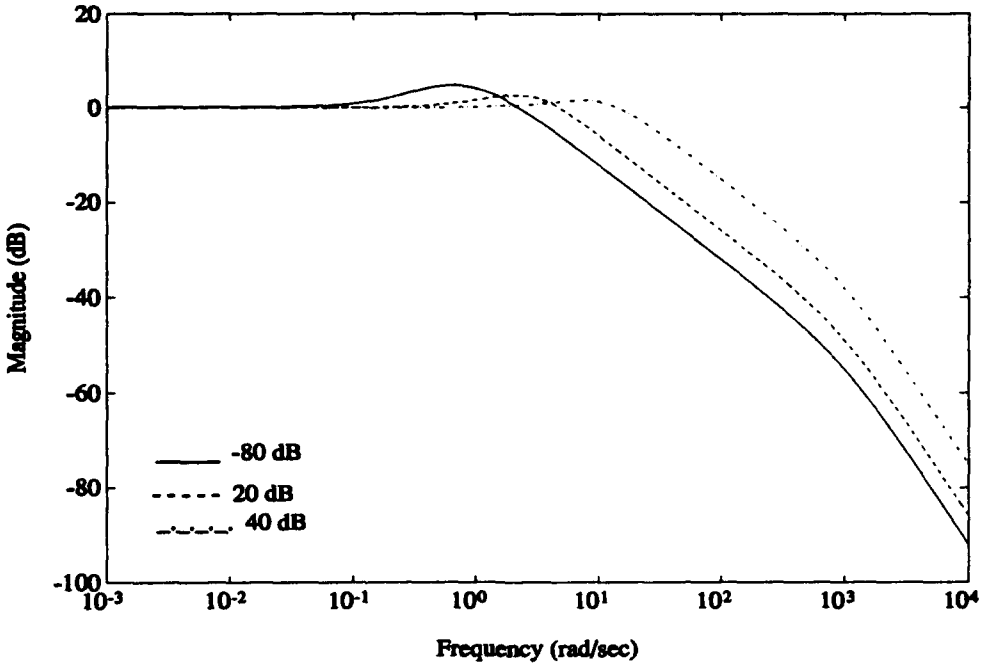

Figure 6-22. 1-DOF Bode Magnitude Plot of $|T|$ for Unstable, Minimum Phase System Example (Large Noise Case)

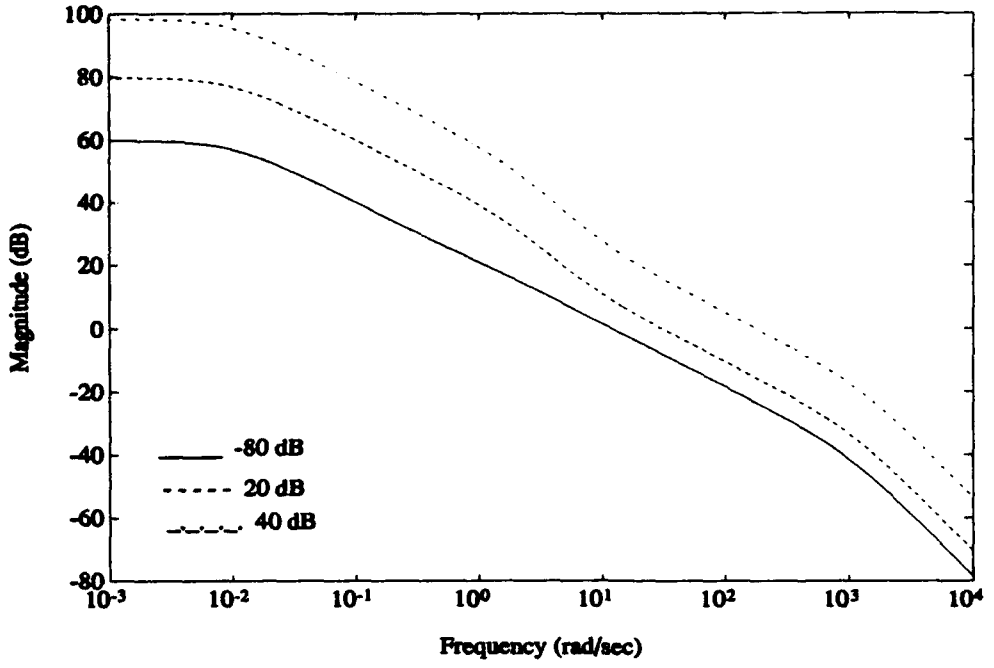

Figure 6-23. 1-DOF Bode Magnitude Plot of $|GK|$ for Unstable, Minimum Phase System Example (Small Noise Case)

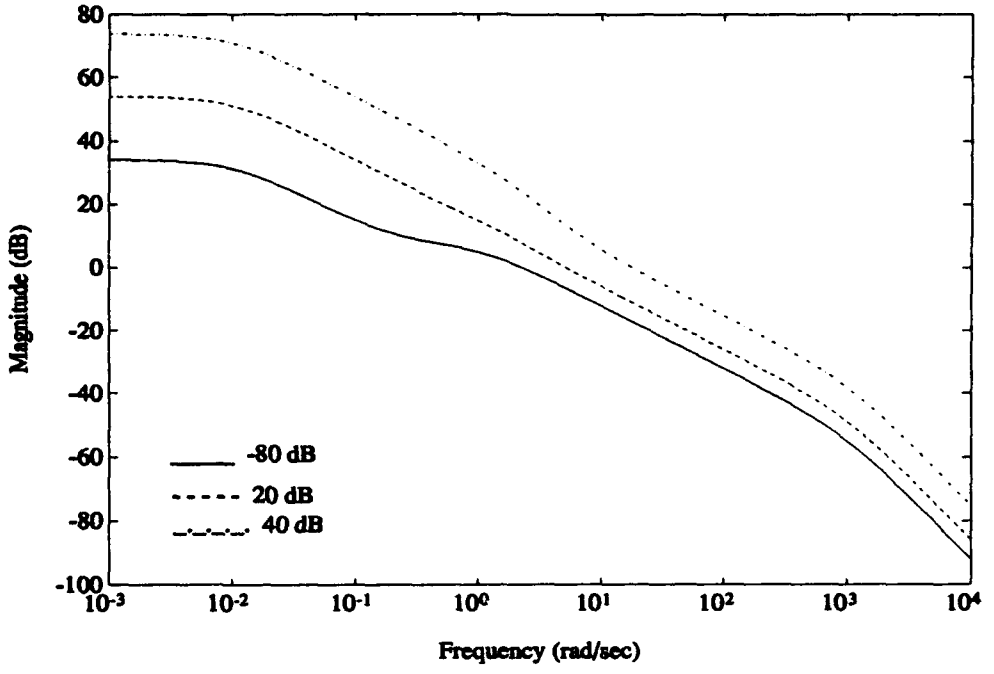

Figure 6-24. 1-DOF Bode Magnitude Plot of $|GK|$ for Unstable, Minimum Phase System Example (Large Noise Case)

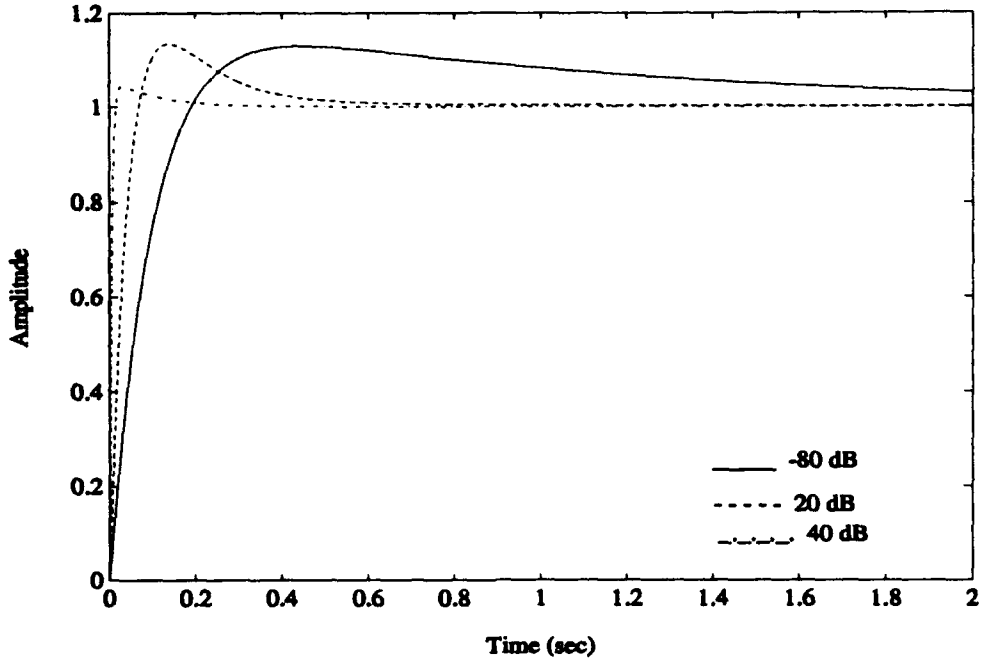

Figure 6-25. 1-DOF Step Responses for Unstable, Minimum Phase System Example (Small Noise Case)

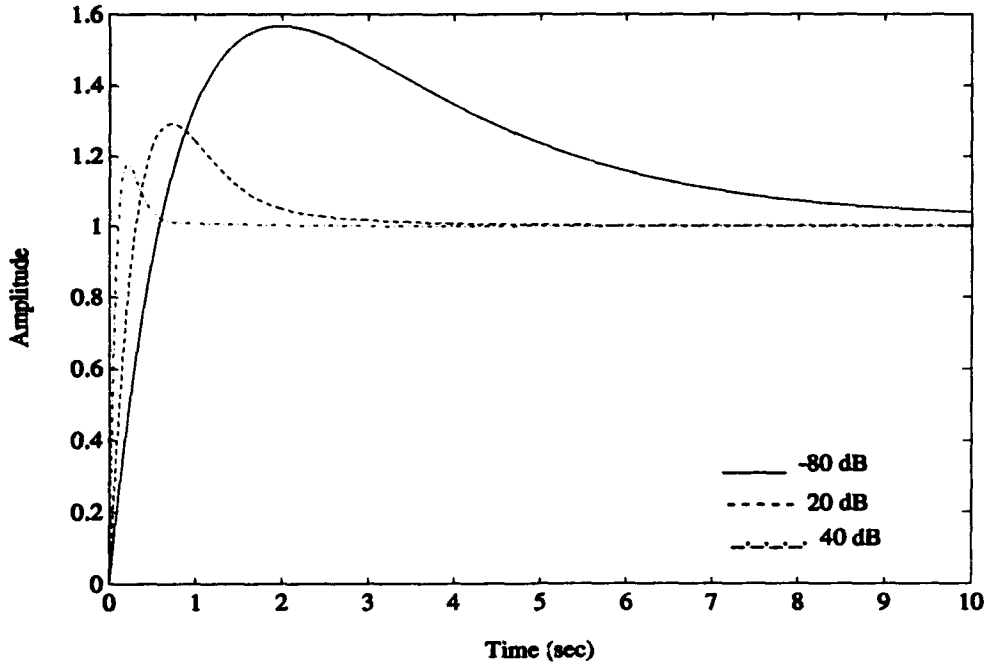

Figure 6-26. 1-DOF Step Responses for Unstable, Minimum Phase System Example (Large Noise Case)

6.2.2 2-DOF Case. Figures 6-27 and 6-28 show plots of the 2-DOF sensitivity function. They are virtually identical to the equivalent plots in the stable, minimum phase system. Figures 6-29 and 6-30 show plots of the complimentary sensitivity function. These plots show a slight increase in magnitude just before rolling off in the small noise case, indicating the slight deterioration of the stability margins compared to the stable case. In the large noise-small disturbance case, the DC gain of $|T|$ is slightly above 0 dB instead of there being only a slight hump, again indicating worse margins. In Figures 6-31 and 6-32, the plots of $|GK_1|$ and $|GK_2|$ for the small noise case are largely unchanged from the stable example, as are the plots for the large noise case, in Figures 6-33 and 6-34. Once again, $|GK_2|$ shapes itself to ensure that it rolls off below 0 dB at least 10 rad/sec. The plot of $|SGK_2|$ is identical to Figure 6-17 and shows the 2-DOF system bandwidth for tracking command inputs. The 2-DOF step response is also identical to that of the 2-DOF stable example in Figure 6-18.

The primary difference between the stable, minimum phase system and the unstable, minimum phase case is the shape of the complimentary sensitivity plot. In the unstable case, the function $|T|$ shows an increase in magnitude before rolling off, indicating a worsening of the stability margins, which is to be expected when going from a stable to an unstable plant.

6.2.3 Comparison Between 1-DOF and 2-DOF Cases. All of the loop shape plots for the 1-DOF and 2-DOF systems are virtually the same as they were in the stable system example, except for the complimentary sensitivity function plots. The 2-DOF sensitivity function plots again show that since $|GK_1|$ is not required to be large

at low frequency, $|S|$ is larger at low frequency than the corresponding 1-DOF case when the disturbance is small relative to the measurement noise. In both the 1-DOF and 2-DOF cases, $|T|$ exhibits a rise in magnitude at some point before rolling off, indicating a decrease in stability margins. In the small disturbance-large noise case, the DC gain of $|T|$ is above 0 dB in the 2-DOF case, which never occurs in the 1-DOF case, due to the requirement for the 1-DOF loop gain to be large at low frequency (for both disturbance rejection and tracking).

Overall, an unstable pole has virtually no effect on the tracking ability of the 2-DOF system, while it has noticeable effects on the performance of the 1-DOF system. The 1-DOF step responses show that an unstable pole generally increases the amount of overshoot. In the 2-DOF case, $|GK_2|$ is shaped in such a way that perfect tracking is maintained (from the plot of $|SGK_2|$) over a larger frequency range than the 1-DOF case.

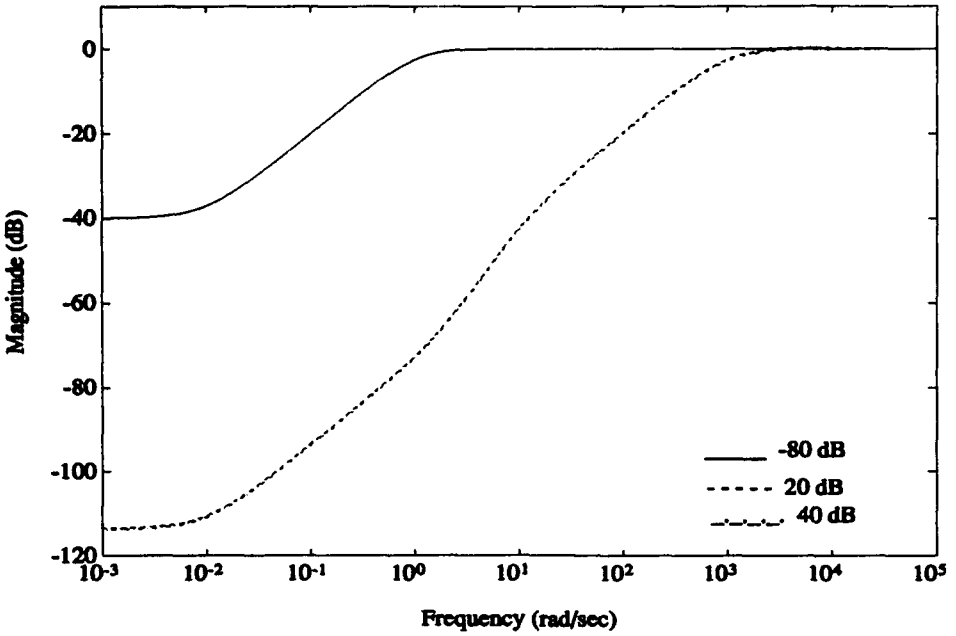

Figure 6-27. 2-DOF Bode Magnitude Plot of |S| for Unstable, Minimum Phase System Example (Small Noise Case)

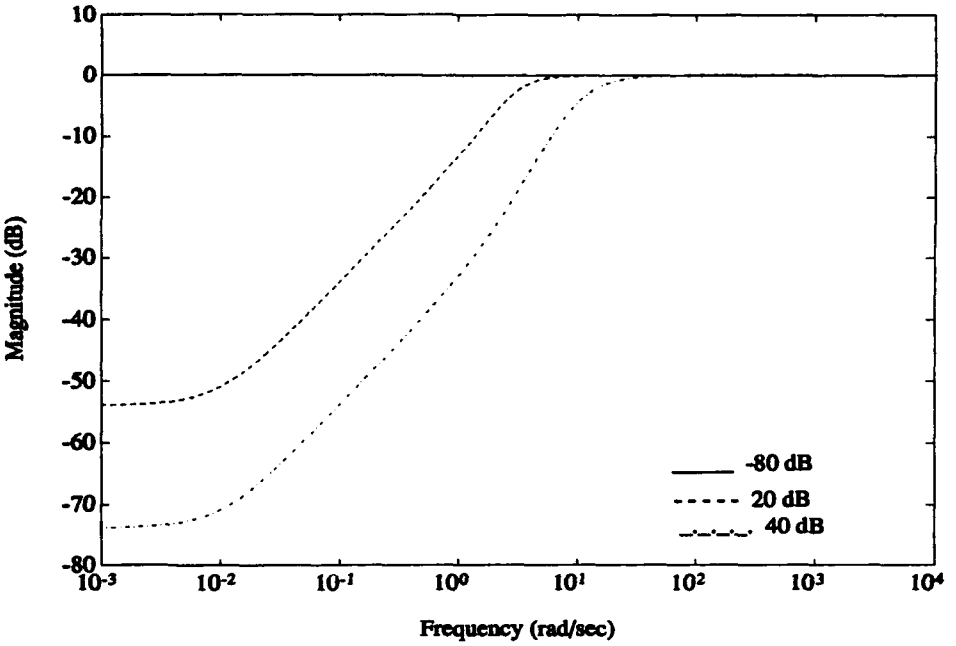

Figure 6-28. 2-DOF Bode Magnitude Plot of |S| for Unstable, Minimum Phase System Example (Large Noise Case)

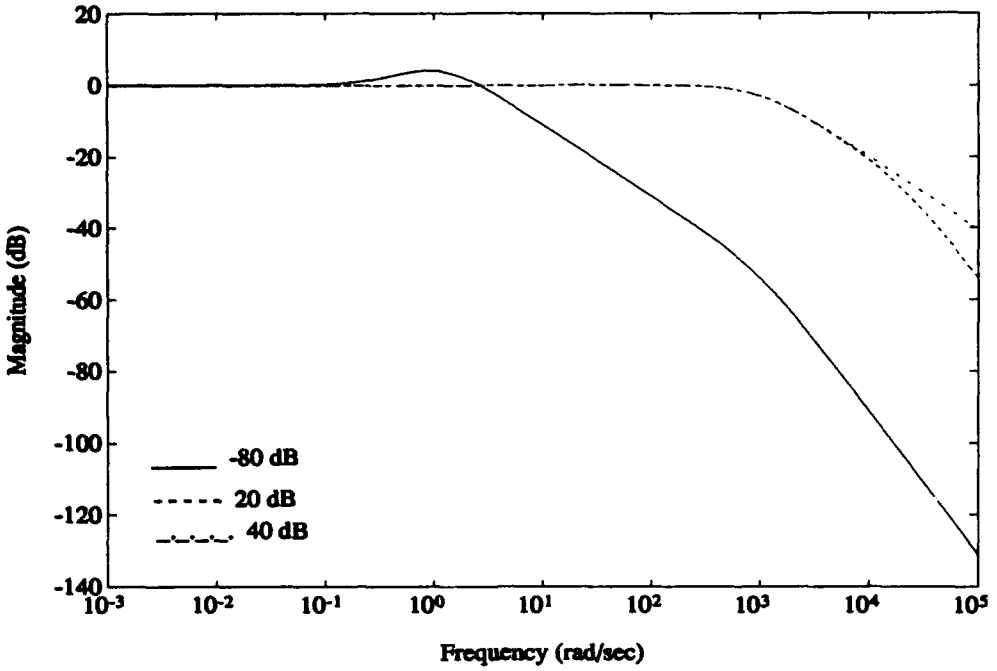

Figure 6-29. 2-DOF Bode Magnitude Plot of |T| for Unstable, Minimum Phase System Example (Small Noise Case)

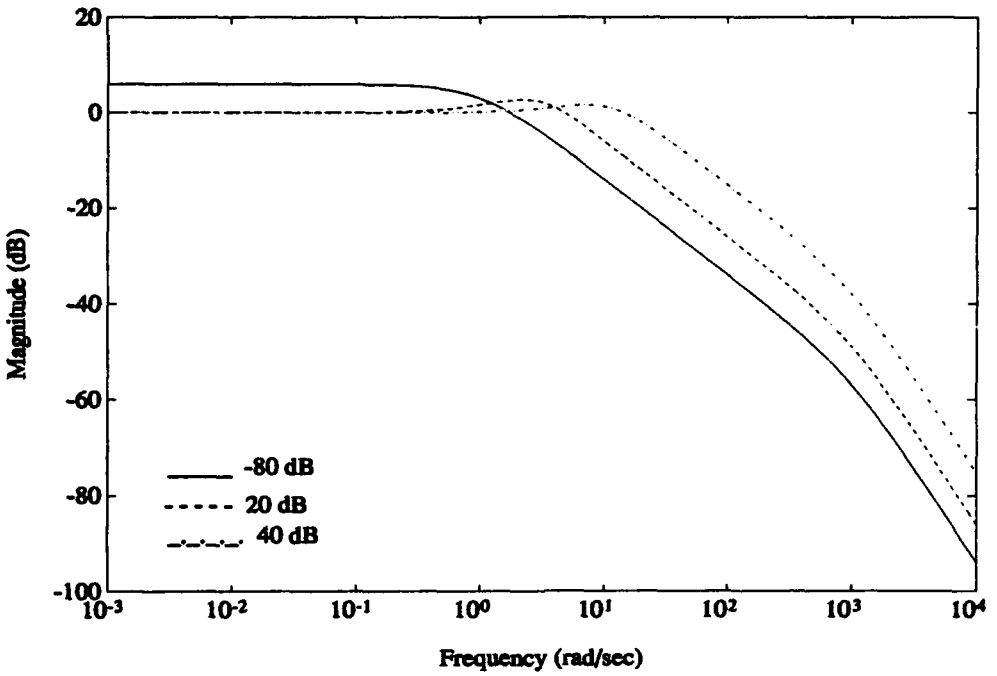

Figure 6-30. 2-DOF Bode Magnitude Plot of |T| for Unstable, Minimum Phase System Example (Large Noise Case)

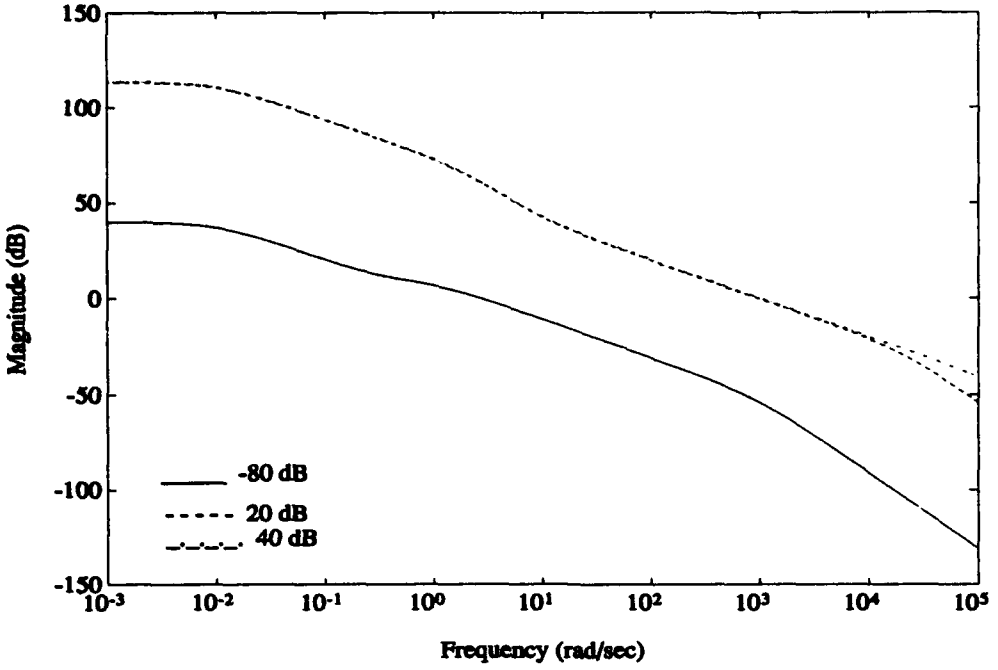

Figure 6-31. 2-DOF Bode Magnitude Plot of $|GK_1|$ for Unstable, Minimum Phase System Example (Small Noise Case)

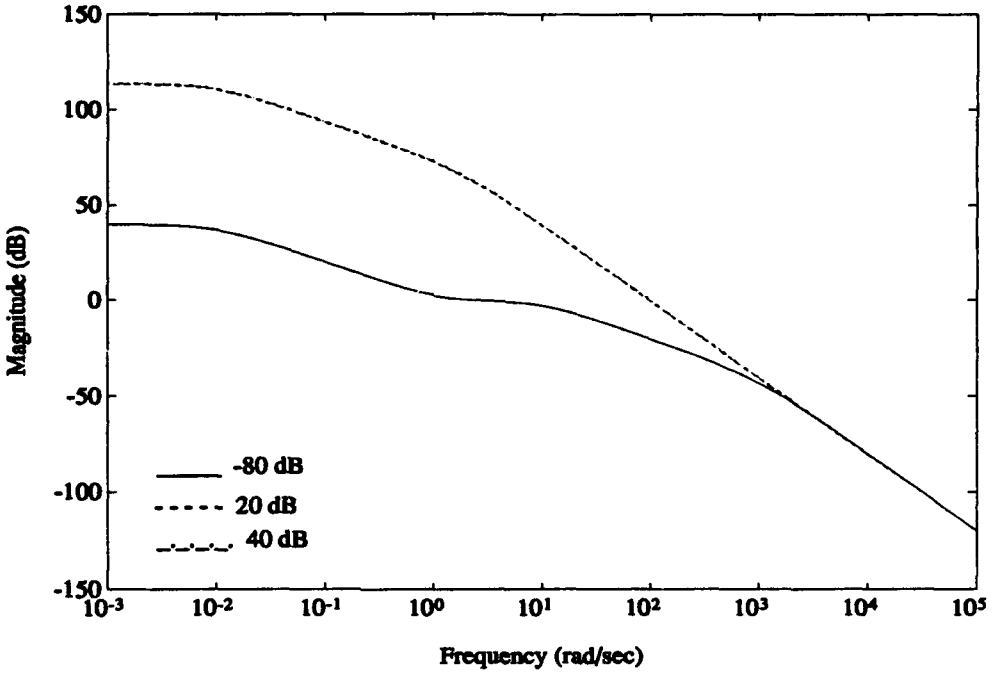

Figure 6-32. 2-DOF Bode Magnitude Plot of $|GK_2|$ for Unstable, Minimum Phase System Example (Small Noise Case)

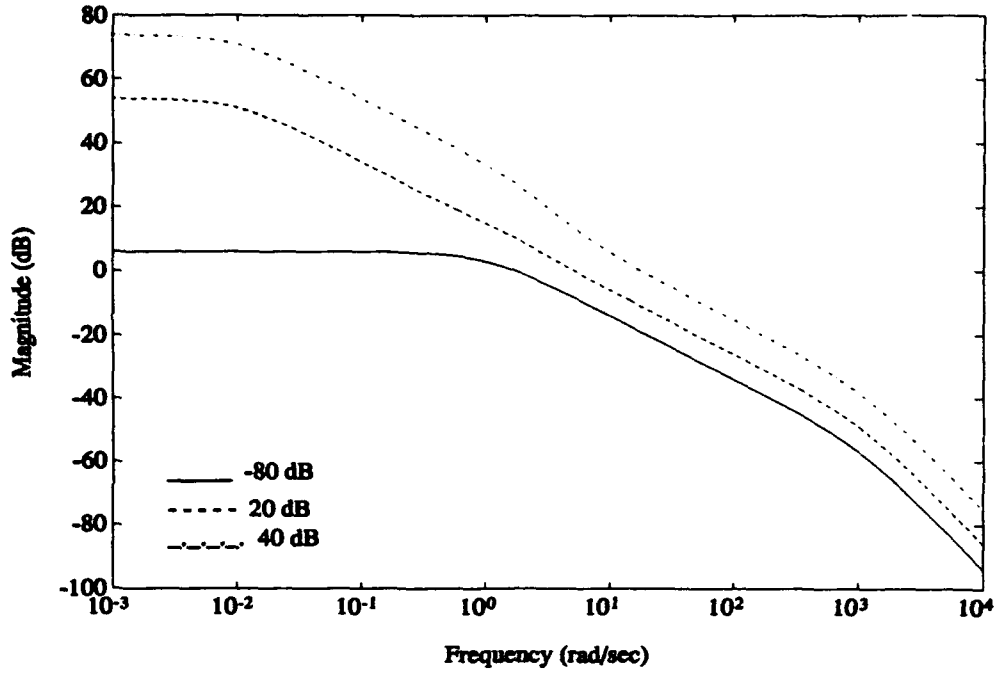

Figure 6-33. 2-DOF Bode Magnitude Plot of $|GK_1|$ for Unstable, Minimum Phase System Example (Large Noise Case)

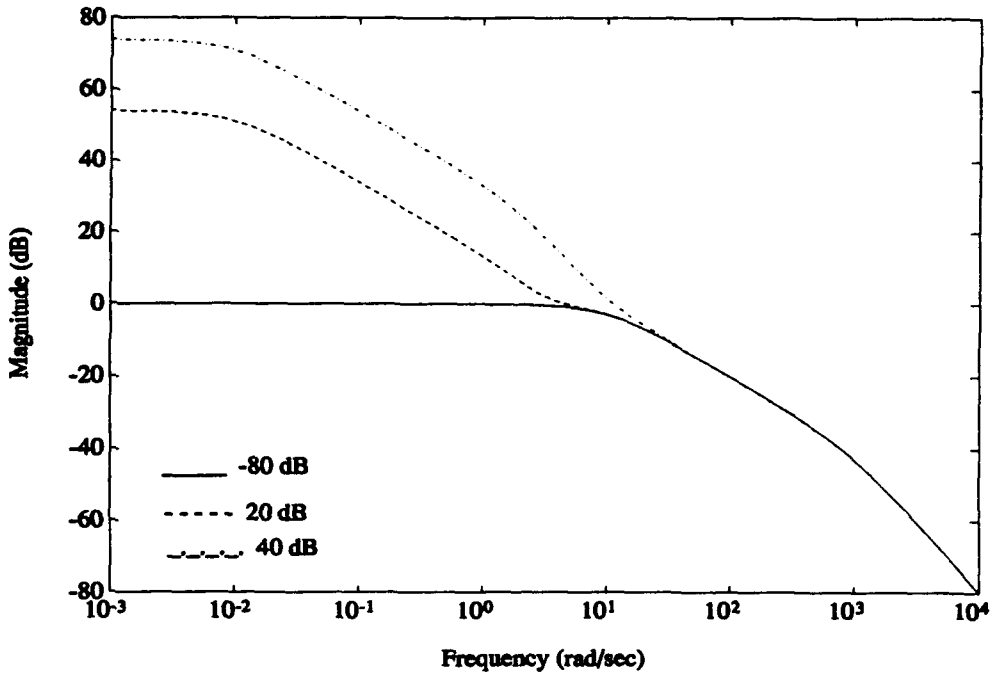

Figure 6-34. 2-DOF Bode Magnitude Plot of $|GK_2|$ for Unstable, Minimum Phase System Example (Large Noise Case)

6.3 Stable, Nonminimum Phase System

The next two examples presented represent nonminimum phase systems, which often pose challenging control problems. Using feedback control, poles in undesirable locations can be moved to more favorable closed loop locations, but undesirable zeros are a burden which cannot be directly remedied -- zeros cannot be re-assigned to different locations.

6.3.1 1-DOF Case. Figures 6-35 and 6-36 show plots of the sensitivity function, $|S|$. The most noticeable characteristic of these plots is the large amount of overshoot exhibited by the functions. The existence of a nonminimum phase zero has the effect of attracting stable poles toward the right-half plane (on a root locus plot) as gain is increased; therefore, the stability margins are expected to be lower for this example than either of the two minimum phase examples described thus far. The plots of $|T|$ in Figures 6-37 and 6-38 reiterate the decreased stability margins in that they also show a significant rise in magnitude before rolling off at the appropriate bandwidth frequency. The amount of overshoot in $|S|$ and $|T|$ is a bit more pronounced in the small noise case than it is in the large noise case. This is because in the small noise case, the size of $|GK|$ is permitted to be larger overall, thereby placing the closed loop poles in a position where the response is faster, but some pole(s) may be closer to instability.

Figures 6-39 and 6-40 show plots of the loop shape, $|GK|$. Both plots still exhibit high gain at low frequency, but the effect of the nonminimum phase zero is evident in their shapes. Since zeros cannot be moved under feedback control, the next best manner in which to handle the situation is to minimize the amount of energy

placed at the frequency of the nonminimum phase zero. This is shown in the two figures by the fact that none of the lines is above 0 dB past 2 rad/sec, which corresponds to the zero at s = +2. In fact, that particular frequency effectively presents a "barrier" under which the magnitude of *GK* must pass in order to produce stable closed loop systems. In the small noise case, |*GK*| normally has higher gain at low frequency and does not cross the 0 dB line until at least 10 rad/sec. For both noise levels with a nonminimum phase zero, however, |*GK*| passes under the 2 rad/sec barrier and then stays just below 0 dB out to frequencies beyond 100 rad/sec before rolling off, thus trying to maintain the highest amount of energy possible over all frequencies.

Figures 6-41 and 6-42 show the step responses for the stable, nonminimum phase system. As expected, the initial tendency of nonminimum phase systems is to initially "go the wrong way." Once again, the general trends are as before -- the settling times get faster as the disturbance gets bigger in both the large and small noise cases, but the large noise case produces slower settling times than the small noise case does. In the large disturbance case, the settling times are about the same for both noises, but the initial undershoot is much larger in the small noise case. This is in keeping with the fact that as |*GK*| is made larger in a nonminimum phase system, the response gets faster, but some pole(s) may move closer to the imaginary axis, causing more oscillatory motion. When the disturbances are smaller in the large noise case, there is not as much undershoot, but the settling times become quite a bit slower.

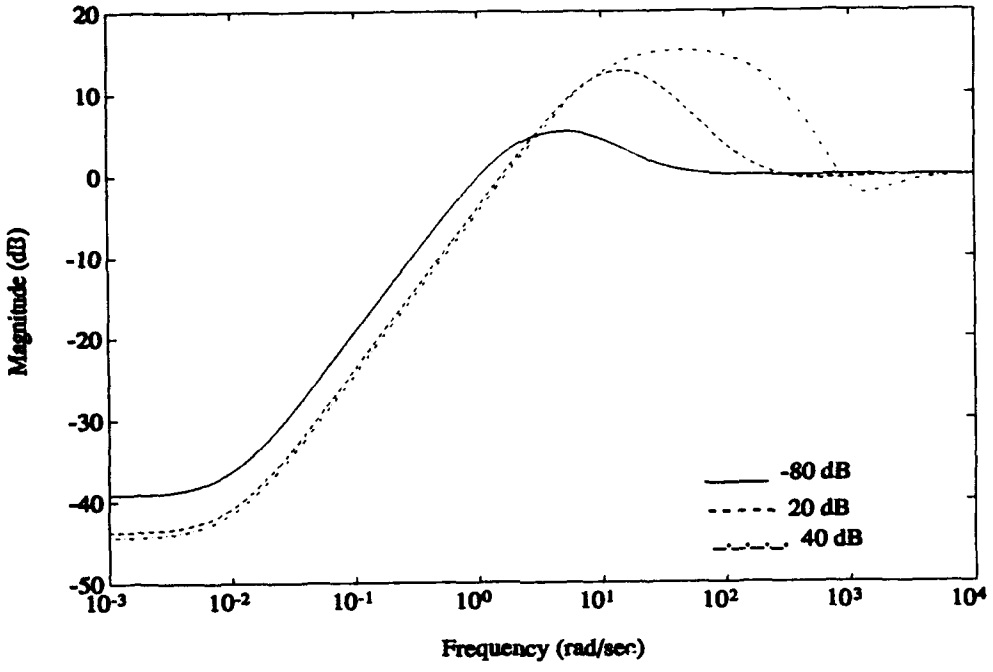

Figure 6-35. 1-DOF Bode Magnitude Plot of $|S|$ for Stable, Nonminimum Phase System Example (Small Noise Case)

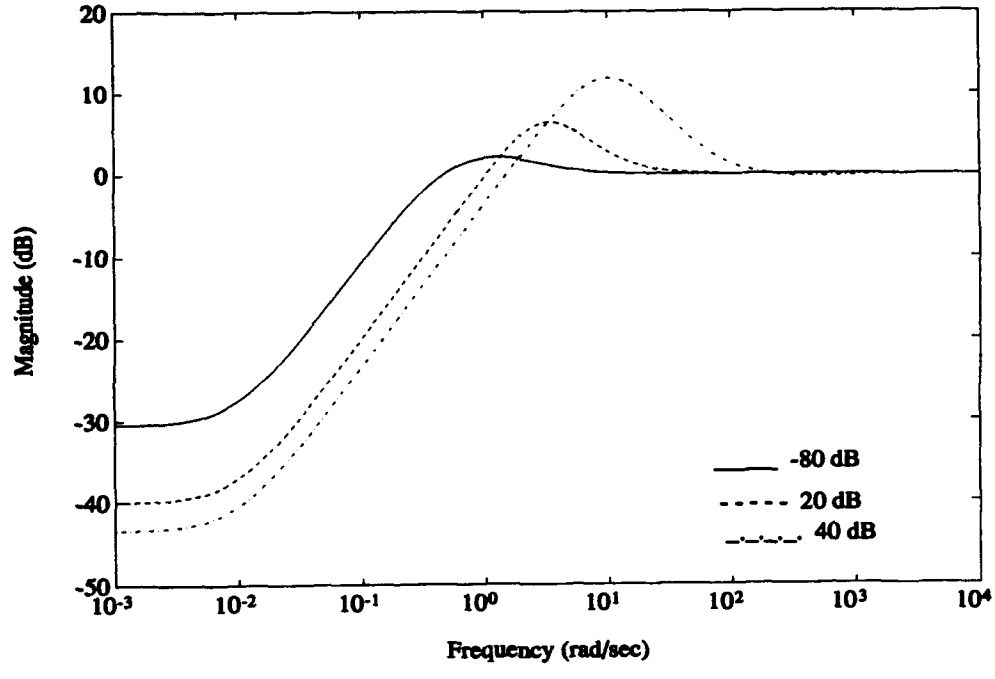

Figure 6-36. 1-DOF Bode Magnitude Plot of $|S|$ for Stable, Nonminimum Phase System Example (Large Noise Case)

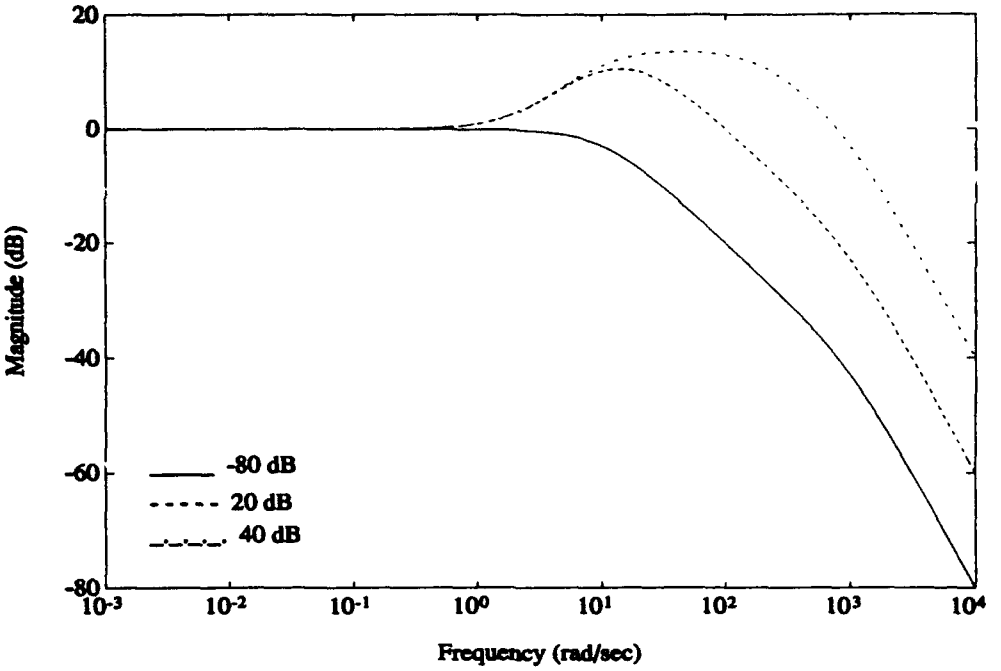

Figure 6-37. 1-DOF Bode Magnitude Plot of |T| for Stable, Nonminimum Phase System Example (Small Noise Case)

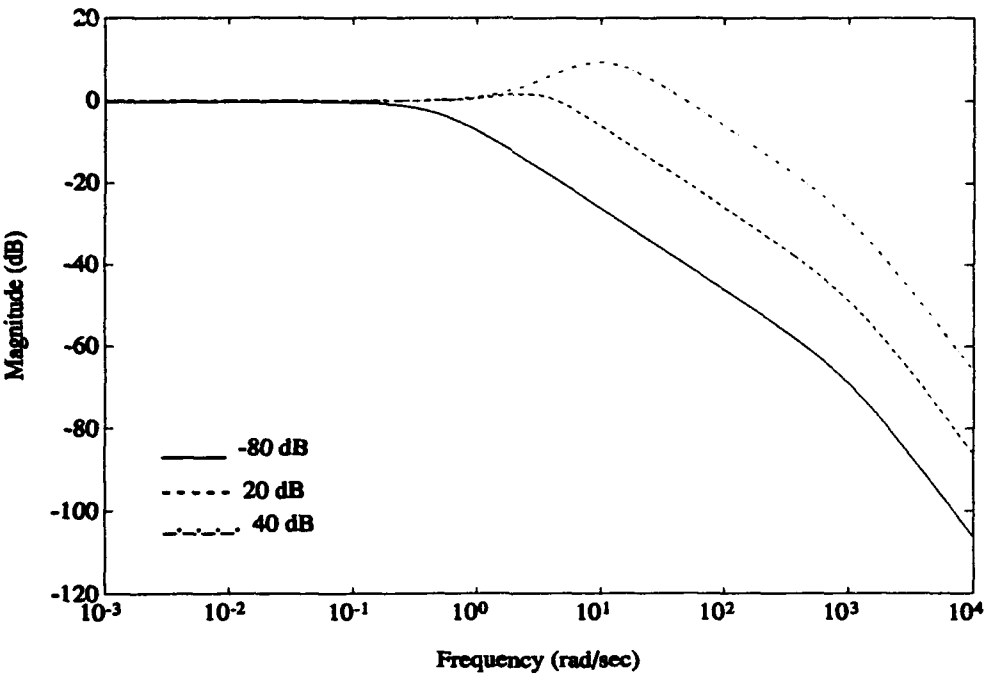

Figure 6-38. 1-DOF Bode Magnitude Plot of |T| for Stable, Nonminimum Phase System Example (Large Noise Case)

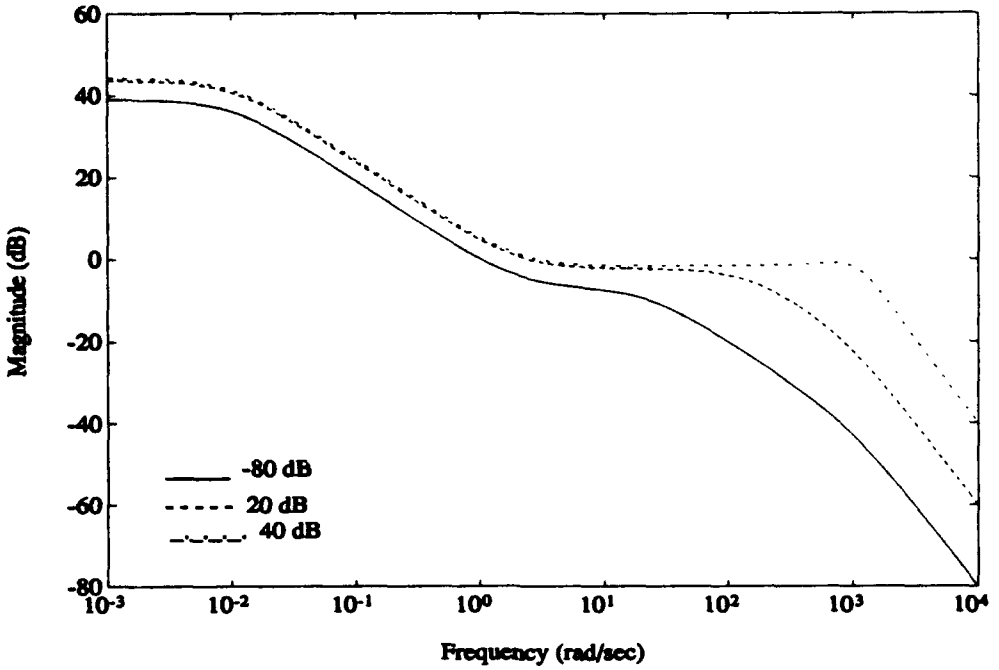

Figure 6-39. 1-DOF Bode Magnitude Plot of $|GK|$ for Stable, Nonminimum Phase System Example (Small Noise Case)

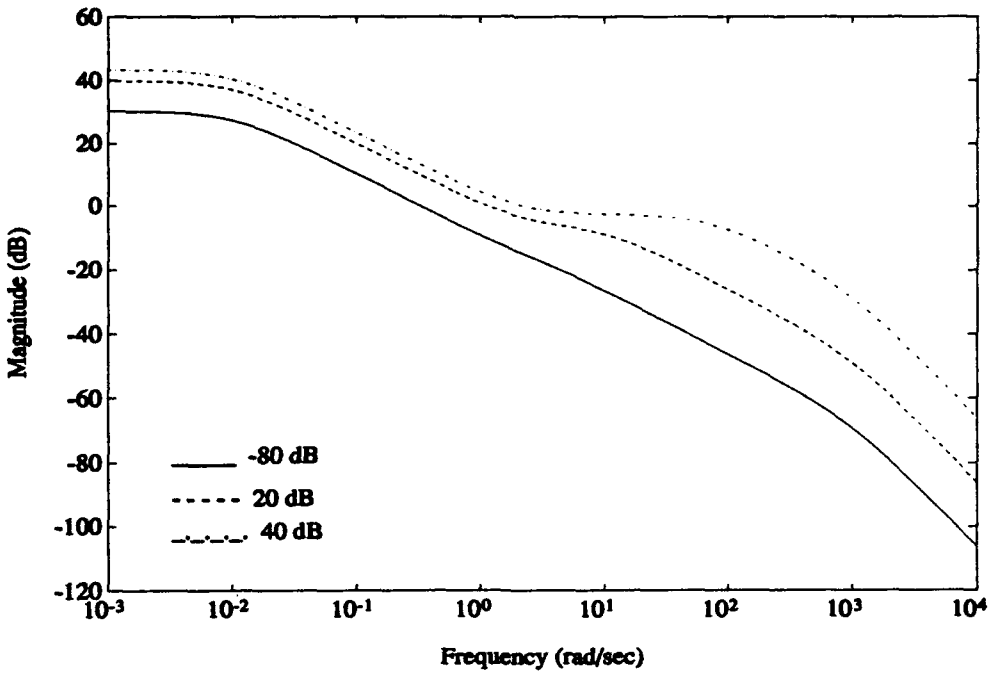

Figure 6-40. 1-DOF Bode Magnitude Plot of $|GK|$ for Stable, Nonminimum Phase System Example (Large Noise Case)

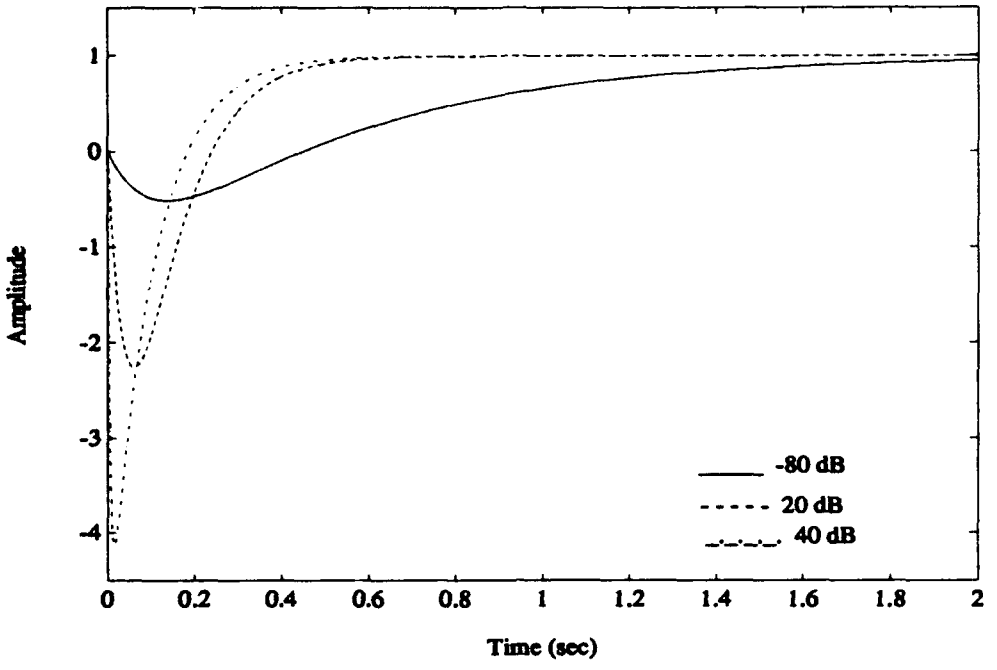

Figure 6-41. 1-DOF Step Responses for Stable, Nonminimum Phase System Example (Small Noise Case)

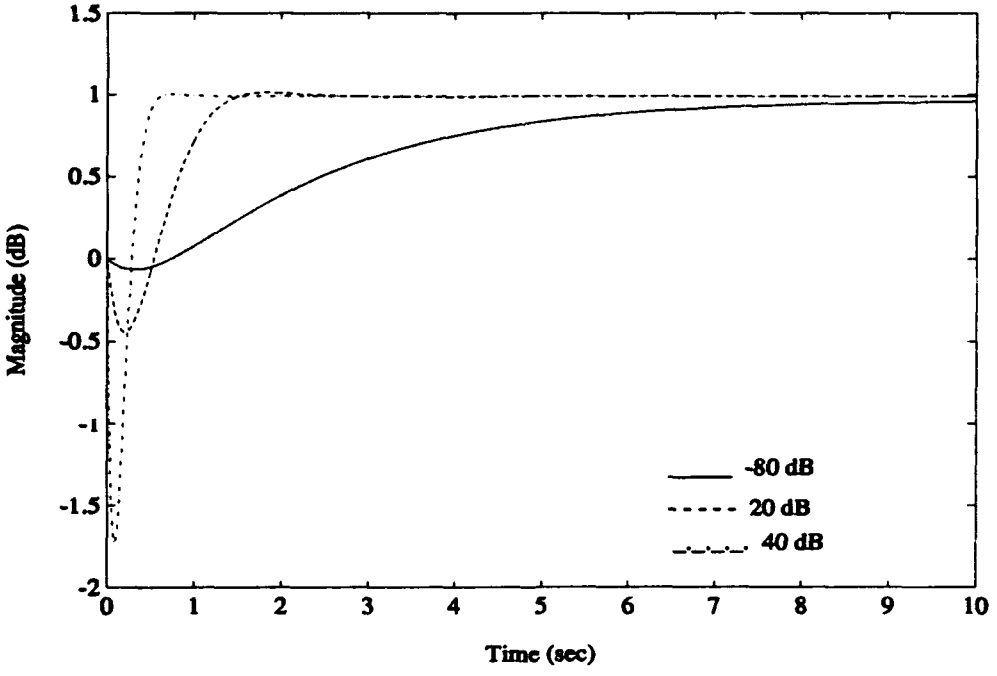

Figure 6-42. 1-DOF Step Responses for Stable, Nonminimum Phase System Example (Large Noise Case)

6.3.2 2-DOF Case. The 2-DOF sensitivity functions are plotted in Figures 6-43 and 6-44. The general shape of the plots is the same as that of "good" loop shapes (from Chapter III), but there is a significant amount of overshoot in both the small and large noise cases. The functions in the small noise case have a bit more overshoot than those in the large noise case, due the fact that the loop gain is higher overall. In the large noise-small disturbance case, the size of $|GK_1|$ is so small that $|S|$ is at 0 dB at virtually all frequencies. Figures 6-45 and 6-46 show plots of the complimentary sensitivity function. These plots also indicate the decrease in stability margins by the large increase in magnitude before rolling off. The other trends for these plots are in agreement with the previous examples.

Figures 6-47 and 6-48 show plots of $|GK_1|$ and $|GK_2|$ for the small noise case. In the small disturbance case, $|GK_1|$ exhibits high gain at low frequency and low gain at high frequency, but since the assumed disturbance level is so low, the plot is not affected by the barrier at 2 rad/sec. In the two larger disturbance cases, however, $|GK_1|$ is required to be large at low frequency, but it must also pass under the barrier at 2 rad/sec. Figures 6-49 and 6-50 show plots of $|GK_1|$ and $|GK_2|$ for the large noise case. The effect of the large noise, once again, is to drive down the size of $|GK_1|$, especially in the small disturbance case The barrier at 2 rad/sec is evident in the plots of both $|GK_1|$ and $|GK_2|$. Figure 6-51 shows a plot of $|SGK_2|$, indicating the frequency range over which the system will track commands. Figure 6-52 shows the 2-DOF step response.

6.3.3 Comparison Between 1-DOF and 2-DOF Cases. In keeping with previous trends, the plots of the sensitivity function show close agreement between the

1-DOF and 2-DOF cases when the measurement noise level is small. In the large noise case, the DC gain of $|S|$ increases more rapidly in the 2-DOF case than it does in the 1-DOF case as the size of the assumed disturbance decreases. The plots of the complimentary sensitivity function also follow previous trends, with the bandwidth frequency increasing as the assumed disturbance gets larger in the small noise case. In the large noise case, the same trends are present, but in the 2-DOF large noise-small disturbance case, the DC gain of $|T|$ is -100 dB. In the small noise case, the plots of $|GK_1|$ are very similar to the plots of $|GK|$ in the 1-DOF case, but the 2-DOF plot for the largest disturbance case rolls off at a higher frequency than the corresponding 1-DOF plot. This is because $|GK_1|$ is not constrained to any tracking requirement, and the measurement noise is not large enough to warrant holding down its size. Since the measurement noise is so small, $|GK_1|$ tends to dominate the system's behavior; thus, the shape of $|GK_2|$ is more or less the same as that of $|GK_1|$. It should be noted that both $|GK_1|$ and $|GK_2|$ still must fall beneath the barrier at 2 rad/sec to accommodate the zero at s = +2. In the large noise case, the shape of $|GK_1|$ and $|GK_2|$ follow the same pattern that they do in the other classes of examples.

The 2-DOF step response's settling time of about three seconds is not as fast as some of the 1-DOF responses (in the small noise case), but it does not have as much initial undershoot or overshoot of the final value as they do. Once again, the 2-DOF system produces the same step response, regardless of the level of the plant disturbance or measurement noise level.

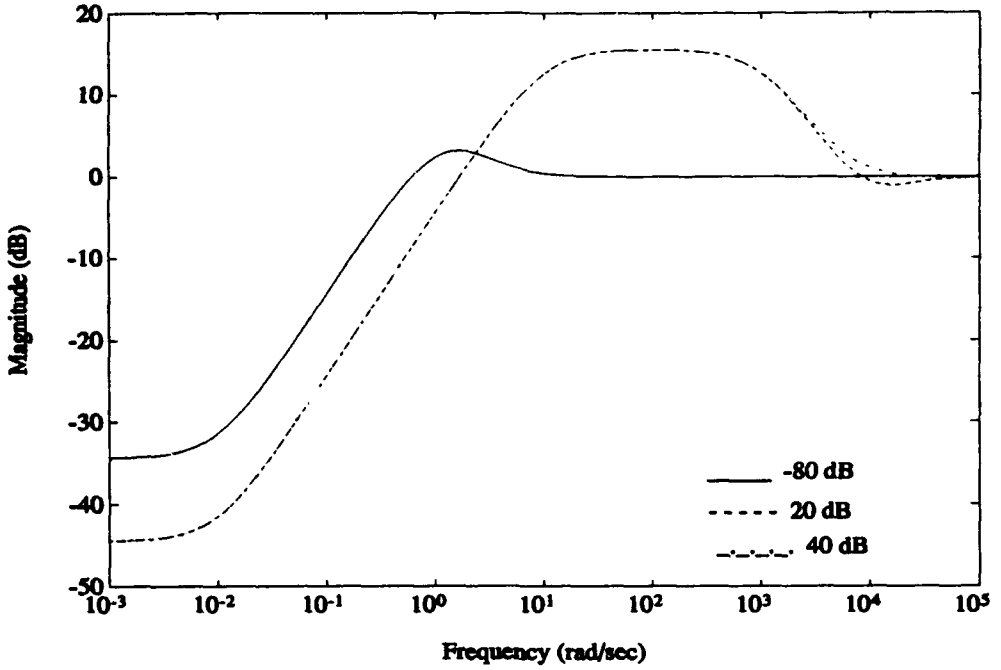

Figure 6-43. 2-DOF Bode Magnitude Plot of |S| for Stable, Nonminimum Phase System Example (Small Noise Case)

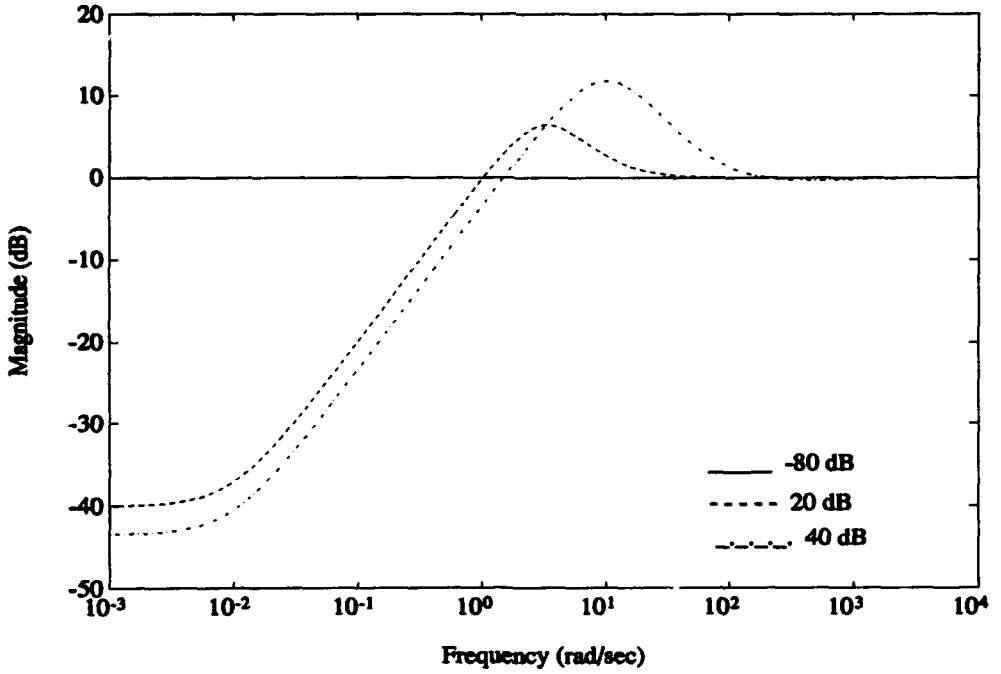

Figure 6-44. 2-DOF Bode Magnitude Plot of |S| for Stable, Nonmin[illegible]num Phase System Example (Large Noise Case)

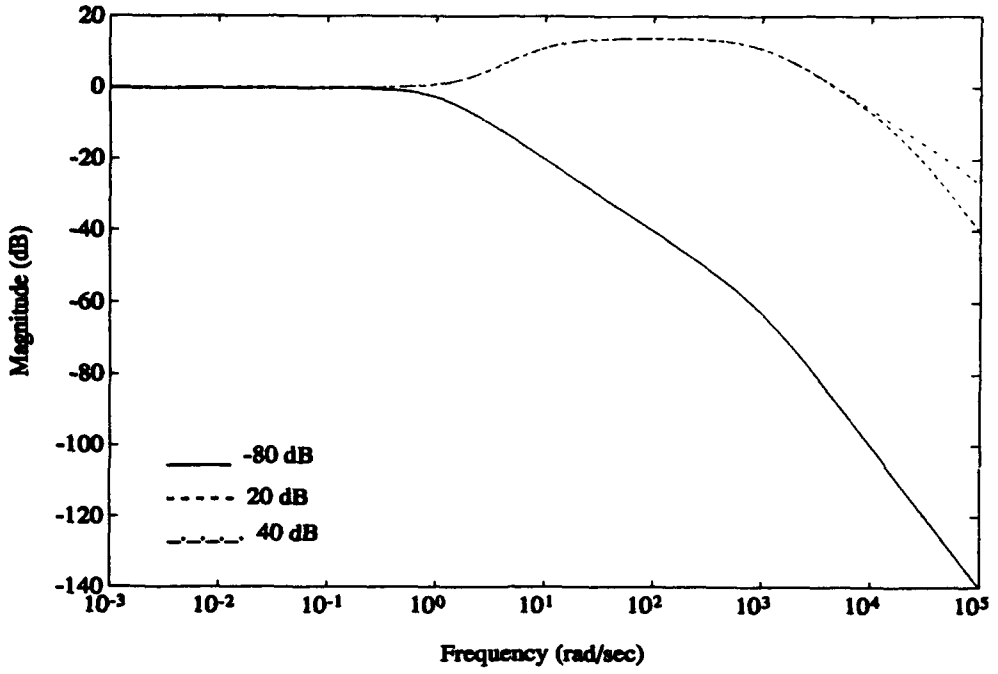

Figure 6-45. 2-DOF Bode Magnitude Plot of |T| for Stable, Nonminimum Phase System Example (Small Noise Case)

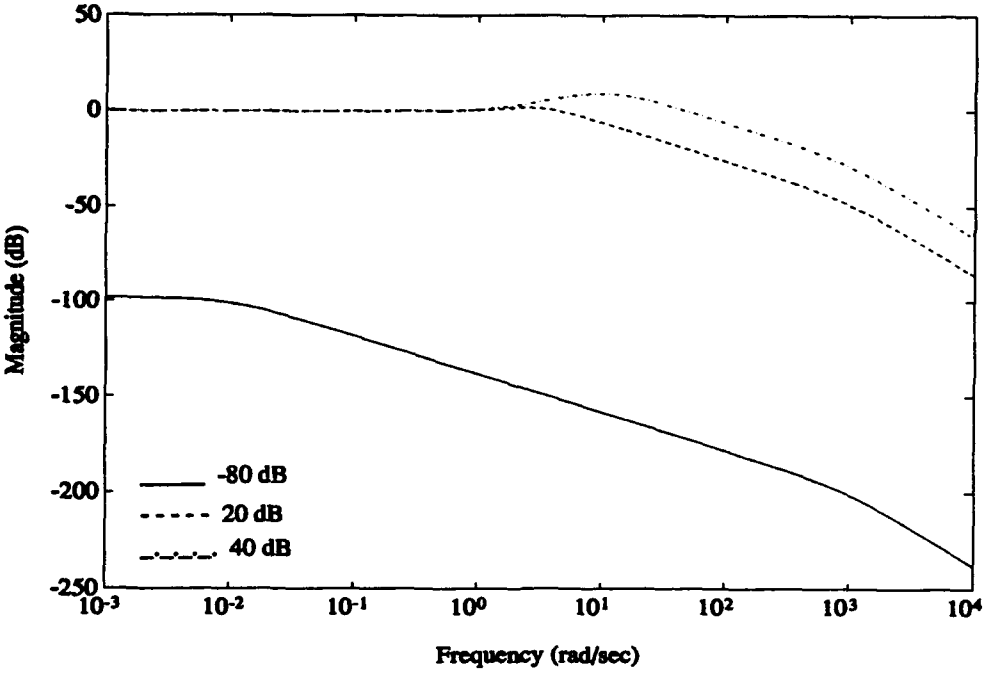

Figure 6-46. 2-DOF Bode Magnitude Plot of |T| for Stable, Nonminimum Phase System Example (Large Noise Case)

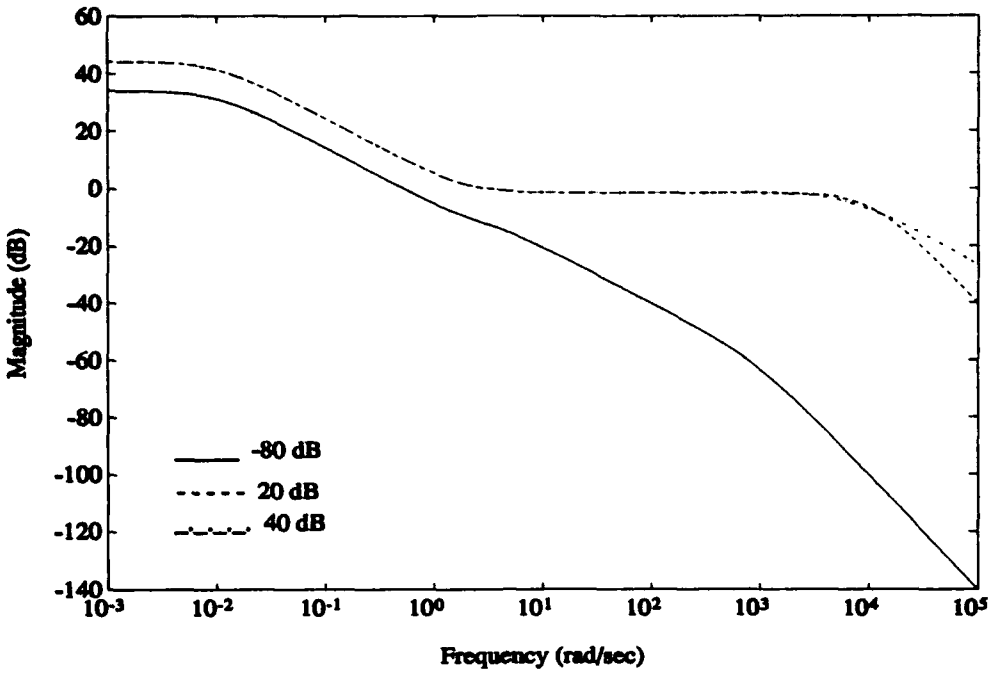

Figure 6-47. 2-DOF Bode Magnitude Plot of $|GK_1|$ for Stable, Nonminimum Phase System Example (Small Noise Case)

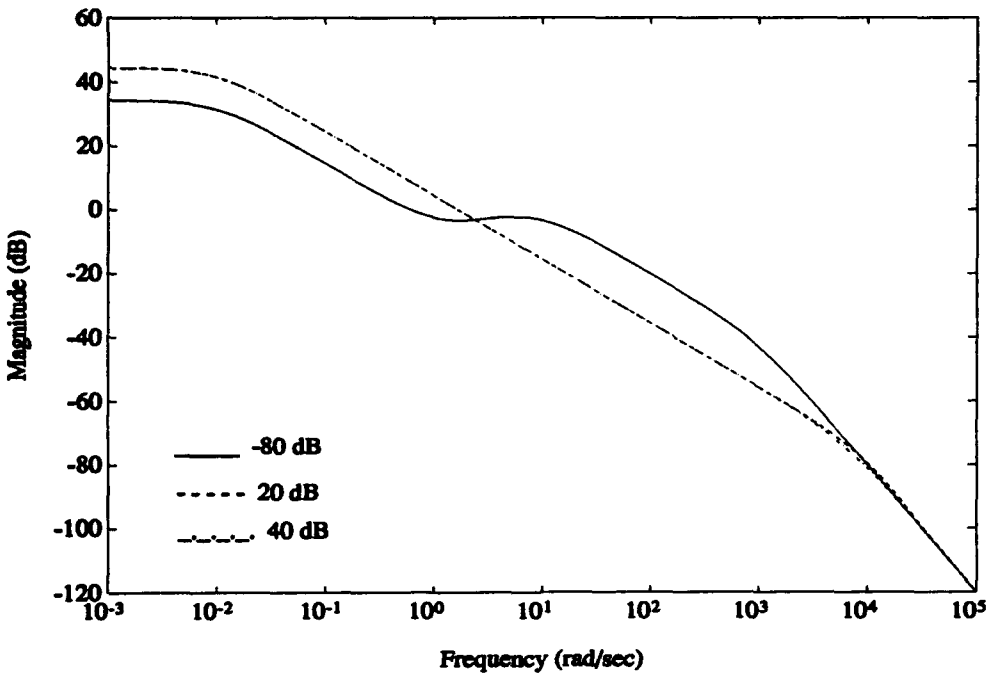

Figure 6-48. 2-DOF Bode Magnitude Plot of $|GK_2|$ for Stable, Nonminimum Phase System Example (Small Noise Case)

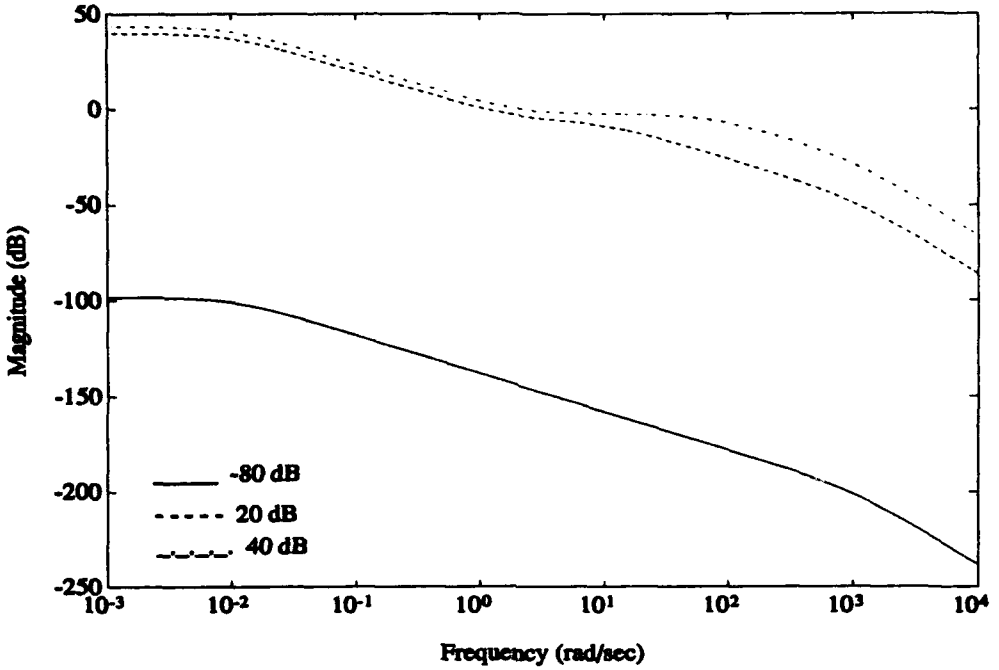

Figure 6-49. 2-DOF Bode Magnitude Plot of $|GK_1|$ for Stable, Nonminimum Phase System Example (Large Noise Case)

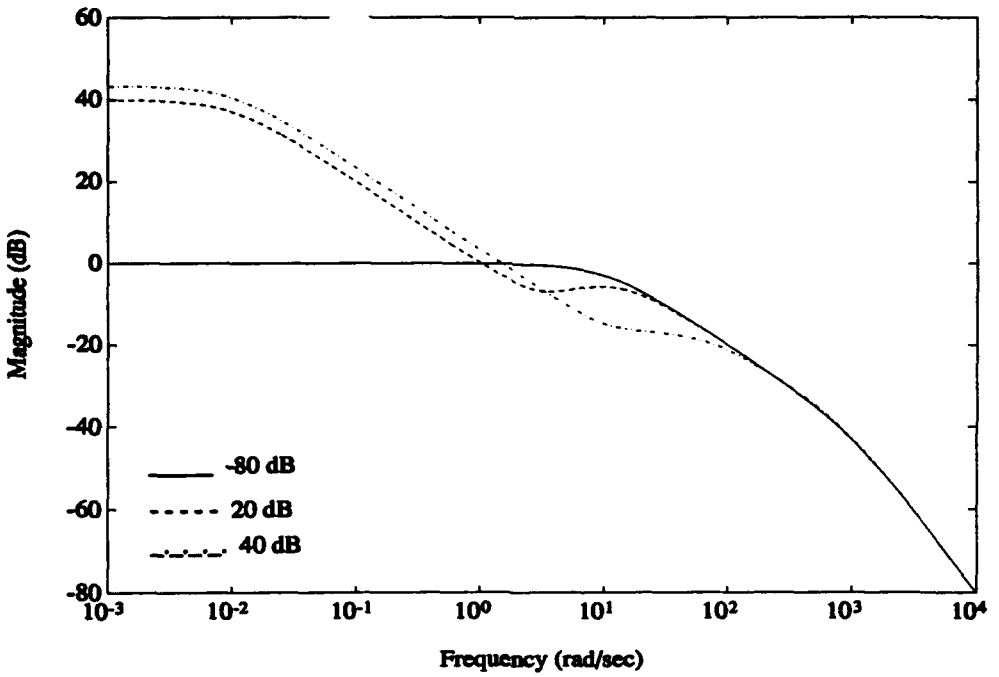

Figure 6-50. 2-DOF Bode Magnitude Plot of $|GK_2|$ for Stable, Nonminimum Phase System Example (Large Noise Case)

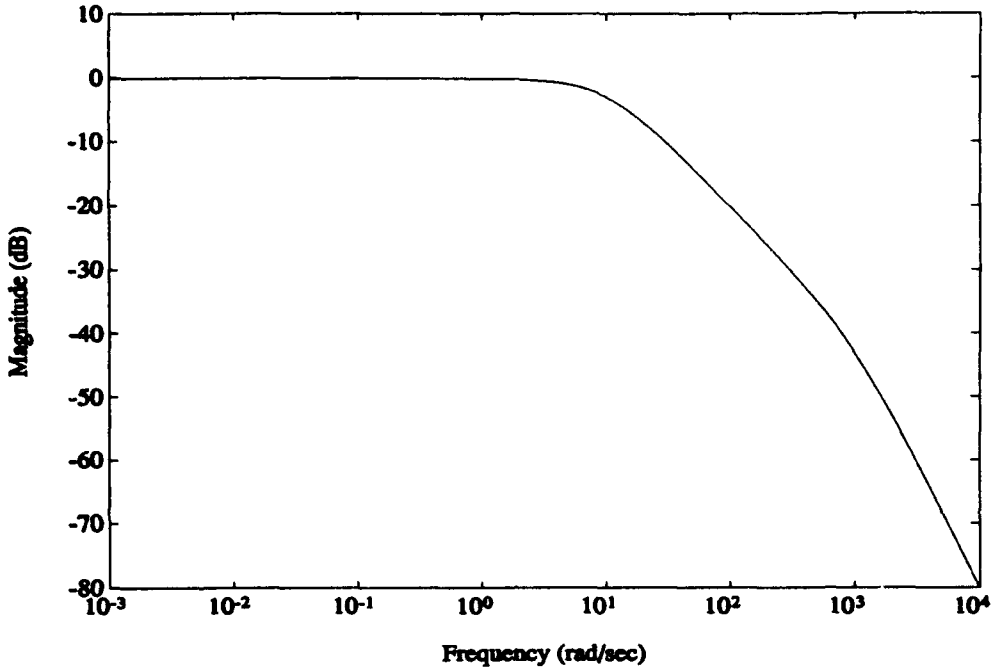

Figure 6-51. 2-DOF Bode Magnitude Plot of $|SGK_2|$ for Stable, Nonminimum Phase System Example (any size noise)

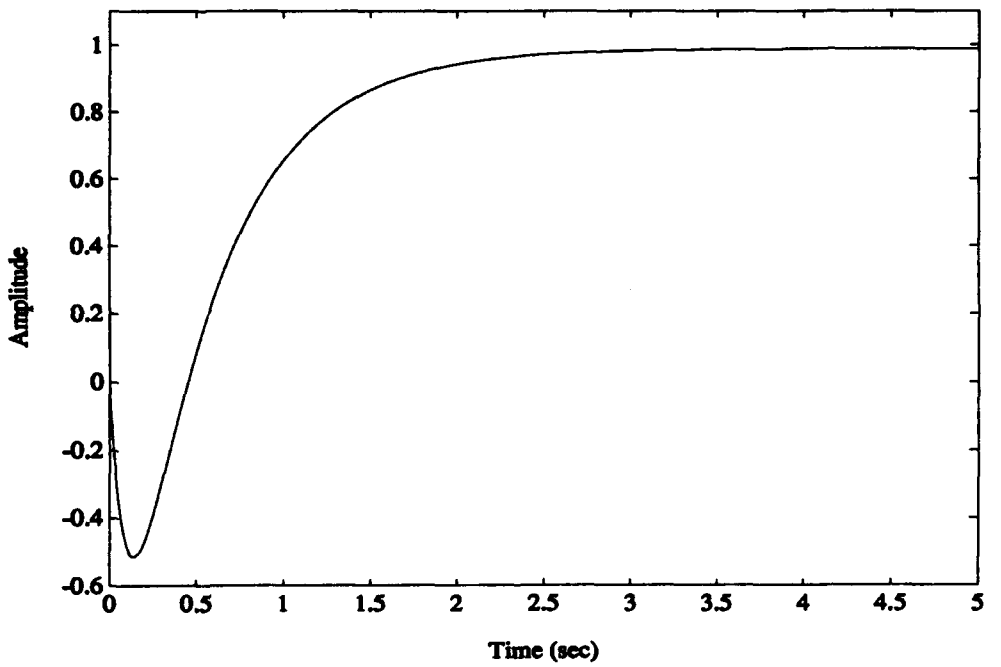

Figure 6-52. 2-DOF Step Response for Stable, Nonminimum Phase System Example (any size noise)

6.4 Unstable, Nonminimum Phase System

6.4.1 1-DOF Case. Figures 6-53 and 6-54 show plots of the sensitivity function. They are very similar to the stable, nonminimum phase case, but the functions do not get as small at low frequency, and the overshoot is much more pronounced. The presence of right-half plane poles *and* zeros erodes the stability margins more than in any other case, and the size of $|GK|$ is held down overall as a result. The graphs of the complimentary sensitivity function, in figures 6-55 and 6-56, add further evidence of low stability margins, with bigger increases in magnitude before rolling off. The shape of $|GK|$ (Figures 6-57 and 6-58) reiterates the requirement that the function stay below 0 dB at the 2 rad/sec nonminimum phase zero frequency. In the small noise-large disturbance case, the function "lips up" above 0 dB at 2000 rad/sec in an effort to regain some overall energy before rolling off, even though it still avoids violating the barrier at 2 rad/sec.

The 1-DOF step responses are shown in Figures 6-59 and 6-60. These responses exhibit characteristics of both unstable and nonminimum phase behavior, as expected, and show the same general trends as the stable, nonminimum phase case. In the small noise case, the initial undershoot increases as the level of the assumed plant disturbance increases. In the large noise case, the initial undershoot also increases, but the subsequent overshoot of the final value decreases slightly, as the assumed disturbance level increases.

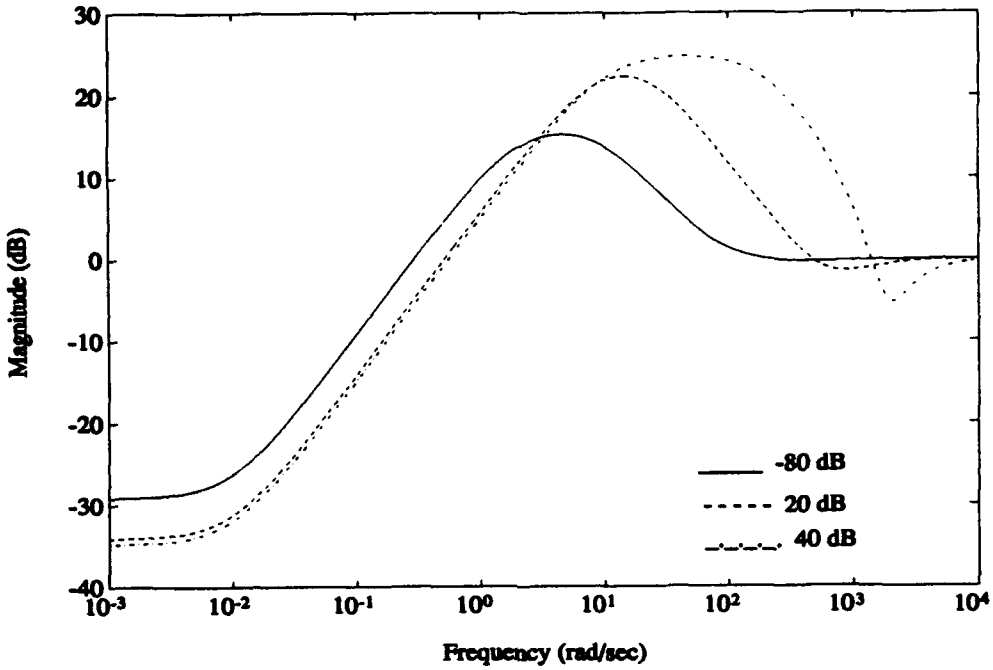

Figure 6-53. 1-DOF Bode Magnitude Plot of |S| for Unstable, Nonminimum Phase System Example (Small Noise Case)

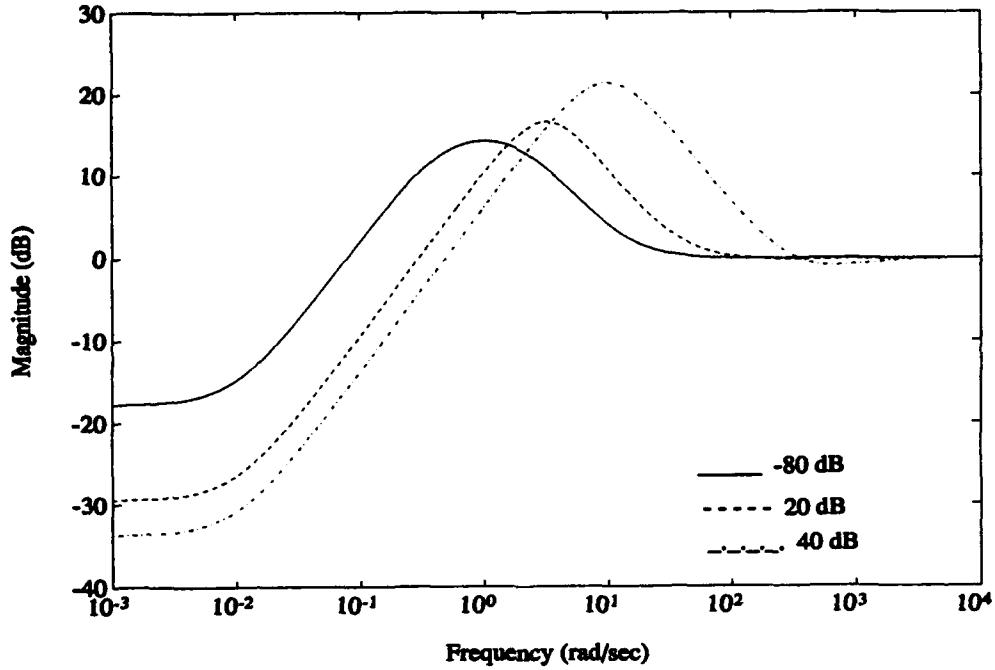

Figure 6-54. 1-DOF Bode Magnitude Plot of |S| for Unstable, Nonminimum Phase System Example (Large Noise Case)

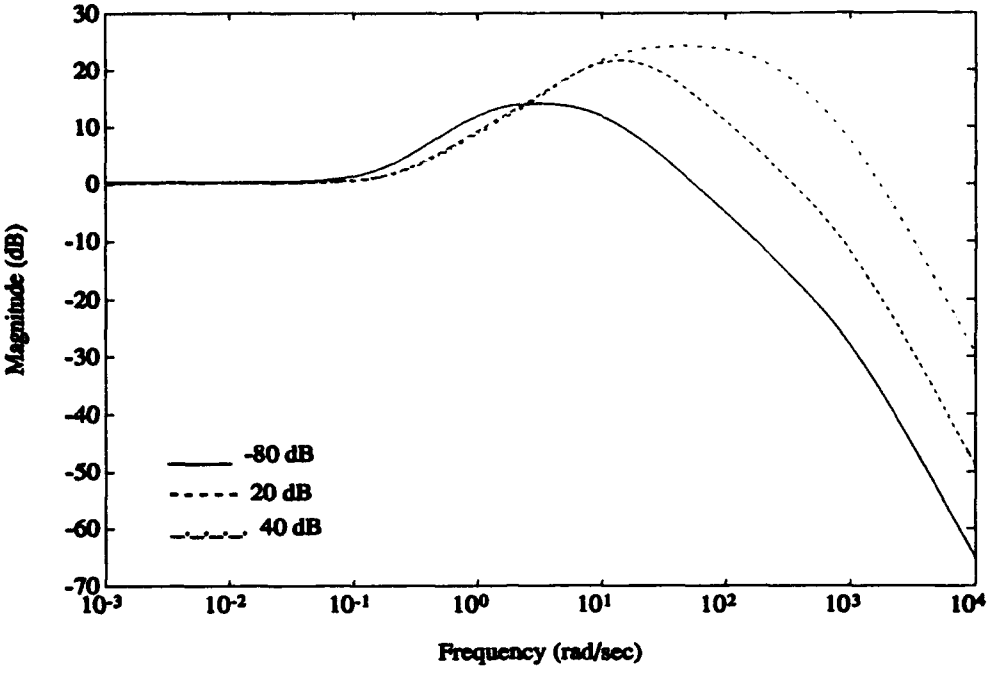

Figure 6-55. 1-DOF Bode Magnitude Plot of $|T|$ for Unstable, Nonminimum Phase System Example (Small Noise Case)

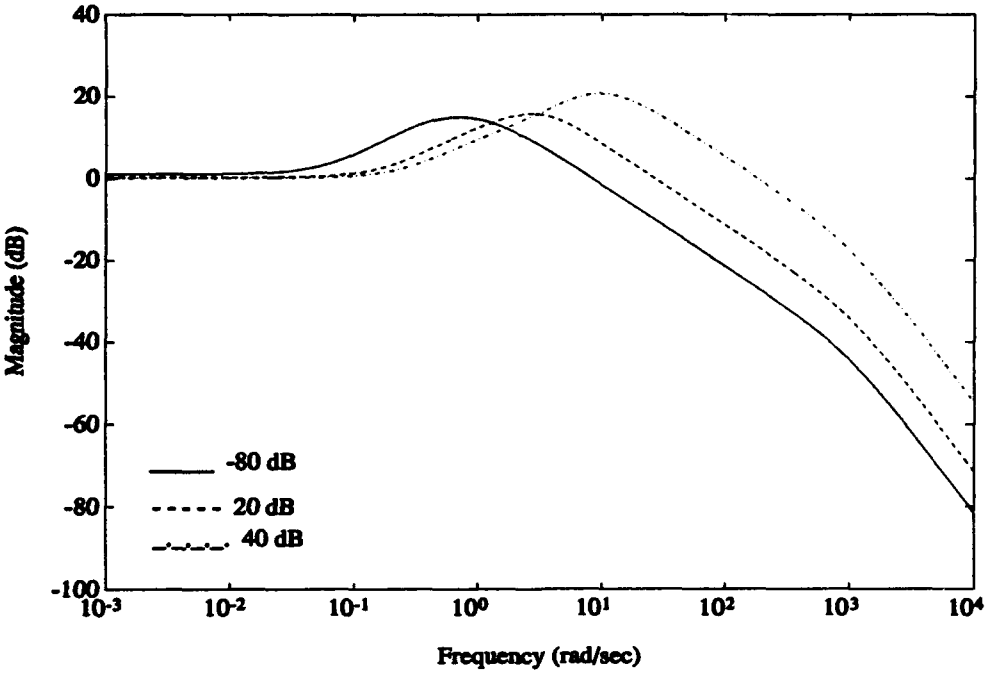

Figure 6-56. 1-DOF Bode Magnitude Plot of $|T|$ for Unstable, Nonminimum Phase System Example (Large Noise Case)

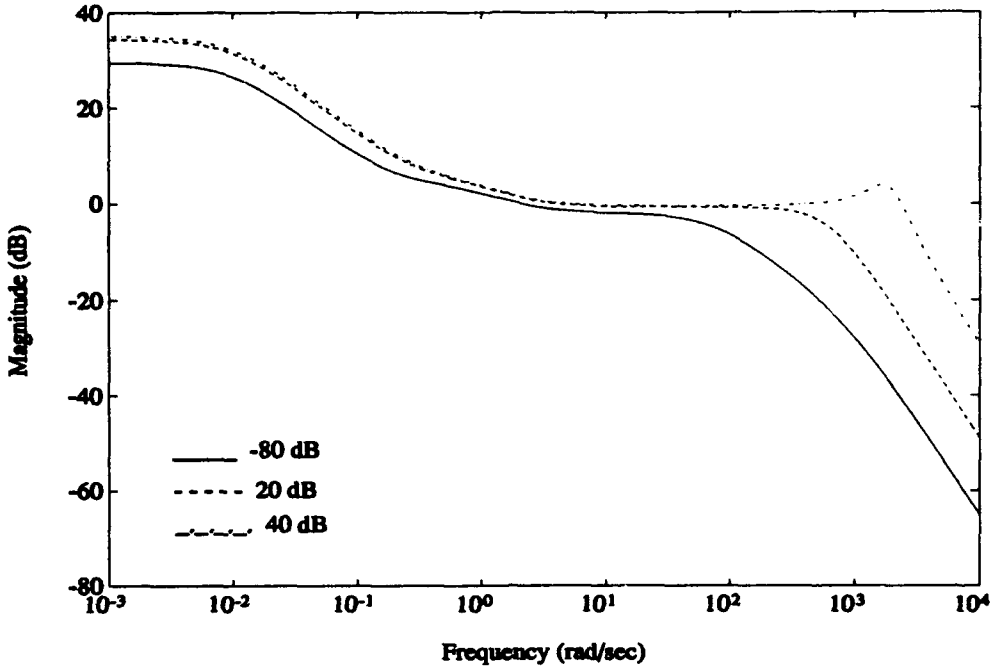

Figure 6-57. 1-DOF Bode Magnitude Plot of $|GK|$ for Unstable, Nonminimum Phase System Example (Small Noise Case)

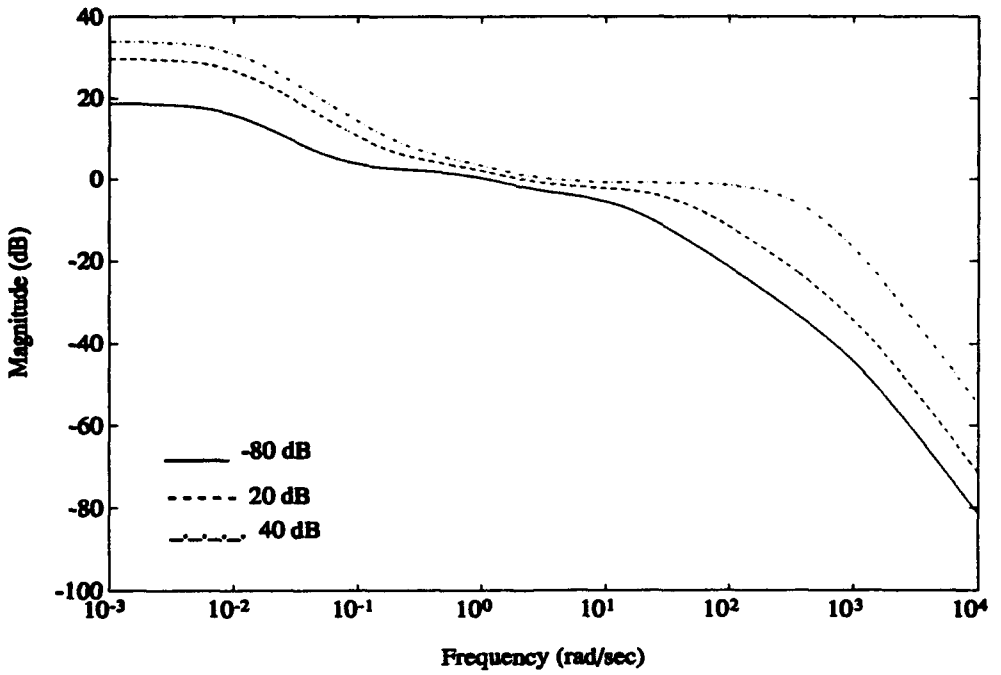

Figure 6-58. 1-DOF Bode Magnitude Plot of $|GK|$ for Unstable, Nonminimum Phase System Example (Large Noise Case)

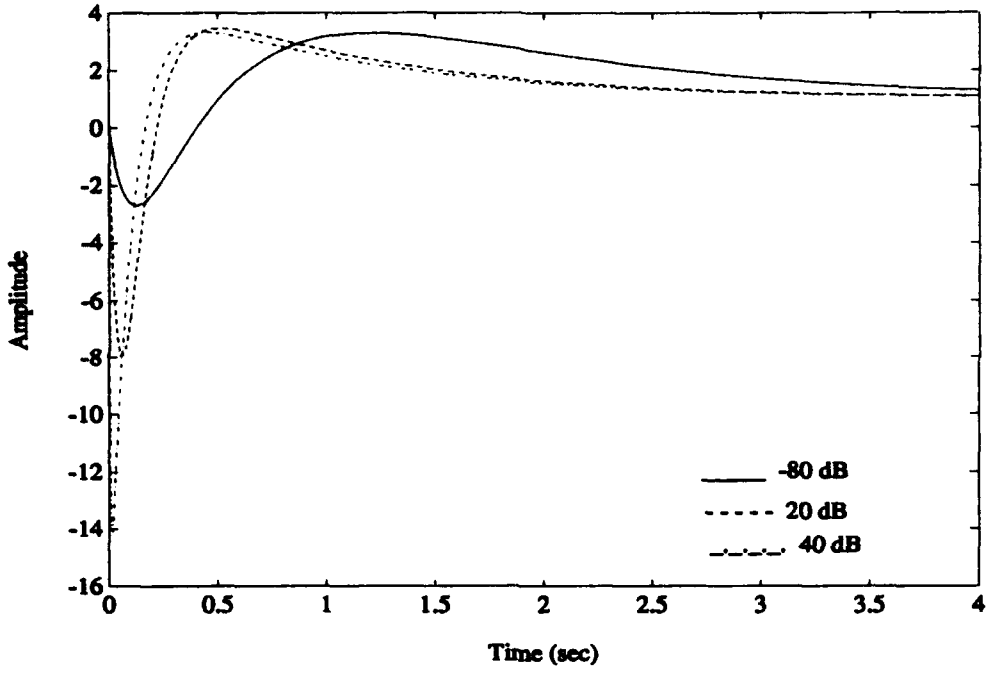

Figure 6-59. 1-DOF Step Responses for Unstable, Nonminimum Phase System Example (Small Noise Case)

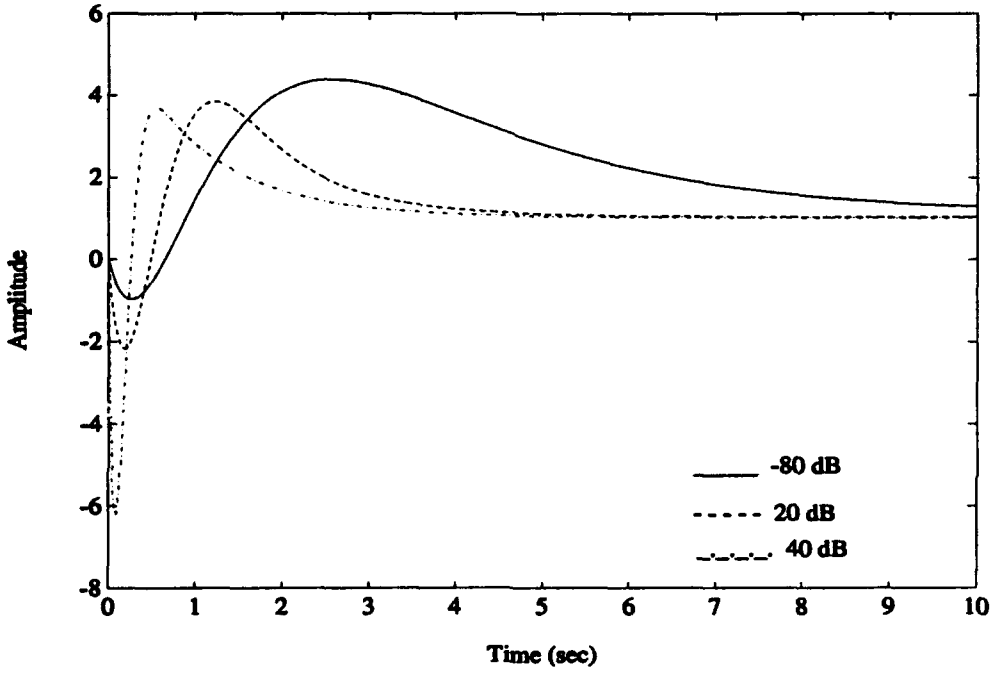

Figure 6-60. 1-DOF Step Responses for Unstable, Nonminimum Phase System Example (Large Noise Case)

6.4.2 2-DOF Case. The plots of the sensitivity function are shown in Figures 6-61 and 6-62. The primary difference in these plots from the other 2-DOF examples is that the overshoot above 0 dB is much higher, indicating worse stability margins. In the large noise-small disturbance case, the DC gain of $|S|$ is about 13 dB, showing how small $|GK_1|$ must be at low frequency to accommodate the large noise. Figures 6-63 and 6-64 show plots of the complimentary sensitivity function. In the large noise-small disturbance case, the DC gain of $|T|$ is also above 0 dB (this time at about 18 dB). The other trends are unchanged from the previous examples.

Figures 6-65 and 6-66 show plots of $|GK_1|$ and $|GK_2|$ for the small noise case, and Figures 6-67 and 6-68 show plots of $|GK_1|$ and $|GK_2|$ for the large noise case. The only significant difference between these plots and those of the stable, nonminimum phase system is the large noise-small disturbance case of $|GK_2|$. In this case, the DC gain of the function is at about -15 dB instead of the normal 0 dB, which shows the flexibility of the shape of $|GK_2|$ in taking on whatever magnitude is necessary to track the command input. In both the large and small noise cases, the plots fall below 0 dB before they reach 1 rad/sec so that no energy is put into the system at the frequencies of the unstable pole or zero.

The plots of $|SGK_2|$ and the 2-DOF step response are identical to Figures 6-51 and 6-52, respectively.

6.4.3 Comparison Between 1-DOF and 2-DOF Cases. The unstable, nonminimum phase system example represents the most challenging of the SISO examples presented. Thus, the loop shape plots exhibit all of the characteristics associated with right-half plane poles and zeros. Both the 1-DOF and the 2-DOF

systems show a great deal of overshoot above the 0 dB line in the sensitivity and complimentary sensitivity plots. As in the other types of examples, when the assumed noise is large compared to the plant disturbance in the 2-DOF case, the DC gain of S becomes larger (as in the 1-DOF case), and in some cases, it is above 0 dB (which does not occur in the 1-DOF case). In the complimentary sensitivity plots, the 2-DOF case shows that as the assumed noise becomes larger relative to the disturbance, the rolloff frequency decreases (as in the 1-DOF case), and in the smallest disturbance case, the DC gain of $|T|$ is above 0 dB (which does not occur in the 1-DOF case). The most noticeable difference between the 1-DOF and 2-DOF system is, once again, in the step responses. In the 1-DOF case, the responses exhibit increasing initial undershoot as the assumed disturbance level increases (due to the nonminimum phase zeros), as well as significant overshoot of the final value (due to the unstable poles). The 2-DOF system, however, utilizes the capabilities of the prefilter to maintain tracking over a wide frequency range and still produces the optimal step response for the given tracking weight, which, for this case, exhibits minimum initial undershoot and no overshoot of the final value.

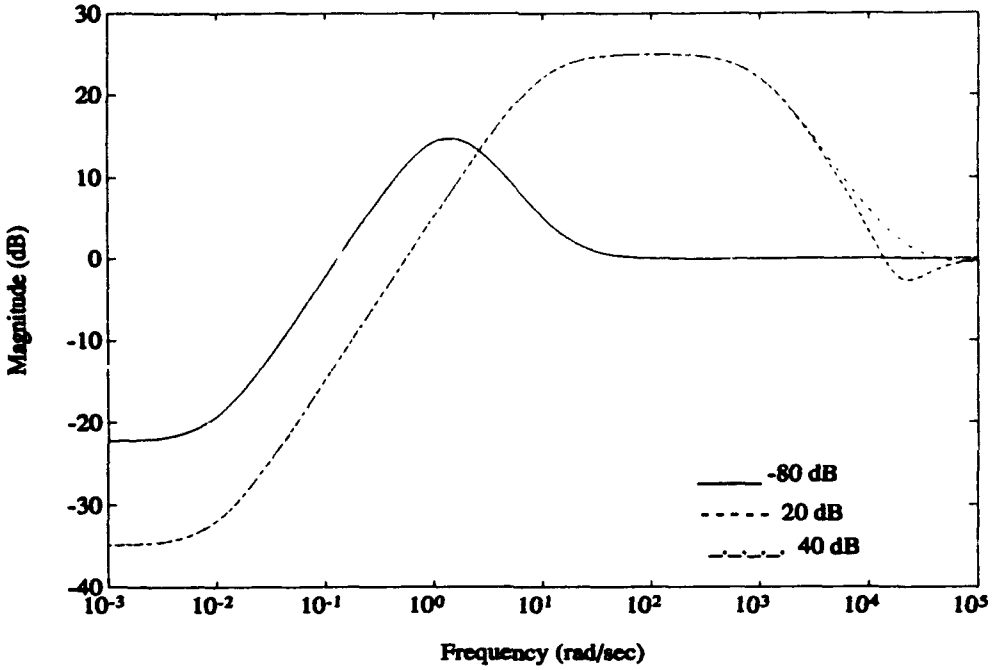

Figure 6-61. 2-DOF Bode Magnitude Plot of |S| for Unstable, Nonminimum Phase System Example (Small Noise Case)

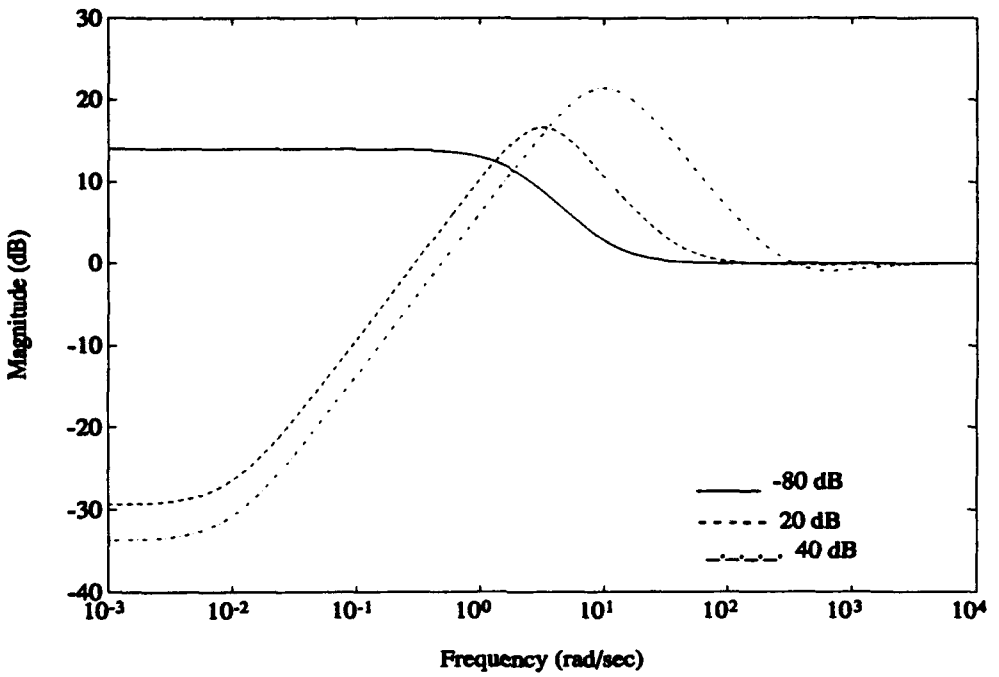

Figure 6-62. 2-DOF Bode Magnitude Plot of |S| for Unstable, Nonminimum Phase System Example (Large Noise Case)

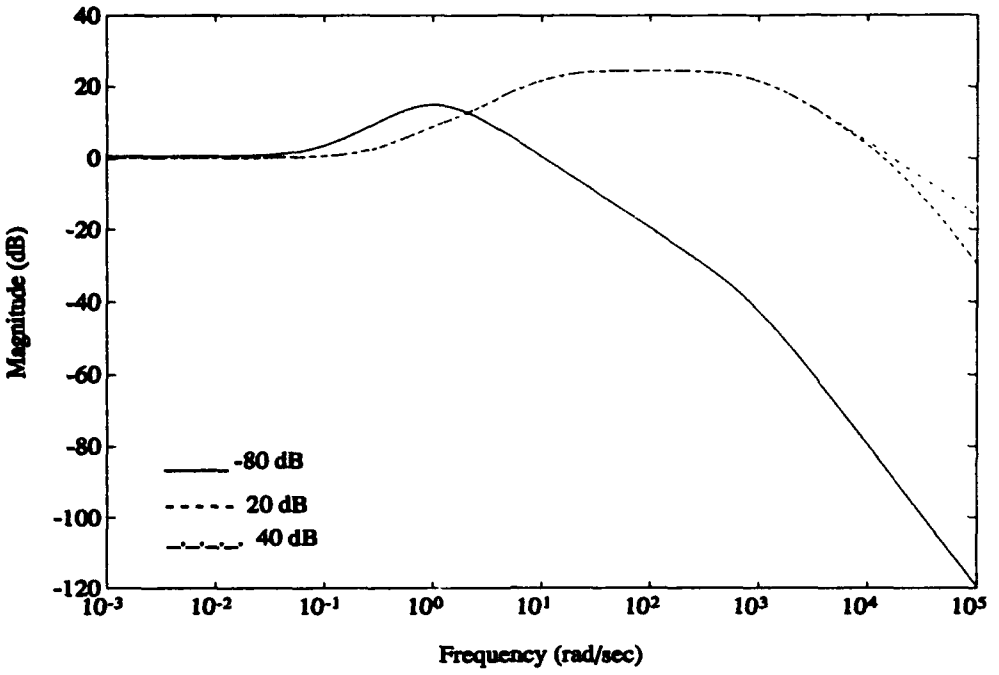

Figure 6-63. 2-DOF Bode Magnitude Plot of $|T|$ for Unstable, Nonminimum Phase System Example (Small Noise Case)

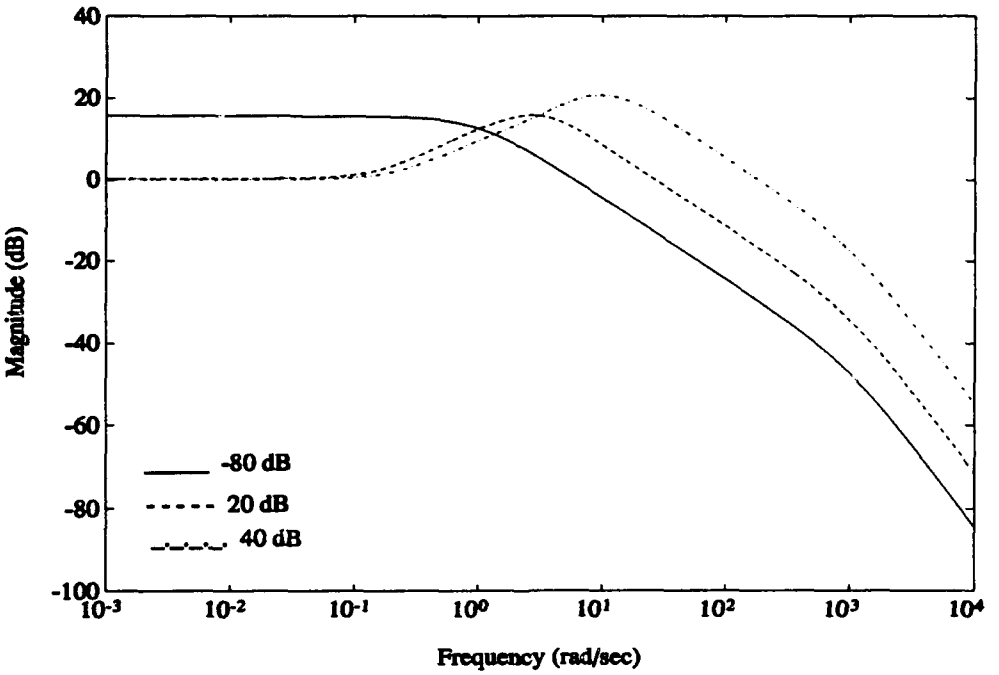

Figure 6-64. 2-DOF Bode Magnitude Plot of $|T|$ for Unstable, Nonminimum Phase System Example (Large Noise Case)

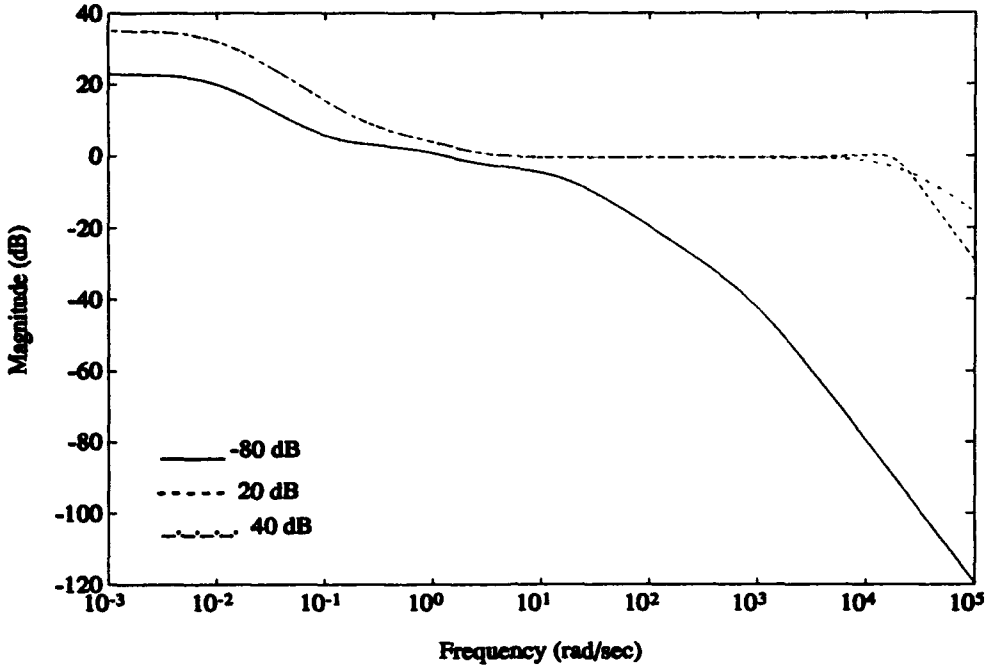

Figure 6-65. 2-DOF Bode Magnitude Plot of $|GK_1|$ for Unstable, Nonminimum Phase System Example (Small Noise Case)

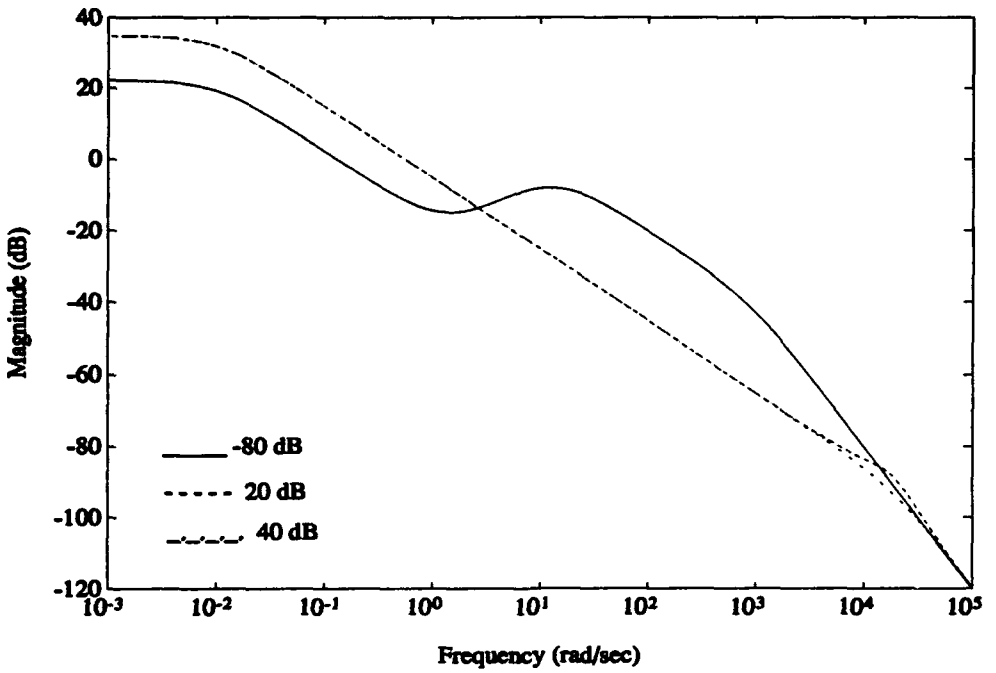

Figure 6-66. 2-DOF Bode Magnitude Plot of $|GK_2|$ for Unstable, Nonminimum Phase System Example (Small Noise Case)

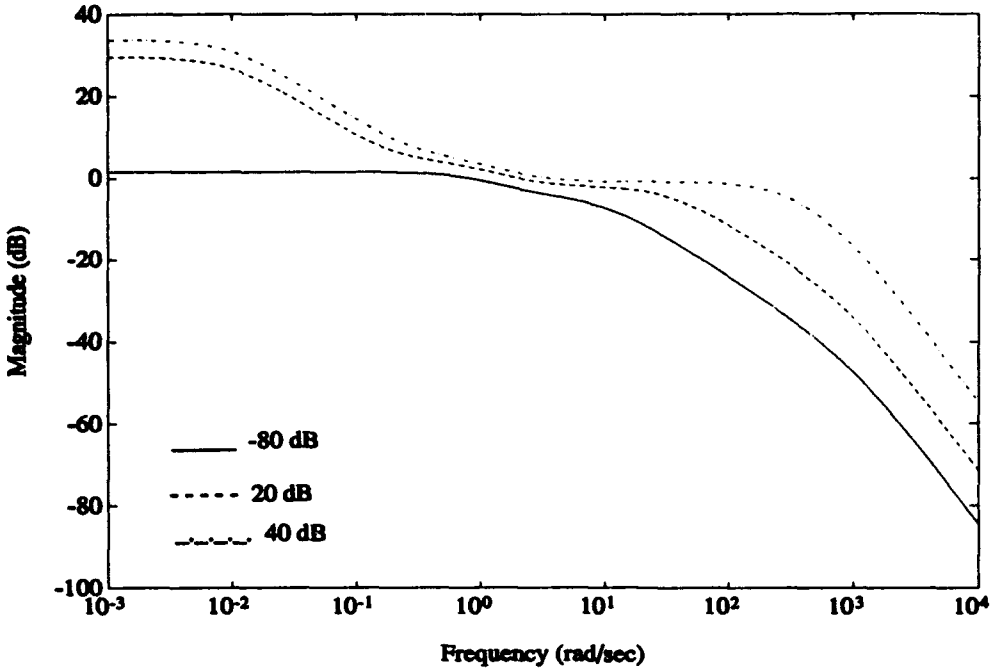

Figure 6-67. 2-DOF Bode Magnitude Plot of $|GK_1|$ for Unstable, Nonminimum Phase System Example (Large Noise Case)

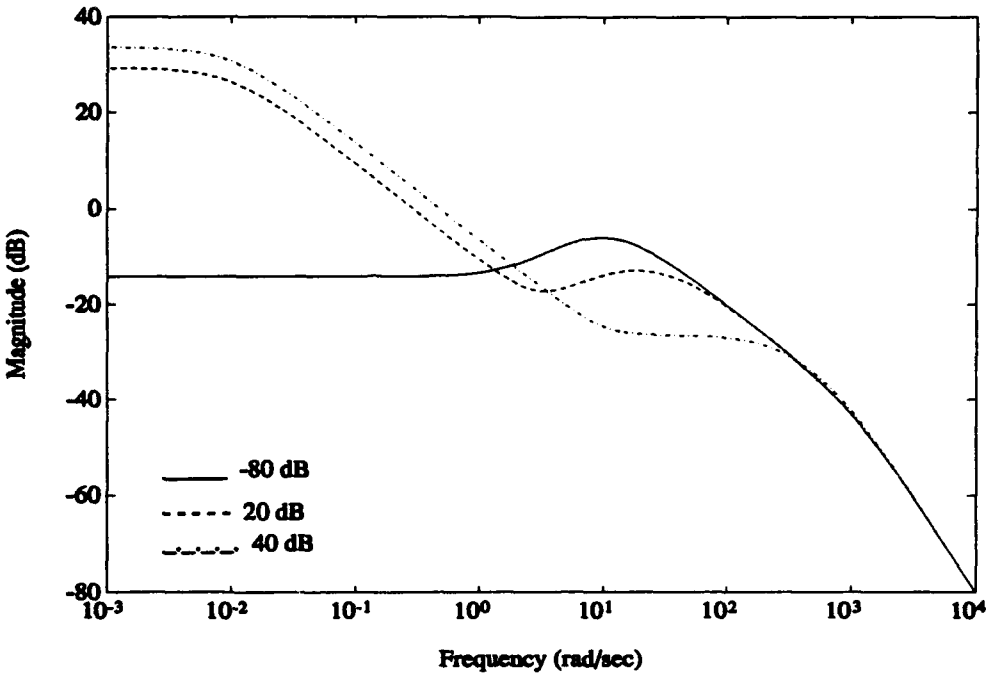

Figure 6-68. 2-DOF Bode Magnitude Plot of $|GK_2|$ for Unstable, Nonminimum Phase Example (Large Noise)

6.5 System Type Examples

In this section, the effects of applying different inputs to both 1-DOF and 2-DOF systems are investigated to find out whether 2-DOF systems offer the same advantages that they do when the input is only a step. The example to be used is the unstable, nonminimum phase plant from section 6.4, looking only at the large noise case. This plant was chosen because it is the most challenging to control, and the differences between the 1-DOF and 2-DOF time responses are the most obvious (especially in the large noise case).

Recall from Chapters II and III that system type is defined as the degree of the polynomial input for which the steady state error is equal to a non-zero constant. Furthermore, if the system is type 0, then it produces a constant error to a step input; if the system is type I, then it tracks a step input perfectly and produces a constant error to a ramp input; if the system is type II, then it tracks step and ramp inputs perfectly and produces a constant error to a parabolic input; and so on. These concepts are repeated here because they have a direct bearing on what is expected in the time response plots for the aforementioned example.

Also, recall from Chapter V that the tracking weight, W_3, in the H_2 optimization setup can also be used to shape the tracking behavior of the system with regard to system type. If W_3 resembles an integrator, then the system will exhibit type I behavior; if it resembles a ramp input, then the system will exhibit type II behavior; etc. The shaping of W_3 is the method that will be used to produce the various system types in both the 1-DOF case and the 2-DOF case. In both cases, the number of low frequency poles near the origin used to model W_3 is directly proportional to the

number of low frequency poles near the origin in the resulting compensator. It should be noted that in the 2-DOF case, the number of poles at or near the origin in either K_1 or K_2 cannot necessarily be attributed to system type behavior, in general. Since H_2 compensators are being utilized, however, K_1 and K_2 share the same poles, and in this particular case, the number of poles at or near the origin in the compensators has a direct bearing on the system type behavior. For comparison purposes, the following values for the tracking weight were utilized to produce the various system type behaviors (through type III):

$$W_3 = \frac{10}{s + 0.001} \qquad (Type\ I) \tag{6.5}$$

$$W_3 = \frac{100}{(s + 0.001)^2} \qquad (Type\ II) \tag{6.6}$$

$$W_3 = \frac{1000}{(s + 0.001)^3} \qquad (Type\ III) \tag{6.7}$$

These weights are plotted in Figure 6-69. Since the only performance characteristic of interest regarding system type is the ability of the system to track different inputs, the only plots that will be presented in this section will be time response plots.

6.5.1 Type I System. The examples presented in this chapter in sections 6.1 through 6.4 were essentially type I systems. In all cases, the tracking weight had a pole at s = -0.01. In these system type examples, the pole(s) was moved a bit closer to the origin (to s = -0.001) just to illustrate the effect of having the poles of the compensator very close to the origin.

Figures 6-70 and 6-71 show the step responses of the 1-DOF and 2-DOF systems, respectively. The 1-DOF response is almost identical to Figure 6-60, in that

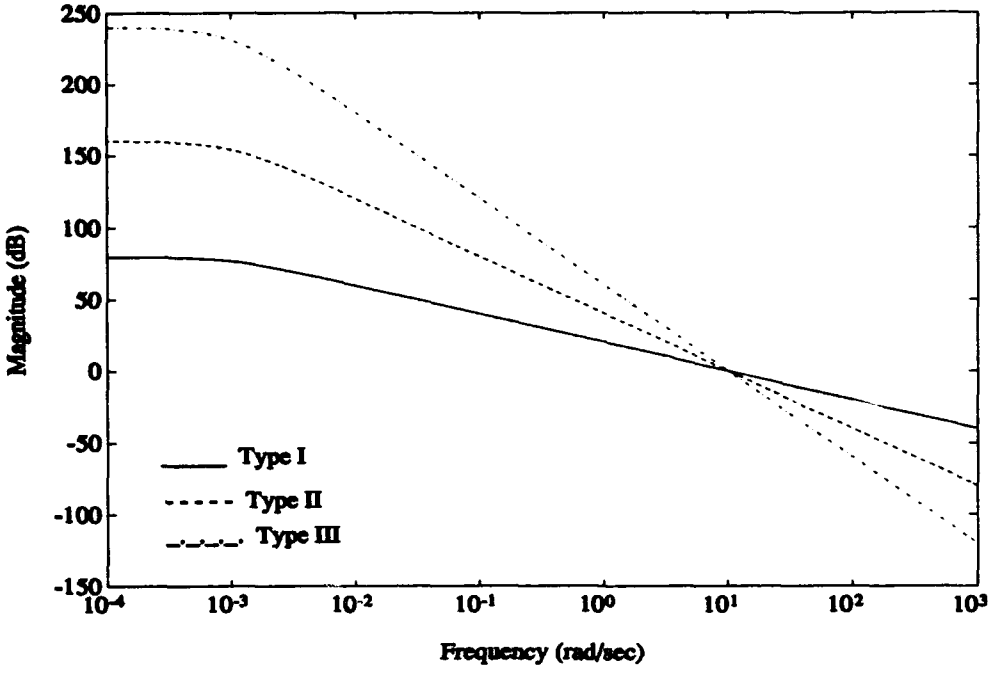

Figure 6-69. Bode Magnitude Plot of Tracking Weights for System Type Examples

it exhibits extreme nonminimum phase behavior (initial undershoot) and overshoot of the final value. The trends in the response for the increasing disturbance are as previously described -- as the disturbance size increases, the initial undershoot increases and the settling time gets faster. Depending on the disturbance, this system settles out between 4 and 10 seconds, with its oscillatory motion ranging from -6 to +4.25. The 2-DOF step response exhibits no overshoot of the final value, settles out in about 3 seconds, and shows an initial undershoot of -0.5. Clearly, the 2-DOF system produces a much more favorable step response in this case (note scale changes to emphasize differences).

The errors to a ramp input are shown in Figures 6-72 and 6-73. These errors

are expected to reach a constant non-zero value for both systems since they are both type I. The 2-DOF system steadies out in under three seconds at a value of +1.1. The 1-DOF system steadies out between 6 and 25 seconds, at values ranging from -2 to -13. The overshoot for all three disturbance sizes is about 1.8.

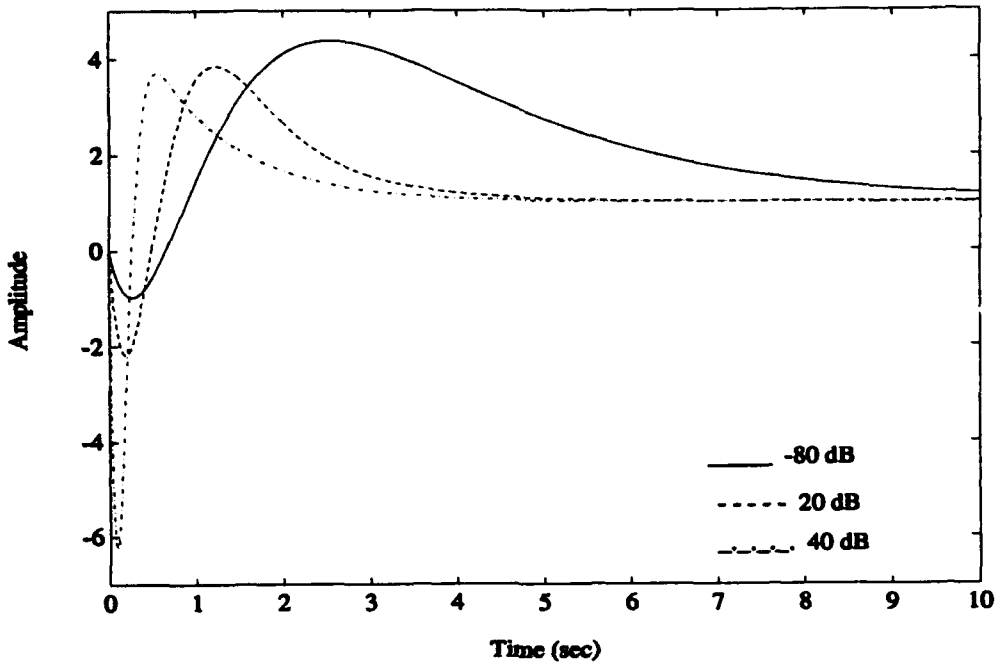

Figure 6-70. 1-DOF Step Responses for Type I System Example

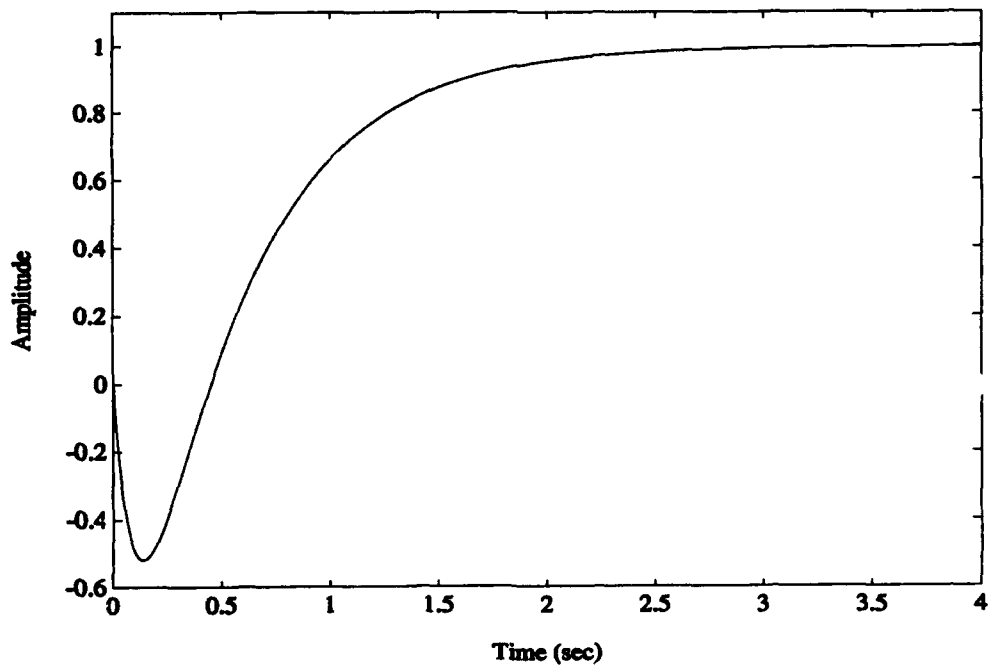

Figure 6-71. 2-DOF Step Response for Type I System Example

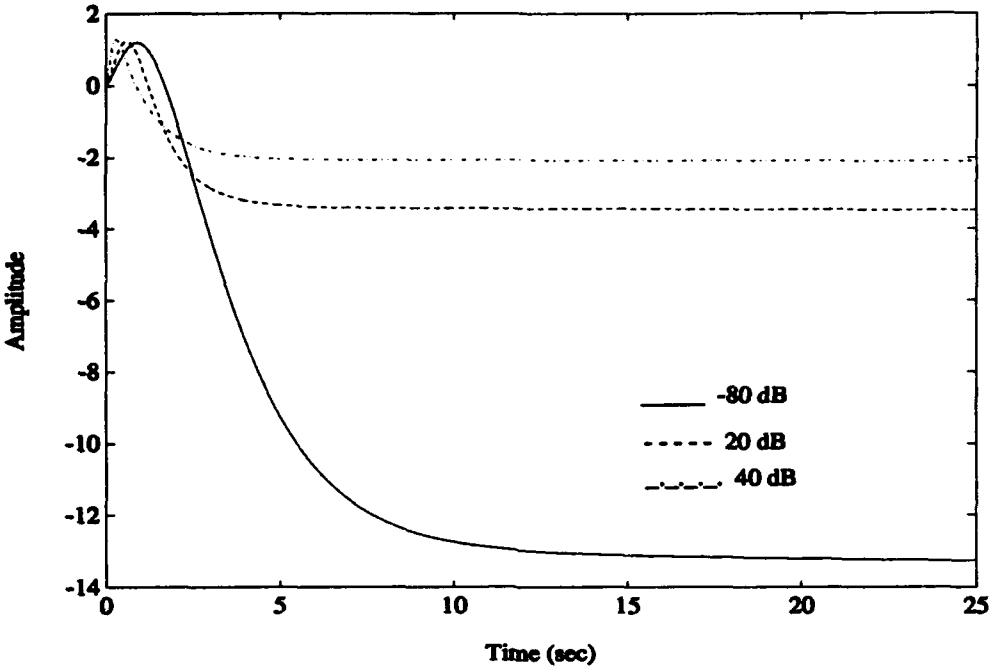

Figure 6-72. 1-DOF Error Responses to a Ramp Input (Type I System Example)

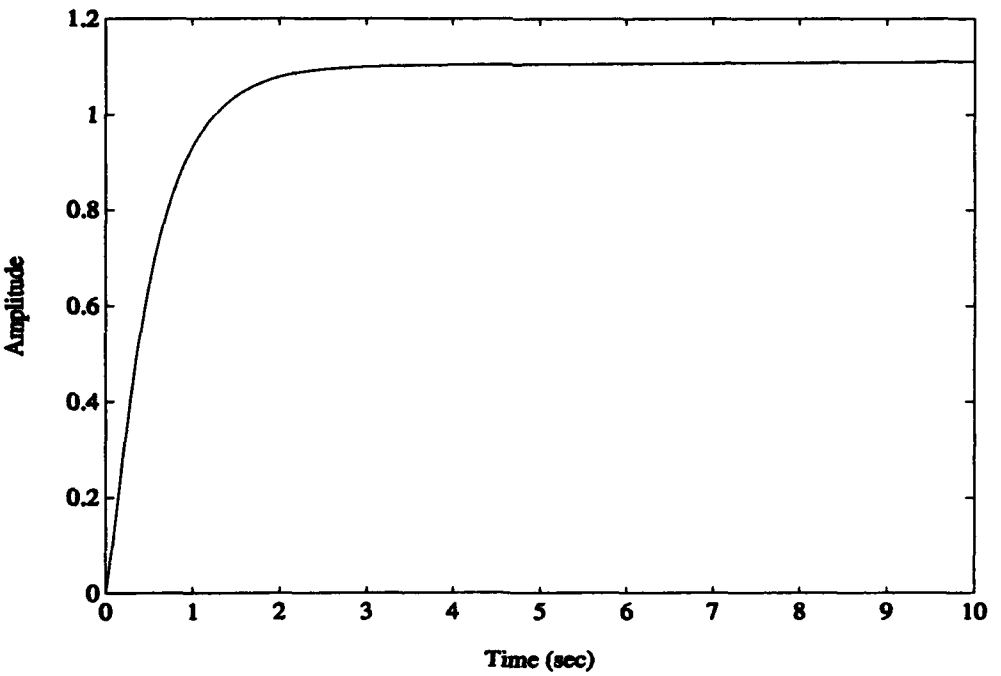

Figure 6-73. 2-DOF Error Response to a Ramp Input (Type I System Example)

6.5.2 Type II System. For this case, another pole near the origin has been added to the tracking weight, producing an additional equivalent pole in the compensator of both systems. The 1-DOF and 2-DOF step responses are shown in Figures 6-74 and 6-75. In the 1-DOF case, the responses all settle out in about 4-5 seconds, which is a marked improvement over the type I case, but the oscillatory motion is much greater, especially in the large disturbance case. It ranges between -30 and +22. The 2-DOF response shows the same trend by showing a quicker settling time of 2.5 seconds and more oscillatory motion than in the type I case, ranging from -4.1 to +2.5.

The ramp error responses are shown in Figures 6-76 and 6-77. Because these are now type II systems, they now track ramp commands perfectly. Depending on the disturbance level, the 1-DOF system settles out at zero between 5 and 15 seconds, with oscillatory motion ranging between -2.1 and +3.2. The 2-DOF system settles out at zero in about 3 seconds, with an initial overshoot of +0.9.

The parabola error responses are shown in Figures 6-78 and 6-79. As expected, both systems produce constant errors to a parabolic inputs. The 1-DOF system settles out between 4 and 15 seconds at values between -16.5 and -2.2. The small disturbance case is significantly slower and has a larger error than the two larger disturbances. The 2-DOF system settles out in about 3 seconds at a value of 1.3, with no initial undershoot.

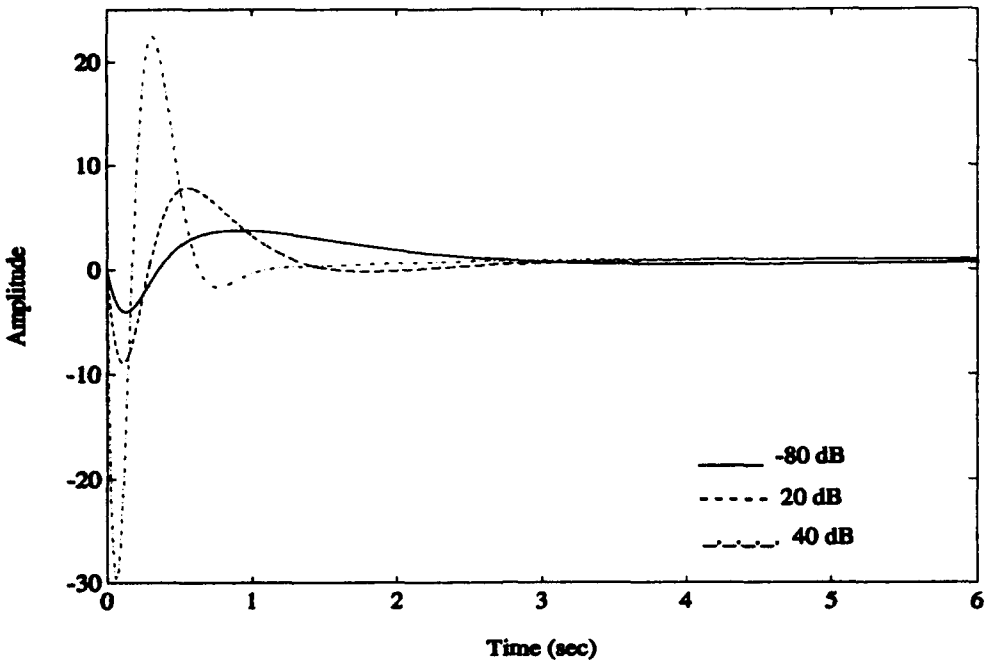

Figure 6-74. 1-DOF Step Responses for Type II System Example

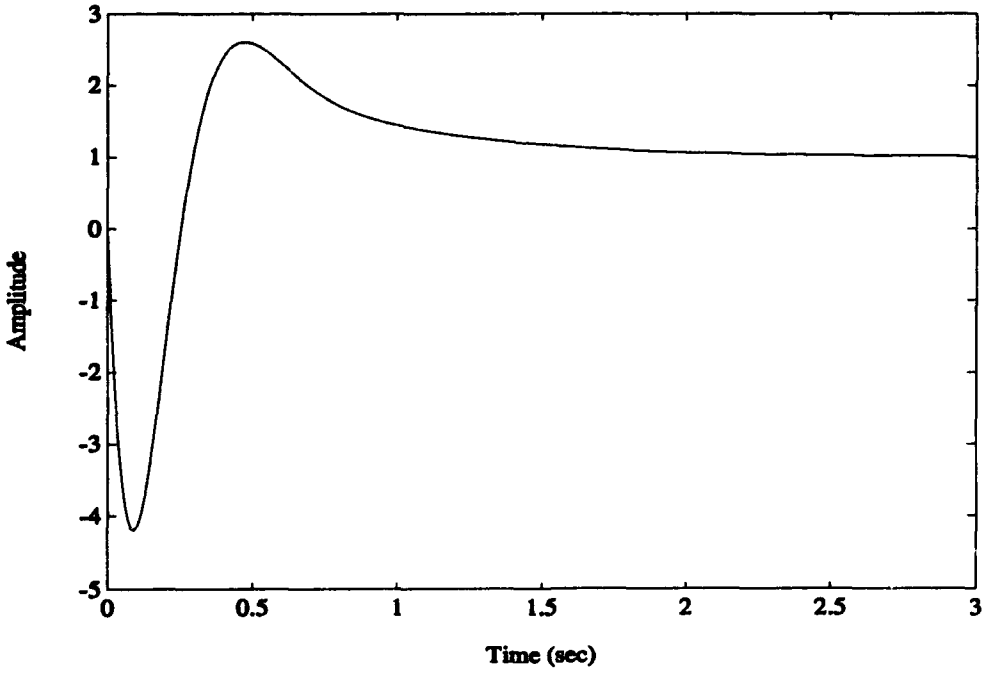

Figure 6-75. 2-DOF Step Response for Type II System Example

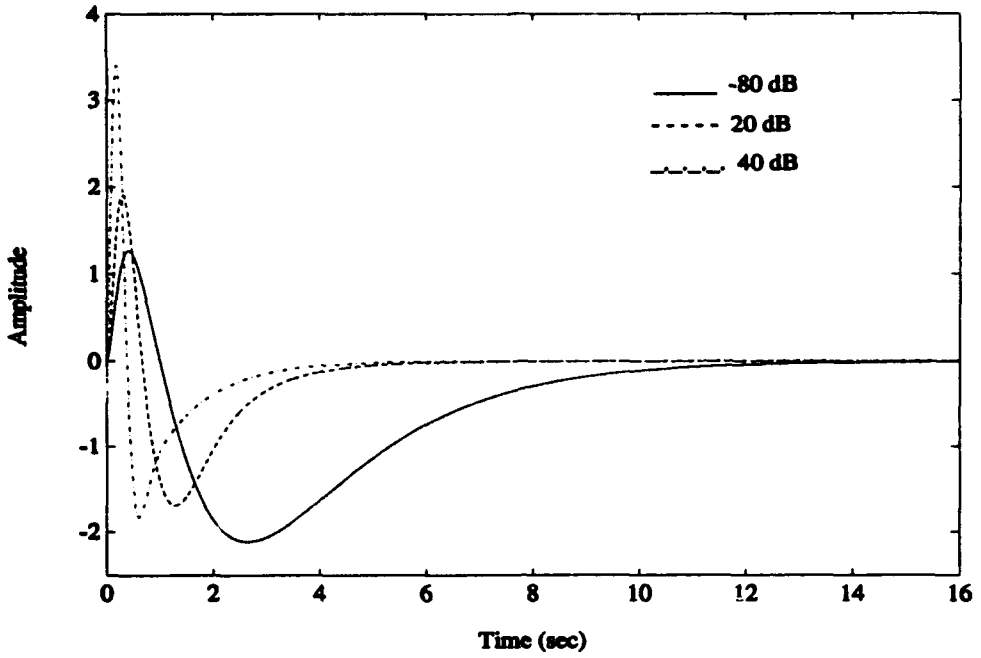

Figure 6-76. 1-DOF Error Responses to a Ramp Input (Type II System Example)

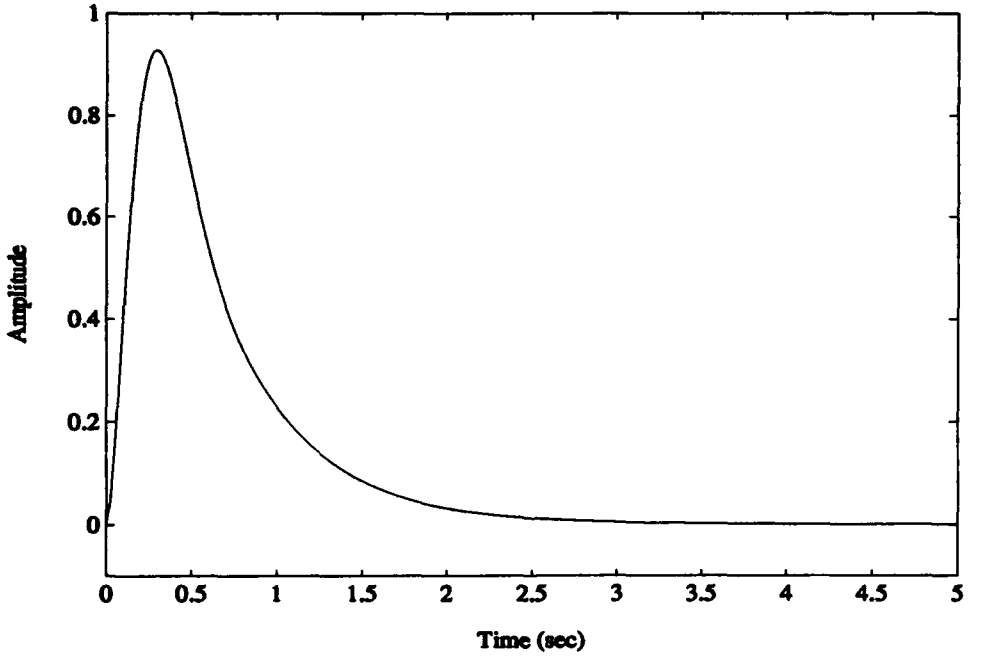

Figure 6-77. 2-DOF Error Response to a Ramp Input (Type II System Example)

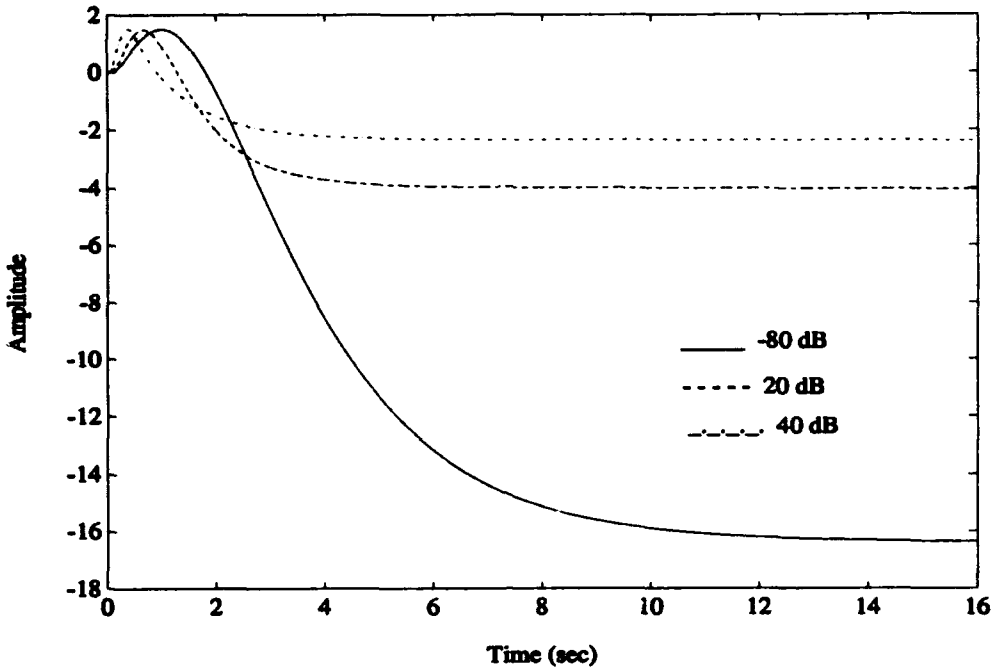

Figure 6-78. 1-DOF Error Responses to a Parabolic Input (Type II System Example)

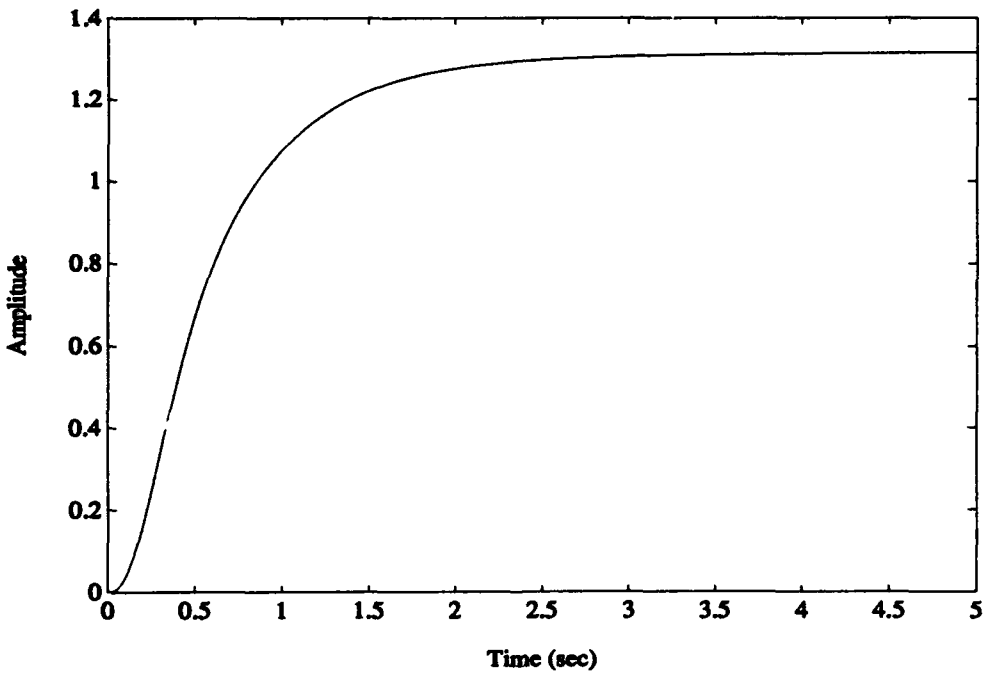

Figure 6-79. 2-DOF Error Response to a Parabolic Input (Type II System Example)

6.5.3 Type III System. For this final case, there are now three poles near the origin in the tracking weight, which produce three poles near the origin in the 1-DOF and 2-DOF compensators. Both systems should be able to track step, ramp, and parabolic inputs with zero steady state error. The 1-DOF and 2-DOF step responses are shown in Figures 6-80 and 6-81. The settling times continue to get faster, but the amount of overshoot also increases, especially in the 1-DOF case. The 1-DOF settling times all fall under two seconds, while the overshoot for the large disturbance is ±130. The 2-DOF settling time is about one second, with oscillatory motion ranging between -20 and +16.

The ramp error responses are shown in Figures 6-82 and 6-83. The 1-DOF system settles out between 4 and 10 seconds (depending on the disturbance level), with the overshoot at ±12. The 2-DOF system settles out in 2.5 seconds with oscillatory motion ranging between -1.1 and +2.4.

The parabola error responses are shown in Figures 6-84 and 6-85. The two larger disturbances in the 1-DOF case produced a settling time of about 6 seconds, but the smallest disturbance case resulted in the system going unstable, due to numerical errors. If there had been a true triple pole at the origin, then the system would have produced zero steady state error. However, the W_3 tracking weight only contains a close approximation to a triple pole at the origin, and the truncation error caused by the approximation eventually affects the system response, especially when the measurement noise is large relative to the plant disturbance. A better approximation would also be to make the DC gain of W_3 larger. The 2-DOF error response settles out in three seconds, with an initial overshoot of +1.1.

It is interesting to note that for the small disturbance case for the type III system, the 1-DOF step response looks a lot like the 2-DOF step response with respect to the settling time and amount of oscillatory motion. When the 1-DOF system is given ramp and parabolic inputs, however, the responses become much worse. The reason for this goes back to the idea that the tracking weight does not really have a triple pole at the origin. From Figure 6-69, the type III tracking weight does have a large amount of energy at low frequency, enabling a favorable 1-DOF step response. As previously mentioned, when the input is higher order, the 1-DOF responses rapidly deteriorate.

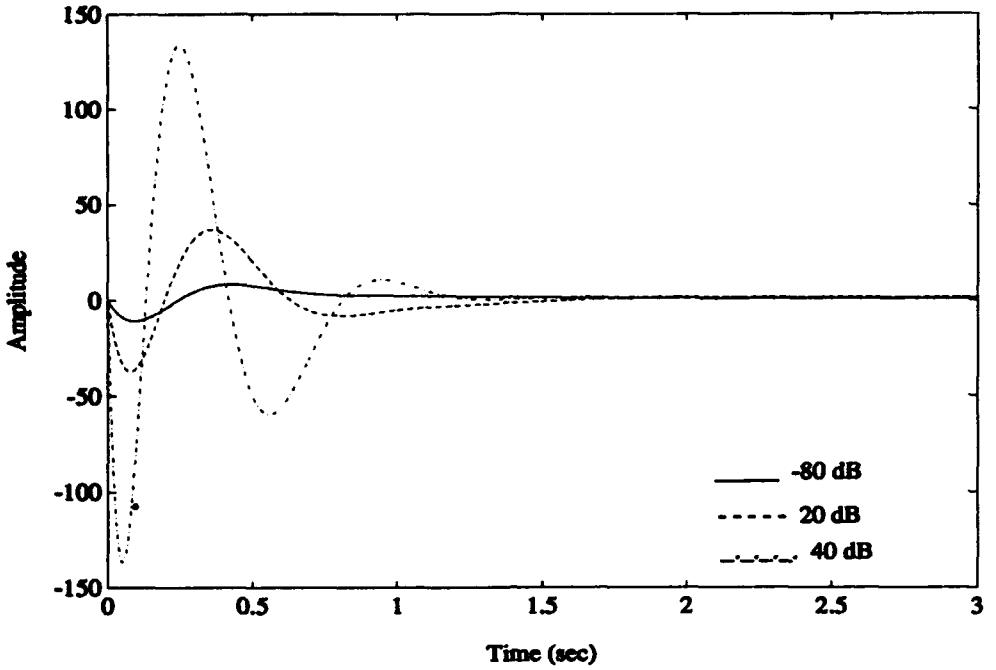

Figure 6-80. 1-DOF Step Responses for Type III System Example

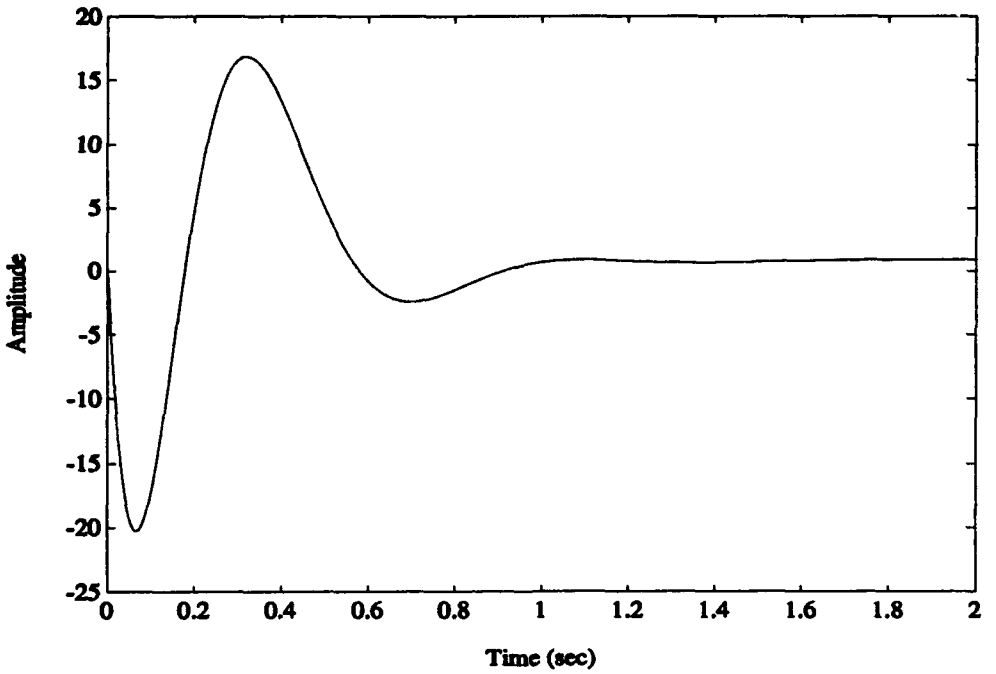

Figure 6-81. 2-DOF Step Response for Type III System Example

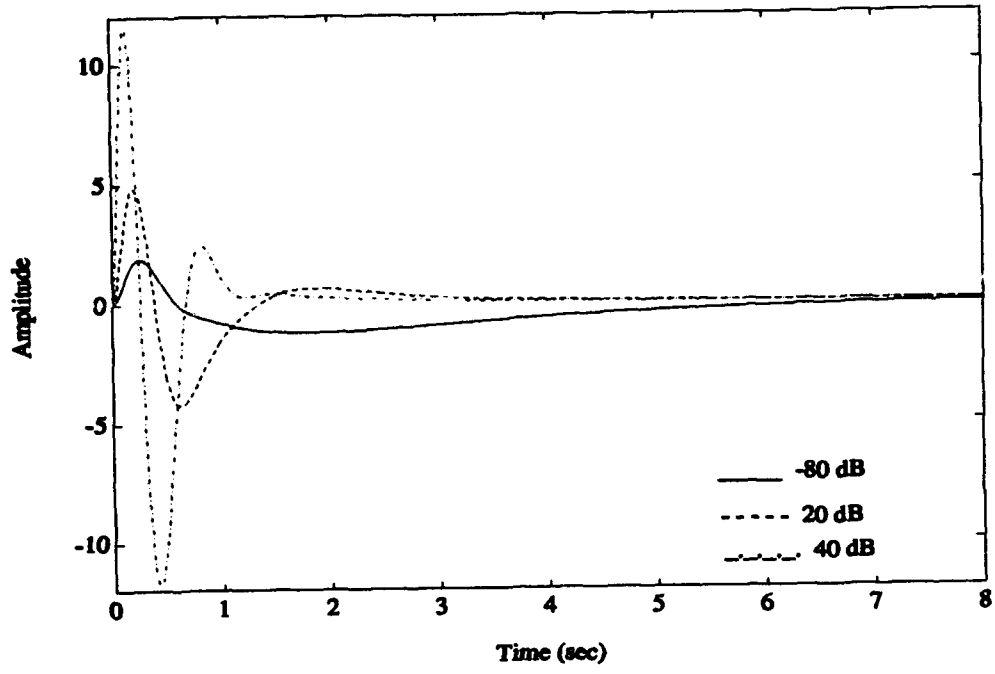

Figure 6-82. 1-DOF Error Responses to a Ramp Input (Type III System Example)

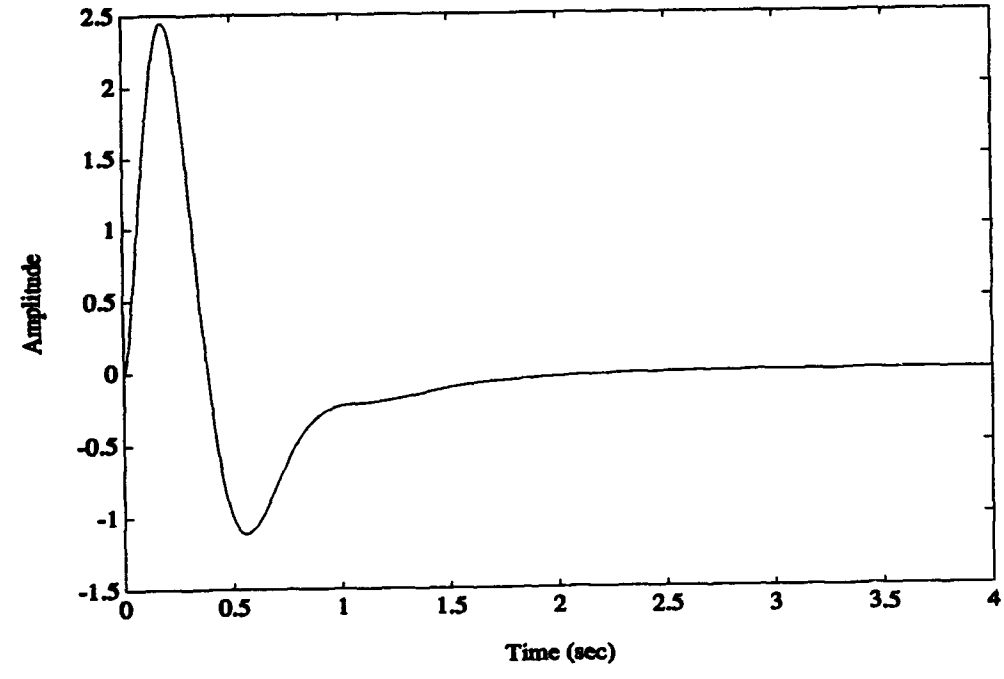

Figure 6-83. 2-DOF Error Response to a Ramp Input (Type III System Example)

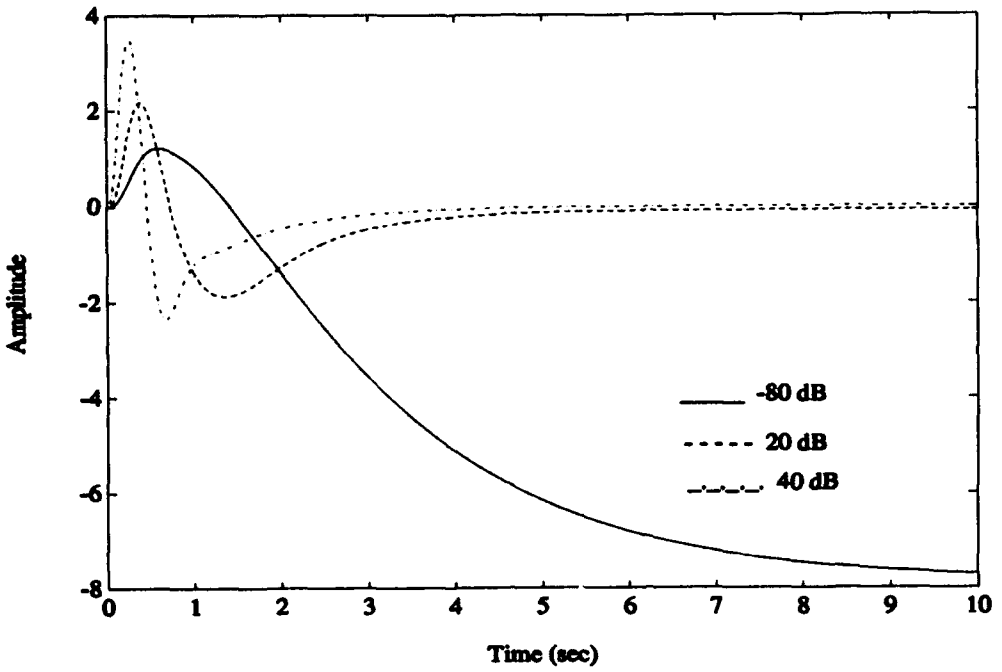

Figure 6-84. 1-DOF Error Responses to a Parabolic Input (Type III System Example)

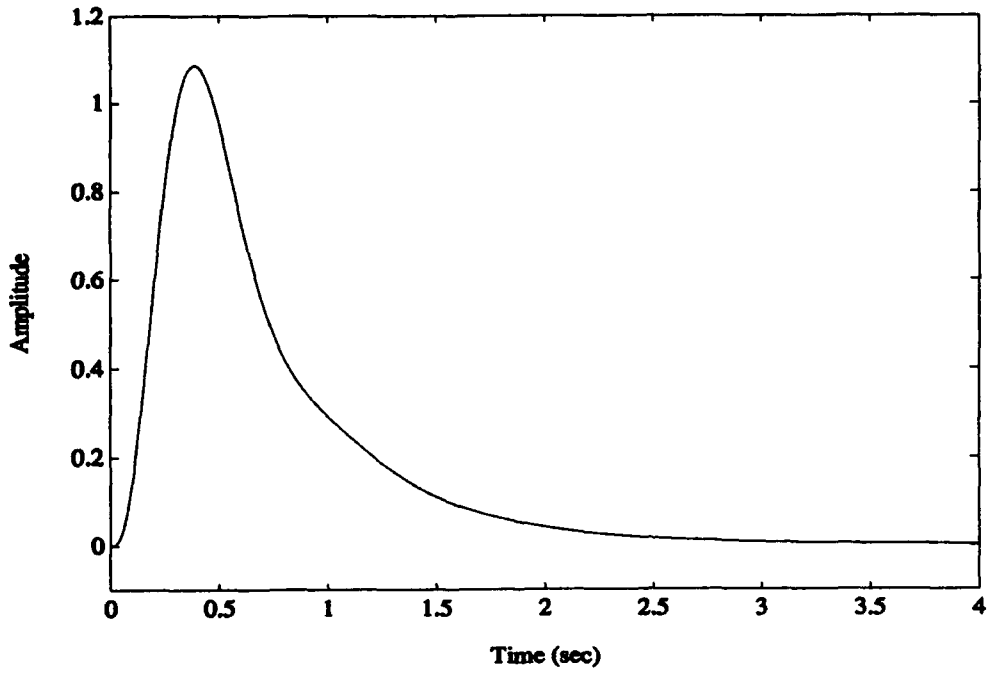

Figure 6-85. 2-DOF Error Response to a Parabolic Input (Type III System Example)

6.6 Low Frequency Measurement Noise Example

In all of the examples presented thus far, both the 1-DOF and 2-DOF systems have been modeled with plant disturbances that contain definite low frequency content (Figure 5-3) and measurement noises that contain definite high frequency content (Figure 5-4). One of the basic ideas emphasized in Chapter V is that the system loop shape, whether 1-DOF or 2-DOF, must exhibit certain properties at low frequencies to deal with commands and disturbances, and other properties at high frequencies to deal with measurement noises. The idea that the measurement noise may contain frequency content in the same range that commands and disturbances fall has not been considered. This section of the chapter will explore the effects of low frequency measurement noise on system loop shape and the corresponding time responses.

The plant to be used for this example is once again the unstable, nonminimum phase system from section 6.4. The measurement noise weight from the H_2 optimization setup, W_5, must be modified to overlap the frequency range that is used to model the plant disturbances. The modified measurement noise weight is given by

$$W_5 = \frac{20\,(s + 0.0001)}{s + 0.001} \tag{6.8}$$

The Bode magnitude plot of this weight compared to the medium sized disturbance weight (with a DC gain of 20 dB) is shown in Figure 6-86. The medium-sized disturbance weight is shown on the plot only to show the overlap of the frequencies. All three disturbance weights will be reflected in the loop shape and time response plots for this example. The frequency and time response plots generated from this

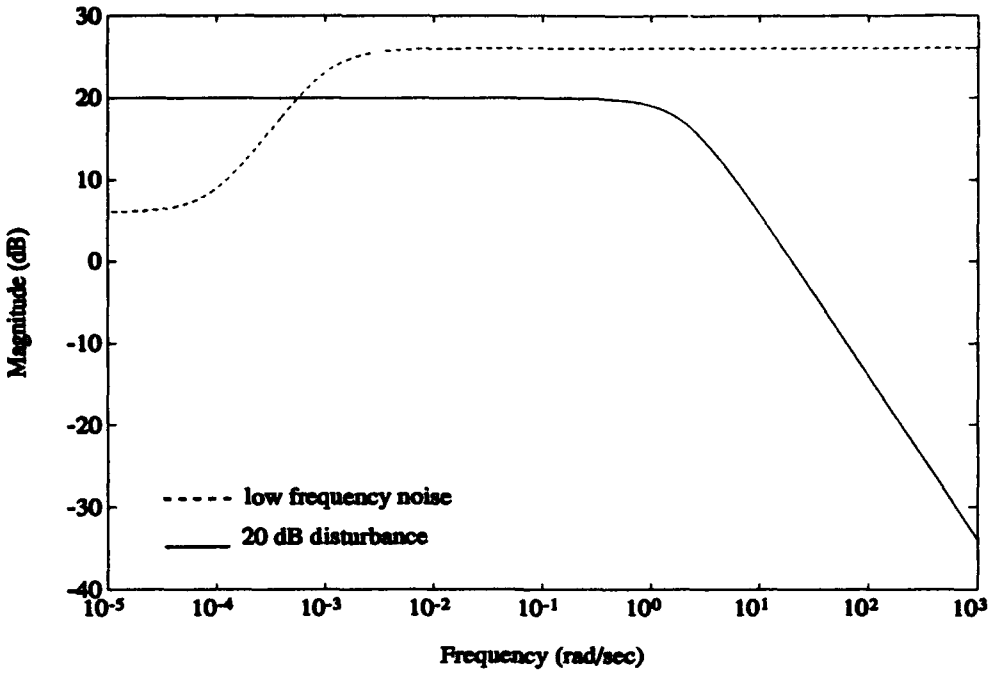

Figure 6-86. Bode Magnitude Plot of Low Frequency Measurement Noise Weight

example are intended to be compared to the large noise plots from the unstable, nonminimum phase example from section 6.4.

For the 1-DOF case, traditional loop shaping theory states that $|GK|$ must be large at low frequency for good disturbance rejection and small at high frequency for good measurement noise rejection. The previous examples have shown that when the measurement noise is large relative to the disturbance, the size of $|GK|$ is driven down over all frequencies. Thus, in the small disturbance case, $|GK|$ is expected to be small overall, regardless of the frequency range of the noise. When the disturbance is larger, the size of $|GK|$ is not as predictable. In general, it should be expected that the size of $|GK|$ will be driven by the low frequency measurement noise; therefore, $|GK|$ should be

driven down at the frequency where the noise first becomes significant. In any case, the time responses should be worse than the case where the noise is restricted to the high frequency region.

For the 2-DOF case, there is still a potential conflict between disturbance rejection and measurement noise rejection, in that they both depend on the size of $|GK_1|$. When the disturbance is small, there should be no problem for the 2-DOF system to accomplish both objectives because $|GK_1|$ does not need to be large to reject the disturbance, and it should be small to reject the noise anyway. $|GK_2|$ compensates for the reduced size of $|GK_1|$ by shaping itself in such a way that tracking is maintained over as large a frequency range as possible. For the large disturbance-large noise case, however, there is still a conflict between the disturbance and noise rejection objectives. From a logical standpoint, it appears that this could result in a worse time response than the case where the noise contains only higher frequencies.

6.6.1 1-DOF Results. Figure 6-87 shows the 1-DOF sensitivity function for the low frequency measurement noise case. It is immediately apparent that in the two smaller disturbance cases, $|S|$ is at 0 dB between 0.0001 and 0.1 rad/sec, which suggests that $|GK|$ is very small in this region. Recalling the steady state error barrier from Figure 2-3, it does not appear that the functions in the two smaller disturbance cases resemble "good" sensitivity functions. $|S|$ for the largest disturbance resembles a more conventional sensitivity function.

Figure 6-88 shows a plot of the complimentary sensitivity function. Again, the functions for the two smaller disturbance cases exhibit undesirable behavior in that they "droop" below the 0 dB line at frequencies before rolling off, indicating that $|GK|$

is small in that region. Figure 6-89 verifies the fact that $|GK|$ is indeed small in the frequency region that $|T|$ exhibits the droop (in the small disturbance cases). The DC gain of $|GK|$ is also very low for those two cases compared to the large disturbance case.

The step responses in Figure 6-90 indicate that when the assumed disturbance is large, the response is virtually unchanged from the case where the measurement noise is only at high frequency (Figure 6-60). When the disturbance is smaller, however, shape of the response does not change much, but the steady state value does not even reach unity. The reason for this is that $|GK|$ is very small in the region where the disturbance and measurement noise frequencies overlap, which is where it needs to be large to produce a favorable response. It should be emphasized here that in the large disturbance case, the step response showed perfect tracking performance using the evaluation model from Chapter V, which has no noises acting on the system. Since the assumed large disturbance causes $|GK|$ to be large at low frequency, and $|T|$ is at 0 dB in the frequency range where the measurement noise first becomes large, the system would track both the command input and the noise in that frequency range. In fact, if the evaluation model were altered so that low frequency measurement noise acted on the system, then the step response would show the amplified noise in it.

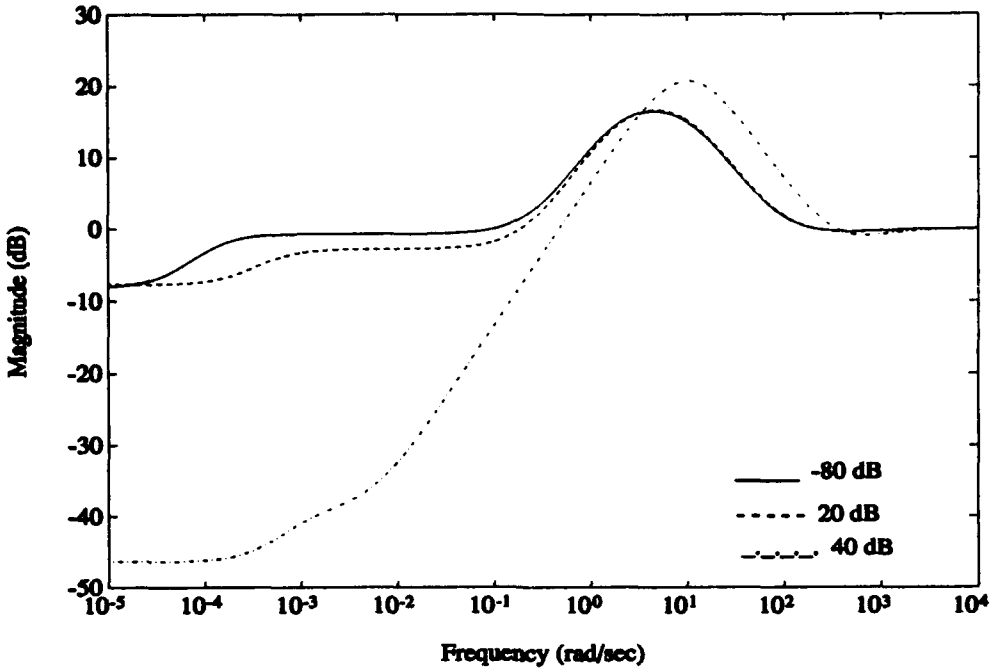

Figure 6-87. 1-DOF Bode Magnitude Plot of $|S|$ for Low Frequency Measurement Noise Example

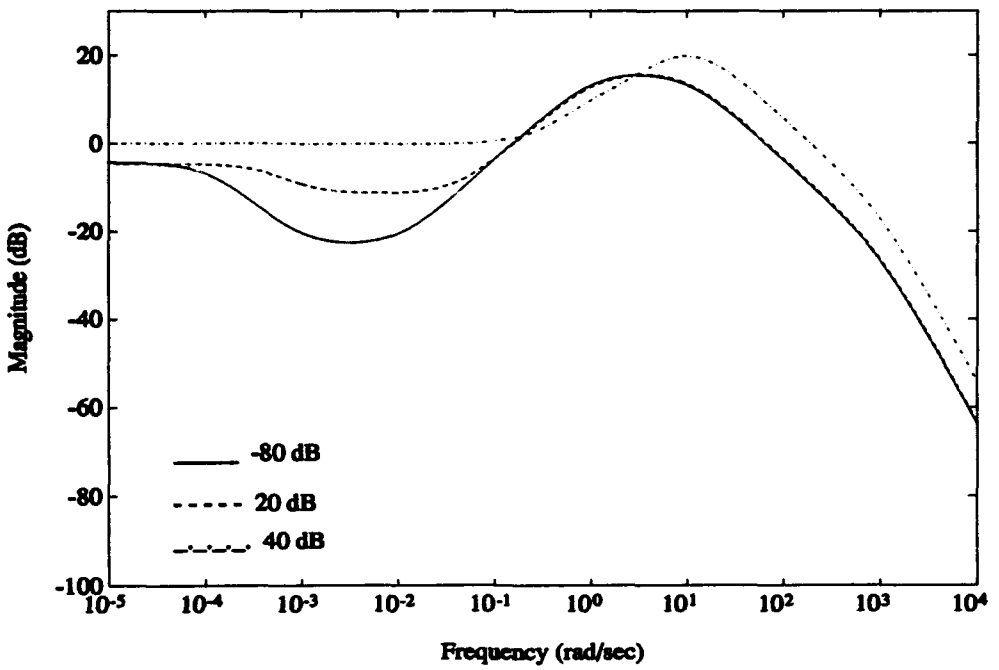

Figure 6-88. 1-DOF Bode Magnitude Plot of $|T|$ for Low Frequency Measurement Noise Example

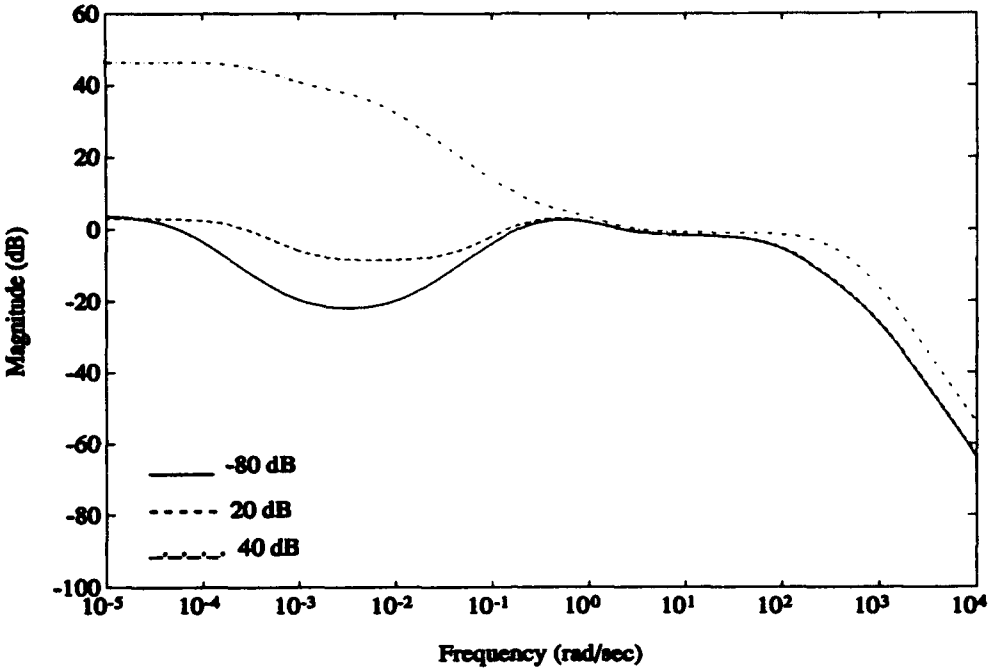

Figure 6-89. 1-DOF Bode Magnitude of $|GK|$ for Low Frequency Measurement Noise Example

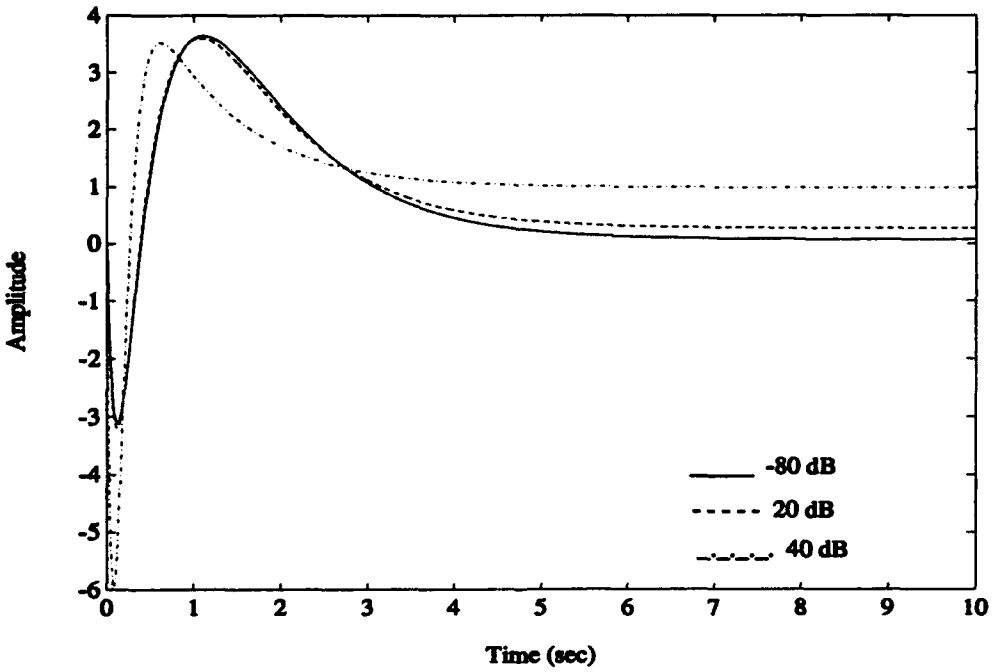

Figure 6-90. 1-DOF Step Responses for Low Frequency Measurement Noise Example

6.6.2 2-DOF Results. Figures 6-91 and 6-92 show the 2-DOF sensitivity and complimentary sensitivity functions. For the small disturbance cases, $|S|$ is at 0 dB between 0.0001 and 0.1 rad/sec, and $|T|$ exhibits a "droop" in this frequency range. In the large disturbance cases, $|S|$ and $|T|$ more closely resemble respective "good" shapes. Figures 6-93 and 6-94 show the magnitude plots of $|GK_1|$ and $|GK_2|$. In the large disturbance case, $|GK_1|$ exhibits high gain at low frequency and low gain at high frequency and is virtually matched by $|GK_2|$. In the two smaller disturbance cases, however, $|GK_1|$ has the same droop that $|T|$ does, but $|GK_2|$ is at 0 dB in this frequency range. The plot of $|SGK_2|$ in Figure 6-95 shows that the 2-DOF system tracks commands perfectly up to the bandwidth frequency of 10 rad/sec. The step response in Figure 6-96 shows that even with a significant low frequency measurement noise, the 2-DOF system still produces the same step response with the noiseless evaluation model as the case where the noise contains strictly high frequencies (Figure 6-52).

6.6.3 Comparison Between 1-DOF and 2-DOF Cases. The 1-DOF and 2-DOF sensitivity and complimentary sensitivity function plots are virtually identical. The primary difference between the 1-DOF and 2-DOF systems comes in the shape of the loop transfer functions. $|GK|$ in the 1-DOF system and $|GK_1|$ in the 2-DOF system are almost identical in that the small disturbance cases still have the low frequency droop. In the 2-DOF case, however, $|GK_2|$ remains at 0 dB throughout the range of the droop, thereby maintaining its command following bandwidth. As previously mentioned, the 1-DOF step responses in the small disturbance cases are unable to track commands without producing a large steady state error, while the 2-DOF system does not show any error. The 1-DOF step response in the large disturbance case does not

show any steady state error, but its initial undershoot is significantly larger than that of the 2-DOF case. In the large disturbance case, the 2-DOF step response is subject to the same caveat as the 1-DOF response -- that is, since the system tracks commands perfectly in the 0.0001 to 0.1 rad/sec frequency range, it will also track measurement noise in that frequency range. Thus, when the assumed disturbance is large, the resulting 1-DOF and 2-DOF controllers would show significant amounts of noise in their step responses if there is low frequency measurement noise in the evaluation model. When the assumed disturbance is smaller, however, neither type of system allows the low frequency noise to pass through to the output. The penalty for the 1-DOF system in this case is that it is also unable to track commands and shows a large steady state error to a step input. The 2-DOF system compensates for the reduced loop gain by reshaping the K_2 controller to maintain perfect tracking and shows no steady state error to a step command.

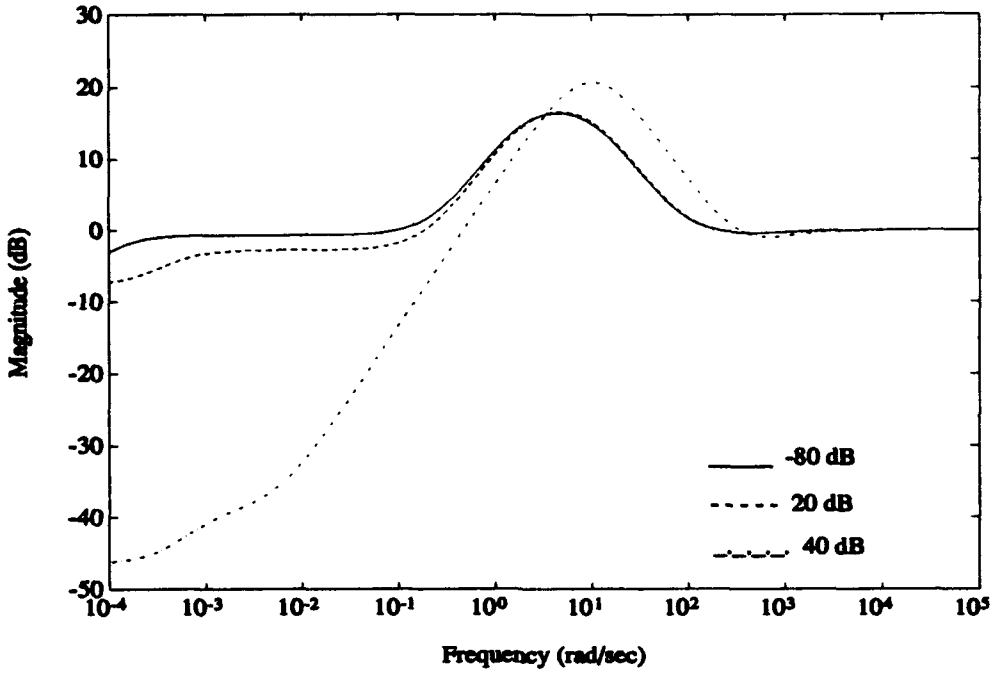

Figure 6-91. 2-DOF Bode Magnitude Plot of \|S\| for Low Frequency Measurement Noise Example

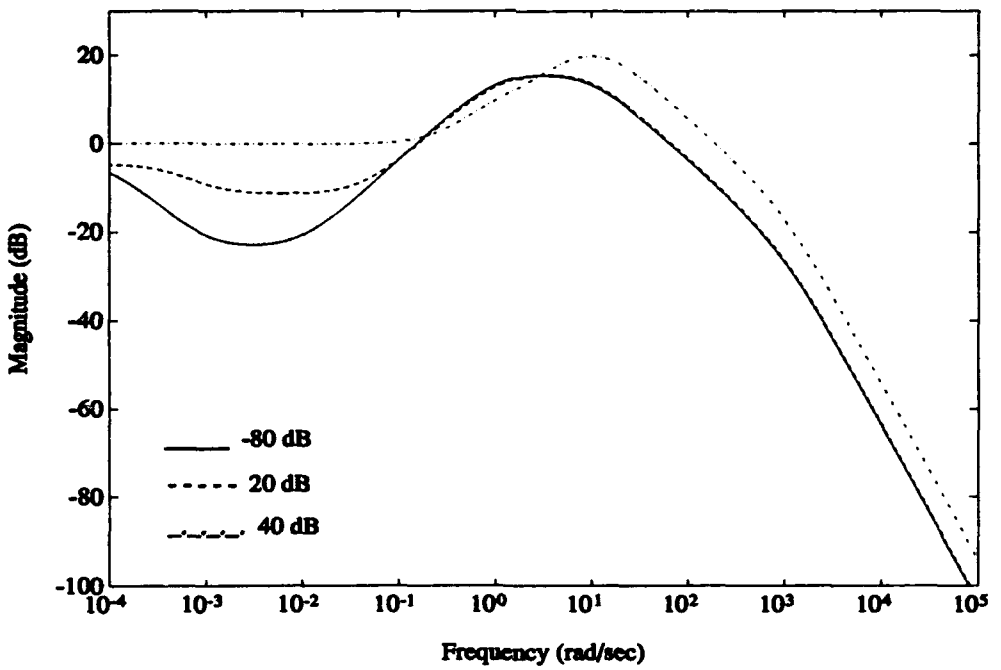

Figure 6-92. 2-DOF Bode Magnitude Plot of \|T\| for Low Frequency Measurement Noise Example

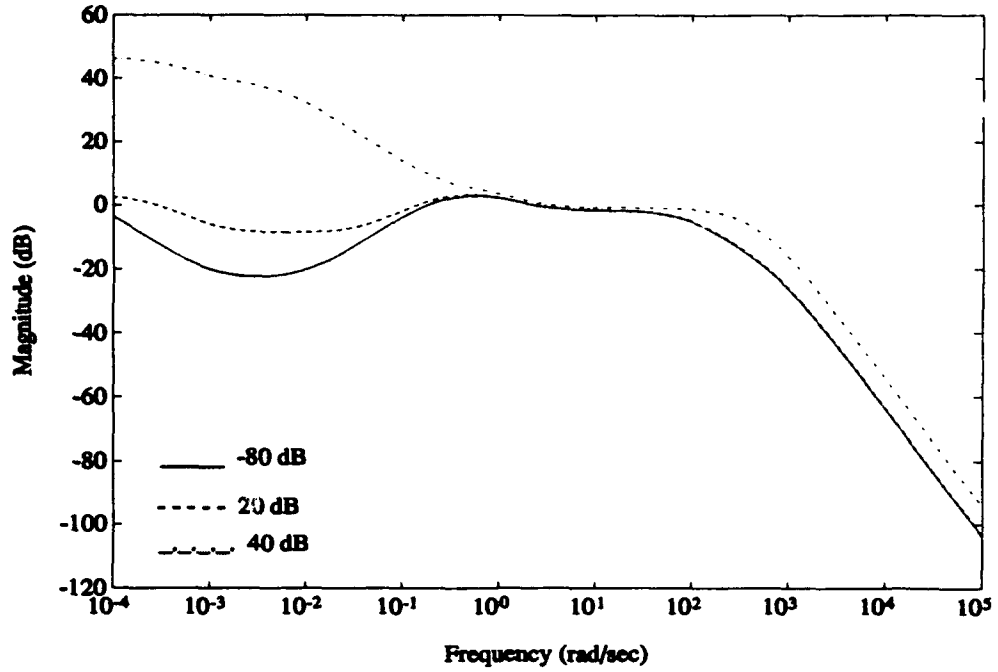

Figure 6-93. 2-DOF Bode Magnitude Plot of $|GK_1|$ for Low Frequency Measurement Noise Example

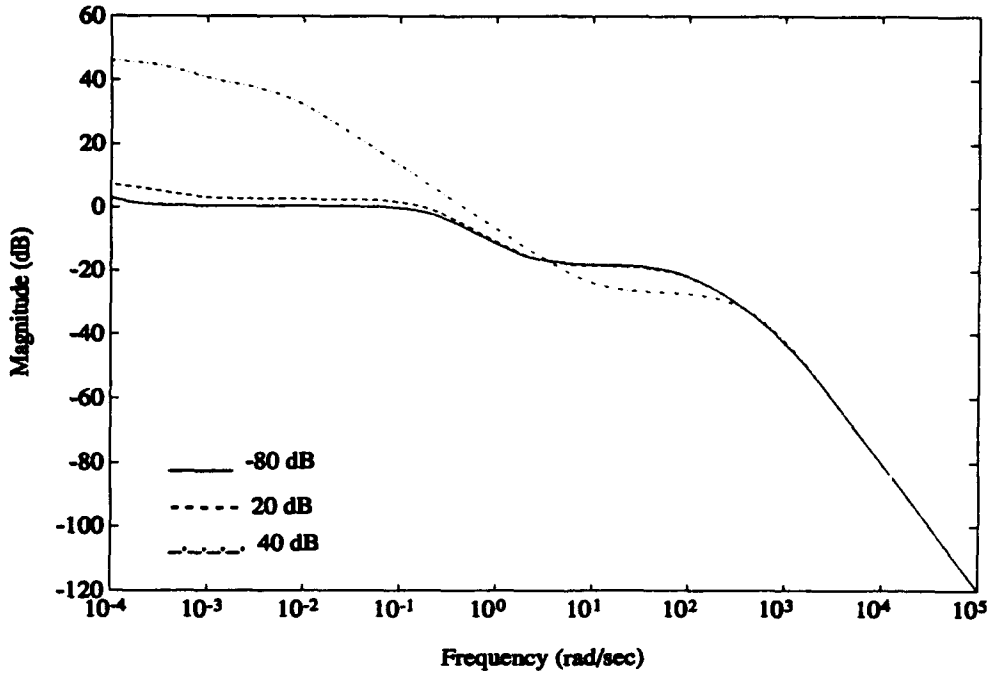

Figure 6-94. 2-DOF Bode Magnitude Plot of $|GK_2|$ for Low Frequency Measurement Noise Example

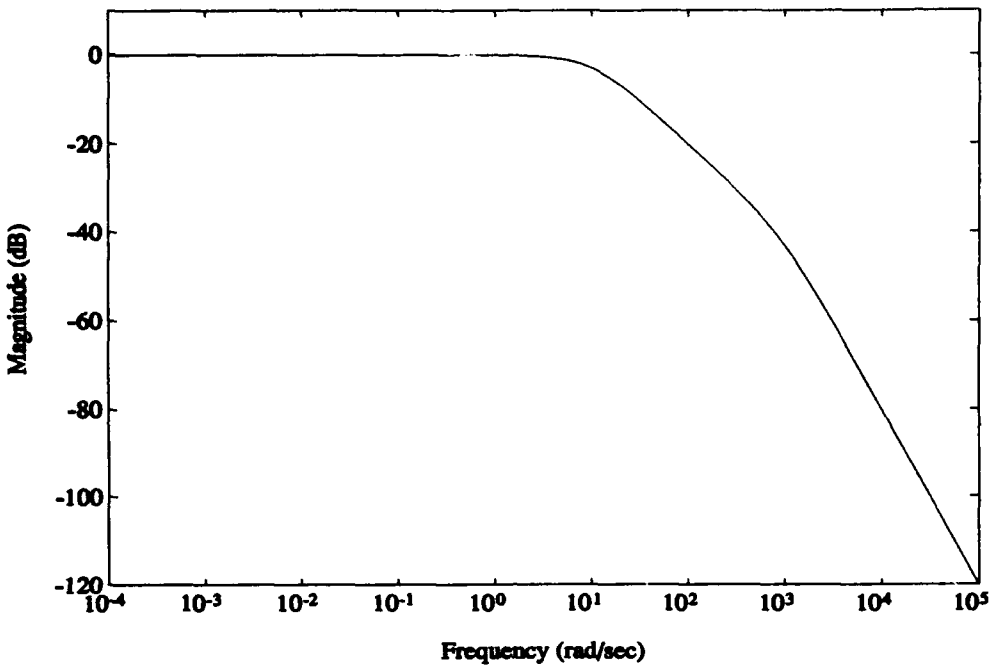

Figure 6-95. 2-DOF Bode Magnitude Plot of $|SGK_2|$ for Low Frequency Measurement Noise Example

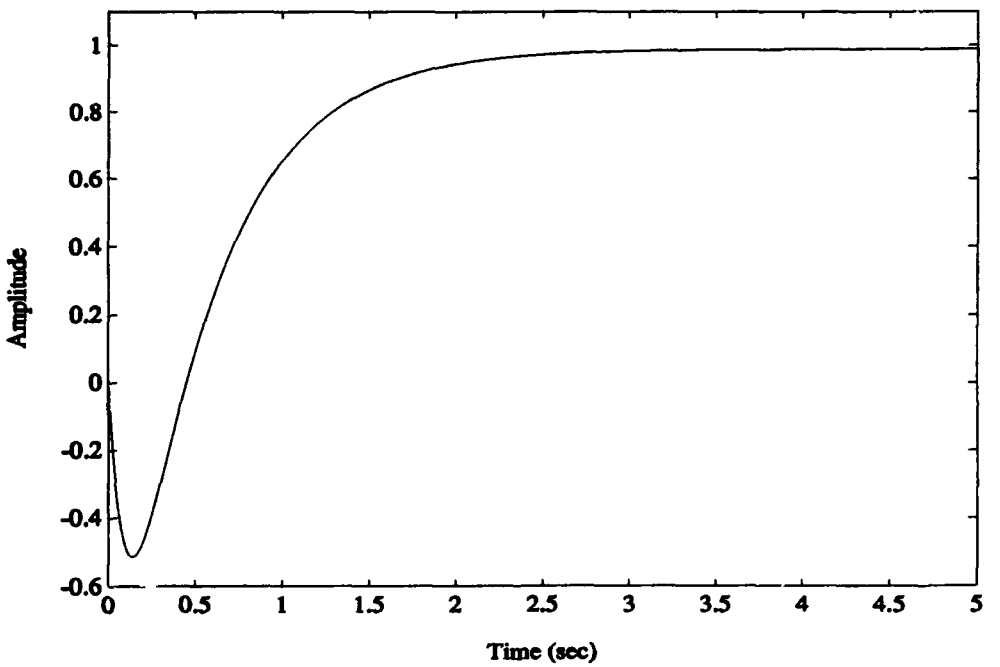

Figure 6-96. 2-DOF Step Response for Low Frequency Measurement Noise Example

6.7 Chapter Summary

Although this chapter makes heavy use of graphs to illustrate the similarities and differences between 1-DOF and 2-DOF controllers, there are several generalities that can be extracted from the information. With regard to stability margins, it is obvious from the graphs of $|S|$ and $|T|$ that unstable poles cause a marked decrease in the margins, but nonminimum phase zeros have an even more detrimental effect on them. The most important conclusions to draw, however, deal with the ability of the two systems to track commands. In the 1-DOF cases, the following trends were observed (using the stable, minimum phase system as a baseline):

i) In all cases, the rise times and settling times improve as the size of the plant disturbance is increased. These two times become slower when going from a small measurement noise to a large one.

ii) The effect of unstable poles on the step response is to increase the overshoot of the final value. In general, the amount of overshoot decreases as the disturbance increases in magnitude. The settling times are also slightly slower.

iii) The primary effect of nonminimum phase zeros is, of course, to cause the step response to initially head in a negative direction. The magnitude of this undershoot increases and the settling time gets faster as the disturbance size increases. A large measurement noise decreases the magnitude of the undershoot and slows the settling time.

iv) In the unstable, nonminimum phase system, all of the above trends are evident in the step responses, showing that the trends are not mutually exclusive. In fact, this type of example serves as a good model to illustrate the differences between

the 1-DOF and 2- DOF approaches because it is a "worst case" scenario.

In all of the classes of examples, the 2-DOF cases only produced a single step response. This is because the H_2 optimal 2-DOF controller produces the step response that is the "best" overall for a given tracking weight, no matter what the size of the plant disturbance or measurement noise is. For the tracking weight given in Chapter V, the following observations were made regarding the 2-DOF step responses: (1) In the minimum phase case, it gave the fastest response that does not exhibit any overshoot; (2) In the nonminimum phase case, it gave the response with the lowest-sized initial undershoot, fastest settling time, and no overshoot of the final value. With all of these constraints, the 2-DOF response may not always be the most practical solution in everyday use. For instance, if restrictions are relaxed to allow a 10% overshoot, then the rise time could become quite a bit faster. If the 2-DOF tracking weight is adjusted to roll off at a higher frequency, then the resulting step response would exhibit a faster rise time with more overshoot. The 1-DOF controllers also allow for this possibility, but the problem with the 1-DOF controllers is that they are susceptible to changes in disturbance and measurement noise. The 2-DOF approach guarantees a response with the aforementioned characteristics regardless of the size of the disturbance or measurement noise.

The system type examples show that even with different types of inputs, the 2-DOF system still produces better tracking results over the spectrum of plant disturbance and measurement noise sizes. The 1-DOF system is prone to exhibit more oscillatory motion with poles near the origin in the compensator than the 2-DOF system is. The 2-DOF system still exhibits the "best" overall responses with higher

order inputs.

The low frequency noise example perhaps best shows the advantages of using 2-DOF controllers. The plots indicate that when the measurement noise contains energy in the same range as the plant disturbance, the noise is more dominant, and the loop gain will be low to lessen its effects. In the 2-DOF case, the prefilter compensator makes up for the smaller size of $|GK_1|$ by shaping itself to maintain a high bandwidth frequency for command following. The 1-DOF system simply has no mechanism to put forth high gain at low frequency, yet avoid the effects of low frequency measurement noise.

The bottom line to this chapter is that 2-DOF controllers exhibit much better tracking characteristics than 1-DOF controllers for a variety of classes of plants and system types. The next chapter examines the differences between the two systems in a MIMO example.

VII. Tail-Controlled Missile Example (MIMO)

As previously mentioned in Chapters II and III, loop shaping concepts can also be applied to the multivariable case. The primary change is that restrictions on the sizes of various loop transfer functions are now placed on the minimum or maximum singular values of the function. The example presented in this chapter is an autopilot for a tail-controlled missile and is taken from [1:16-17]. It is a point design in the flight envelope of the missile and is not intended to be a design used for operational purposes. The purpose of this example is to once again show the differences in loop shapes and time responses between 1-DOF and 2-DOF systems.

The linearized model of the missile plant consists of eight states, given by

$$\bar{x} = \begin{bmatrix} \delta p \\ \delta q \\ \delta r \\ \alpha \\ \beta \\ p \\ q \\ r \end{bmatrix} = \begin{bmatrix} \textit{fin actuator state (roll)} \\ \textit{fin actuator state (pitch)} \\ \textit{fin actuator state (yaw)} \\ \textit{pitch-plane angle of attack} \\ \textit{yaw-plane angle of attack} \\ \textit{roll rate} \\ \textit{pitch rate} \\ \textit{yaw rate} \end{bmatrix} \tag{7.1}$$

The inputs consist of roll-fin, pitch-fin, and yaw-fin deflections. The plant state space matrices are given by

$$A = \begin{bmatrix} -4.0000E+02 & 0.0000E+00 & 0.0000E+00 & 0.0000E+00 \\ 0.0000E+00 & -4.0000E+02 & 0.0000E+00 & 0.0000E+00 \\ 0.0000E+00 & 0.0000E+00 & -4.0000E+02 & 0.0000E+00 \\ -8.7349E-01 & 1.3044E+02 & -4.5412E-01 & -9.8435E-01 \\ -2.4611E-01 & 6.2620E-01 & -1.2753E+02 & -9.2340E-02 \\ 3.3304E+06 & 1.2009E+06 & -4.2461E+03 & -2.6737E+02 \\ -1.0950E+03 & 1.2844E+05 & 5.8025E+01 & -1.9462E+02 \\ -1.2044E+02 & 5.6387E+02 & 1.2598E+05 & 6.9673E-01 \end{bmatrix} \tag{7.2}$$

$$\begin{bmatrix} 0.0000E+00 & 0.0000E+00 & 0.0000E+00 & 0.0000E+00 \\ 0.0000E+00 & 0.0000E+00 & 0.0000E+00 & 0.0000E+00 \\ 0.0000E+00 & 0.0000E+00 & 0.0000E+00 & 0.0000E+00 \\ -9.2340E-02 & 0.0000E+00 & 1.0000E+00 & 0.0000E+00 \\ -9.8435E-01 & 0.0000E+00 & 0.0000E+00 & -1.0000E+00 \\ 2.6737E+02 & -1.5949E+00 & 0.0000E+00 & 0.0000E+00 \\ -6.9672E-01 & 0.0000E+00 & -1.5498E+00 & 0.0000E+00 \\ 1.9462E+02 & 0.0000E+00 & 0.0000E+00 & -1.5498E+00 \end{bmatrix}$$

$$B = \begin{bmatrix} 1 & 0 & 0 \\ 0 & 1 & 0 \\ 0 & 0 & 1 \\ 0 & 0 & 0 \\ 0 & 0 & 0 \\ 0 & 0 & 0 \\ 0 & 0 & 0 \\ 0 & 0 & 0 \end{bmatrix} \tag{7.3}$$

$$C = \begin{bmatrix} 0.0000E+00 & 0.0000E+00 & 0.0000E+00 & 0.0000E+00 \\ 0.0000E+00 & 0.0000E+00 & 0.0000E+00 & 0.0000E+00 \\ 0.0000E+00 & 0.0000E+00 & 0.0000E+00 & 0.0000E+00 \\ -5.4953E+02 & 1.3982E+03 & -2.8476E+05 & -2.0619E+02 \\ -1.9504E+03 & 2.9126E+05 & -1.0140E+03 & -2.1979E+03 \end{bmatrix} \tag{7.4}$$

$$\begin{bmatrix} 0.0000E+00 & 1.0000E+00 & 0.0000E+00 & 0.0000E+00 \\ 0.0000E+00 & 0.0000E+00 & 1.0000E+00 & 0.0000E+00 \\ 0.0000E+00 & 0.0000E+00 & 0.0000E+00 & 1.0000E+00 \\ -2.1979E+03 & 0.0000E+00 & 0.0000E+00 & 0.0000E+00 \\ -2.0619E+02 & 0.0000E+00 & 0.0000E+00 & 0.0000E+00 \end{bmatrix}$$

The system has no transmission zeros, and the poles are given by

$$\lambda \in \left\{ \begin{array}{c} -1.5949 \\ -1.2209 + 13.922j \\ -1.2209 - 13.922j \\ -1.3133 + 13.974j \\ -1.3133 - 13.974j \\ -400 \\ -400 \\ -400 \end{array} \right\} \tag{7.5}$$

The plant outputs available for measurement (from the C matrix) are the angular rate in each of the three axes (p, q, and r) and the acceleration in each of the two lateral axes (N_y and N_z). The only outputs of interest in this example are the two accelerations and the roll rate. Specifically, the control objective is to have the system track a 10 g N_z command, with N_y and p commanded to zero.

Since this is a MIMO example, the loop shapes are now represented by singular value plots instead of single-line Bode magnitude plots. Thus, it would be difficult to observe trends with multiple singular value plots on a single graph. To alleviate this situation, only plots resulting from the smallest and largest plant disturbances will be presented in this chapter. Furthermore, only the minimum and maximum singular values for each disturbance will be plotted. The singular values for each disturbance will be plotted with a single line type, and the disturbances will still be identified by their DC gain. In this manner, two singular value plots can be plotted together on one graph, and the trends can still be easily observed. As in the other examples, the plots in which small measurement noises were used will be on the top of the page, and the ones in which large noises were used will be on the bottom.

7.1 1-DOF Setup and Results

The first problem immediately encountered when solving this example is the fact that there are five outputs available for measurement, but only three commanded inputs. Since unity feedback theory requires that the number of commanded inputs equal the number of outputs being fed back, then the problem arises as to what to do with the remaining two plant outputs. A 5 x 3 selector matrix can be placed in judicious locations in the 1-DOF H_2 optimization block diagram from Figure 5-1 in order to make maximum use of the outputs in the controller design. As it turns out, after several iterations of placing the selector matrices in different locations, the two remaining outputs (q and r) have no bearing on the system's tracking performance. It is generally not a valid assumption to ignore plant outputs that are not commanded, but that assumption is valid in this particular case. Therefore, for the purposes of the 1-DOF controller designs in this chapter, the plant C matrix will be truncated to reflect only the three outputs of interest. This setup also results in the compensator with the lowest order, which is desirable from a practical standpoint. With the C matrix modified in this manner, the system has transmission zeros located at s = +28.6, s = +25.5, s = -30.1, and s = -27.1, indicating that this is a nonminimum phase system. Figure 5-1 is still valid for use in the H_2 algorithm, the only difference being that all of the signals are now three-dimensional vector signals, and the weight blocks represent 3 x 3 transfer function matrices. The weights are the same as those mentioned in Chapter V, except they now have been multiplied by the identity matrix. Equations (5.1) and (5.2) are also still valid representations of the input-to-output transfer function matrix and the system state space, respectively.

Figures 7-1 and 7-2 show plots of the MIMO sensitivity function, $|S|$, for the small and large noise cases, respectively. Using the ideas from Chapter II, it is expected that the maximum singular value of S, $\bar{\sigma}[S]$, should be small at low frequency. As the disturbance gets larger, $\bar{\sigma}[S]$ gets smaller. In the large noise case, these same trends are present, except in the small disturbance case, $\bar{\sigma}[S]$ is not as small at low frequency as it is in the small noise case. In the large noise-large disturbance case, $\bar{\sigma}[S]$ is about the same magnitude as it is in the small noise-large disturbance case, but the minimum singular value of S, $\underline{\sigma}[S]$, is much lower at low frequency in the small noise-large disturbance. This is because with a smaller noise, the system could potentially exhibit higher loop gain at low frequency, as in the SISO case. The "hump" above 0 dB is larger in the small noise cases than it is in the large noise cases (indicating worse stability margins) because when more gain is put into a nonminimum phase system, the response gets faster, but the system comes closer to instability.

The system complimentary sensitivity function, $|T|$, is shown in Figures 7-3 and 7-4 for each noise size. For good noise rejection, $\bar{\sigma}[T]$ must be small at high frequency, and the MIMO bandwidth is defined as the frequency where $\bar{\sigma}[T]$ rolls off. As the disturbance size increases, the bandwidth frequency gets larger, as expected. In the large noise case, the trends are the same, but the bandwidths are significantly lower, as in the SISO case. Once again, in the small noise case, there is a larger increase in the function magnitude before rolling off than in the large noise case

because the larger loop gain causes worse stability margins in this system.

Figures 7-5 and 7-6 show plots of the loop transfer function $|GK|$. As described in Chapter II, $\underline{\sigma}[GK]$ must be large at low frequency for good tracking and disturbance rejection, and $\overline{\sigma}[GK]$ must be small at high frequency for good measurement noise rejection. These trends are observed in the figures. As the disturbance size increases, $\underline{\sigma}[GK]$ also gets bigger, as does the separation between $\underline{\sigma}[GK]$ and $\overline{\sigma}[GK]$. The trends are identical in both the small and large noise cases, but in the large noise case, the the plots are shifted downward, reflecting the reduced loop gain.

Figures 7-7 and 7-8 show the N_z responses to a 10 g step. In the small noise case, the response settles out slightly faster in the large disturbance case (0.5 seconds vs. 0.6 seconds), but there is also higher overshoot (both positive and negative) than the small disturbance case. In the large noise case, the large disturbance response still settles out in less than a second (0.7 seconds), but the small disturbance response has a settling time of over 10 seconds. The overshoot in the large disturbance case is much higher, however. In both noise size cases, the effect of increasing the disturbance is to decrease the settling time, but at the same time increase the magnitude of the oscillatory motion. These exact trends are true of the N_y responses (Figures 7-9 and 7-10) and the roll rate responses (Figures 7-11 and 7-12).

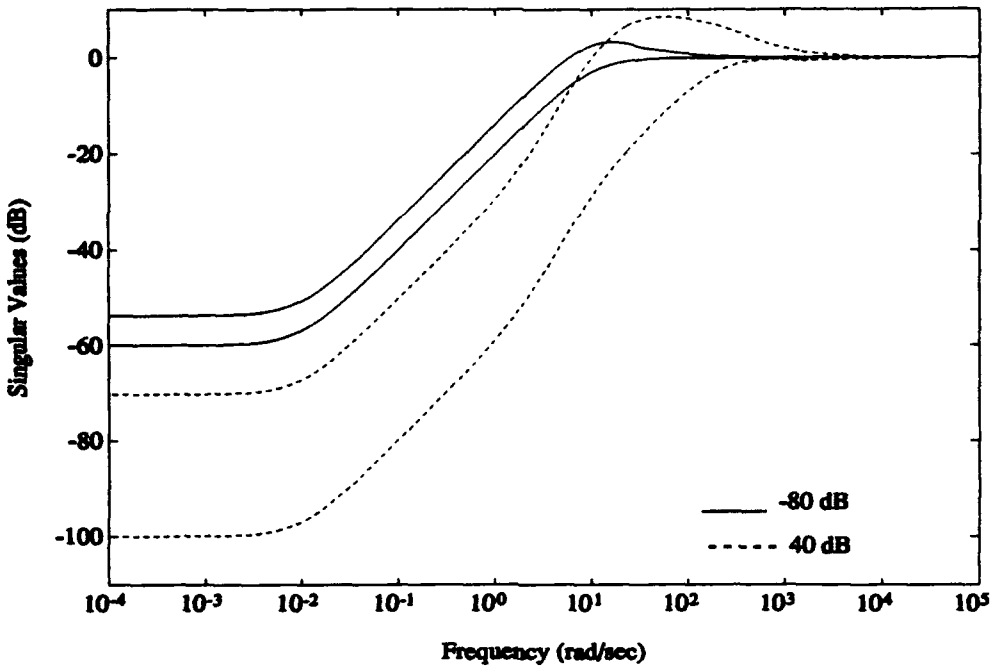

Figure 7-1. 1-DOF Singular Value Plot of $|S|$ for Tail-Controlled Missile Example (Small Noise Case)

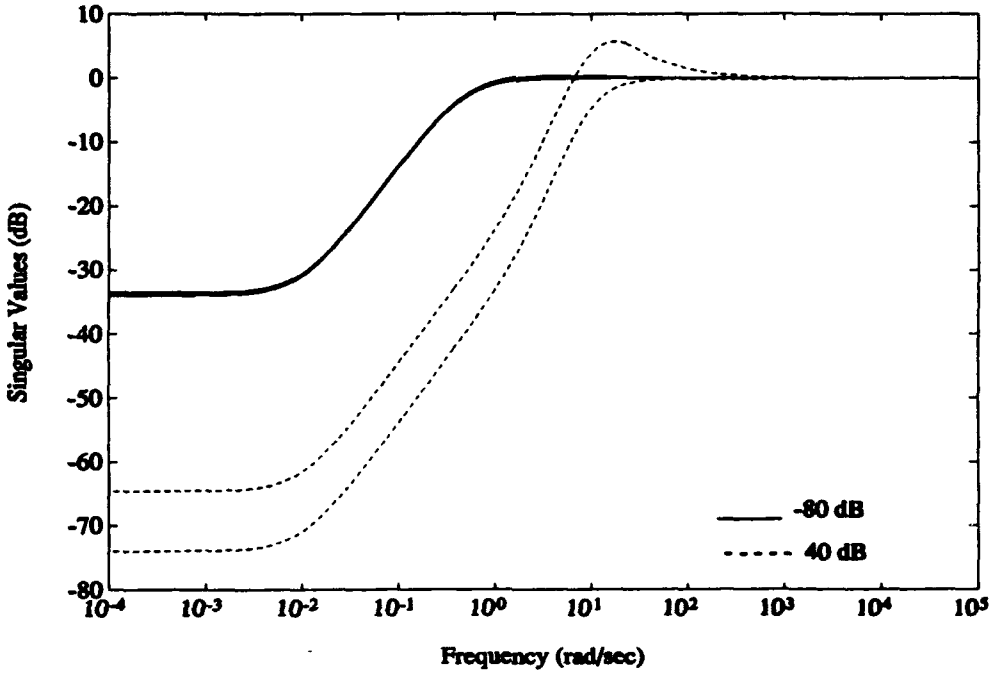

Figure 7-2. 1-DOF Singular Value Plot of $|S|$ for Tail-Controlled Missile Example (Large Noise Case)

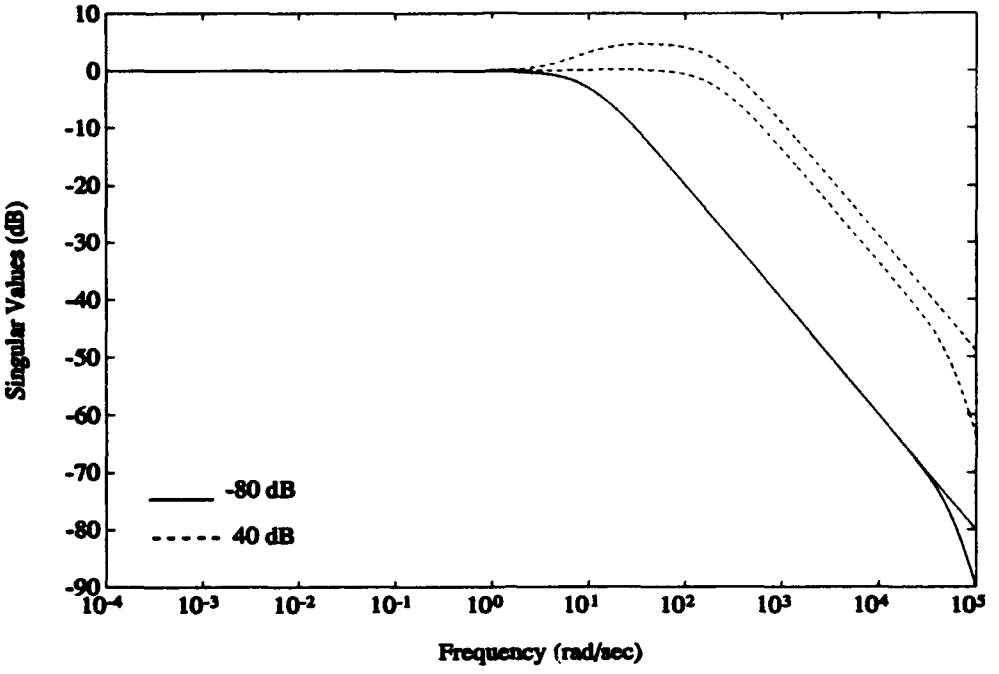

Figure 7-3. 1-DOF Singular Value Plot of $|T|$ for Tail-Controlled Missile Example (Small Noise Case)

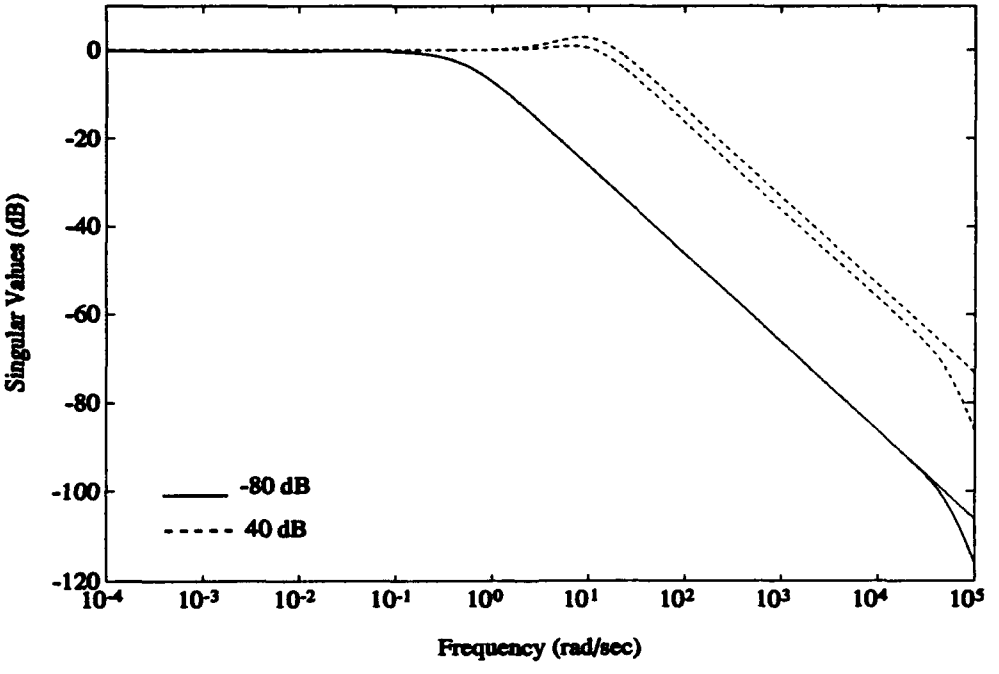

Figure 7-4. 1-DOF Singular Value Plot of $|T|$ for Tail-Controlled Missile Example (Large Noise Case)

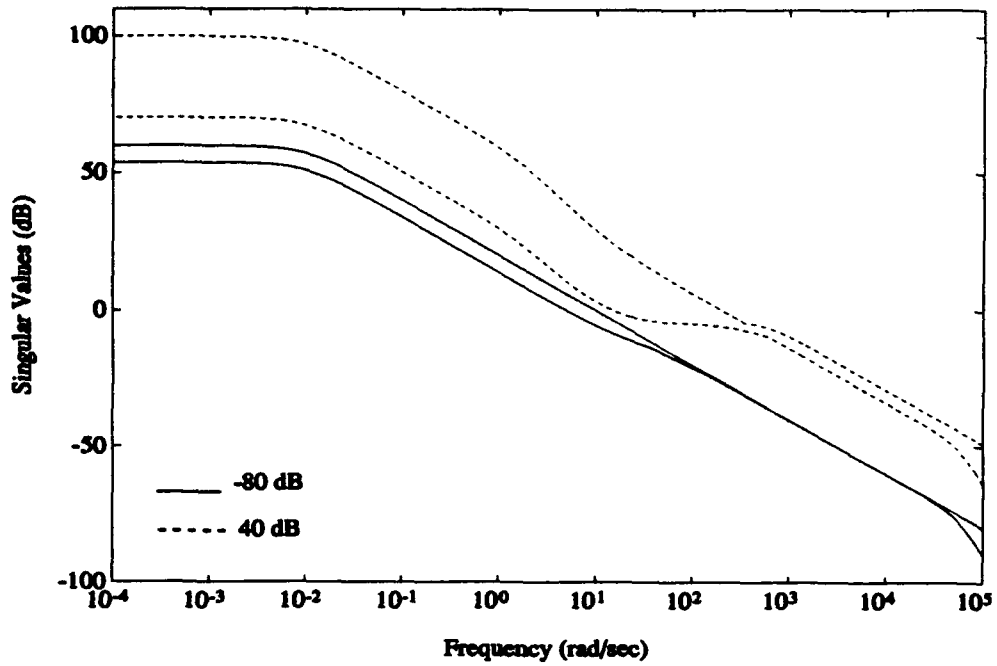

Figure 7-5. 1-DOF Singular Value Plot of $|GK|$ for Tail-Controlled Missile Example (Small Noise Case)

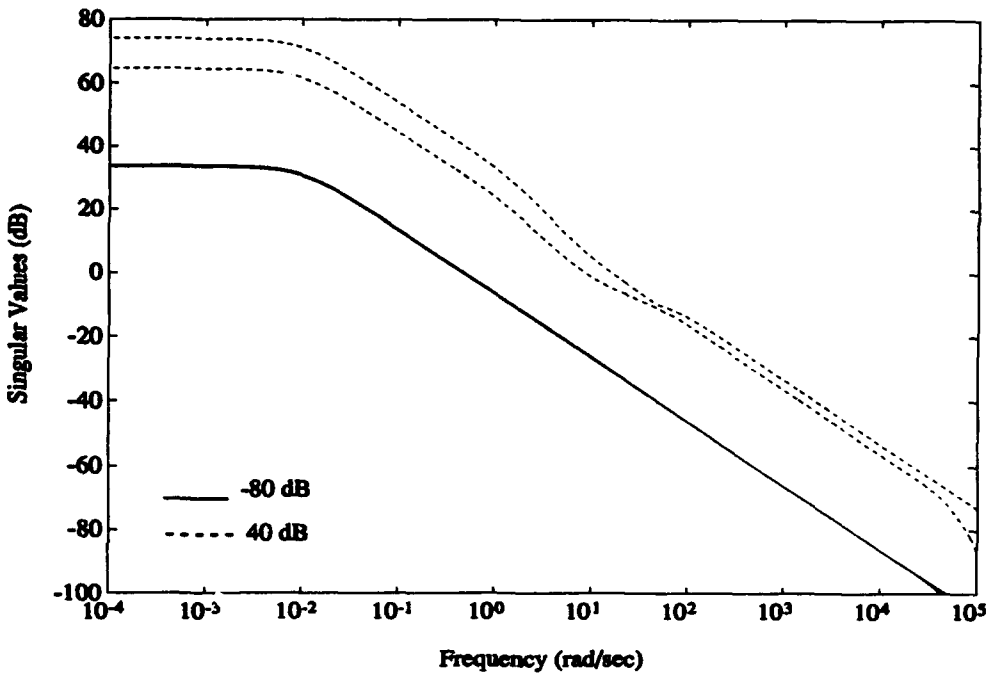

Figure 7-6. 1-DOF Singular Value Plot of $|GK|$ for Tail-Controlled Missile Example (Large Noise Case)

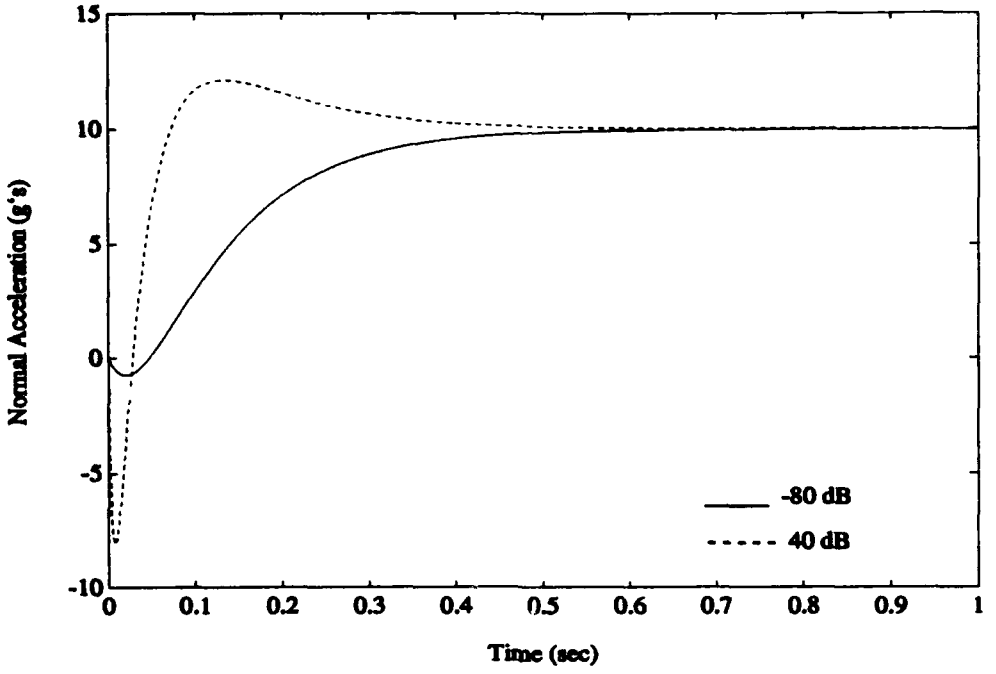

Figure 7-7. 1-DOF N_z Response to a 10 g Step for Tail-Controlled Missile Example (Small Noise Case)

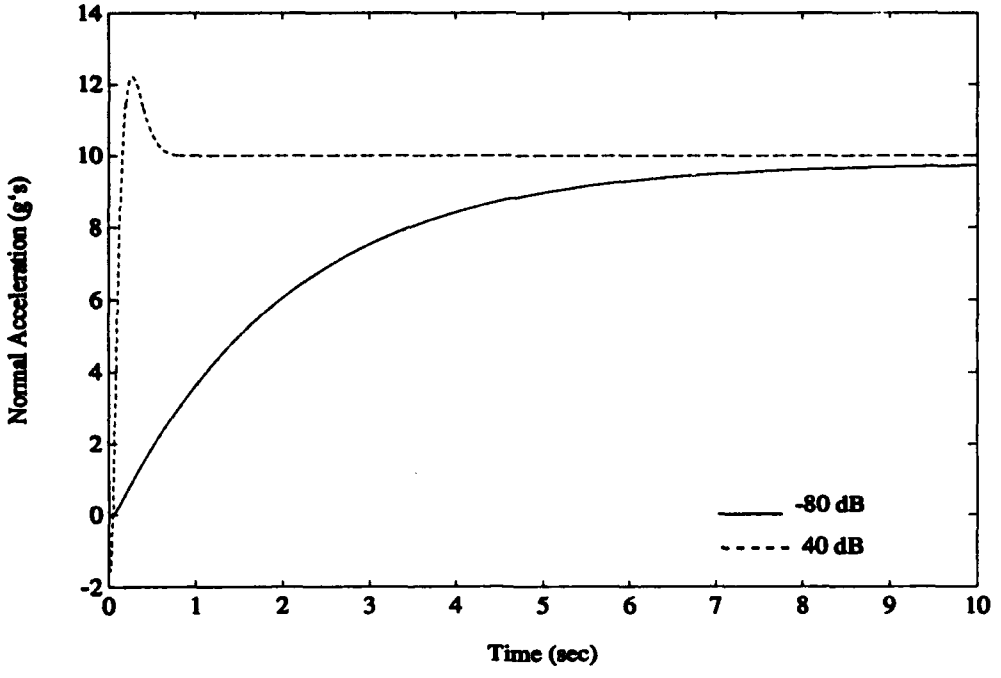

Figure 7-8. 1-DOF N_z Response to a 10 g Step for Tail-Controlled Missile Example (Large Noise Case)

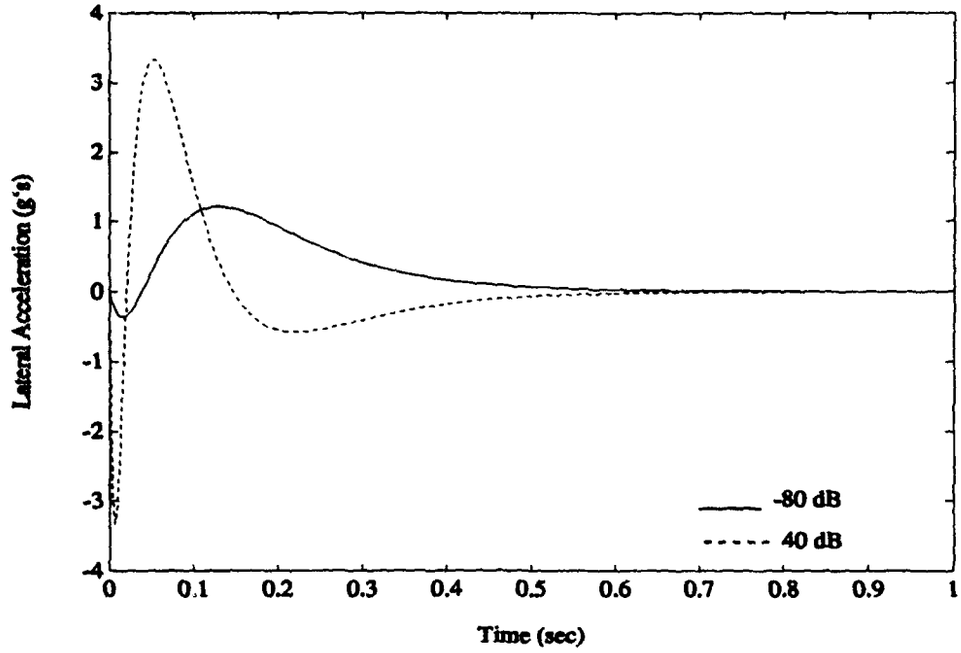

Figure 7-9. 1-DOF N_y Response to a 10 g Step in N_z for Tail-Controlled Missile Example (Small Noise Case)

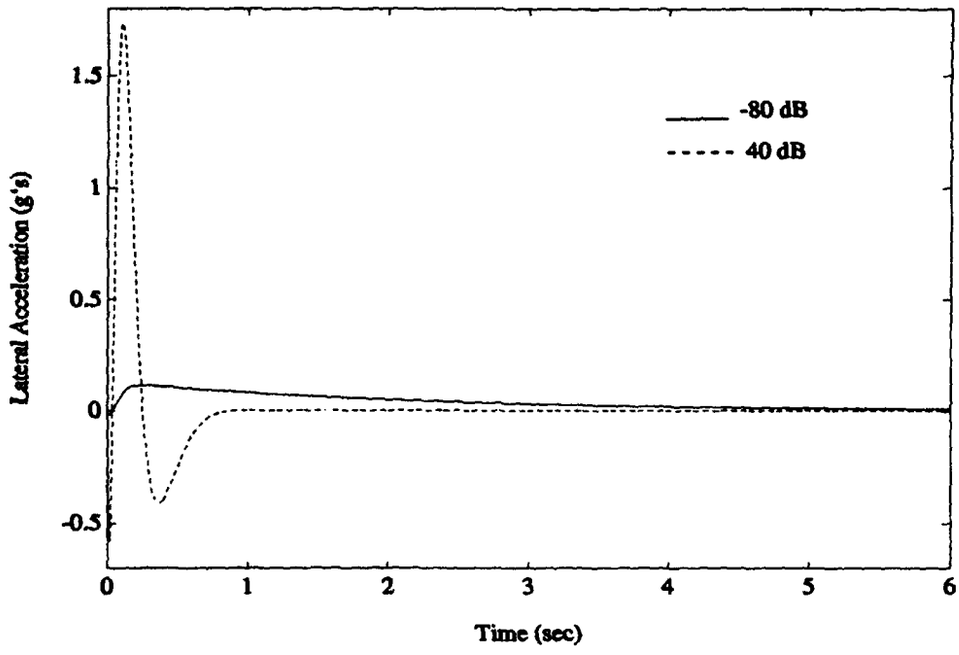

Figure 7-10. 1-DOF N_y Response to a 10 g Step in N_z for Tail-Controlled Missile Example (Large Noise Case)

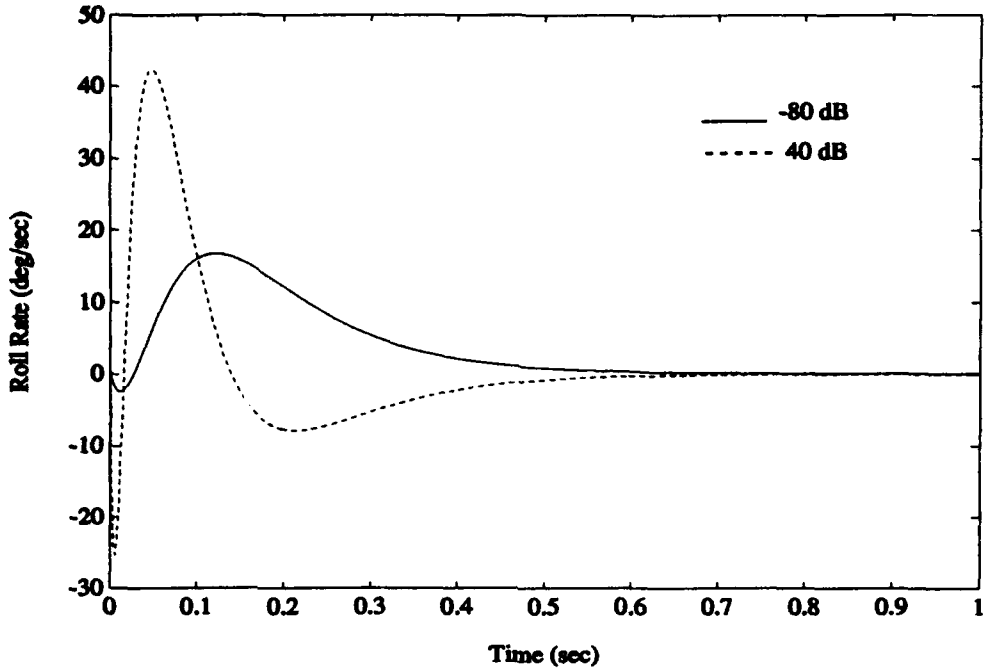

Figure 7-11. 1-DOF Roll Rate Response to a 10 g Step in N_z for Tail-Controlled Missile Example (Small Noise Case)

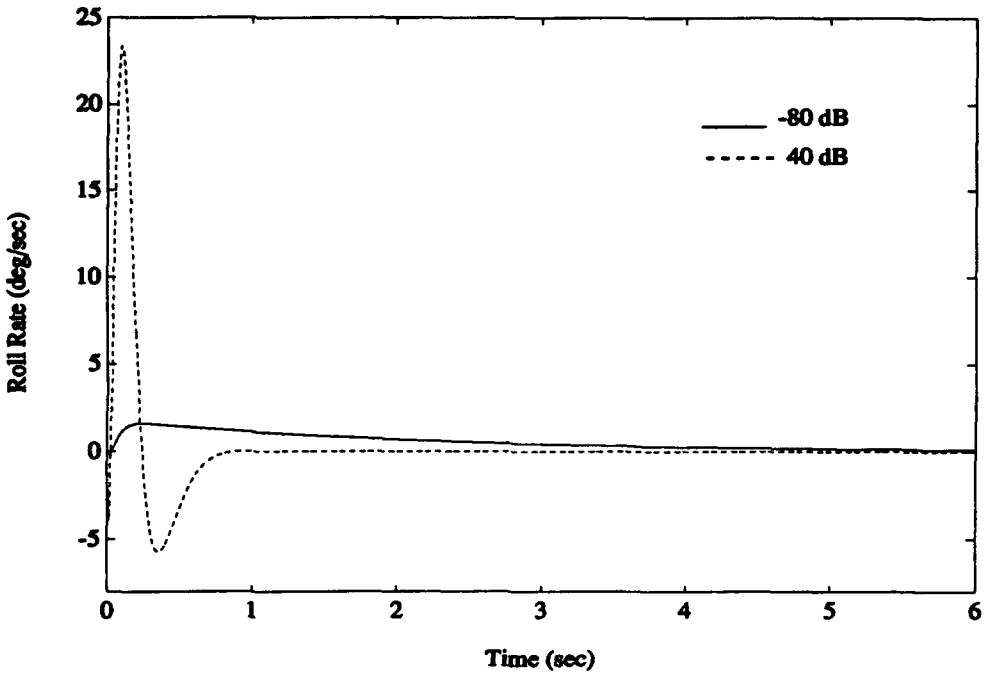

Figure 7-12. 1-DOF Roll Rate Response to a 10 g Step in N_z for Tail-Controlled Missile Example (Large Noise Case)

7.2 2-DOF Setup and Results

Section 7.1 revealed that the 1-DOF H_2 block diagram setup has some limitations as far as being able to utilize all of the possible plant outputs in the design of the compensator. The 2-DOF setup contains a bit more flexibility than the 1-DOF setup does because the K_1 compensator is located *after* the plant in the control loop instead of before it. In this manner, all five of the plant outputs can be fed directly into K_1 instead of "throwing away" two states. The K_1 compensator then becomes a non-square 3 x 5 transfer function matrix. The modified 2-DOF setup is shown in Figure 7-13. The M block in the figure is the selector matrix that is used to convert the plant output signal from five outputs to three and is given by

$$M = \begin{bmatrix} 1 & 0 & 0 & 0 & 0 \\ 0 & 0 & 0 & 1 & 0 \\ 0 & 0 & 0 & 0 & 1 \end{bmatrix} \tag{7.6}$$

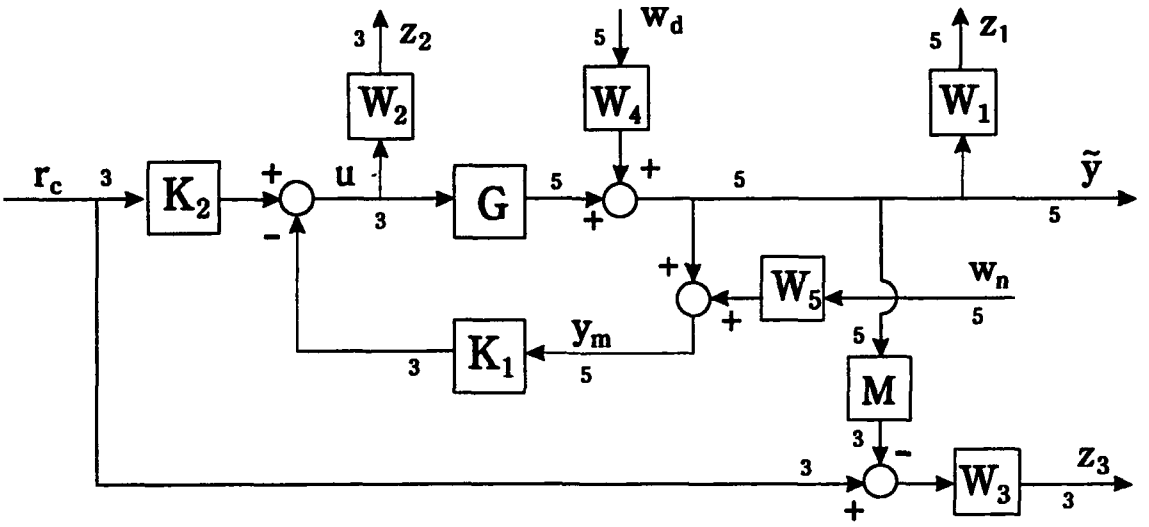

Figure 7-13. 2-DOF MIMO H_2 Optimization Block Diagram

The numbers located at various points around the figure represent the number of inputs or outputs that are contained in the respective vector signal. Equation (5.4) is still a valid representation of the input-to-output transfer function matrix, except for the last row, the z_3 output, which needs to reflect the addition of the selector matrix. The modified transfer function matrix is given by

$$\begin{bmatrix} z_1 \\ z_2 \\ z_3 \end{bmatrix} = \begin{bmatrix} W_1SGK_2 & W_1SW_4 & -W_1TW_5 \\ W_2[I - K_1SG]K_2 & -W_2K_1SW_4 & -W_2K_1SW_5 \\ W_3[I - MSGK_2] & -W_3MSW_4 & W_3MTW_5 \end{bmatrix} \begin{bmatrix} r_c \\ w_d \\ w_n \end{bmatrix} \qquad (7.7)$$

The state space has only a few minor modifications from equation (5.6) and is not shown here.

The 2-DOF MIMO sensitivity function, $|S|$, is shown in Figures 7-14 and 7-15. Since the quantity GK_1 is the product of a 5 x 3 matrix and a 3 x 5 matrix, the resulting matrix is 5 x 5, but its rank is only three. Therefore, there are two singular values that are equal to zero over all frequencies, although they are not shown in the figures. In the small noise case, $\bar{\sigma}[S]$ is very similar to the 1-DOF case, in that it decreases as the disturbance size increases. In the large disturbance case, however, $\underline{\sigma}[S]$ is much lower than it is in the 1-DOF case, indicating the potential for higher loop gain. In the large noise case, some of the same trends are present as in the SISO case, such as the singular values all being zero when the disturbance is small, showing the K_1 compensator minimizing the effects of the noise.

Figures 7-16 and 7-17 show plots of the MIMO complimentary sensitivity

function. As in the SISO case, the bandwidth increases as the disturbance size increases. When the disturbance is large, in both the small and large noise cases, $\bar{\sigma}[T]$ rises above 0 dB before rolling off, indicating deteriorating stability margins due to increased loop gain in a nonminimum phase system. In the small noise-large disturbance case, the singular values do not roll off until after 10,000 rad/sec, compared to 100 rad/sec in the 1-DOF case. In the large noise-small disturbance case, $\bar{\sigma}[T]$ has a DC gain of nearly -100 dB, again showing K_1 minimizing the effects of the noise.

Figures 7-18 and 7-19 show $\sigma[GK_1]$ and $\sigma[GK_2]$ for the small noise case. In the large disturbance case, the separation between $\underline{\sigma}[GK_1]$ and $\bar{\sigma}[GK_1]$ is much bigger than it is in the small disturbance case, which shows the potential for higher loop gain, as expected from the sensitivity plots. Also, since the noise is so small, the K_2 compensator does not really come in to play, and the singular values of GK_1 and GK_2 are almost the same over all frequencies.

Figures 7-20 and 7-21 show $\sigma[GK_1]$ and $\sigma[GK_2]$ for the large noise case. In the large disturbance case, the trends are the same as they are in the small noise case. In the small disturbance case, however, $\underline{\sigma}[GK_1]$ is held down by the dominant measurement noise, and all of the singular values of GK_2 are at 0 dB to maintain tracking performance, as in the SISO case.

Figure 7-22 shows a plot of $|SGK_2|$, which is the same for all of the plant disturbance and measurement noise combinations, showing the bandwidth frequency

for tracking commands. Figure 7-23 shows a plot of the N_z step response. It has an initial undershoot of less than -1 and a settling time of about 0.6 seconds, with no overshoot of the final value. This response is virtually identical to the small noise-small disturbance case for the 1-DOF system and represents the best response possible without any overshoot of the final value. The responses of N_y and roll rate (Figures 7-24 and 7-25, respectively) exhibit responses with the same characteristics of minimizing the over- and undershoot.

Overall, this MIMO example served to reiterate the concepts derived in Chapter III and those learned from the SISO examples in Chapter VI. Whenever the measurement noise is large enough to dominate the system, the 2-DOF system is able to react by driving down the singular values of GK_1 to minimize its effects and readjusting the singular values of GK_2 to maintain favorable tracking. The 1-DOF system responses are particularly susceptible to the effects of large measurement noise, which serves to increase the overshoot and settling time. For the given tracking weight, the 2-DOF system still produces the best overall time responses from the standpoint of exhibiting no overshoot of the final value and minimizing the initial undershoot, regardless of the disturbance or measurement noise sizes. For this MIMO example, the 2-DOF system also proves to make use of all five available measurements, which the 1-DOF system does not. In a more complicated MIMO example, where knowledge of certain measurements may be crucial to controlling other commands, the 2-DOF system would be at a distinct advantage.

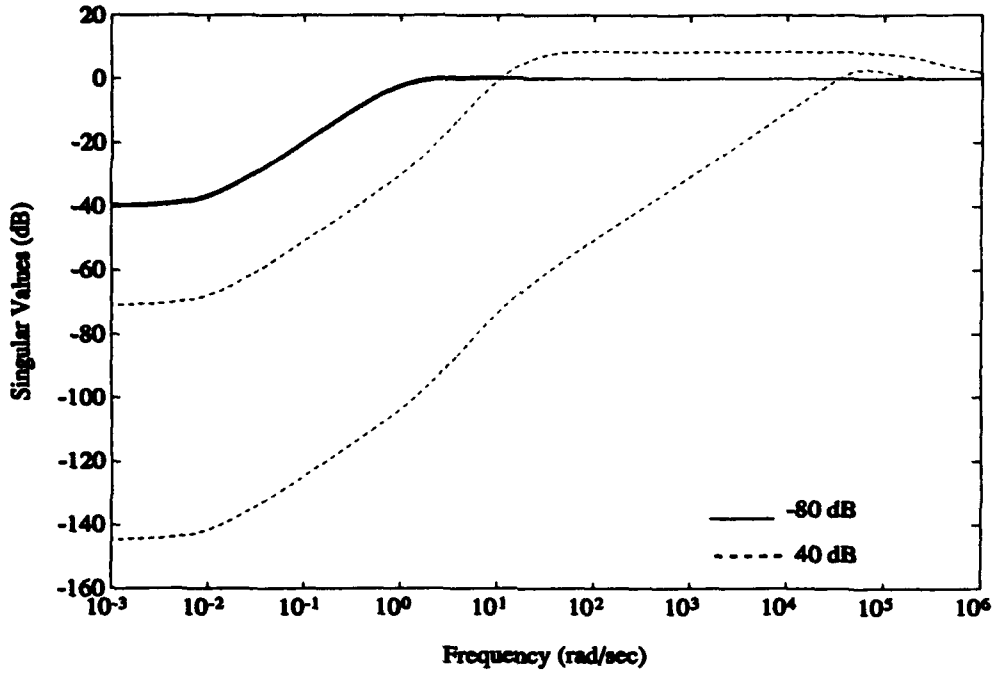

Figure 7-14. 2-DOF Singular Value Plot of $|S|$ for Tail-Controlled Missile Example (Small Noise Case)

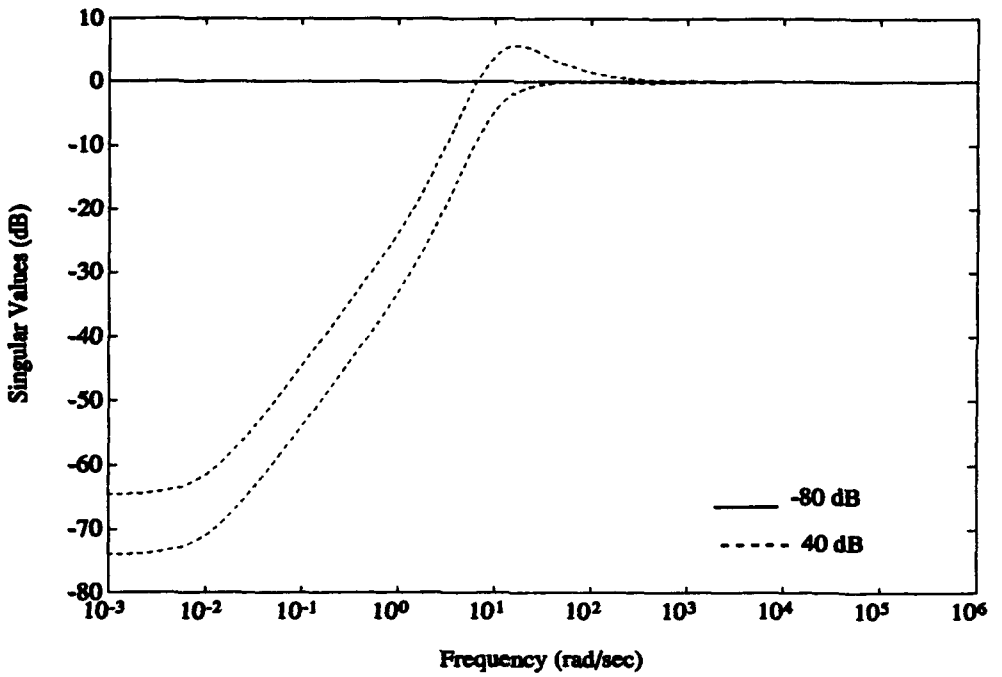

Figure 7-15. 2-DOF Singular Value Plot of $|S|$ for Tail-Controlled Missile Example (Large Noise Case)

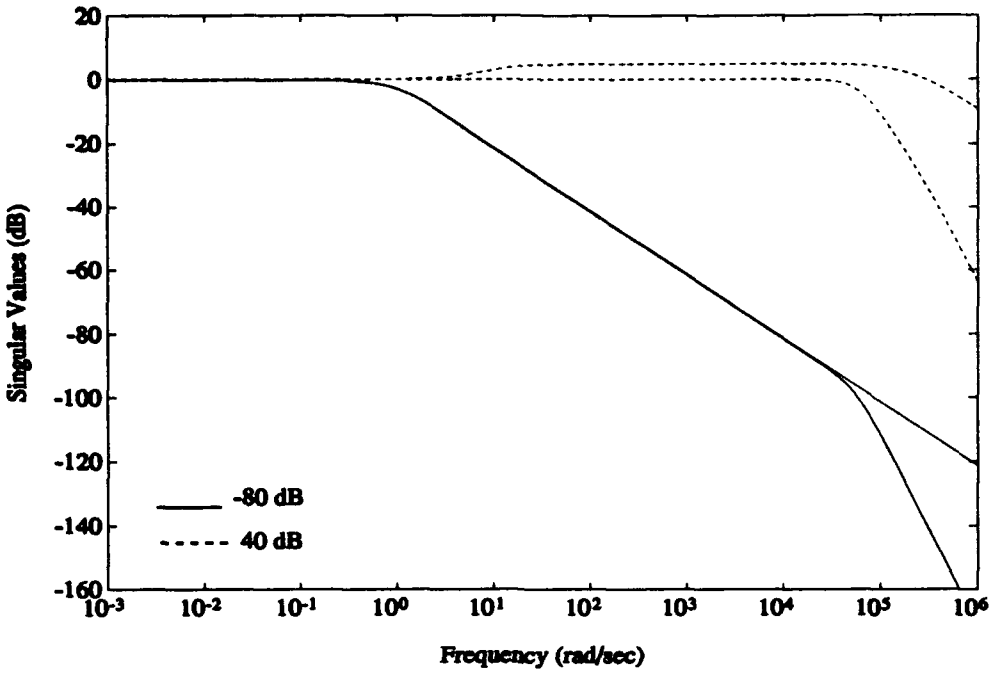

Figure 7-16. 2-DOF Singular Value Plot of $|T|$ for Tail-Controlled Missile Example (Small Noise Case)

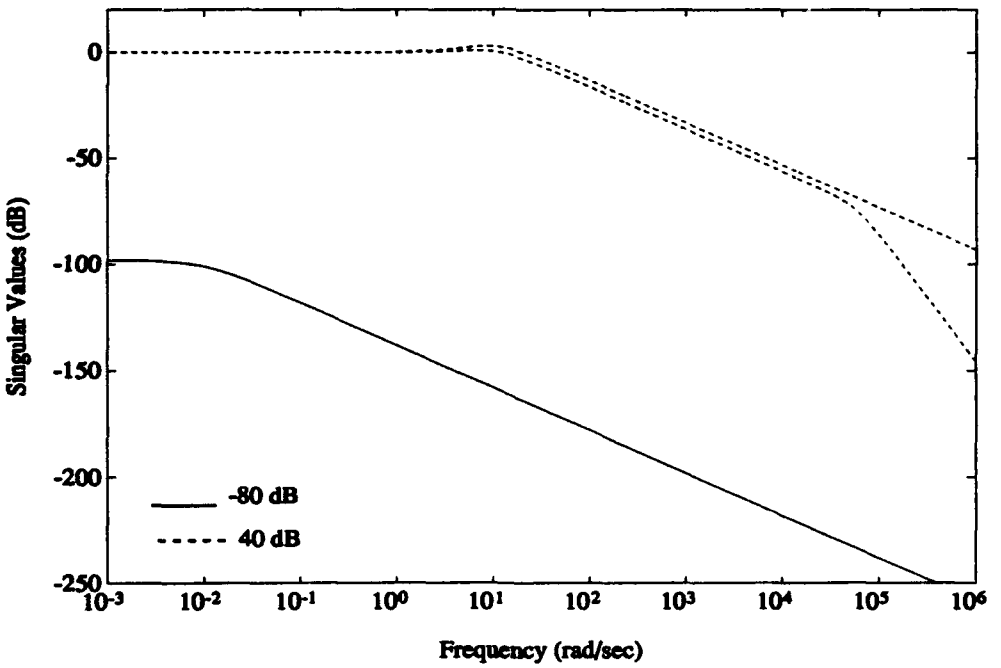

Figure 7-17. 2-DOF Singular Value Plot of $|T|$ for Tail-Controlled Missile Example (Large Noise Case)

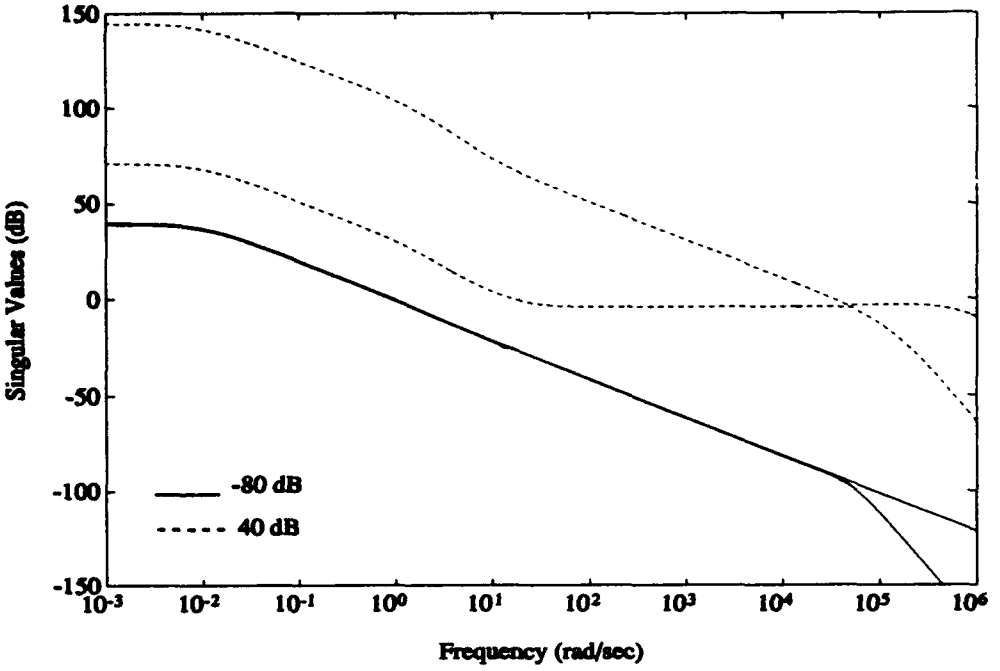

Figure 7-18. 2-DOF Singular Value Plot of $|GK_1|$ for Tail-Controlled Missile Example (Small Noise Case)

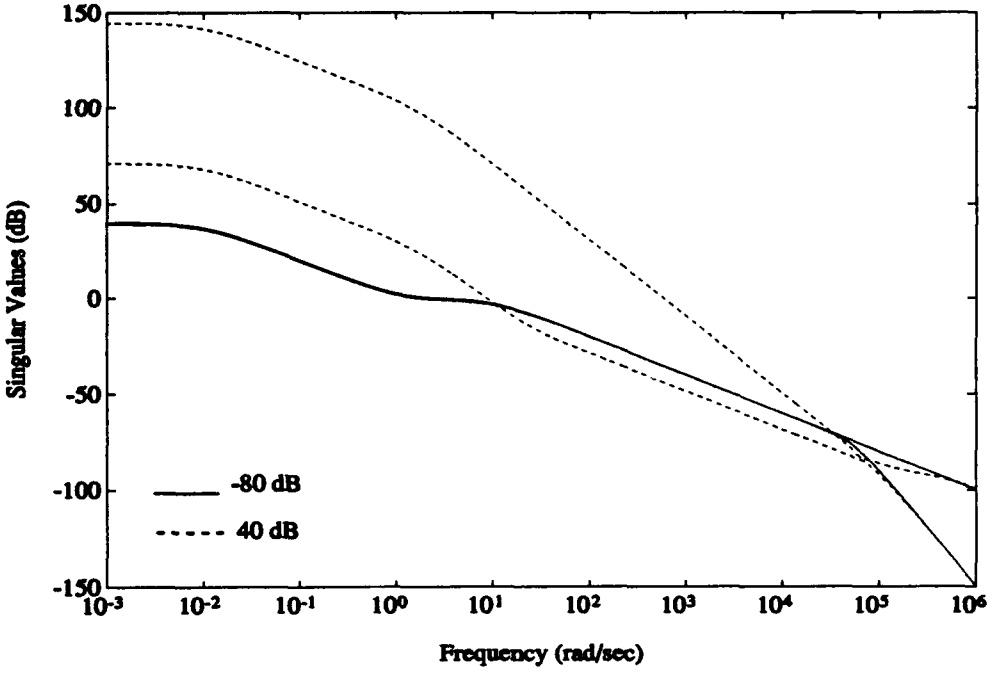

Figure 7-19. 2-DOF Singular Value Plot of $|GK_2|$ for Tail-Controlled Missile Example (Small Noise Case)

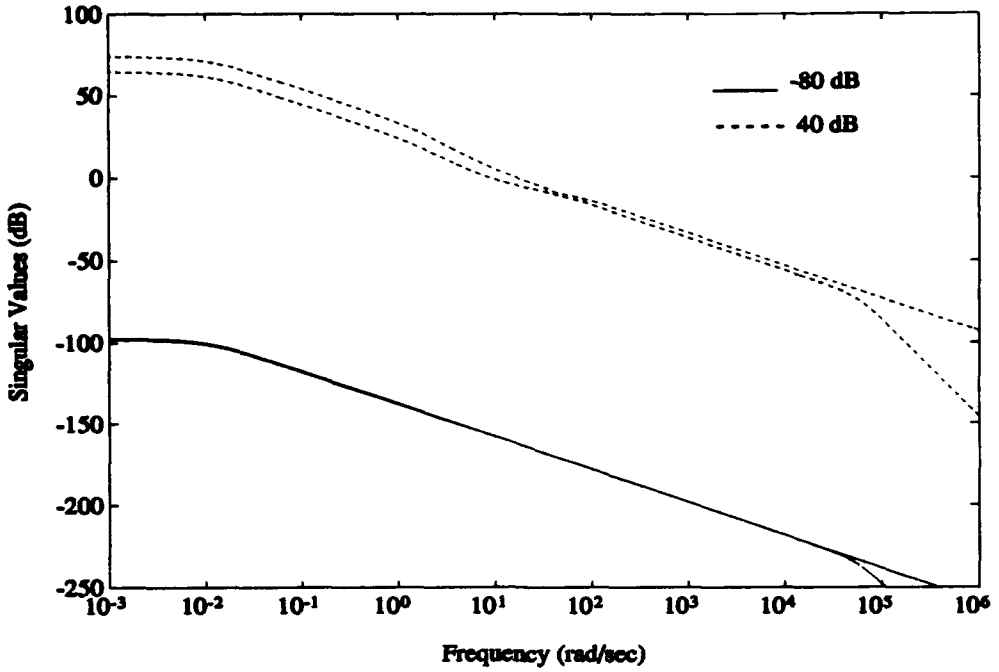

Figure 7-20. 2-DOF Singular Value Plot of $|GK_1|$ for Tail-Controlled Missile Example (Large Noise Case)

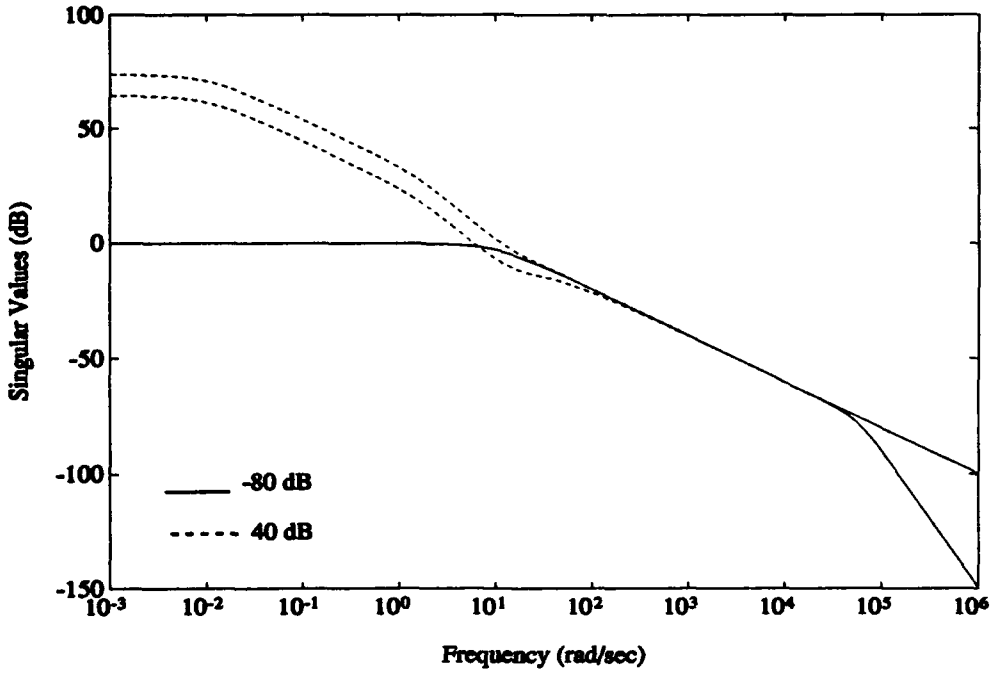

Figure 7-21. 2-DOF Singular Value Plot of $|GK_2|$ for Tail-Controlled Missile Example (Large Noise Case)

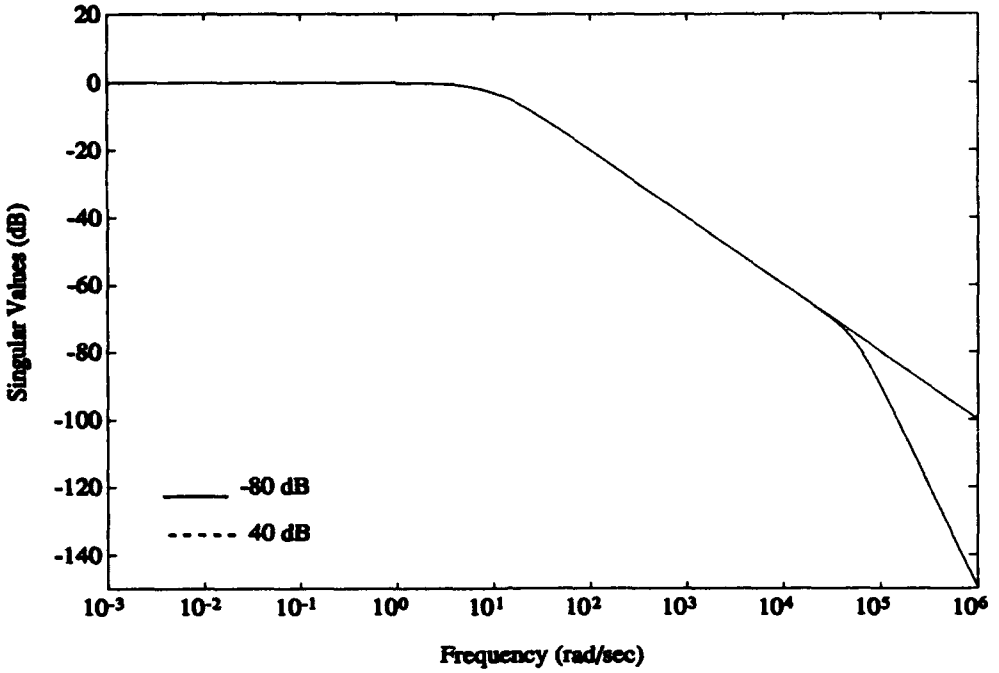

Figure 7-22. 2-DOF Singular Value Plot of $|SGK_2|$ for Tail-Controlled Missile Example (any size noise)

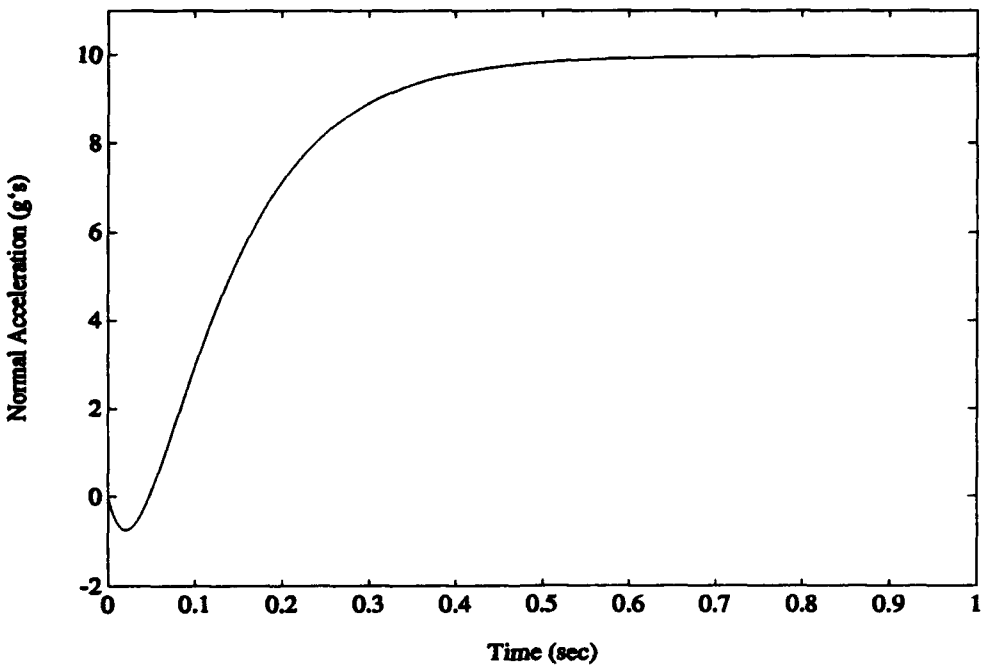

Figure 7-23. 2-DOF N_z Response to a 10 g Step for Tail-Controlled Missile Example (any size noise)

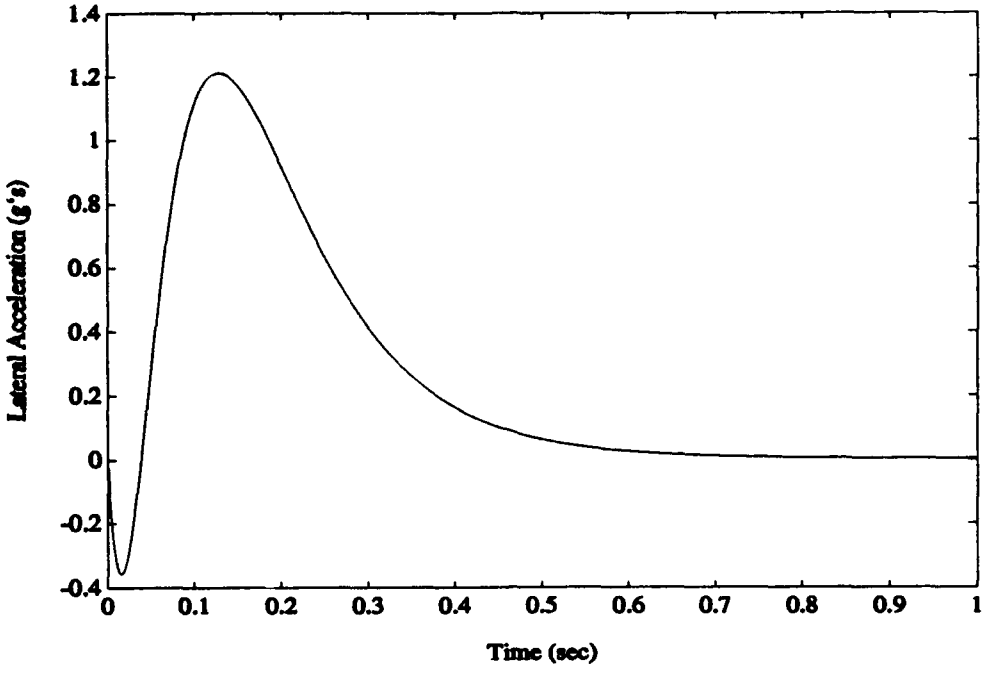

Figure 7-24. 2-DOF N_y Response to a 10 g Step in N_z for Tail-Controlled Missile Example (any size noise)

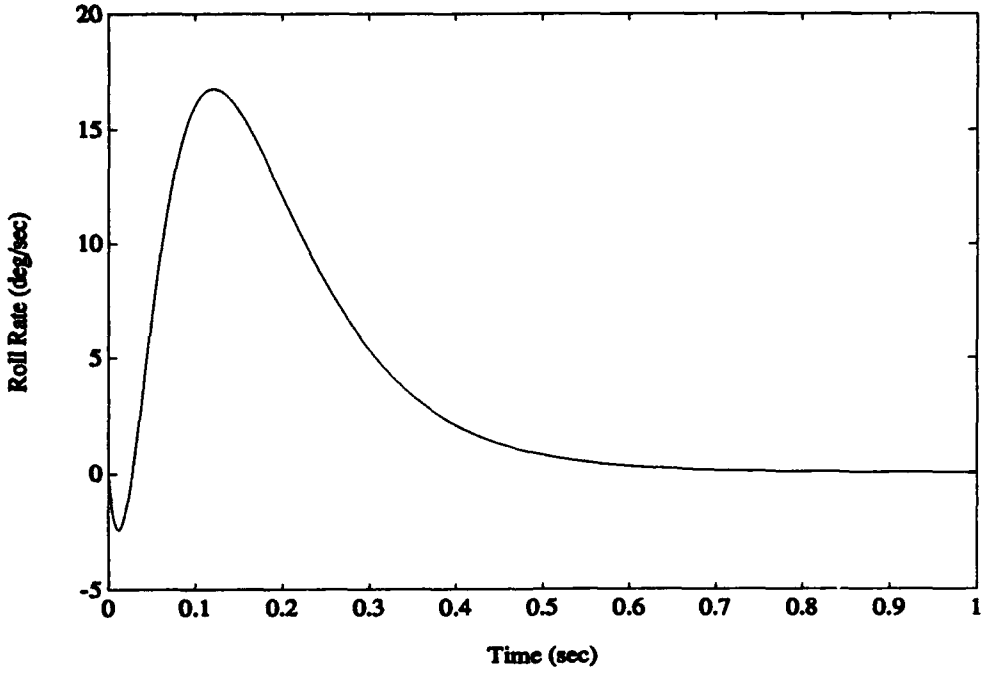

Figure 7-25. 2-DOF Roll Rate Response to a 10 g Step in N_z for Tail-Controlled Missile Example (any size noise)

VIII. Conclusions and Recommendations

8.1 Summary and Conclusions

At the beginning of this thesis, it was stated that 2-DOF systems were assumed to exhibit better tracking qualities than 1-DOF systems, and two of the main questions to answer were how much and under what conditions they were better. The approach to quantifying the differences between the two systems started out with a summary of the rules governing loop shaping in the 1-DOF case, and through the extension of these concepts to the 2-DOF case, key differences were identified. Several types of examples were then completed in order to try to achieve the basic control objectives of tracking commands and rejecting plant disturbances and measurement noises utilizing both types of systems.

In the four basic SISO examples, the frequency responses gave the basic closed loop shapes that could be expected to be encountered in control system design. Although the nominal plant model was low order and could be considered very simple, it did allow for the effects of putting a pole or zero into the right-half plane to be easily observed. It turned out that nonminimum phase zeros had the most detrimental effect on the tracking ability of both systems, sharply reducing the stability margins and causing the step responses to initially head in the opposite direction. The fact that zeros cannot be moved through feedback control is a universal problem in control theory. Unstable poles also had adverse effects on the systems, particularly by reducing the stability margins.

Most importantly, the four SISO examples revealed the conditions under which 2-DOF controllers really have an advantage over 1-DOF controllers. In cases where the plant disturbance was large, the time responses of both systems were very similar. In fact, the 1-DOF responses often showed faster rise and settling times. The one variable which brought out the differences was measurement noise. Since the system reference command and measurement noise are related to the output by the same transfer function in the 1-DOF system, it is readily apparent that there is always a potential conflict between command following and noise rejection. The noise level could be viewed as a "knob" that can be directly tuned to degrade the tracking performance of the system. In all of the examples, increased measurement noise caused more overshoot and longer settling times in the 1-DOF step responses. The 2-DOF controller's structure effectively decouples the requirements necessary for noise rejection and command following performance by allowing the feedback controller to concentrate on attenuating measurement noise and the prefilter controller to adjust accordingly to maintain tracking over as wide a frequency range as possible.

The effects of measurement noise on tracking performance was made more clear in the low frequency measurement noise example. When the measurement noise frequencies dip into the region normally reserved for plant disturbances and command inputs, the classic tradeoff between tracking and noise rejection in 1-DOF systems begins to break down, as the system must try to simultaneously attenuate the noise while at the same time place energy into tracking commands -- an impossible task The 1-DOF step response for this example showed that as the noise level increased, so

did the steady state error in the response, due to the fact that no loop gain could be applied at the frequencies where high gain is normally required for a low steady state error. The 2-DOF system alleviated this problem by shaping the feedback controller to resemble that of the 1-DOF system, thereby holding down the effects of the noise. Meanwhile, the prefilter controller "picked up the slack" by shaping itself in such a way as to preserve its tracking characteristics. In fact, the 2-DOF system acted as if it could not tell the difference between high or low frequency measurement noise. However, if the evaluation model were changed so that low frequency measurement noise actually entered the system, then both the 1-DOF and 2-DOF systems would exhibit "noisy" responses in the case where the controllers were designed with both a large plant disturbance and large measurement noise in mind.

The SISO system type examples demonstrated one of the defining characteristics of H_2 2-DOF controller tracking performance. That is, in each of the examples, the 2-DOF system produced the response that had the fastest settling time, subject to the constraint of having no overshoot. In nonminimum phase systems, the amount of initial undershoot was also minimized. Even the error responses for ramp and parabolic inputs showed the 2-DOF controller's response to have very little oscillatory motion. A possible criticism of the limits of the 2-DOF time response for the given tracking weight is that 1-DOF controllers produce responses which have faster rise and settling times under certain conditions, such as when the measurement noise level is low compared to the disturbance level. That perceived drawback can be dismissed when the fact that the 2-DOF controller produces responses with the aforementioned constraints *regardless* of the size of the plant disturbance or

measurement noise is considered. The tracking weight can be altered to contain more high frequency content in order to improve the speed of the transient response (and allow more overshoot). In addition, it is possible to move the poles of the prefilter to different locations after the optimization algorithm is complete, thereby improving the response without affecting the disturbance or noise rejection properties of the system.

The tail-controlled missile MIMO example reiterated all of the concepts just discussed for the SISO case and brought out another area where 2-DOF controllers may offer possible advantages. When a plant is modeled as a non-square system (different number of outputs than inputs), as the missile in this example was, 1-DOF systems are limited insofar as how they make use of all available information. Since the input to the compensator is the difference between the command inputs and the measured outputs, then the number of outputs used by the optimization algorithm is limited by the number of command inputs. In 2-DOF systems, on the other hand, the feedback controller is located after the plant in the control loop. Therefore, the feedback controller can be non-square and thus make use of all of the plant outputs yet at the same time feed back only the appropriate number of outputs to be summed with the command inputs.

The concept of a 2-DOF controller has been around for several years, but it is still relatively new from the point of view that there are virtually no textbooks that include it as part of a basic discussion of linear control theory. The primary purpose of this work was to take the concept of a 2-DOF controller and compare it to the basic 1-DOF model as far as what it takes to achieve control objectives. Through the examples presented, it is hoped that it has become clear that a 2-DOF controller offers

significant design advantages over the conventional 1-DOF model over a wide variety of conditions.

8.2 Recommendations for Future Research

The 2-DOF controllers employed in thesis made use of the H_2 optimization method, which has the limitation of constraining the feedback compensator and the prefilter to share the same poles. There has been some work done on designing each compensator separately in an effort to optimize each one without being limited by the other. One potential research topic would be to investigate the techniques of designing the two controllers separately and comparing them to designs where the controllers are designed in a single step. Also, since the 2-DOF system is a basic control system model, other optimization techniques could be applied to it, such as LQG, H_∞, and mixed H_2/H_∞. Finally, it would be interesting to see just what 2-DOF systems are capable of in practical applications. If simulations indicate that they produce superior time responses regardless of any plant disturbances or measurement noises, then 2-DOF controllers would make excellent candidates for precision control applications.

References

1. Brown, J.M. II, D.B. Ridgely and R.N. Paschall. "Autopilot Design for a Tail-Controlled Missile Using LQG/LTR with Eigenstructure Reassignment," submitted to the 1994 American Controls Conference and the *Journal of Guidance, Control, and Dynamics.*

2. Doyle, J.C., K. Glover, P.P. Khargonekar and B.A. Francis. "State-Space Solutions to Standard H_2 and H_∞ Control Problems," *IEEE Transactions on Automatic Control*, Vol. 34, No. 8: 831-847 (August 1989).

3. Franklin, G.F., J.D. Powell and A. Emami-Naeini. *Feedback Control of Dynamic Systems* (Second Edition). Addison-Wesley Publishing Company, Reading, MA, April 1991.

4. Hara, S. and T. Sugie. "Independent Parameterization of Two-Degree-of-Freedom Compensators in General Robust Tracking Systems," *IEEE Transactions on Automatic Control*, Vol. 33, No. 1: 59-67 (January 1988).

5. Limebeer, D.J.N., E.M. Kasenally and J.D. Perkins. "On the Design of Robust Two Degree of Freedom Controllers," *Automatica*, Vol. 29, No. 1:157-168 (July 1992).

6. Ridgely, D.B. *A Nonconservative Solution to the General Mixed H_2/H_∞ Optimization Problem*. PhD dissertation. Massachusetts Institute of Technology, Cambridge, MA, 1991.

7. Ridgely, D.B. and S. Banda. *Introduction to Robust Multivariable Control.* AFWAL-TR-85-3102. February 1986.

8. Soroka, E. and U. Shaked. "A Decoupling Approach to the Design of the Two-Degree-of-Freedom Tracking Control Systems," *Proceedings of 25th Conference on Decision and Control.* 661-665. Athens, Greece, December 1986.

9. Yaesh, I. and U. Shaked. "Two-Degree-of-Freedom H_∞ Optimization of Multivariable Feedback Systems," *IEEE Transactions on Automatic Control*, Vol. 36, No. 11: 1272-1276 (November 1991).

10. Youla, D.C. and J.J. Bongiorno, Jr. "A Feedback Theory of Two-Degree-of-Freedom Optimal Wiener-Hopf Design," *IEEE Transactions on Automatic Control*, Vol. AC-30, No. 7: 652-665 (July 1985).

Vita

Captain Michael J. Stephens was born in New York City on 3 December 1967. He graduated from Atholton High School in Columbia, MD in 1985 and attended the U.S. Air Force Academy, graduating with a Bachelor of Science in Aeronautical Engineering in May 1989. Upon graduation, he received a regular commission in the USAF and served his first tour of duty at Eglin AFB, Florida. While there, he served as an aeroballistics research engineer in the Armament Directorate of Wright Laboratory, where he was responsible for conducting experimental aerodynamic research on various munitions. During this time he also earned a Master of Business Administration degree from the University of West Florida, graduating in December 1991. He entered the Graduate School of Engineering, Air Force Institute of Technology, in May 1992 to pursue a Master of Science degree in Aeronautical Engineering.

December 1993 Master's Thesis

OPTIMAL CONTROL DESIGN ADVANTAGES UTILIZING TWO-DEGREE-OF-FREEDOM CONTROLLERS

Michael J. Stephens, Captain, USAF

Air Force Institute of Technology, WPAFB OH 45433

AFIT/GAE/ENY/93D-27

N/A

The purpose of this study was to investigate and describe the differences between a one-degree-of-freedom (1-DOF) controller, in which a controller is placed in a single location in the control loop, and a two-degree-of-freedom (2-DOF) controller, in which two separate controllers are designed -- one in the feedback loop and the other as a prefilter in the forward loop. The approach involved summarizing the major rules governing loop shaping for performance and robustness in the 1-DOF case and then extending the concepts to the 2-DOF case. H_2 optimization was utilized to perform several types of SISO examples and one MIMO example to verify the concepts. In all cases, the 2-DOF controller exhibited superior tracking performance over a wide range of plant disturbances and measurement noises compared to the 1-DOF model.

Optimal Control, Feedback Control Systems, Controllers, Degrees of Freedom, Tracking 184

Unclassified Unclassified Unclassified UL